SYNTHESIS OF PHOSPHINE STABILIZED GOLD NANOPARTICLES BASED ON 9-BBN AS A NOVEL REDUCING AGENT AND APPLICATION IN CATALYSIS

by

Patrick Musyoki Shem

A dissertation submitted to the faculty of
The University of Utah
in partial fulfillment of the requirements for the degree of

Doctor of Philosophy

Department of Chemistry

The University of Utah

August 2012

The University of Utah Graduate School

STATEMENT OF DISSERTATION APPROVAL

The dissertation of **Patrick Musyoki Shem**

has been approved by the following supervisory committee members:

Jennifer S. Shumaker-Parry	, Chair	**06-21-2012** Date Approved
Joel M. Harris	, Member	**06-21-2012** Date Approved
Marc D. Porter	, Member	**06-22-2012** Date Approved
Kenneth J. Woycechowsky	, Member	**06-22-2012** Date Approved
David W. Grainger	, Member	Date Approved

and by **Henry S. White**, Chair of the Department of **Chemistry**

and by Charles A. Wight, Dean of The Graduate School.

ABSTRACT

A simple, versatile single step method to synthesize phosphine-stabilized gold nanoparticles (TPP-AuNPs) of narrow size distribution using the mild reducing agent 9-borabicyclo [3.3.1]nonane (9-BBN) was developed. This single step procedure produces particles of less than 2 nm in diameter. The use of 9-BBN offers many advantages over other commonly used reducing agents. The particle growth process can be controlled and the particle size can be tuned by carefully controlling the conditions under which the reduction takes place. In addition, the approach is inexpensive and greener because the use of phase transfer reagents and the attendant rigorous purification steps are eliminated. Since 9-BBN is a mild reducing agent, the synthesis is compatible with a wide variety of ω-functionalized capping ligands.

TPP-AuNPs can be used as precursors to AuNPs functionalized with various ligands by way of ligand exchange reactions to obtain AuNPs stabilized with different *ω*-functionalized alkythiols, other phosphines and bipyridines. The *in-situ* addition of capping ligands other than TPP to the reaction was demonstrated to reduce the need for ligand exchange reactions.

TPP-AuNPs also are soluble in water, thereby expanding their potential applications. The stability of TPP-AuNPs in water as a function of salt and sodium borohydride concentration, solvents with different dielectric constants, pH and temperature was investigated. The NPs were found to be stable in water as evidenced by

UV-vis spectroscopy, TEM imaging and zeta potential measurements over time. Addition of salt and $NaBH_4$ induced aggregation of the NPs.

The catalytic activity of TPP-AuNPs in aqueous solution was investigated using two model reactions: reduction of 4-nitrophenol by $NaBH_4$ and the electron transfer reduction of hexacyanoferrate (III) by $NaBH_4$. The rate constants for the reduction reactions were found to depend on the surface area of the TPP-AuNPs. The TPP-AuNPs were recycled, however aggregation of the NPs was observed at the end of the reduction. The kinetic data for both reactions for the unsupported TPP-AuNPs was better compared with that for supported AuNP catalytic systems, indicating the good catalytic activity of TPP-AuNPs for these reactions.

For Shem Munyalo and Sarah Mwikali Ndumbu

TABLE OF CONTENTS

LIST OF TABLES

LIST OF SCHEMES

ACKNOWLEDGEMENTS

I would like to express my sincere gratitude to my research advisor, Prof. Jennifer Shumaker-Parry for her guidance and mentoring during my research. I am very grateful for the many opportunities for scientific growth afforded to me during my time in the Shumaker-Parry group. I would also like thank my dissertation committee members, Prof. Joel M. Harris, Prof. Marc D. Porter, Prof. Kenneth J. Woycechowsky and Prof. David W. Grainger for serving in my dissertation committee and for their helpful advice and suggestions.

I wish to express my thanks to current and former members of the Shumaker-Parry group for the interactive and dynamic learning environment they fostered in the lab. I am especially indebted to Dr. Rajesh Sardar (IUPUI) who was a postdoctoral researcher in the Shumaker-Parry lab when I joined in 2008. He mentored me during the beginning of my graduate career and I learned a great deal during the discussions we had in the lab.

I extend my sincere gratitude to Nancy Chandler of the University of Utah Electron Microscopy Core Facility for teaching me how to use the transmission electron microscope and for her help with troubleshooting on numerous occasions.

Finally, I thank my family for their support and encouragement.

CHAPTER 1

GENERAL INTRODUCTION

1.1 Introduction

Since ancient times, metal nanoparticles have been produced for various uses. Interest in metal sols, especially gold sols emanated from the different colors they exhibited in different environments. The most famous example is the Lycurgus Cup.[1] When the cup is illuminated at different angles, it changes color. It appears red due to absorption and green due to scattering. Another example is Purple of Cassius which was made from gold salts and tin (II) chloride was used as a coloring agent for glass, enamel and silk fabric.[2] Colloidal gold sols also were used for medical purposes, for example *aurum potabile* or "drinkable gold" potions.[3] The first documented scientific study of colloidal gold nanoparticles is attributed to Michael Faraday.[4, 5] By reducing chloroaurate with white phosphorus in a carbon disulfide-water mixture, Faraday synthesized a colloidal gold solution which was deep red in color. He also observed the Tyndall effect in the colloidal solution. [5] This marked the beginning of modern colloid science in which systematic studies of colloids of different metals have been undertaken. The unique optical and electronic properties of the metal nanoparticles depend on the size, shape, surface chemistry, the distance between the nanoparticles and the refractive index of the surrounding medium of the nanoparticles.[6] As a result, in recent times,

synthesis of metal nanoparticles has required that the size, surface chemistry and shape among other properties must be tuned precisely. Recent advances in colloidal synthesis have led to the development of new synthetic strategies that have made control of nucleation and growth of nanoparticles achievable. In turn, the properties of the nanoparticles can thus be tuned as desired. Gold nanoparticles (AuNPs) represent one class of nanoparticle systems that has been studied widely and this dissertation will focus on AuNPs with special emphasis on phosphine stabilized AuNPs.

1.2 Unique properties of gold nanoparticles

Nanoparticles are composed of several parts: the core (made up of metal atoms), stabilizing shell and stabilizing ligands (Figure 1.1). Stabilizing ligands may include ions, organic molecules, polymers or biomolecules. Gold nanoparticles have attracted immense interest because they exhibit many unique properties which are size and shape dependent. The diameter of the nanoparticles and the wavelength of the electrons in the nanoparticles are similar, giving rise to these properties.[7] Some of the unique properties include surface plasmon resonance,[8, 9] surface enhanced Raman scattering,[10] size dependent catalytic activity,[11] quantized charging[12] and electronic quantum confinement.[13, 14] The electronic character of the nanoparticles depends on the number of atoms they possess which is directly related to the size of the nanoparticle.[15] In addition, the reactivity of the nanoparticles depends on the nature of the ligand passivating the nanoparticles[16, 17] and the fraction of surface atoms.[18] As the size of the nanoparticles decreases, the fraction of atoms at the surface increases leading to an increase in the reactivity of the nanoparticle.[19] The stabilizing ligands also determine the solubility and

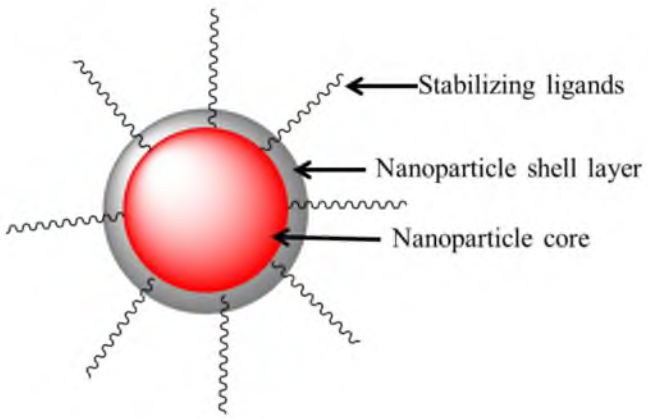

Figure 1.1. Schematic illustrating the components of a nanoparticle: the core, shell and stabilizing ligands.

stability of the nanoparticles.[20, 21] Phosphine capped nanoparticles that contain both phosphorus and chlorine also exhibit magnetism.[7] Gold nanoparticles also exhibit a strong resistance to oxidation compared to other metal nanoparticles, for example, silver.[22, 23] These properties offer numerous possibilities for technological applications.

1.3 Applications of phosphine stabilized nanoparticles

The bulk of recent work on gold nanoparticles has focused on thiol stabilized nanoparticles. Since they were first used in electron microscopy to enhance the visualization of biological samples during imaging,[24] interest in phosphine stabilized gold nanoparticles has increased. One advantage of triphenylphosphine stabilized nanoparticles (TPP-AuNPs) over thiol stabilized NPs is that they can serve as precursors to other functionalized nanoparticles.[25] This is because the triphenylphosphine (PPh_3) ligand is labile and is easily replaced with other ligands.[26] This property of TPP-AuNPs is especially useful because it enables the attachment of molecules with different functional groups to the nanoparticles. It therefore becomes possible to change the

properties of the NPs, for example solubility in different solvents and to build other structures like chains using these NPs as building blocks. TPP-AuNPs have found applications in many areas including catalysis,[27] sensors,[28] optical switches and microelectronics,[13, 29, 30] nanophotonics,[31] immunoassays and immunolabeling,[32, 33] X-ray contrast agents,[34] reprography,[35, 36] drug delivery and targeting platforms.[37] The $Au_{55}[P(C_6H_5)_3]_{12}Cl_6$ cluster which has a diameter of 2 nm, also has been used in nanoelectronic devices because it exhibits Coulomb-blockade-dominated transport at room temperature.[38] This cluster is also catalytically active in both bare and ligand protected forms.[39] These applications have necessitated the development of versatile and scalable synthetic strategies for phosphine stabilized gold nanoparticles.

1.4 Gold nanoparticle synthetic methods

The most commonly used synthetic methods for making gold nanoparticles will be discussed in this section. The Turkevich method in which chloroaurate ions in water are reduced by sodium citrate is the most common method for making gold nanoparticles.[40] The citrate ion in this case is both the reducing and stabilizing agent. Frens demonstrated that by varying the amount of the reducing agent (sodium citrate) added to the reaction mixture, controlled nucleation of the gold nuclei could be achieved.[41] As a result, monodisperse nanoparticles could be obtained. However, the Turkevich method cannot be used to make small nanoparticles and the stabilizing ligand is limited to citrate. On the other hand, gold nanoparticles of small sizes (2 nm in diameter) stabilized by phosphines can be synthesized. Phosphine stabilized gold nanoparticles also can be used as precursors to prepare nanoparticles functionalized with different ligands.[42] Synthesis

of phosphine stabilized gold nanoparticles involves the reduction of Au precursors in the presence of the desired phosphine, usually triphenylphosphine.

Phosphine stabilized nanoparticles were first synthesized as the gold cluster $Au_{55}(PPh_3)_2Cl_6$ by Schmid et al.[43] Briefly, the synthesis involves the reduction of Ph_3PAuCl by diborane in benzene or toluene at high temperatures. The nanoparticles produced were 1.4 ±0 .4 nm in diameter. This synthetic procedure was cumbersome, required anaerobic conditions and used the strong reducing agent, diborane which is a toxic gas.[44] In addition, other products like chlorinated boranes were produced during the synthetic procedure, thereby forcing rigorous purification steps for the product. For these reasons, development of more convenient and scalable methods to produce gold nanoparticles became necessary.

The Brust-Schiffrin method[20] was developed as an alternative to the Schmid method. The Brust method is a two-phase synthetic procedure which uses $NaBH_4$ as the reducing agent. This method produces thiol stabilized gold nanoparticles with a broad size distribution (1-4 nm in diameter).[45] It is difficult to perform post synthetic surface modification and functionalization with other ligands using thiol stabilized gold nanoparticles as precursors due to the strong bond between gold and sulfur. They also cannot be used for catalysis because of the stability availed by the thiol ligands leading to a low fraction of available surface sites for reactions.[45] As a result, various modifications of the Brust synthetic method have been reported for phosphine stabilized gold nanoparticles. Hutchison et al. developed a two phase synthetic procedure for preparing 1.5 nm phosphine stabilized gold nanoparticles as shown in Scheme 1.1.[42] This method uses $NaBH_4$ as the reducing agent to reduce the $HAuCl_4$ precursor.

Scheme 1.1. Synthesis of 1.5 nm triphenylphosphine-stabilized gold nanoparticles

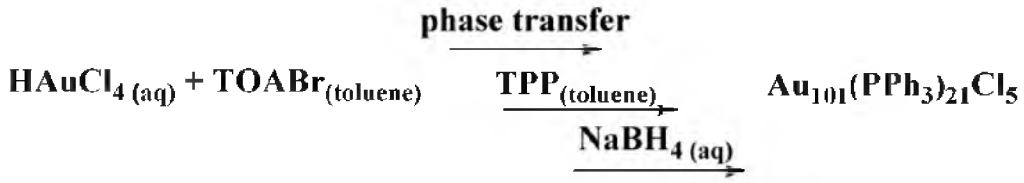

(Reprinted with permission from Dahl, J. A.; Maddux, B. L. S.; Hutchison, J. E. *Chem. Rev.* **2007**, *107*, 2228-2269, Scheme 1. Copyright 2007 American Chemical Society).

The Hutchison synthetic protocol requires the use of a phase transfer agent which introduces impurities into the final product. Rigorous washing and purification steps are therefore necessary to remove the phase transfer agent, byproducts and unreacted material. The purification process consumes a lot of organic solvents (chloroform and pentane) and makes the synthetic procedure longer and expensive. The use of amine-borane complexes as reducing agents in the synthesis of metal nanoparticles also has been reported.[46] However, these complexes are either too mild leading to long reaction times or are so strong that the growth process is hard to control. Zheng et al.[46] used tert-butylamine-borane as the reducing agent. Whereas this is a one-step synthetic procedure which uses a phosphine gold salt precursor ($AuPPh_3Cl$), it was necessary to add thiols to the mixture in order to obtain nanoparticles with a narrow size distribution.

Thus, although a few methods for making phosphine stabilized AuNPs have been developed, these approaches require phase transfer reagents, which introduce impurities to the product. Purification steps are required which makes the process more time consuming and increases the amount of solvent used. The existing methods also limit the types of ω-functionalized alkylthiols and amines that can be used as capping ligands for

AuNP stabilization and functionalization. This limitation is due to the reduction of the functional groups of the capping ligands by the strong reducing agents that are typically used.

We have developed a simple and versatile method for making monodisperse triphenylphosphine (TPP) stabilized AuNPs with diameters of less than 2 nm.[47] This is a single step procedure which uses a mild reducing agent 9-Borabicyclo[3.3.1]nonane (9-BBN). The use of 9-BBN offers many advantages over other commonly used reducing agents. 9-BBN avails the ability to control the particle growth process. The particle size can be tuned by carefully controlling the conditions under which the reduction takes place. In addition, the approach is inexpensive and greener because the use of phase transfer reagents and the attendant rigorous purification steps are eliminated. Since 9-BBN is a mild reducing agent, the synthesis is compatible with a wide variety of ω-functionalized capping ligands, making *in-situ* functionalization of the NPs with desired ligands possible. This reduces the need for post functionalization procedures, for example, ligand exchange which is a technique commonly used to introduce ligands with desired functional groups to NPs postsynthesis. A theoretical model of the structure of 2 nm TPP-AuNPs is presented in Figure 1.2.

1.5 Mechanisms of nanoparticle formation

In order to develop a consistent and reproducible synthetic process for NPs, it is very important to understand the mechanism of formation and growth of the NPs. Generally, there are three steps involved in the formation of NPs: nucleation, growth and stabilization. When nucleation and growth occur simultaneously, NPs with a broad size distribution are formed.[48] Numerous studies have been undertaken in order to decouple

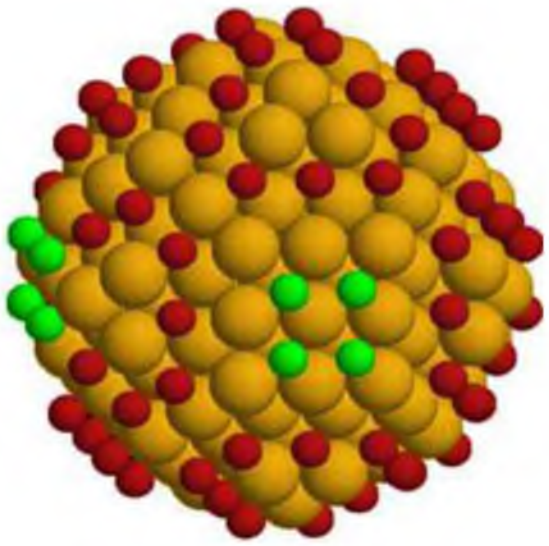

Figure 1.2. Theoretical model of 2 nm TPP-AuNPs. Yellow, red and green correspond to the gold core atoms, phosphorus and chlorine atoms, respectively. (Reprinted with permission from Muñoz-Márquez, M.; Guerrero, E.; Fernández, A.; Crespo, P.; Hernando, A.; Lucena, R.; Conesa, J. *J. Nanopart. Res.* **2010**, *12*, 1307-1318, Figure 2. Copyright 2010 Springer Science+Business Media B.V).

the three processes with the aim of gaining information about the contribution of each step to the emergence of the NPs. This information can be used to manipulate each step and gain control of the synthetic process under all conditions. Study after study has confirmed that even slight modifications in the synthetic conditions alters the mechanism of NP formation and may lead to NPs with different characteristics. For example, in the Hutchison synthesis described earlier, changing the solvents used in the reaction resulted in NPs with different core diameter even though the precursor and the reducing agent were not changed. When a toluene/water mixture was used as the solvent, NPs with a core diameter of 1.5 nm were obtained.[42] Using ethanol as the solvent resulted in NPs with a 0.8 nm core diameter.[49]

LaMer theory has been used to explain the formation of monodisperse colloids.[50] This theory was originally developed to describe the formation of sulfur sols in solution.

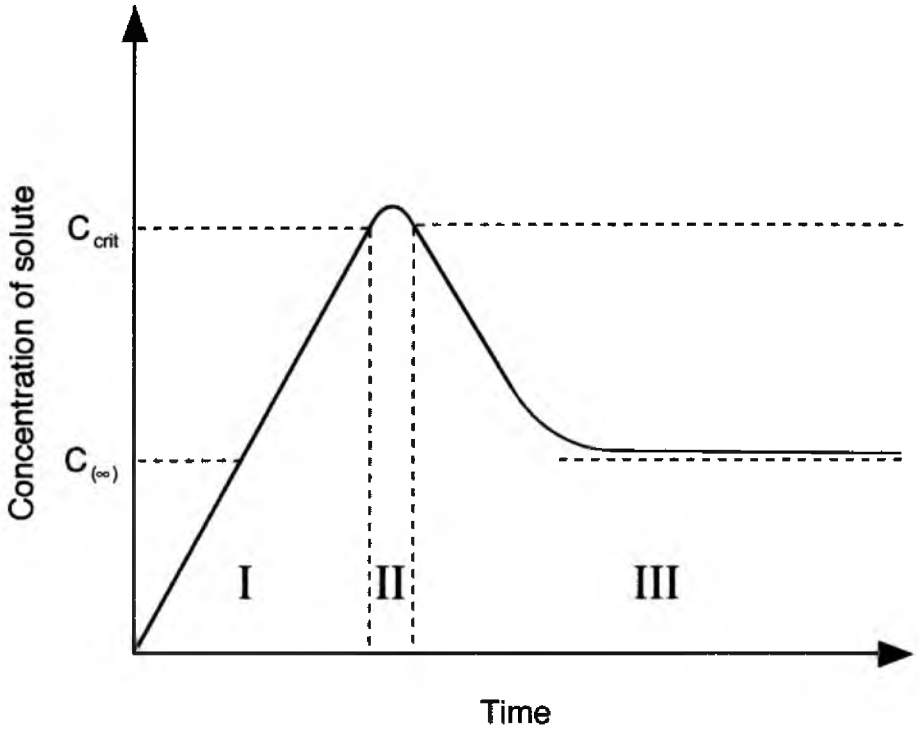

Figure 1.3. Representation of the formation of NPs according to LaMer theory. $C_{(\infty)}$ is the concentration of bulk solute and C_{crit} is the critical concentration for nucleation, respectively. The regions I, II, and III represent prenucleation stage, nucleation stage, and growth stage, respectively. (Reprinted with permission from Sugimoto, T.; Shiba, F.; Sekiguchi, T.; Itoh, H. *Colloids Surf. A* **2000**, *164*, 183-203, Figure 1. Copyright 2000 Elsevier).

Later, it was extended to explain the formation of different colloidal solutions which were mainly monodisperse and spherical.[51] The LaMer theory is based on a nucleation and diffusion model.[52] According to the theory, nucleation occurs in a short burst during which time gold atoms nucleate to form primary particles and this nucleation terminates with the start of the growth stage. Since this step is time limited, control of the size of the NPs occurs during this time. No additional nucleation occurs in the growth stage.[53] In the growth stage, particles grow by the deposition of atoms onto the primary particles through a diffusion driven process.[54] These processes are depicted in Figure 1.3.

Recent studies have shown that most solution phase syntheses which result in monodisperse NPs do not proceed according to the LaMer theory.[55-59] LaMer theory ignores particle-particle interactions and does not account for the aggregation of small nanoparticles.[60] In addition to the small NPs, the theory does not adequately describe the growth mechanisms for NPs whose size is greater than 100 nm.[57] It has been reported in order for small NPs in a colloidal solution to achieve stability, they aggregate on time scales faster than those predicted by the LaMer theory.[61] Theoretical and experimental evidence shows that NP size uniformity can be achieved by this aggregative growth mechanism.[51, 58, 62] For many colloidal systems, X-ray studies have shown that the NPs are not single crystals, providing further proof for aggregative growth.[62] This has led to the development of the aggregative growth mechanism to explain the growth mechanism of most solution phase synthesis. A recent report by Richards et al. indicates that in the early stages of nucleation, the classical LaMer mode of nucleation growth occurs, although it does not predominate.[63] Fits of the data to kinetic models indicated that overall, the aggregative model described the growth of the AgNPs in the study. An investigation of the one phase synthesis of NPs stabilized by different ligands which utilizes an amine-borane reducing agent and Au(I) salt precursor,[46] indicates that the growth mechanism of the NPs follows a combination of growth modes.[64]

It is therefore clear that the growth mechanism of NPs especially during the early stages is complicated. An adequate description of nucleation and growth of NPs requires the use of a variety of experimental techniques. Real time measurement of the processes which occur on the millisecond time scale, like nucleation, is a challenge. Time resolved *in-situ* studies of NPs are therefore needed to fully understand NP formation mechanisms.

X-ray adsorption fine structure (XAFS) is a technique that can be used to monitor the reduction of the salt precursors and also the NP growth process.[65] X-ray absorption near-edge spectroscopy (XANES) also can be used to monitor reduction kinetics and the oxidation state of the metal species.[66] The size, shape and number of formed NPs can be determined by small angle x-ray scattering (SAXS) while both SAXS and wide angle x-ray scattering (WAXS) can provide information about the crystallinity of the formed NPs.[67] This has led to the use of a combination of the methods described above *in-situ* and in real-time to obtain data that describes the NP formation process fully. For example, these methods have been combined with *in-situ* transmission electron microscopy (TEM), scanning electron microscopy (SEM) and UV-vis absorption spectroscopy. [67-69] A limitation of these techniques is that access to synchrotron radiation sources is required. This has hampered widespread use of these techniques to study NP growth mechanisms.

1.6 Nanoparticle characterization methods

One of the commonly used methods for characterizing AuNPs is UV-vis spectroscopy. When the free electrons in the conduction band of the gold nanoparticles are excited in the UV-vis region, they oscillate in the presence of the electromagnetic field of the incoming light in a coherent manner (Figure 1.4).[70, 71] A localized surface plasmon resonance (LSPR) band arises due to the oscillations of the NP conduction electrons. The wavelength at which this band is observed falls between 500-600 nm for gold and is dependent on the particle size, shape and the dielectric medium.[72] By monitoring changes in the absorbance and wavelength of the surface plasmon resonance,

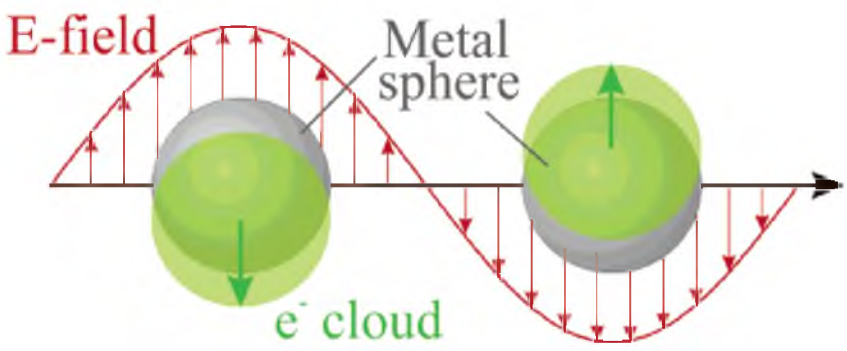

Figure 1.4. Schematic representation of a localized surface plasmon. (Reprinted with permission from Kelly, K. L.; Coronado, E.; Zhao, L. L.; Schatz, G. C. *J. Phys. Chem. B* **2003**, *107*, 668-677, Figure 1. Copyright 2003 American Chemical Society).

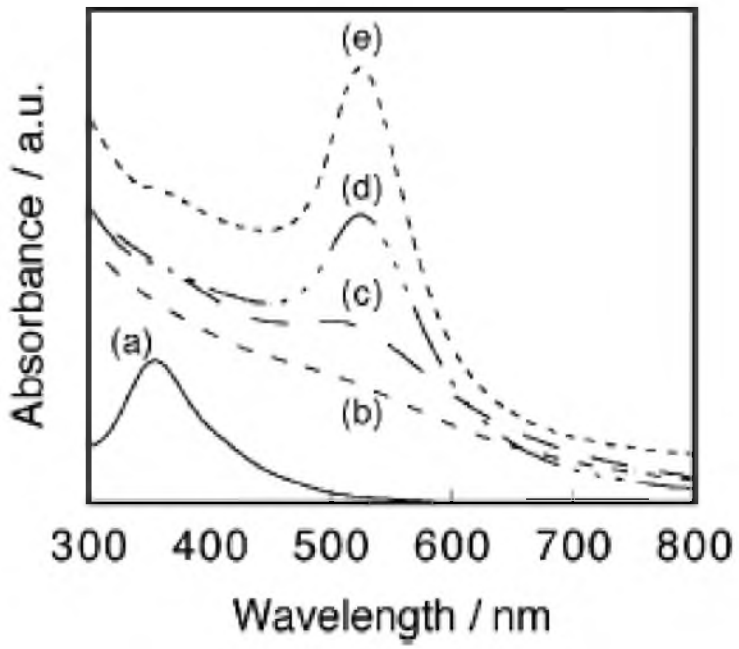

Figure 1.5. Dodecanethiol-protected Au nanoparticles with mean diameters of (a) 1.5 ± 0.2 nm, (b) 3.4 ± 0.3 nm, (c) 5.4 ± 0.7nm, (d) 6.8 ± 0.5 nm and (e) 9.7 ± 0.9 nm. (Reprinted with permission from Shimizu, T.; Teranishi, T.; Hasegawa, S.; Miyake, M. *J. Phys. Chem. B* **2003**, *107*, 2719-2724, Figure 1. Copyright 2003 American Chemical Society).

the size of the nanoparticles can be inferred from the position of the surface plasmon band.[71] For small nanoparticles (< 2 nm), this oscillation is damped due to the low electron density in the conduction band, leading to the no observance of a significant plasmon resonance.[8] Instead a featureless absorption feature is observed.[42] Figure 1.5 shows the LSPR spectra of nanoparticles of different sizes.

In addition to size, the plasmon resonance of nanoparticles is sensitive to changes in shape, and can therefore be used to determine whether the nanoparticles are aggregated or not.[73] A good indicator of aggregation is the broadening and shift of the resonance peak towards longer wavelengths. The LSPR also is sensitive to the nature of the ligands on the surface of the nanoparticle. This is because the ligands can either increase or decrease the electron density in the NPs, leading to a change in the position of the LSPR.[74] The nature of the solvents (dielectric environment) also affects the LSPR.[75] Due to these limitations, the position of the LSPR cannot be used to conclusively determine the size of the NPs. Other methods are used to corroborate the data obtained by UV-vis absorption spectroscopy analysis.

Zeta (ζ) potentials provide information about the net charge of the nanoparticles in solution.[53] The ζ potential determines how the nanoparticles in solution interact. Therefore, ζ potential measurements are commonly used to determine the stability of a nanoparticle suspension. The ζ potential is determined in most systems by applying a potential in a cell with two electrodes containing the nanoparticle solution. The nanoparticles move to the electrode of opposite charge and the electrophoretic mobility of the particles is measured.[76] The data are converted to ζ potential using the Smoluchowski equation.[77] Values of $\pm$ 30 mV are considered to indicate a stable colloidal solution.[78]

Zeta potential depends on pH, temperature and the surface chemistry of the nanoparticle.[79]

Dynamic light scattering (DLS) can be used to obtain the size distribution of the nanoparticles in a sample. It is a simple, rapid and nondestructive method for obtaining the size of nanoparticles dissolved in a variety of solvents.[80] However, DLS does not measure the core size of the nanoparticles directly, instead it measures the hydrodynamic radius of the NPs. DLS depends on the scattered light intensity to determine particle size which biases the method towards the detection of nanoparticles with larger sizes.[81] It is therefore not very useful for small nanoparticles (i.e., less than 2 nm in diameter). Transmission electron microscopy (TEM) is the most widely used method to obtain information about the structure and size distribution of metal clusters.[72] One drawback is that the sample preparation for TEM analysis can introduce artifacts. A major setback in size determination by TEM is the increased core size due to NP ripening on the TEM grid during the course of drying the sample.[60, 67, 69] The exposure of samples to the electron beam is known to cause atom rearrangement and coalescence if samples are exposed for extended times in the beam. In addition, standard TEM has poor resolution for nanoparticles of the sizes produced in the studies discussed in this dissertation (< 2 nm). This is because of the poor contrast between the nanoparticles and the support material which leads to bias towards larger nanoparticles.[82] Distinguishing between clusters that differ only slightly in core size also is challenging due to poor contrast.[83] The result is limited accuracy in the determination of the cluster sizes.

High resolution TEM (HRTEM) is a method used to determine the faceting and crystallinity of AuNPs. HRTEM can be used to achieve a better resolution for small

nanoparticles and therefore obtain more accurate cluster diameters. While HRTEM gives a better view of the nanoparticle lattices, it is difficult to distinguish between clusters that differ by only a few metal atoms in their cores. High-angle annular dark-field scanning transmission microscopy (HAADF-STEM) is a method designed to overcome the limitations of TEM and HRTEM described above.[84] HAADF-STEM also offers better contrast for small nanoparticles because it excludes lower angle Bragg deflections during data collection in favor of high angle incoherently scattered electrons.[84] HAADF-STEM can be used to further characterize the gold clusters in order to undertake a more precise determination of the number of atoms per nanocluster.[83] This information can be used to obtain an accurate molecular formula for the cluster.

X-ray photoelectron spectroscopy (XPS) is a surface chemical analysis method used to obtain information about the chemical composition of the samples.[83] This information is useful in determining the overall molecular formula of the cluster.[47, 85] XPS also can be used to quantitatively determine how much ligand is present on the surface of the NPs. The photoelectron energy peak positions of the atoms indicate whether the ligands being investigated are bound to the nanoparticles. For example, the P($2p_{3/2}$) binding energy position at 131.6 eV for triphenylphosphine on Au indicates non-oxidized phosphorus binding to Au.[86] For oxidized phosphorus, the P($2p_{3/2}$) peak position would shift to higher binding energy to 132.8 eV. It is therefore possible to distinguish between oxidized and non-oxidized species of an atom. High resolution XPS also provides information about the oxidation states of the gold atoms in the nanoparticles.[87] This is usually achieved by background subtraction and deconvolution of the high resolution spectra.

Infrared spectroscopy is used to obtain the vibrational stretching and bending modes of molecules when they interact with infrared radiation. Characteristic fingerprint IR signatures of the molecules can be used for identification of chemical species and to derive conformation data from the IR spectrum.[88-90] Infrared spectroscopy can be done to ascertain the absence or presence of the stabilizing ligands and provide information about the interaction of the ligands and the AuNPs. Attenuated total reflectance-IR spectroscopy (ATR-IR) is a technique that can be used to perform infrared spectroscopy of aqueous samples. This is because it eliminates interference due to the water band in the aqueous nanoparticle samples.[91] In addition, it eliminates path length and concentration issues which are common in transmission IR. In ATR-IR, an infrared beam undergoes total internal reflection when it comes into contact with a crystal with a high refractive index at a specific angle. An evanescent wave is created which then penetrates into the sample deposited on the crystal. Information about absorption from the attenuated wave generates an IR spectrum.

Nuclear magnetic resonance spectroscopy (NMR) can be used to determine the dynamics of molecules in either solid form or in solution.[92] Spectrum resonances of the ligands attached to the nanoparticles can be obtained by ^{1}H and ^{31}P NMR spectroscopy.[93] By observing the shape of the resonances (whether broadened or not) and how they shift (upfield or downfield), information about the nature of the molecules and how they are coordinated to Au can be obtained. In addition, the presence or absence of impurities can be determined. For this dissertation study, ^{1}H and ^{31}P NMR will be useful for structural characterization of PPh_3 binding to AuNPs. Therefore, definitive characterization of nanoparticles requires the use of a variety of methods. *In-situ* methods like SAXS

coupled with *in-situ* UV-vis absorption spectroscopy and TEM would be very useful to overcome the limitations of the individual methods discussed above. This will also help to corroborate data obtained from each of the methods.

1.7 Main goal of the research project

The main goal of the dissertation research is the synthesis, characterization and application of TPP-AuNPs in catalysis. A simple and versatile one-step approach for making TPP-AuNPs that can be extended to a wide variety of ligands and noble metal salts will be developed. The versatility of this method will be demonstrated by performing ligand exchange reactions to produce NPs stabilized with different ω-functionalized alkyl thiols and bipyridyls. *In-situ* functionalization of soft ligand stabilized AuNPs will be performed to prepare bipyridyl stabilized AuNPs which have potential applications in molecular electronics and solar cells.

In order to achieve better control of nanoparticle size and distribution, it is important that the kinetics of the nanoparticle growth are better understood. This is particularly important since multiple thermodynamic and kinetic factors determine the NP growth mechanism. For example the nucleation stage is very sensitive to factors such as reactant concentration, temperature, molar ratios of reactants, presence of surfactants and speed of stirring. Slight variations in these experimental conditions lead to changes in nuclei concentration and nanoparticles of various sizes. A study of the growth kinetics of phosphine stabilized gold nanoparticles has not been undertaken so far. Since the properties of the NPs depend on their size and structure, understanding the growth processes that produce these NPs is essential in order to develop and design NPs for

specific practical applications and to extend this synthetic procedure to other metals and ligands.

The TPP-AuNPs and their derivatives will be characterized using electron microscopy and spectroscopy techniques. Particle sizes will be determined using transmission electron microscopy (TEM), cluster diameters using high resolution transmission electron microscopy (HRTEM), high-angle annular dark-field scanning transmission microscopy (HAADF-STEM), crystal structure using small angle electron diffraction (SAED), elemental composition using X-ray photoelectron spectroscopy (XPS) and cluster purity and composition using thermogravimetric analysis (TGA). Structural characterization and cluster dynamics information of the TPP-AuNPs will be obtained using attenuated total reflectance-IR spectroscopy (ATR-IR), ^{1}H and ^{31}P NMR spectroscopy.

Stability of TPP-AuNPs will be investigated as a function of ionic strength, solvents, pH and temperature. $NaBH_4$ will be used to induce aggregation for this study. Stability data will be collected using UV-vis spectroscopy, zeta potential measurements and microscopy. The catalytic activity of the TPP-AuNPs in water will be determined using two model reactions: the reduction of 4-aminophenol to 4-nitrophenol and the electron transfer reactions involving the reduction of hexacyanoferrate (III) to hexacyanoferrate (II) by $NaBH_4$.

1.8 Outline of the dissertation

Chapter 2 discusses the synthesis of triphenylphosphine stabilized nanoparticles using 9-BBN as the reducing agent. The advantages of using the mild reducing agent are

presented. The benefits of the new synthetic procedure are highlighted. Briefly, in addition to being able to synthesize stable nanoparticles of less than 2 nm in size, control of the synthetic procedure is possible by varying the reaction conditions to produce nanoparticles of different sizes. Characterization of the prepared TPP-AuNPs will be described in detail. The versatility of this synthetic procedure is demonstrated by preparing TOP stabilized AuNPs.

Chapter 3 describes the ligand exchange reactions involving the TPP-AuNPs. We demonstrate that TPP-AuNPs can be used as precursors to make NPs functionalized with ligands bearing different functional groups. The ability to incorporate ligands with different functional groups to the TPP-AuNPs by replacing the TPP ligand extends the utility of the NPs by extending the variety of solvents in which they are soluble, for example. We also explore the feasibility of preparation of bipyridyl stabilized AuNPs from the TPP-AuNPs precursors.

Chapter 4 describes the synthesis of soft ligand stabilized nanoparticles. The synthesis involves the reduction of a phosphine-based gold precursor by the mild reducing agent 9-Borabicyclo[3.3.1]nonane (9-BBN) in the absence of stabilizing agents. AuNPs which are ~4.0 nm stabilized by soft ligands in organic solvents are produced. The soft ligands offer the potential for easy and complete displacement after synthesis by the desired strong binding ligands. Due to the relatively weak affinity of the phosphine ligands, *ex-situ* addition of stronger ligands prevents the growth of the nanoparticles and leads to longer term stabilization of the AuNPs. AuNPs with narrow size dispersion are produced. The utility of this synthesis is demonstrated by simple *in-situ* surface modification of the synthesized AuNPs with 2,2'- and 4,4'-bipyridyl leading to the 2,2'-

and 4,4'-bipyridyl-functionalized AuNPs. The synthesis of the soft ligand nanoparticles is also used to study the kinetics of formations of the NPs and to determine when the *in-situ* addition of ligands yields NPs of uniform size.

Chapter 5 describes the investigation of the stability of TPP-AuNPs in water as a function of salt and sodium borohydride concentration, solvents with different dielectric constants, pH and temperature. UV-vis spectroscopy, zeta potential measurements, high resolution TEM imaging and selected area electron diffraction are used to study the stability of the NPs and determine the changes in structure that they undergo. The roles of TPP ligand and the solvents in imparting stability to the NPs are described. The increased stability was attributed to hydrogen binding as a result of π-π stacking of the phenyl rings of the triphenylphosphine ligands.

Chapter 6 presents the investigation of the catalytic activity of triphenyl-phosphine stabilized gold nanoparticles (TPP-AuNPs) in aqueous solution. The reduction of 4-nitrophenol (4-NP) by sodium borohydride catalyzed by the TPP-AuNPs served as the model reaction for the study. High- resolution transmission electron microscopy (HRTEM) analysis indicated that the NPs were predominantly single crystalline with (111) lattice fringes and selected area electron diffraction (SAED) confirmed the crystalline nature of the NPs. We found that the reduction of 4-NP proceeded after an induction period dependent on the concentration of 4-NP and the amount of catalyst added to the reaction mixture. Investigations using different concentrations of sodium borohydride indicated that an increase in the borohydride concentration did not change the induction time. In order to obtain kinetic data, we performed the catalysis at four different temperatures between 25 and 40 ^{o}C and with different borohydride

concentrations. We determined the rate constants by monitoring the concentration of 4-nitrophenol using UV-vis absorption spectroscopy. The TPP-AuNPs were able to be recycled, even though aggregation of the NPs was observed at the end of the reduction. The rate constants were found to depend on the surface area of the TPP-AuNPs and hence the percentage of surface atoms. This relationship is evidence that the reaction most likely occurs on the surface of the NPs. The activation energy and the entropy of activation for the reaction also were determined. The kinetic data obtained for the unsupported TPP-AuNPs was comparable with that for supported gold catalytic systems, indicating the good catalytic activity of TPP-AuNPs.

Chapter 7 describes the reduction of hexacyanoferrate (III) to hexacyanoferrate (II) by sodium borohydride as a model redox reaction, using water soluble TPP-AuNPs as the catalyst. In the absence of TPP-AuNPs, the reaction takes considerable time to complete. On addition of TPP-AuNPs, there was significant increase in the rate constant observed. A linear relationship between the rate constant and the nanoparticle concentration as well as the surface area of the NPs was observed. This was an indication that the NPs served as catalysts for the reaction. The reaction was first order with respect to hexacyanoferrate (III) and AuNPs concentration. The rate of reduction depended on the borohydride concentration linearly at the borohydride concentrations studied. The rate constants and activation energy of the reaction were determined at the 25-40^{o}C temperature range. The activation energy was 23.6 ± 2.8 kJ/mol for the unsupported catalysts (TPP-AuNPs) used in this study. This work demonstrates that TPP-AuNPs can act as efficient catalysts for electron transfer/redox reactions in an aqueous environment.

In Chapter 8, a summary of the results obtained in the dissertation study is presented with recommendations for future work.

1.9 References

(1) Freestone, I.; Meeks, N.; Sax, M.; Higgitt, C. *Gold Bulletin* **2007**, *40*, 270-277.

(2) Clark, R. J. H., Ed. *The Chemistry of Gold*; Elsevier Scientific: New York, 1978.

(3) Hauser, E. A. *J. Chem. Educ.* **1952**, *29*, 456.

(4) Faraday, M. *Philos. Trans. R. Soc. London* **1857**, *147*, 145.

(5) Edwards, P. P.; Thomas, J. M. *Angew. Chem. Int. Ed.* **2007**, *46*, 5480-5486.

(6) Nath, N.; Chilkoti, A. *Anal. Chem.* **2004**, *76*, 5370-5378.

(7) Muñoz-Márquez, M.; Guerrero, E.; Fernández, A.; Crespo, P.; Hernando, A.; Lucena, R.; Conesa, J. *J. Nanopart. Res.* **2010**, *12*, 1307-1318.

(8) Maye, M. M.; Han, L.; Kariuki, N. N.; Ly, N. K.; Chan, W. B.; Luo, J.; Zhong, C. J. *Anal. Chim. Acta* **2003**, *496*.

(9) Willets, K. A.; Van Duyne, R. P. *Annu. Rev. Phys. Chem.* **2007**, *58*, 267-297.

(10) Feng, Y.; Xing, S.; Xu, J.; Wang, H.; Lim, J. W.; Chen, H. *Dalton Trans.* **2010**, *39*, 349-351.

(11) Tsunoyama, H.; Sakurai, H.; Negishi, Y.; Tsukuda, T. *J. Am. Chem. Soc.* **2005**, *127*, 9374-9375.

(12) Schaaff, T. G.; Knight, G.; Shafigullin, M. N.; Borkman, R. F.; Whetten, R. L. *J. Phys. Chem. B* **1998**, *102*, 10643.

(13) Zhong, C. J.; Maye, M. M. *Adv. Mater.* **2001**, *13*, 1507-1511.

(14) Volokitin, Y.; Sinzig, J.; de Jongh, L. J.; Schmid, G.; Vargaftik, M. N.; Moiseevi, I. I. *Nature* **1996**, *384*, 621-623.

(15) Caragheorgheopol, A.; Chechik, V. *Phys. Chem. Chem. Phys.* **2008**, *10*, 5029-5041.

(16) Guo, R.; Song, Y.; Wang, G.; Murray, R. W. *J. Am. Chem. Soc.* **2005**, *127*, 2752-2757.

(17) Somorjai, G. A.; Park, J. Y. *Angew. Chem. Int. Ed.* **2008**, *47*, 9212-9228.

(18) Narayanan, R.; Tabor, C.; El-Sayed, M. *Top. Catal.* **2008**, *48*, 60-74.

(19) Zhang, P.; Sham, T. K. *Appl. Phys. Lett.* **2002**, *81*, 736-738.

(20) Brust, M.; Walker, M.; Bethell, D.; Schiffrin, D. J.; Whyman, R. *J. Chem. Soc., Chem. Commun.* **1994**, 801-802.

(21) Leff, D. V.; Brandt, L.; Heath, J. R. *Langmuir* **1996**, *12*, 4723-4730.

(22) Boyen, H. G.; Kästle, G.; Weigl, F.; Koslowski, B.; Dietrich, C.; Ziemann, P.; Spatz, J. P.; Riethmüller, S.; Hartmann, C.; Möller, M.; Schmid, G.; Garnier, M. G.; Oelhafen, P. *Science* **2002**, *297*, 1533-1536.

(23) Aikens, C. M.; Schatz, G. C. *J. Phys. Chem. A* **2006**, *110*, 13317-13324.

(24) Hainfeld, J. F. *Science* **1987**, *236*, 450-453.

(25) Brown, L. O.; Hutchison, J. E. *J. Am. Chem. Soc.* **1999**, *121*, 882-883.

(26) Wang, W.; Murray, R. W. *Langmuir* **2005**, *21*, 7015-7022.

(27) Schmid, G. *Chem. Rev.* **1992**, *92*, 1709-1727.

(28) Anker, J. N.; Hall, W. P.; Lyandres, O.; Shah, N. C.; Zhao, J.; Van Duyne, R. P. *Nat Mater* **2008**, *7*, 442-453.

(29) Feldheim, D. L.; Grabar, K. C.; Natan, M. J.; Mallouk, T. E. *J. Am. Chem. Soc.* **1996**, *118*, 7640-7641.

(30) Schön, G.; Simon, U. *Colloid Polym. Sci.* **1995**, *273*, 101-117.

(31) Maier, S. A.; Kik, P. G.; Atwater, H. A.; Meltzer, S.; Harel, E.; Koel, B. E.; Requicha, A. A. G. *Nat Mater* **2003**, *2*, 229-232.

(32) Hainfeld, J. F.; Furuya, F. R. *J. Histochem. Cytochem.* **1992**, *40*, 177-184.

(33) Gupta, S.; Huda, S.; Kilpatrick, P. K.; Velev, O. D. *Anal. Chem.* **2007**, *79*, 3810-3820.

(34) Hainfeld, J. F.; Slatkin, D. N.; Focella, T. M.; Smilowitz, H. M. *Br J Radiol* **2006**, *79*, 248-253.

(35) Shi, W.; Sahoo, Y.; Swihart, M. T.; Prasad, P. N. *Langmuir* **2005**, *21*, 1610-1617.

(36) Hamilton, J. F.; Baetzold, R. C. *Science* **1979**, *205*, 1213-1220.

(37) Huang, X.; Neretina, S.; El-Sayed, M. A. *Adv. Mater.* **2009**, *21*, 4880-4910.

(38) Clarke, L.; Wybourne, M. N.; Brown, L. O.; Hutchison, J. E.; Yan, M.; Cai, S. X.; Keana, J. F. W. *Semicond. Sci. Technol.* **1998**, *13*, A111-A114.

(39) Schmid, G. *Chem. Soc. Rev.* **2008**, *37*.

(40) Turkevich, J.; Stevenson, P. C.; Hillier, J. *Discuss. Faraday Soc.* **1951**, *11*, 55.

(41) Frens, G. *Nature Phys Sci* **1973**, *241*, 20-22.

(42) Weare, W. W.; Reed, S. M.; Warner, M. G.; Hutchison, J. E. *J. Am. Chem. Soc.* **2000**, *122*, 12890-12891.

(43) Schmid, G.; Pfeil, R.; Boese, R.; Bandermann, F.; Meyer, S.; Calis, G. H. M.; van der Velden, J. W. A. *Chem. Ber.* **1981**, *114*, 3634-3642.

(44) Schmid, G. *Inorg. Synth.* **1990**, *27*, 214-218.

(45) Brust, M.; Fink, J.; Bethell, D.; Schiffrin, D. J.; Kiely, C. *J. Chem. Soc., Chem. Commun.* **1995**, 1665-1666.

(46) Zheng, N.; Fan, J.; Stucky, G. D. *J. Am. Chem. Soc.* **2006**, *128*, 6550-6551.

(47) Shem, P. M.; Sardar, R.; Shumaker-Parry, J. S. *Langmuir* **2009**, *25*, 13279-13283.

(48) Sugimoto, T.; Shiba, F.; Sekiguchi, T.; Itoh, H. *Colloids Surf A* **2000**, *164*, 183-203.

(49) Woehrle, G. H.; Hutchison, J. E. *Inorg. Chem.* **2005**, *44*, 6149-6158.

(50) LaMer, V. K.; Dinegar, R. H. *J. Am. Chem. Soc.* **1950**, *72*, 4847-4854.

(51) Privman, V.; Goia, D. V.; Park, J.; Matijevic, E. *J. Colloid Interface Sci.* **1999**, *213*, 36-45.

(52) Sugimoto, T. *Chem. Eng. Technol.* **2003**, *26*, 313-321.

(53) Hunter, R. J. *Foundations of Colloid Science*, 2nd ed.; Oxford University Press Inc.: New York, 2001.

(54) Hiramatsu, H.; Osterloh, F. E. *Chem. Mater.* **2004**, *16*, 2509-2511.

(55) Compton, O. C.; Osterloh, F. E. *J. Am. Chem. Soc.* **2007**, *129*, 7793-7798.

(56) Suber, L.; Sondi, I.; Matijevic, E.; Goia, D. V. *J. Colloid Interface Sci.* **2005**, *288*, 489-495.

(57) Park, J.; Privman, V.; Matijevic, E. *J. Phys. Chem. B* **2001**, *105*, 11630-11635.

(58) van Embden, J.; Sader, J. E.; Davidson, M.; Mulvaney, P. *J. Phys. Chem. C* **2009**, *113*, 16342-16355.

(59) Njoki, P. N.; Luo, J.; Kamundi, M. M.; Lim, S.; Zhong, C.-J. *Langmuir* **2010**, *26*, 13622-13629.

(60) Shields, S. P.; Richards, V. N.; Buhro, W. E. *Chem. Mater.* **2010**, *22*, 3212-3225.

(61) Bogush, G. H.; Zukoski Iv, C. F. *J. Colloid Interface Sci.* **1991**, *142*, 19-34.

(62) Sugimoto, T. *Fine particles : Synthesis, Characterization, and Mechanisms of Growth* Marcel Dekker New York 2000.

(63) Richards, V. N.; Rath, N. P.; Buhro, W. E. *Chem. Mater.* **2010**, *22*, 3556-3567.

(64) Koerner, H.; MacCuspie, R. I.; Park, K.; Vaia, R. A. *Chem. Mater.* **ASAP** DOI: 10.1021/cm202633v.

(65) Nishimura, S.; Takagaki, A.; Maenosono, S.; Ebitani, K. *Langmuir* **2009**, *26*, 4473-4479.

(66) Polte, J. r.; Ahner, T. T.; Delissen, F.; Sokolov, S.; Emmerling, F.; Thünemann, A. F.; Kraehnert, R. *J. Am. Chem. Soc.* **2010**, *132*, 1296-1301.

(67) Abecassis, B.; Testard, F.; Spalla, O.; Barboux, P. *Nano Lett.* **2007**, *7*, 1723-1727.

(68) Polte, J.; Erler, R.; Thünemann, A. F.; Sokolov, S.; Ahner, T. T.; Rademann, K.; Emmerling, F.; Kraehnert, R. *ACS Nano* **2010**, *4*, 1076-1082.

(69) McKenzie, L. C.; Haben, P. M.; Kevan, S. D.; Hutchison, J. E. *J. Phys. Chem. C* **2010**, *114*, 22055-22063.

(70) Schaaff, T. G.; Knight, G.; Shafigullin, M. N.; Borkman, R. F.; Whetten, R. L. *J. Phys. Chem. B* **1998**, *102*, 10643-10646.

(71) Link, S.; El-Sayed, M. A. *J. Phys. Chem. B* **1999**, *103*, 8410-8426.

(72) Schmid, G.; Corain, B. *Eur. J. Inorg. Chem.* **2003**, 3081.

(73) Jain, P. K.; Lee, K. S.; El-Sayed, I. H.; El-Sayed, M. A. *J. Phys. Chem. B* **2006**, *110*, 7238-7248.

(74) Goettmann, F.; Moores, A.; Boissière, C.; Le Floch, P.; Sanchez, C. *Small* **2005**, *1*, 636-639.

(75) Zhang, H.; Wang, D. *Angew. Chem. Int. Ed.* **2008**, *47*, 3984-3987.

(76) Pons, T.; Uyeda, H. T.; Medintz, I. L.; Mattoussi, H. *J. Phys. Chem. B* **2006**, *110*, 20308-20316.

(77) French, R. A.; Jacobson, A. R.; Kim, B.; Isley, S. L.; Penn, R. L.; Baveye, P. C. *Environ. Sci. Technol.* **2009**, *43*, 1354-1359.

(78) Zhang, Z.; Wu, Y. *Langmuir* **2010**, *26*, 9214-9223.

(79) Sapsford, K. E.; Tyner, K. M.; Dair, B. J.; Deschamps, J. R.; Medintz, I. L. *Anal. Chem.* **2011**, *83*, 4453-4488.

(80) Jans, H.; Liu, X.; Austin, L.; Maes, G.; Huo, Q. *Anal. Chem.* **2009**, *81*, 9425-9432.

(81) Pettibone, J. M.; Hudgens, J. W. *ACS Nano* **2011**, *5*, 2989-3002.

(82) Menard, L. D.; Xu, H.; Gao, S.-P.; Twesten, R. D.; Harper, A. S.; Song, Y.; Wang, G.; Douglas, A. D.; Yang, J. C.; Frenkel, A. I.; Murray, R. W.; Nuzzo, R. G. *J. Phys. Chem. B* **2006**, *110*, 14564-14573.

(83) Menard, L. D.; Gao, S.-P.; Xu, H.; Twesten, R. D.; Harper, A. S.; Song, Y.; Wang, G.; Douglas, A. D.; Yang, J. C.; Frenkel, A. I.; Nuzzo, R. G.; Murray, R. W. *J. Phys. Chem. B* **2006**, *110*, 12874-12883.

(84) Yang, J. C.; Bradley, S.; Gibson, J. M. *Microsc. Microanal.* **2000**, *6*, 353-357.

(85) Schaaff, T. G.; Shafigullin, M. N.; Khoury, J. T.; Vezmar, I.; Whetten, R. L.; Cullen, W. G.; First, P. N.; Gutierrez-Wing, C.; Ascensio, J.; Jose-Yacaman, M. J. *J. Phys. Chem. B* **1997**, *101*, 7885-7891.

(86) Uvdal, K.; Persson, I.; Liedberg, B. *Langmuir* **1995**, *11*, 1252-1256.

(87) McNeillie, A.; Brown, D. H.; Smith W, E.; Gibson, M.; Watson, L. *J. Chem. Soc., Dalton Trans.* **1980**, 767 - 770.

(88) Kariis, H.; Westermark, G.; Persson, I.; Liedberg, B. *Langmuir* **1998**, *14*, 2736-2743.

(89) John, G. H.; May, I.; Sarsfield, M. J.; Steele, H. M.; Collison, D.; Helliwell, M.; McKinney, J. D. *Dalton Trans.* **2004**, 734-740.

(90) Zeldin, M.; Mehta, P.; Vernon, W. D. *Inorg. Chem.* **1979**, *18*, 463-466.

(91) Tanaka, T.; Nagao, S.; Ogawa, H. *Anal. Sci.* **2001**, *17(Suppl.)*, i1081−i1083.

(92) Sharma, R.; Holland, G. P.; Solomon, V. C.; Zimmermann, H.; Schiffenhaus, S.; Amin, S. A.; Buttry, D. A.; Yarger, J. L. *J. Phys. Chem. C* **2009**, *113*, 16387-16393.

(93) Petroski, J.; Chou, M. H.; Creutz, C. *Inorg. Chem.* **2004**, *43*, 1597-1599.

CHAPTER 2

ONE-STEP SYNTHESIS OF PHOSPHINE-STABILIZED GOLD NANOPARTICLES USING THE MILD REDUCING AGENT 9-BBN

2.1 Introduction

Phosphine-stabilized gold nanoparticles (AuNPs) comprise an important class of nanomaterials finding broad application in areas such as nanoscale electronics development, catalysis, imaging, sensing, and new therapeutic approaches. For example, phosphine-stabilized AuNPs have served as effective catalysts for asymmetric organic transformations.[1-3] In addition, these nanoparticles have been used as staining agents in biological imaging, immunoassays, and labeling of biological molecules such as proteins.[4-7] In general, organic-ligand-stabilized metal clusters (~2.0 nm) can serve as building blocks for two- or three-dimensional superlattices[8, 9] and in detection of organic and biological molecules.[10, 11] The structural[12-15] and electronic properties[16-18] of these clusters make them candidates for incorporation into nanoscale electronic and photonic

---

Reprinted with permission from Shem, P. M.; Sardar, R.; Shumaker-Parry, J. S. *Langmuir* 2009, *25*, 13279-13283. Copyright 2009, American Chemical Society. The first author designed and conducted all experimental and characterization work reported except as indicated. The author also composed the manuscript corresponding to Chapter 2. Sardar, R. carried out the high resolution TEM imaging (HRTEM) and provided experimental design guidance. Shumaker-Parry, J. S provided experimental design and editorial guidance.

devices.[19-23] Phosphine-stabilized AuNPs may serve as the starting materials for production of nanoparticles functionalized by other ligands, such as thiols, amines, and other phosphines, in order to control material properties. For example, the use of a phosphine ligand as a stabilizer enables easy replacement by thiolated surfactants[24-26] which may extend the solubility of the nanoparticles in aqueous media for nanobiotechnology[10, 11, 27] and aqueous-based catalysis applications.[28] For all of these applications, synthesis of small, uniform, stable nanoparticles is the initial challenge.

In the literature, very few protocols are reported for synthesis of phosphine-stabilized AuNPs with average diameters of <2.0 nm.[6, 29] Schmid reported the synthesis of phosphine-stabilized Au_{55} with narrow size dispersion.[30] The approach produces 1.4 ± 0.4 nm AuNPs when the Ph_3PAuCl complex is reduced by diborane (B_2H_6). Due to the use of diborane, the synthetic protocol requires extra precautions and makes the synthesis complicated. Additionally, the particles produced are inherently unstable in dilute solution and at high temperature and are difficult to isolate in a pure state.[31] A more convenient and safer synthetic method was reported by Hutchison and coworkers in order to generate triphenylphosphine (TPP)-stabilized 1.5 nm AuNPs using a modified version of the Brust two-phase protocol.[32, 33] This synthesis requires a phase transfer reagent which makes the process long and expensive. Additionally, vigorous cleaning steps are required to remove the phase transfer agent, byproduct, and unreacted reducing agent sodium borohydride ($NaBH_4$) in order to use those particles, especially for biological applications. A simple and inexpensive method of synthesizing phosphine-stabilized gold nanoparticles with narrow size dispersion without the use of a phase transfer agent or rigorous purification steps would be an advancement for this class of materials.

Here we report a simple, one-step synthesis of phosphine stabilized AuNPs which produces high purity nanoparticles with narrow size dispersion and enables tuning of particle size. This synthesis is based on the mild reducing agent 9-borabicyclo-[3.3.1]nonane (9-BBN). Recently, it was shown that 9-BBN could be used to synthesize ω-functionalized alkylthiol- and azide terminated disulfide-stabilized AuNPs.[29] The slow reduction by 9-BBN leads to good control over particle size and size dispersion. Here we demonstrate the versatility of the reducing agent 9-BBN to produce phosphine-stabilized AuNPs. We show that, by controlling the reaction conditions, AuNPs with diameters from 1.2 to 2.8 nm may be produced.

2.2 Experimental procedures

2.2.1 Materials

Chloro(triethylphosphine)gold(I) (97%), triphenylphosphine (99%), trioctylphosphine (99.8%), 0.5 M THF solution of 9-Borabicyclo[3.3.1]nonane (9-BBN), 11-mercapto-1-undecanoic acid (MUA), 1-dodecanethiol (DDT) and toluene (HPLC grade) were obtained from Sigma Aldrich. Acetonitrile (HPLC grade) was obtained from Fisher Scientific. Dichloromethane (99.8%) was obtained from Fluka while hexanes were obtained from EMD Chemicals. Deuterated dichloromethane was obtained from Cambridge Isotope Laboratories Inc. All chemicals and solvents were used as received.

2.2.2 UV-visible Spectroscopy

UV-vis absorption spectra were collected at room temperature using a Perkin-Elmer Lambda 19 UV/Vis/NIR spectrophotometer over the 300-800 nm range. All data

were corrected for background absorption using the solvent used to dissolve the respective sample.

2.2.3 Transmission Electron Microscopy

Transmission Electron Microscopy (TEM) micrographs were obtained using a Tecnai-12 instrument operating at 100 KV accelerating voltage. Before the TEM sample preparation, the sample was centrifuged at 4000 r.p.m. for 10 min to remove any large aggregates. From the centrifuged solution, one drop of reaction mixture was deposited on a 150-mesh formvar-coated copper grid, and excess solution was removed by wicking with filter paper to avoid particle aggregation. The grid was then allowed to dry before being imaged. Particle size analysis was conducted by analyzing at least 200 particles in the TEM images using Scion Image Beta 4.02 Software. Higher resolution transmission electron micrographs (HRTEM) were collected using a JOEL 2010F-FAS instrument at 200 KV operating voltage.

2.2.4 X-ray Photoelectron Spectroscopy (XPS)

XPS data were obtained on a Kratos AxisUltraDLD using monochromatic Aluminium K alpha source (1486.6 eV) with a pass energy of 40 eV and a step size of 0.1 eV. The spectrometer was calibrated using Ag $3d_{5/2}$ peak. The binding energy (BE) scale was calibrated using the C1s peak with a BE set at 285.0 eV. The dwell time was 300 ms and the peaks were analyzed relative to the C1s. The samples were prepared as films on a silicon wafer which had been thoroughly cleaned using piranha solution and rinsed copiously with nanopure water and ethanol and dried with nitrogen.

2.2.5 ^{31}P and ^{1}H NMR

^{31}P NMR spectra were obtained using a Varian Inova 500 MHz NMR working at a ^{31}P frequency of 202.2 MHz. The ^{31}P chemical shifts were referenced to 85% H_3PO_4. ^{31}P spectra were obtained for each solution at -55°C with a sweep width of 40,000 Hz and a relaxation delay of 40.4 sec. The acquisition time was 0.409 sec with a 90^0 pulse width of 7.4 μs and 4 transients (TPP) and 1024 transients for TPP-AuNPs . Samples were dissolved in CD_2Cl_2 and placed in a 5 mm NMR tube for analysis. ^{1}H NMR spectra were obtained using a Bruker 400 MHz NMR using CD_2Cl_2 as solvent. The ^{1}H NMR chemical shifts were referenced to the residual proton resonance of the solvent.

2.2.6 Synthesis of triphenylphosphine (TPP) stabilized gold nanoparticles (AuNPs)

In a mixture of acetonitrile and toluene (10:40 ml), 0.017 gm (0.05 mmol) of chloro(triethylphosphine)gold(I) (Et_3PAuCl) was dissolved. 0.0786gms (0.3mmol) of triphenylphosphine (TPP) were added to the mixture at room temperature. The contents were stirred for 30 min after which 0.4 ml of 9-BBN (0.2 mmol) was injected into the mixture. After an additional 30 min of stirring, a solid appeared. The reaction mixture was centrifuged and the solid was collected. The solid then was washed at least twice with hexane to remove any impurities. After drying by nitrogen flow, a black solid was obtained and analyzed by various spectroscopic and microscopic techniques. Using identical molar ratio of reagents, reductions were also carried out at 40 ^{0}C and 50 ^{0}C.

2.2.7 Synthesis of trioctylphosphine (TOP) stabilized gold nanoparticles (AuNPs)

In a mixture of acetonitrile:toluene (10:40 ml), 0.017 gms (0.05mM) of Et_3PAuCl was dissolved. 133.8 µl (0.3mM) TOP was added to the mixture. The contents were stirred at room temperature for 30 min. Ten µl of TOA and 0.8ml of 9-BBN were simultaneously injected into the mixture and the contents stirred. A total of 9 hrs of stirring resulted in a fine dispersion of particles, which was collected through centifugation, washed with hexane and analyzed by spectroscopic and microscopic techniques.

2.3 Results and discussion

2.3.1 Synthesis of TPP-AuNPs

We demonstrate a simple, one-step synthesis of phosphine-stabilized AuNPs using the mild reducing agent 9-BBN (Scheme 2.1). The AuNPs were synthesized when Et_3PAuCl (0.017 gm, 0.05 mmol) was dissolved in 50 mL of a 1:4 volume ratio mixture of acetonitrile:toluene containing TPP (0.0786 gm, 0.3 mmol) and the reaction mixture was stirred for 30 min at room temperature. At this juncture, 0.4 mL of 0.5 M THF solution of 9-BBN (0.2 mmol) was injected with constant stirring for an additional 30 min. At the end of the stirring, a black solid was obtained which was then centrifuged, washed with hexane and dried under N_2.

We obtained 0.007 gm of purified black solid from 0.017 gm of Et_3PAuCl. The final solid product could be redispersed either in dichloromethane (DCM) or acetonitrile for spectroscopic and microscopic analysis.

Scheme 2.1 Synthetic pathway for TPP-stabilized AuNPs.

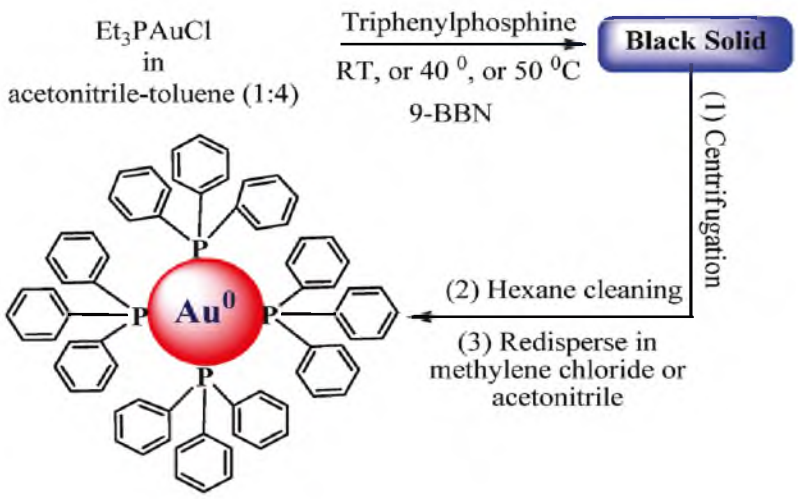

2.3.2 Characterization of TPP-AuNPs

The UV-visible spectrum of the redispersed particles displays an absorption maximum (λ_{max}) at ~505 nm (Figure 2.1A). The shape of the spectrum is similar to that observed by Whetten and co-workers for the absorption spectra of AuNPs in the size range of 2-3 nm.[16] The synthesized particles also were analyzed by transmission electron microscopy (TEM) to determine the size and size dispersion (Figure 2.1B). The particles are narrowly dispersed with an average size of 1.7 ± 0.4 nm**.** The size of the particles from TEM analysis indicates that the absorption behavior measured by UV-visible spectroscopy must be dominated by the larger AuNPs. TEM and HRTEM analysis of AuNPs synthesized at room temperature shows the particles are well dispersed on the TEM grid (Figure 2.1B and 2.1C). This result suggests that the particles are stabilized by TPP which keeps the particles dispersed and prevents them from aggregating during the synthesis.

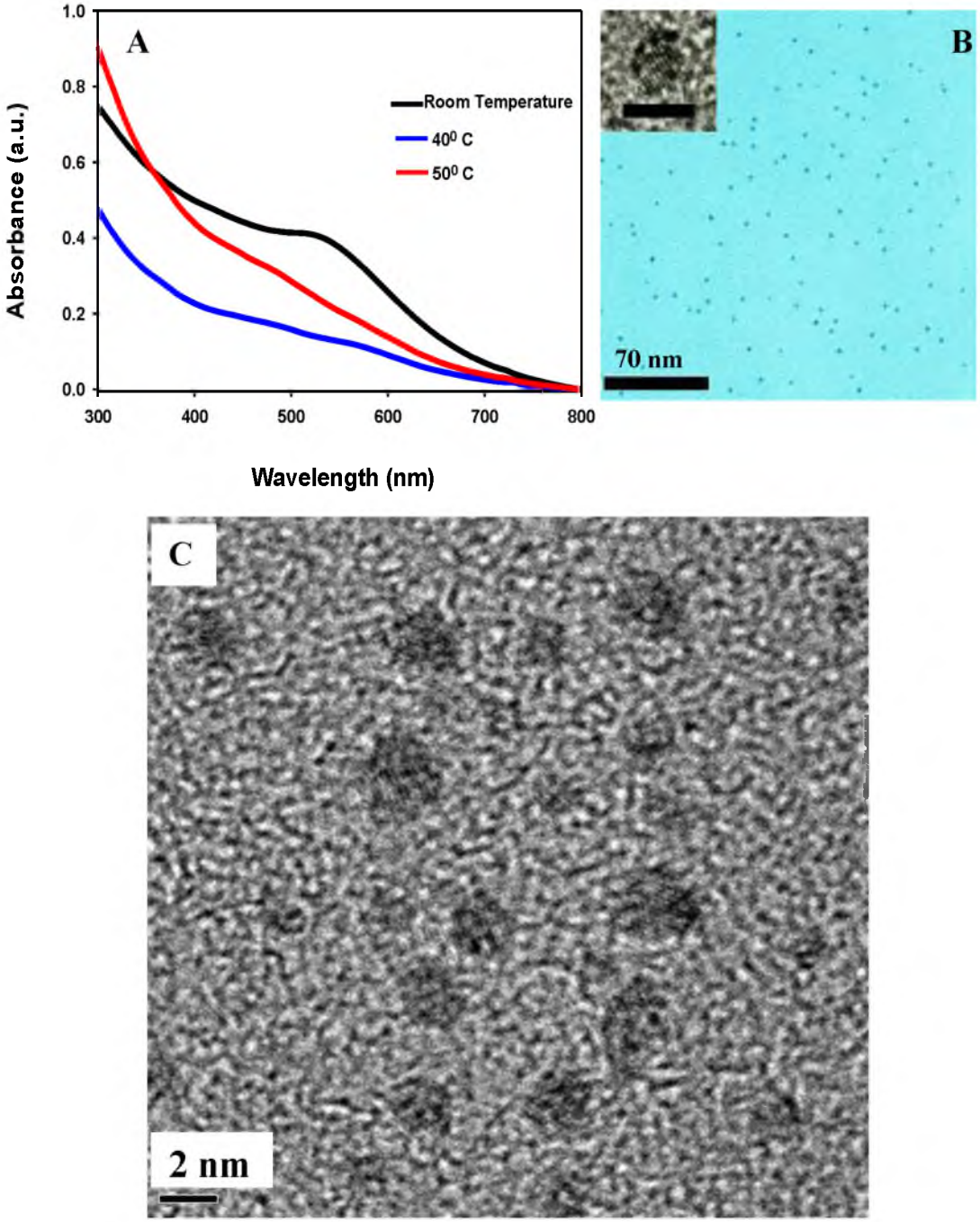

Figure 2.1. TPP-AuNPs prepared using the 9-BBN method. (A) UV-visible absorption spectra of TPP-AuNPs synthesized at room temperature, 40 ^{0}C and 50 ^{0}C. (B) TEM image of TPP-stabilized AuNPs synthesized at room temperature. Inset is a high resolution TEM (HRTEM) image of a single NP with a 2 nm scale bar. (C) HRTEM image of the TPP-stabilized AuNPs synthesized at room temperature.

To determine the elemental composition, the electronic state of the elements, and the purity, the AuNPs were analyzed by X-ray photoelectron spectroscopy (XPS). The XPS spectrum (Figure 2.2) shows all of the Au peaks including the Au 4f peak. The peak position of the Au 4f doublet ($4f_{5/2}$, 87.8 eV and $4f_{7/2}$, 84.1 eV), the peak-to-peak distance (3.7 eV) and the absence of a shoulder due to unreacted Au ions (Au^{+}) that would appear at 84.9 eV clearly verifies that all of the Au is present in the Au^{0} oxidation state (Figure 2.3).[34] A peak at 131.6 eV is observed which is due to coordinated P(2p) from the TPP molecules.[35] In addition, the carbon 1s at 285.1 eV also is observed. The XPS results show the TPP-stabilized AuNPs sample is 98% pure (including Au, C, P, and Cl). In addition, 1.7% oxygen also was detected. The XPS analysis yielded 86 mass percent of Au. The purity of the sample is higher than what previously has been reported for TPP-stabilized AuNPs.[32] The average molecular formula for the clusters was determined to be $Au_{146}(PPh_3)_{15}Cl_7$ by estimating that there are ~146 atoms in a particle of average size of 1.7 nm.[17] The average molecular formula was determined using the elemental ratios of Au:P:Cl (20:2:1) obtained by XPS.[16]

NMR spectroscopy is a useful tool for obtaining information about the coordination chemistry of ligand-stabilized metal nanoparticles, particularly AuNPs.[36-38] The synthesized particles were further analyzed by ^{31}P NMR to confirm and support the XPS and TEM results that the AuNPs are stabilized by TPP molecules adsorbed on surface. The NMR spectrum for pure TPP exhibited a peak at -5.4 ppm at room temperature. In comparison, the ^{31}P NMR peak of TPP coordinated to the AuNPs is expected to be shifted downward.

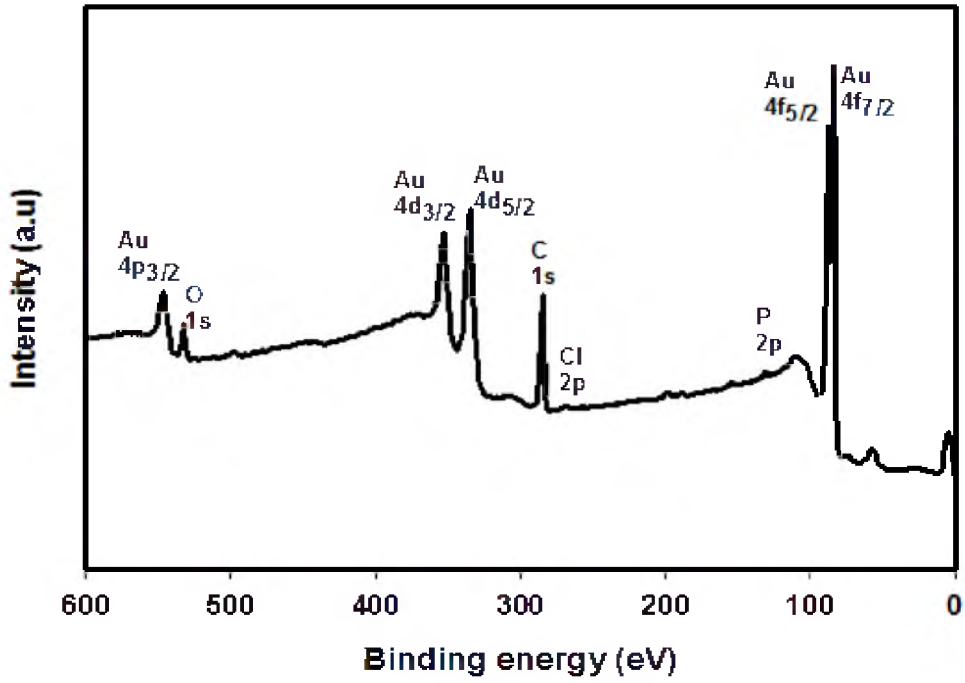

Figure 2.2. XPS spectrum of TPP-stabilized AuNPs synthesized at room temperature.

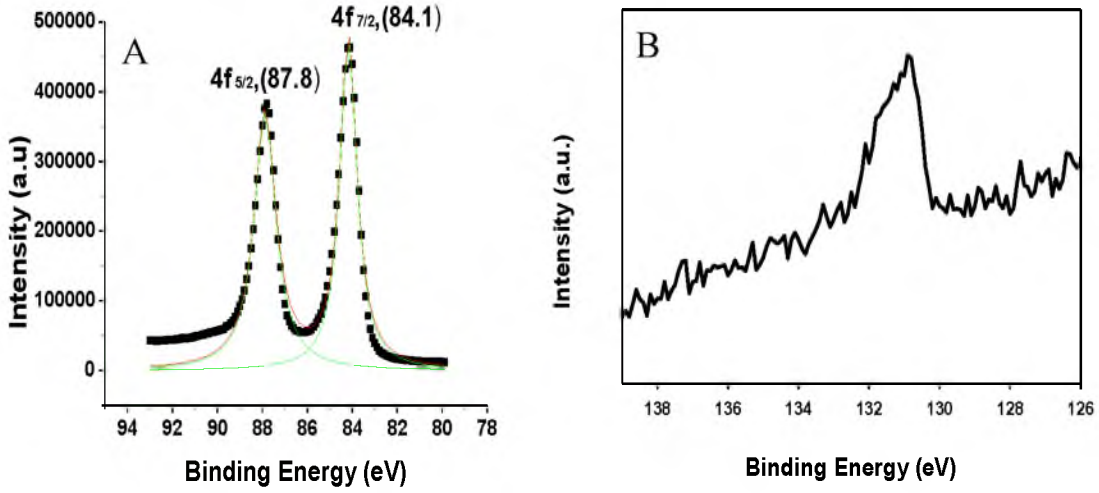

Figure 2.3. (A) XPS Au 4f photoelectron peak fit using a Lorentzian line shape. (B) P 2p high resolution XPS spectrum.

The synthesized TPP-AuNPs in CD_2Cl_2 did not exhibit a ^{31}P NMR signal at room temperature or -5°C. A similar phenomenon also has been observed previously for gold clusters in the < 2.0 nm size regime.[26] After lowering the temperature to -55°C, a peak was observed at 63.0 ppm attributed to TPP coordinated to the AuNPs (Figure 2.4). Previously, Creutz and co-workers described the chemical shift of phosphine stabilized AuNPs with varying numbers of gold atoms.[26] As the number of gold core atoms increases, it is expected that a downward shift of the ^{31}P resonance of the AuNPs will be observed. Creutz and co-workers observed a chemical shift of 42.7 ppm for the Au_{101} cluster. In comparison, the Au_{146} cluster exhibited a chemical shift of 63.0 ppm. The single narrow peak at 63.0 ppm for TPP-AuNPs implies those phosphorous atoms are in a magnetically equivalent environment.[36, 37] The additional peaks in the region of 50-60 ppm could be due to the presence of triphenylphosphine oxide which may form as a result of the oxidation of TPP during the sample preparation.[39] The nanoparticles also were analyzed by ^1H NMR spectroscopy in order to determine the chemical composition. In the ^1H NMR spectrum (Figure 2.5), broad peaks observed in the 7.2-7.4 ppm region are assigned to the protons from the phenyl rings of TPP adsorbed the surface of the AuNPs. The absence of Et_3P methylene and terminal methyl protons resonances at ~1.0 and 3.5 ppm, respectively, indicates that Et_3P is absent from the sample (Figure 2.5). This confirms that the AuNPs are not stabilized by mixed ligands (TPP and Et_3P). The ^1H NMR spectrum also shows small peaks at 7.1 and 7.6 ppm, which could be due to traces of triphenylphosphine oxide. This result correlates with the ^{31}P NMR where additional peaks were observed in the 50-60 ppm region.

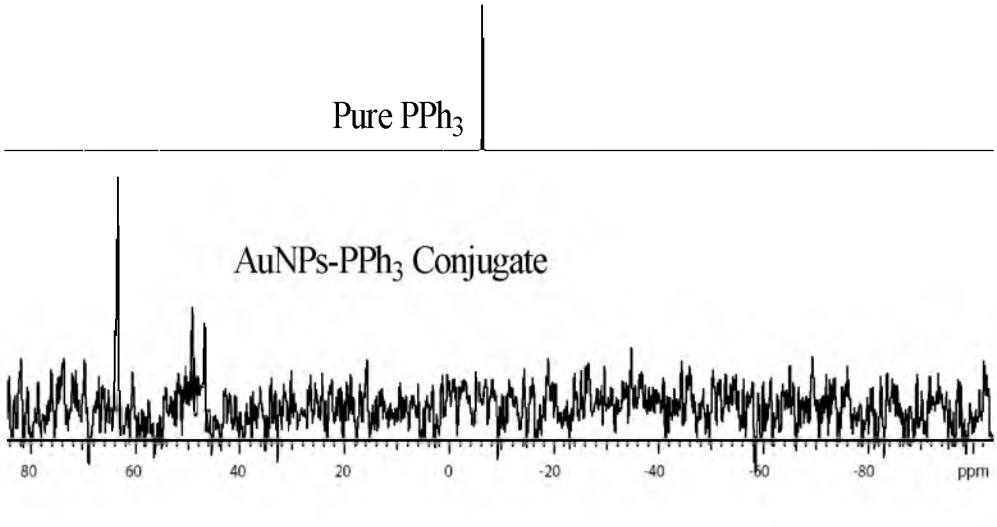

Figure 2.4. ^{31}P NMR spectra for pure TPP (upper panel) and TPP-AuNP conjugates (lower panel). The ^{31}P NMR spectra of pure TPP and TPP-AuNP conjugates were acquired at room temperature and -55^0 C, respectively, in CD_2Cl_2.

Control of nanoparticle size is important for many applications, especially in catalysis where the catalytic efficiency is significantly enhanced due to an increase in the surface-to-volume ratio for small nanoparticles.[40, 41] Generally, the borohydride based reduction method produces particles with diameters of < 2.0 nm, although the average size is difficult to control. The method also requires a large amount of thiols in the reaction medium and several solvent fractionations are essential to remove larger particles. Our simple, 9-BBN based synthesis could avoid these issues. In order to demonstrate the versatility of the synthesis, we explored the impact of temperature on the nanoparticle size and size dispersion of phosphine-stabilized AuNPs by varying the temperature at which the reduction reaction took place. The molar ratios of the reagents were similar to the ones used for room temperature synthesis. After the reduction and purification steps, a black solid was obtained which was redispersed in DCM for analysis.

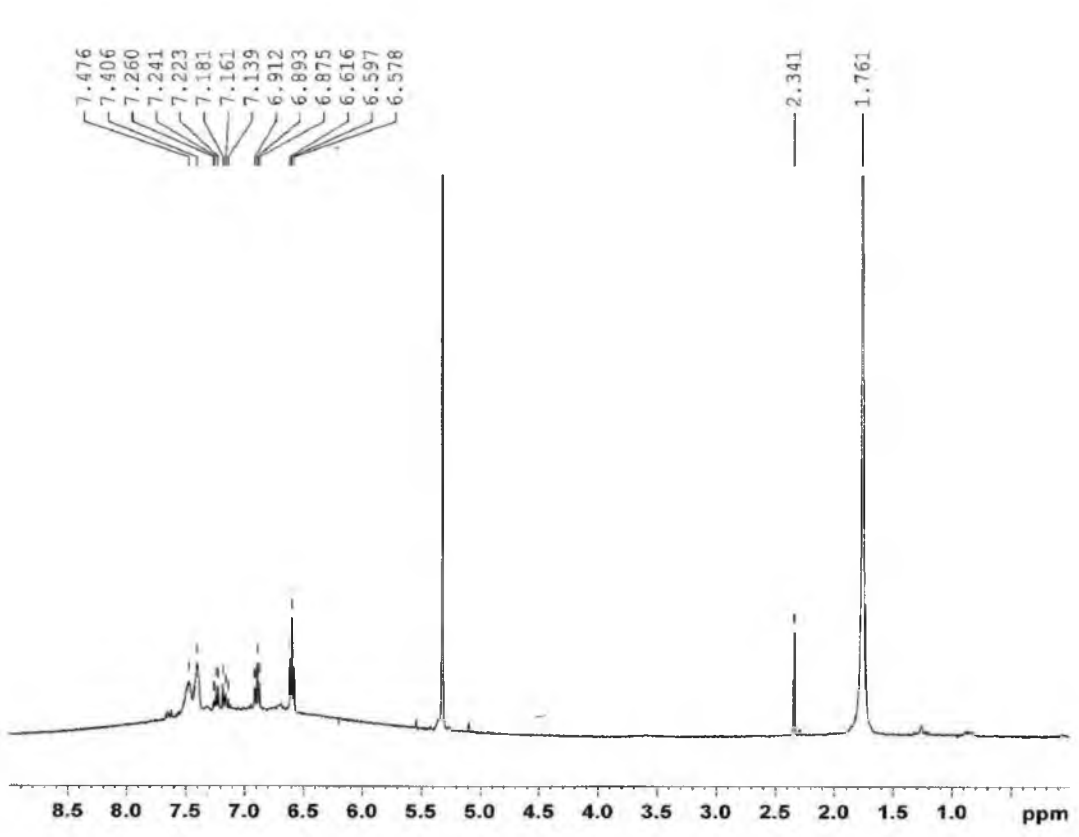

Figure 2.5. ^{1}H NMR spectrum of TPP stabilized AuNPs. The spectra were recorded using CD_2Cl_2 as solvent.

The TPP-stabilized AuNPs synthesized at 40^0 C and 50^0 C were analyzed by UV-visible absorption spectroscopy. The absorption spectra shown in Figure 1.1A may be compared to the spectrum for the particles synthesized at room temperature, where a λ_{max} centered at ~505 nm is observed. In contrast, the UV-visible spectra of AuNPs synthesized at 40^0 C and 50^0 C are featureless which indicate that the particles were < ~1.5 nm and smaller than the particles synthesized at room temperature.[42, 43] Representative TEM images of the AuNPs verify that particle sizes were smaller when higher temperatures were used (Figure 2.6). The particles are of narrow size dispersion

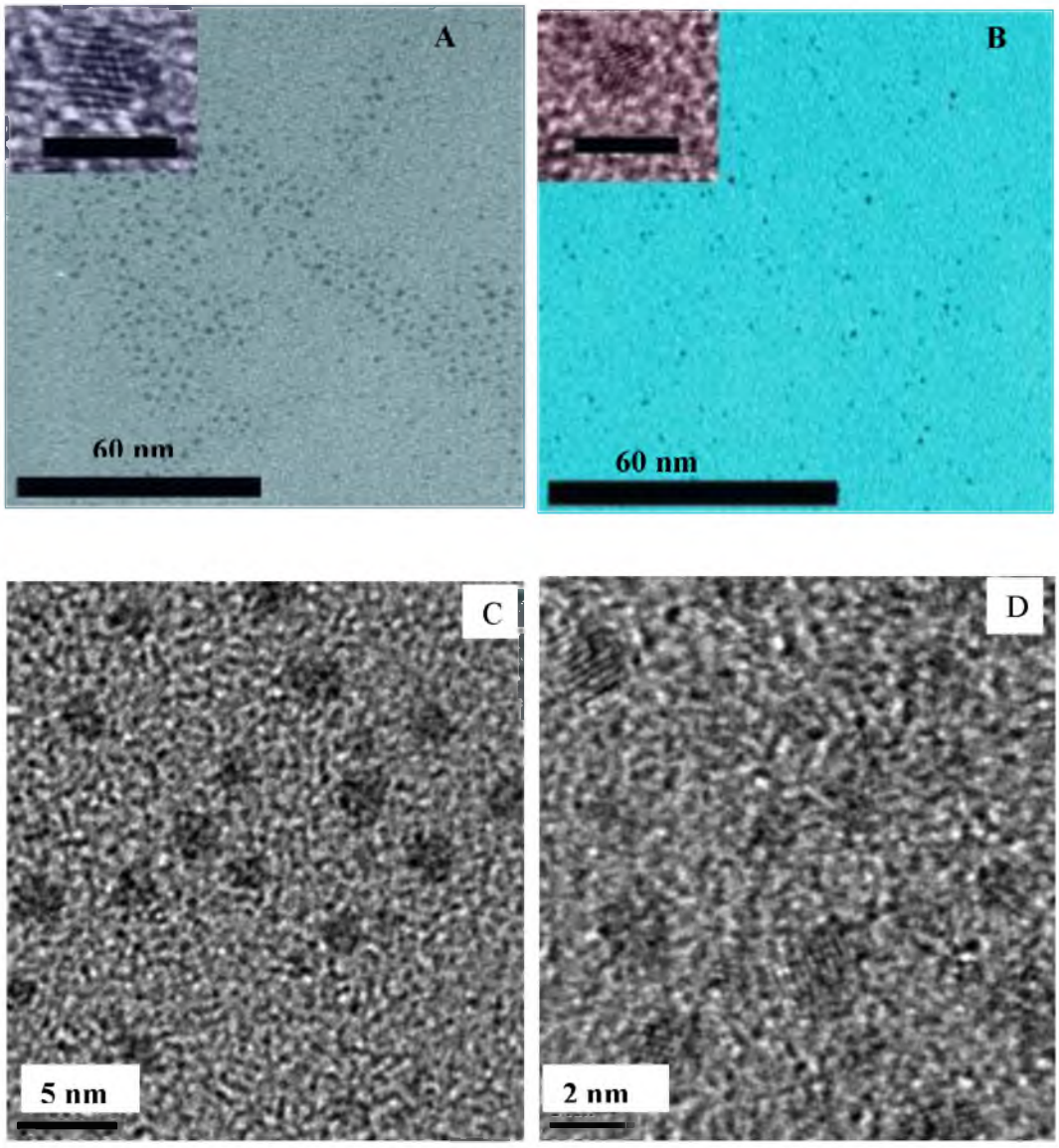

Figure 2.6. TEM images of TPP stabilized AuNPs synthesized at (A) 40^0C and (B) 50^0C. Insets show HRTEM images of single NPs with 2 nm scale bars. (C) HRTEM images of the TPP-AuNPs synthesized at 40^0C and (D) 50^0C.

with sizes of 1.4 ± 0.2 nm and 1.2 ± 0.2 nm for particles synthesized at 40^0 C and 50^0 C, respectively. A comparison of UV-visible absorption maxima and particle size analysis of AuNPs synthesized at the three different temperatures indicates that with an increase of solution temperature, the core size of the resulting particles decreases. Table 2.1 summarizes the results.

2.3.3 Versatility of the 9-BBN synthetic method

The versatility of the 9-BBN based synthetic method is further demonstrated by preparing AuNPs in the presence of trioctylphosphine (TOP) ligand. The synthesis was carried out at room temperature. The UV-visible absorption spectroscopy analysis of the particles in an acetonitrile:toluene solution exhibits a distinct and clearly observable LSPR extinction peak (λ_{max}) centered at 505 nm, (Figure 2.7A). This LSPR peak is indicative of particles larger than 2 nm in size which correlates with the TEM analysis.[42, 43] The size of the TOP-stabilized AuNPs is 2.8 ± 0.7 nm as determined by TEM analysis (Figure 2.7B).

2.3.4 Mechanism of TPP-AuNP formation

It is very important to control the size and shape of nanoparticles during synthesis because these two properties play a big role in how the nanoparticles will be used for various applications. In order to gain control of the synthetic process, it is necessary to understand the mechanism of the reduction process which leads to the nanoparticles.

Table 2.1. Comparison of UV-visible absorption maxima and particle sizes of TPP stabilized AuNPs synthesized at different temperatures.

Temperature (^{0}C)[a]	UV-visible absorption maxima (nm)	particle size (nm)[b]
25	~500	1.5 (0.4)
40	featureless	1.4 (0.2)
50	featureless	1.2 (0.2)

[a] 25 ^{0}C represents room temperature. [b] The number in the parenthesis represents standard deviation. At least 200 particles were counted to determine the particle size.

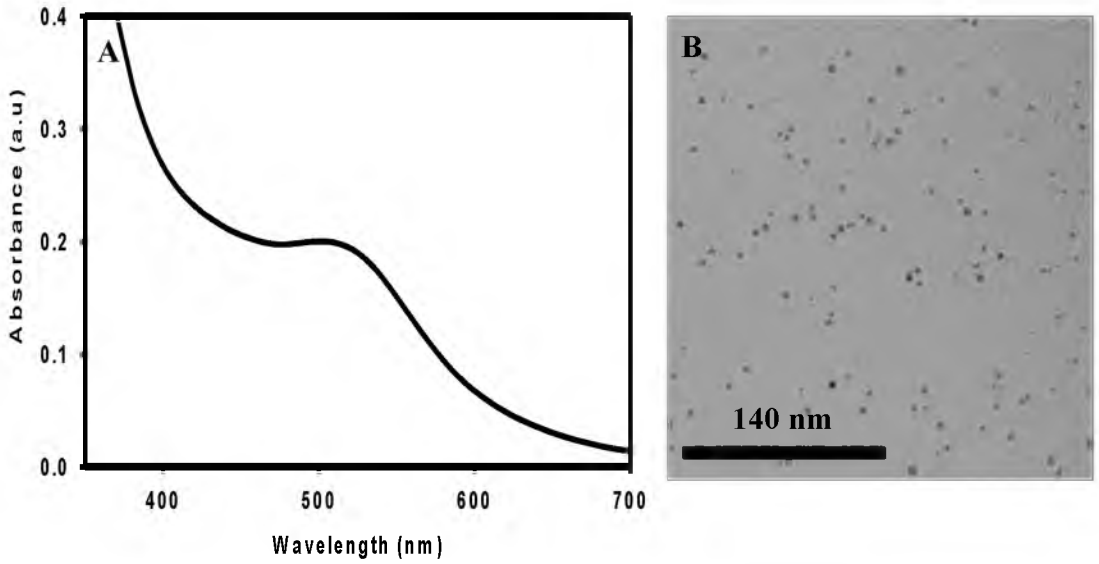

Figure 2.7. (A) UV-visible absorption spectrum and (B) TEM image of TOP-stabilized AuNPs.

Most methods for making triphenylphosphine stabilized gold nanoparticles require a hydride-based reducing agent to reduce the precursor gold salt.[44-46] The hydride provides this electron. Several sources of hydrides have been used as reducing agents including sodium borohydride and 9-BBN. [29, 32, 47] Weare et al. [32] used $NaBH_4$ to reduce the hydrogen tetrachloroaurate salt ($HAuCl_4$) using a modification of the Brust method.[33] Sodium borohydride provides the hydrides needed to reduce the Au(III) to Au(0). The application of 9-BBN to reduce chloro(triethylphosphine) gold(I) salt (Et_3PAuCl) is another method that also uses hydrides to reduce Au(I) to Au(0).[48] A gain of one electron is required to initiate Au cluster formation from the Au salt precursors.[46] The triphenylphosphine ligand attaches to the Au atoms and stabilizes the Au clusters formed.[44] We propose that Et_3PAuCl is reduced by 9-BBN to form the Au_{146} cluster following scheme 2.2.

The LaMer mechanism has been used to describe the growth and formation of near monodisperse nanoparticles in solution.[49] The basis of the LaMer mechanism is that nucleation occurs in a very short period and terminates with the start of the growth stage. Since the nucleation occurs in a short burst and is therefore time limited, control of the size of the NPs occurs during this time. No additional nucleation occurs in the growth stage.[50] Recent studies have shown that the nucleation process is very fast and does not conform to the LaMer mechanism.[51-54] An aggregative nucleation and growth mechanism describes the formation of these small NPs.[54-57] This mechanism explains the nucleation of the small primary NPs in a supersaturated solution followed by aggregation which leads to the formation of larger uniform NPs. Due to the fast formation kinetics, the process cannot be adequately monitored using *ex-situ* microscopy and UV-vis spectroscopy. The nucleation phase is expected to occur in a millisecond timescale. Thus a fast method for monitoring the formation of the nanoparticles, for example *in-situ* small angle X-ray scattering (SAXS) is needed. McKenzie et al. have developed a microscale flow system in which simultaneous *in-situ* SAXS and UV-vis spectroscopy can be done to determine the growth kinetics of the AuNPs in the 0.8-5 nm size range in real time.[58] Synchrotron based methods are suited for this kind of analysis, however, they are not easily accessible.

Scheme 2.2. Reaction pathway for the formation of TPP-AuNPs using the 9-BBN reduction method

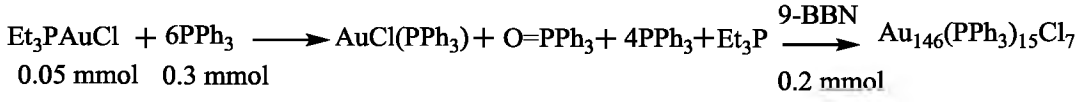

Future work to probe the formation mechanisms should include SAXS analysis. Related studies by McKenzie et al.[58] on systems similar to ours lead us to conclude that a similar mechanism is operative in our system.

2.4 Conclusion

In conclusion, we have presented a new simple and versatile method for synthesizing phosphine-stabilized AuNPs with diameters 1.2-2.8 nm and low size dispersion. The size of these phosphine-stabilized AuNPs can be modulated by controlling the temperature during synthesis. The TPP-AuNPs conjugates display size dependent optical properties. The versatility of this synthetic procedure was demonstrated by preparing TOP-capped AuNPs. The TPP-stabilized nanoparticles can be useful as precursors for preparation of AuNPs functionalized with other ligands through place exchange. The synthetic protocol could be useful in preparation of optically active phosphinate stabilized gold or other noble metal nanoparticles.

2.5 References

(1) Tamura, M.; Fujihara, H. *J. Am. Chem. Soc.* **2003**, *125*, 15742-15743.

(2) Ramírez, J.; Sanaú, M.; Fernández, E. *Angew. Chem. Int. Ed.* **2008**, *47*, 5194-5197.

(3) Fürstner, A.; Morency, L. *Angew. Chem. Int. Ed.* **2008**, *47*, 5030-5033.

(4) Hainfeld, J. F.; Furuya, F. R. *J. Histochem. Cytochem.* **1992**, *40*, 177-184.

(5) Jahn, W. *J. Struct. Biol.* **1999**, *127*, 106-112.

(6) Reardon, J. E.; Frey, P. A. *Biochem.* **1984**, *23*, 3849-3856.

(7) Ackerson, C. J.; Jadzinsky, P. D.; Jensen, G. J.; Kornberg, R. D. *J. Am. Chem. Soc.* **2006**, *128*, 2635-2640.

(8) Kiely, C. J.; Fink, J.; Brust, M.; Bethell, D.; Schiffrin, D. J. *Nature* **1998**, *396*, 444-446.

(9) Schmid, G.; Simon, U. *Chem. Commun.* **2005**, 697-710.

(10) Daniel, M. C.; Astruc, D. *Chem. Rev.* **2004**, *104*, 293-346.

(11) Phillips, R. L.; Miranda, O. R.; You, C.-C.; Rotello, V. M.; Bunz, U. H. F. *Angew. Chem. Int. Ed.* **2008**, *47*, 2590-2594.

(12) Jadzinsky, P. D.; Calero, G.; Ackerson, C. J.; Bushnell, D. A.; Kornberg, R. D. *Science* **2007**, *318*, 430-433.

(13) Heaven, M. W.; Dass, A.; White, P. S.; Holt, K. M.; Murray, R. W. *J. Am. Chem. Soc.* **2008**, *130*, 3754-3755.

(14) Gruene, P.; Rayner, D. M.; Redlich, B.; van der Meer, A. F. G.; Lyon, J. T.; Meijer, G.; Fielicke, A. *Science* **2008**, *321*, 674-676.

(15) Zhu, M.; Aikens, C. M.; Hollander, F. J.; Schatz, G. C.; Jin, R. *J. Am. Chem. Soc.* **2008**, *130*, 5883-5885.

(16) Alvarez, M. M.; Khoury, J. T.; Schaaff, T. G.; Shafigullin, M. N.; Vezmar, I.; Whetten, R. L. *J. Phys. Chem. B* **1997**, *101*, 3706-3712.

(17) Schaaff, T. G.; Shafigullin, M. N.; Khoury, J. T.; Vezmar, I.; Whetten, R. L.; Cullen, W. G.; First, P. N.; Gutierrez-Wing, C.; Ascensio, J.; Jose-Yacaman, M. J. *J. Phys. Chem. B* **1997**, *101*, 7885-7891.

(18) Li, X.-B.; Wang, H.-Y.; Yang, X.-D.; Zhu, Z.-H.; Tang, Y.-J. *J. Chem. Phys.* **2007**, *126*, 084505.

(19) Chen, S.; Ingram, R. S.; Hostetler, M. J.; Pietron, J. J.; Murray, R. W.; Schaaff, T. G.; Khoury, J. T.; Alvarez, M. M.; Whetten, R. L. *Science* **1998**, *280*, 2098-2101.

(20) Boyer, D.; Tamarat, P.; Maali, A.; Lounis, B.; Orrit, M. *Science* **2002**, *297*, 1160-1163.

(21) Feldheim, D. L.; Grabar, K. C.; Natan, M. J.; Mallouk, T. E. *J. Am. Chem. Soc.* **1996**, *118*, 7640-7641.

(22) Thomas, K. G.; Kamat, P. V. *Acc. Chem. Res.* **2003**, *36*, 888-898.

(23) Kamat, P. V.; Barazzouk, S.; Hotchandani, S. *Angew. Chem. Int. Ed.* **2002**, *41*, 2764-2767.

(24) Woehrle, G. H.; Warner, M. G.; Hutchison, J. E. *J. Phys. Chem. B* **2002**, *106*, 9979-9981.

(25) Woehrle, G. H.; Brown, L. O.; Hutchison, J. E. *J. Am. Chem. Soc.* **2005**, *127*, 2172-2183.

(26) Petroski, J.; Chou, M. H.; Creutz, C. *Inorg. Chem.* **2004**, *43*, 1597-1599.

(27) He, L.; Musick, M. D.; Nicewarner, S. R.; Salinas, F. G.; Benkovic, S. J.; Natan, M. J.; Keating, C. D. *J. Am. Chem. Soc.* **2000**, *122*, 9071-9077.

(28) Han, J.; Liu, Y.; Guo, R. *J. Am. Chem. Soc.* **2009**, *131*, 2060-2061.

(29) Sardar, R.; Shumaker-Parry, J. S. *Chem. Mater.* **2009**, *21*, 1167-1169.

(30) Schmid, G. *Inorg. Synth.* **1990**, *27*, 214-218.

(31) Schmid, G.; Hess, H. *Z. Anorg. Allg. Chem.* **1995**, *621*, 1147-1152.

(32) Weare, W. W.; Reed, S. M.; Warner, M. G.; Hutchison, J. E. *J. Am. Chem. Soc.* **2000**, *122*, 12890-12891.

(33) Brust, M.; Walker, M.; Bethell, D.; Schiffrin, D. J.; Whyman, R. *J. Chem. Soc., Chem. Commun.* **1994**, 801-802.

(34) Leff, D. V.; Brandt, L.; Heath, J. R. *Langmuir* **1996**, *12*, 4723-4730.

(35) Zorn, G.; Gotman, I.; Gutmanas, E. Y.; Adadi, R.; Salitra, G.; Sukenik, C. N. *Chem. Mater.* **2005**, *17*, 4218-4226.

(36) Son, S. U.; Jang, Y.; Yoon, K. Y.; Kang, E.; Hyeon, T. *Nano Lett.* **2004**, *4*, 1147-1151.

(37) Kim, S.-W.; Kim, S.; Tracy, J. B.; Jasanoff, A.; Bawendi, M. G. *J. Am. Chem. Soc.* **2005**, *127*, 4556-4557.

(38) Parker, J. F.; Choi, J.-P.; Wang, W.; Murray, R. W. *J. Phys. Chem. C* **2008**, *112*, 13976-13981.

(39) Robinson, P. L.; Barry, C. N.; Kelly, J. W.; Evans, S. A. *J. Am. Chem. Soc.* **1985**, *107*, 5210-5219.

(40) Wilson, O. M.; Knecht, M. R.; Garcia-Martinez, J. C.; Crooks, R. M. *J. Am. Chem. Soc.* **2006**, *128*, 4510-4511.

(41) Zhong, C. J.; Maye, M. M. *Adv. Mater.* **2001**, *13*, 1507-1511.

(42) Wolfe, R. L.; Balasubramanian, R.; Tracy, J. B.; Murray, R. W. *Langmuir* **2006**, *23*, 2247-2254.

(43) Balasubramanian, R.; Guo, R.; Mills, A. J.; Murray, R. W. *J. Am. Chem. Soc.* **2005**, *127*, 8126-8132.

(44) Pettibone, J. M.; Hudgens, J. W. *ACS Nano* **2011**, *5*, 2989-3002.

(45) Muñoz-Márquez, M.; Guerrero, E.; Fernández, A.; Crespo, P.; Hernando, A.; Lucena, R.; Conesa, J. *J. Nanopart. Res.* **2010**, *12*, 1307-1318.

(46) Barngrover, B. M.; Aikens, C. M. *J. Phys. Chem. Lett.* **2011**, *2*, 990-994.

(47) Shem, P. M.; Sardar, R.; Shumaker-Parry, J. S. *Langmuir* **2009**, *25*, 13279-13283.

(48) Sardar, R.; Shumaker-Parry, J. S. *J. Am. Chem. Soc.* **2011**, *133*, 8179-8190.

(49) LaMer, V. K.; Dinegar, R. H. *J. Am. Chem. Soc.* **1950**, *72*, 4847-4854.

(50) Hunter, R. J. *Foundations of Colloid Science*, 2nd ed.; Oxford University Press Inc.: New York, 2001.

(51) Besson, C.; Finney, E. E.; Finke, R. G. *J. Am. Chem. Soc.* **2005**, *127*, 8179-8184.

(52) Drews, T. O.; Katsoulakis, M. A.; Tsapatsis, M. *J. Phys. Chem. B* **2005**, *109*, 23879-23887.

(53) Finney, E. E.; Finke, R. G. *Chem. Mater.* **2008**, *20*, 1956-1970.

(54) Matijevic, E. *Chem. Mater.* **1993**, *5*, 412-426.

(55) Shields, S. P.; Richards, V. N.; Buhro, W. E. *Chem. Mater.* **2010**, *22*, 3212-3225.

(56) Park, J.; Privman, V.; Matijevic, E. *J. Phys. Chem. B* **2001**, *105*, 11630-11635.

(57) Njoki, P. N.; Luo, J.; Kamundi, M. M.; Lim, S.; Zhong, C.-J. *Langmuir* **2010**, *26*, 13622-13629.

(58) McKenzie, L. C.; Haben, P. M.; Kevan, S. D.; Hutchison, J. E. *J. Phys. Chem. C* **2010**, *114*, 22055-22063.

CHAPTER 3

LIGAND EXCHANGE REACTIONS OF TRIPHENYLPHOSPHINE CAPPED GOLD NANOPARTICLES

3.1 Introduction

Ligand exchange reactions, also known as place exchange reactions are a convenient method of preparing nanoparticles (NPs) functionalized with desired functional groups for specific applications.[1, 2] This exchange process makes it possible to incorporate ligands onto nanoparticles after synthesis. This is particularly useful for ligands that are incompatible with the synthesis conditions for reasons ranging from solubility issues to reduction of the ligands by the reducing agent used to prepare the nanoparticles. Starting from a precursor nanoparticle, the initial stabilizing ligand can be removed or displaced. The incoming ligands are carefully chosen to impart the desired chemical functionality to the nanoparticles. Ligand exchange reactions can be used make NPs that are soluble in water or organic solvents depending on the intended application application. [3, 4] Ligand exchange is also used to increase the size of the NPs[5] and to

---

Reprinted with permission from Shem, P. M.; Sardar, R.; Shumaker-Parry, J. S. *Langmuir* 2009, *25*, 13279-13283. Copyright 2009, American Chemical Society. The first author designed and conducted all experimental and characterization work reported except as indicated. The author also composed the manuscript corresponding to Chapter 2. Sardar, R. carried out the high resolution TEM imaging (HRTEM) and provided experimental design guidance. Shumaker-Parry, J. S provided experimental design and editorial guidance.

impart greater stability to the NPs.[6] Several factors are known to influence ligand exchange. Differences in the size of the NP core affects how fast the ligand exchange proceeds.[7] The size range or dispersion (i.e., monodisperse verses polydisperse) of a particular batch of NPs also affects the ligand exchange process.[8] This can be explained by the fact the NPs have different fractions of atoms on the edges, vertices and terraces depending on their size.[9] These surface sites exhibit different reactivity and therefore affect the ligand exchange kinetics of the NPs in question.[10] The nature of the incoming ligand, e.g., the length of the chain of the incoming ligand and the functional groups it possesses, also affects the exchange kinetics.[7, 10] In addition, due to the differences in the reactivity of the NP sites, it is typically not possible to completely exchange all of the ligands on the NP surface.[11-13]

In order to favor exchange, the temporary stabilizing ligands should be easy to remove during the exchange reactions. For gold NPs, two of the most easily replaceable ligands are phosphines[13] and citrates.[14, 15] In this study, we focus on ligand exchange reactions involving triphenylphosphine (TPP) as the initial stabilizing ligand. Phosphine stabilized AuNPs have been used widely as precursor NPs for many ligand exchange reactions.[5, 16-19] An important advantage of phosphine-ligand-stabilized AuNPs is that, under ordinary laboratory conditions, easy and efficient place exchange by various ligands can be performed.[20, 21] As a result, amine, thiol and bipyridyl stabilized AuNPs can be obtained from phosphine stabilized NPs. For example, Murray and co-workers have used ligand exchange of $Au_{55}(PPh_3)_{12}Cl_6$ by thiols and studied the electrochemical behavior of those small clusters.[20, 21] In addition, the original phosphine ligands can be exchanged for other phosphine ligands.[22] However, it should be noted that ligand

exchange involving TPP-AuNPs sometimes preserves the core size of the resulting NPs[16] while at other times it does not.[3]

Phosphine to phosphine exchange occurs when one type of phosphine is exchanged for another. This type of exchange has been used to introduce water soluble ligands onto the surface of the NPs. Examples of such ligands includes the water soluble triphenylphosphine-monosulfonic acid[22] and aminophosphine ligands such as tris-[p-aminomethylphenyl]phosphine.[23] NPs stabilized by these two ligands have been used for biological studies.[24] The kinetics of exchange during phosphine-phosphine exchanges are fast.[25] However, studies have shown that it is impossible to achieve complete ligand exchange for phosphine to phosphine exchanges.[13, 24, 25] This can be attributed to the tendency of phosphine ligands to rapidly dissociate, which leads to instability of such NPs in dilute solutions.[18]

Hutchison and co-workers reported phosphine to amine ligand exchange between 1.4 nm TPP-AuNPs and an alkylamine ligand, 1-pentadecylamine.[6] AuNPs with sizes ranging from 4 nm to 8 nm were obtained depending on the ligand exchange conditions. Even though the resulting NPs were of uniform size, an increase in the diameter of the AuNPs was clearly evident. Detailed analysis of the amine stabilized NPs indicated that the phosphines were completely exchanged. Therefore, phosphine to amine exchange can be used to obtain larger NPs of uniform dispersion that are well ordered.[26]

One of the most studied and widely applied ligand exchanges is the phosphine to thiols ligand exchange. Phosphine to thiol place exchange can achieve complete ligand exchange, and as a result it is a more reliable type of place exchange reaction.[2, 20, 21] This approach facilitates the functionalization of the resulting NPs with a wide variety of ω-

functionalized thiols. Moreover, it is possible to maintain the size of the NP core as demonstrated by Hutchison et al. [27, 28] Loss of Au atoms has been reported during phosphine-to-thiol exchanges even though the size of the NPs does not change significantly.[18, 29] The resulting thiol capped NPs are usually more stable than their phosphine capped counterparts owing to the stronger Au-S bond compared to the Au-P bond. Thiol-stabilized AuNPs have received much attention because of the particles' electronic properties, use in creation of various assemblies, and applications in biological systems.[30-36]

Here, we report on the ligand exchange reactions in which NPs stabilized with different ω-functionalized thiols are prepared from the TPP-AuNP precursors synthesized using the 9-BBN reduction method. We also explore the feasibility of preparing bipyridyl stabilized AuNPs from the TPP-AuNP precursors through ligand exchange. Bipyridyls adsorbed on metal surfaces can act as shuttles in electron transfer reactions. [37, 38] Thus bipyridyl-NPs have potential applications in molecular electronics [39] and in solar cells.[40] Bipyridyl stabilized AuNPs have been prepared from citrate stabilized AuNPs.[41] However, they have not been prepared using phosphine AuNP as precursors. As a result of relying on citrate stabilized NPs as precursors, the size range of the bipyridyl AuNPs that can be prepared is limited. This is because the citrate reduction method does not produce NPs of small sizes (less than 9 nm).[42]

3.2 Experimental section

3.2.1 Materials

Chloro(triethylphosphine)gold(I) (97%), triphenylphosphine (99%), 0.5 M THF solution of 9-Borabicyclo[3.3.1]nonane (9-BBN), 11-mercapto-1-undecanoic acid (MUA), 11-meracpto-1-undecanol (MuOH), 1-dodecanethiol (DDT) and toluene (HPLC grade) were obtained from Sigma Aldrich while 11-bromo-1-undecanethiol (BUT) was obtained from Assemblon Inc. Acetonitrile (HPLC grade) was obtained from Fisher Scientific. Dichloromethane (99.8%) was obtained from Fluka while hexanes were obtained from EMD Chemicals. All of the chemicals and solvents were used as received. Water was purified (>18MΩ.cm) using a Branstead NANOpure Diamond™ system. All glass apparatus were cleaned with aqua regia and thoroughly rinsed with nanopure water and dried in the oven for 24 h at 120 ^{o}C before use. All reactions were carried out at room temperature unless otherwise indicated. PTFE IR cards were obtained from International Crystal Laboratories (Garfield, NJ).

3.2.2 Ligand exchange reactions

TPP-AuNPs were prepared at room temperature as described in Chapter 2. The TPP-AuNPs were then dissolved in DCM or acetonitrile and sonicated and centrifuged. The gold solution was obtained for use in the ligand exchange reactions. For the exchange reactions, four different thiols were used: 11-mercapto-1-undecanoic acid (MUA), 11-meracpto-1-undecanol (MuOH), 1-dodecanethiol (DDT) and 11-bromo-1-undecanethiol (BUT). Two bipyridines were used for the ligand exchange reaction: 2,2'- and 4,4'-bipyridine. To four different vials, 20 ml of the TPP-AuNPs solution and a

magnetic stir bar were added. To each different vial, 0.2mM (0.0437 g MUA, 0.0408 g MuOH, 47.96 µl DDT and 53.45 µl BUT) of thiol was added. The mixtures were stirred for 30 min, after which the contents of the vials were centrifuged and the solid obtained was dissolved in water. Brown colored solutions were obtained which were then analyzed by UV-Vis spectroscopy. MUA-AuNPs were treated with 1.0 mM NaOH to adjust the pH to ~ 8. For the bipyridines, 20 ml of the TPP-AuNPs solution and a magnetic stir bar were added to two vials. To each vial, 0.2mM (0.0312 g) of 2,2'- and 4,4'-bipyridine was added. The mixtures were stirred for 30 min. The contents of the vials were then centrifuged and the solid obtained was dissolved in water or ethanol. UV-Vis spectroscopy was used to analyze the solutions. A drop of each of the thiol and bipyridine AuNP solutions was deposited on a formvar copper grid for TEM analysis.

3.2.3 Spectroscopy and microscopy measurements

UV-vis absorption spectra were collected at room temperature using a Perkin-Elmer Lambda 19 UV/Vis/NIR spectrophotometer over the range of 300-800 nm. All data were corrected for background absorption using the solvent used to dissolve the respective sample. FTIR analysis was performed on a Perkin-Elmer Spectrum 100 Fourier Transform Infrared (FTIR) spectrometer. TPP-AuNPs samples were prepared by depositing 20 µl of the solution containing the TPP-AuNPs on PTFE IR cards. The sample was then dried under nitrogen. Each spectrum was obtained by averaging 4 scans at 4 cm^{-1} resolution. Transmission Electron Microscopy (TEM) micrographs were acquired using a Tecnai-12 instrument operating at 100 KV accelerating voltage. Before the TEM sample preparation, the sample was centrifuged at 4000 r.p.m. for 10 min to

remove any large aggregates. One drop of the solution collected after centrifugation, was deposited on a 150-mesh formvar-coated copper grid, and excess solution was removed by wicking with filter paper to avoid particle aggregation. The grid was then allowed to dry before being imaged. Particle size analysis was conducted by analyzing at least 200 particles in the TEM images using Scion Image Beta 4.02 Software. In Scion Image, after setting the known distance and unit, the 'Analyze Particle' parameter was used to generate a table of particle diameters. This table was then exported into Microsoft Excel for statistical analysis.

Raman spectra were collected using a Raman spectrometer whose configuration has previously been described in detail.[43] Briefly, data were collected using a Kr ion laser at 785 nm. A 300-mW beam was focused onto the sample using a cylindrical lens. The samples were contained in a quartz fluorometer cell. The Raman scattering were collected using a CCD and integrated for 20 s.

3.3 Results and discussion

3.3.1 Ligand exchange reactions involving ω-functionalized alkyl thiols

Incorporation of ligands with different functional groups onto AuNPs allows the production of materials with desired chemical functionalities.[44] The introduction of functional groups including alcohol- or acid-terminated thiols and disulfide ligands is only possible post synthesis for most NP synthetic schemes.[13] This is because the reduction of the functional groups could take place during synthesis. As a result, ligand exchange has remained a widely used strategy for preparing NPs bearing a diverse range

of functional groups. In this study, ω-functionalized alkyl thiols were incorporated into AuNPs by ligand exchange of TPP-AuNPs. The ligand exchange reactions were initiated by dissolving the TPP-AuNPs in dichloromethane (DCM), acetonitrile or water as noted and adding 0.2 mM of the thiols following Scheme 3.1. The reaction mixture was stirred for 30 min and a solid was obtained, purified and re-dissolved in the appropriate solvent as indicated.

After the ligand exchange reactions, the NPs were characterized by UV-vis absorption spectroscopy, TEM and FTIR. Figure 3.1A shows the TPP-AuNPs before the ligand exchange reaction. After the ligand exchange reaction, the DDT capped particles were stable in organic solvent. These DDT-AuNPs were 1.6 ± 0.4 nm in diameter (Figure 3.1B). On the other hand, MUOH-AuNPs were found to be aggregated after ligand exchange. MUA-AuNPs also were not stable in organic medium and the particles formed aggregates. Aggregation of alcohol and acid terminated thiol functionalized NPs has been previously reported.[27, 44]

Scheme 3.1. Ligand exchange reactions of TPP stabilized AuNPs with thiolated ligands.

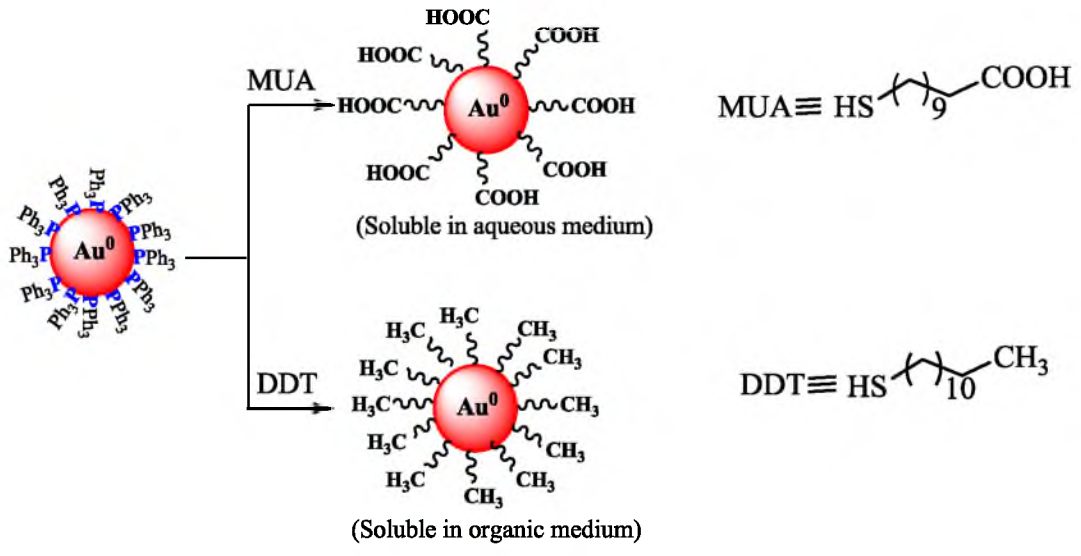

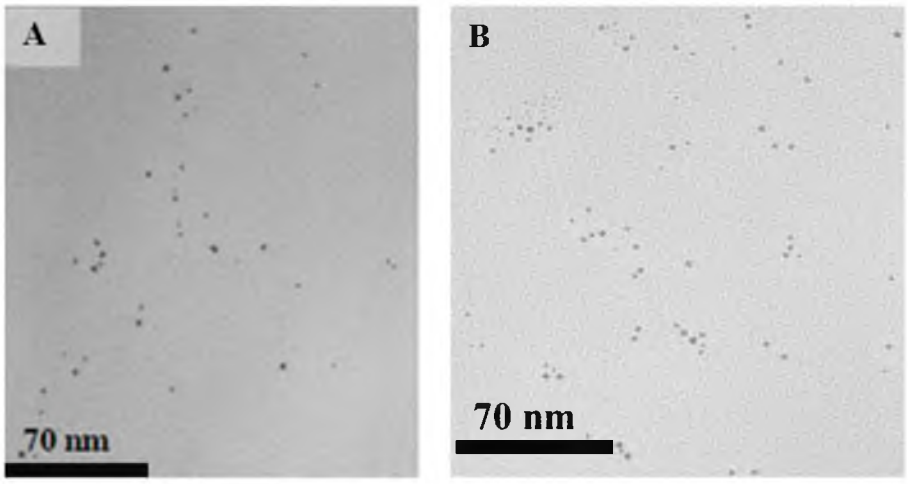

Figure 3.1. TEM image of (A) TPP-AuNPs before ligand exchange and (B) DDT-AuNPs.

This is because their solubility is pH dependent and the functional groups are deprotonated at high pH levels or protonated at low pH levels. For example, ligand exchanges involving carboxylic acid terminated thiols under non-basic conditions leads to the formation of insoluble material.[27] A detailed discussion of the pH dependent solubility of MUA-AuNPs will follow.

The TPP-AuNPs were found to be soluble in water. This was a surprising because the TPP ligands were not derivatized to make them hydrophilic and thus water soluble, as is the case with triphenylphosphine-monosulfonic acid ligand for example.[24] Ligand exchange reactions also were performed using the water soluble TPP-AuNPs. Briefly, TPP-AuNPs were dissolved in water while the ligands (MUA, DDT, MUOH and BUT) were dissolved in DCM. To each solution of MUA, DDT and MUOH in a separate Erlenmeyer flask was added to the TPP-AuNPs. The mixture was stirred for 1 h and then separated using a separatory funnel. The DDT-, MUOH-, and BUT-AuNPs transferred to the organic layer and the MUA-AuNPs transferred to the aqueous layer.

The layer containing the DDT-, MUOH-, and BUT-AuNPs was collected and analyzed. In this study, the size of nanoparticles in water increased from 1.4 ± 0.2 nm to 2.3 ± 0.5 nm for MUA-AuNPs (Figure 3.2A). The size of MuOH-AuNPs was 1.7 ± 0.4 nm as determined by TEM after ligand exchange (Figure 3.2B). It should be noted that these diameter estimates are based on the NPs in the TEM micrographs that were entirely spherical and not aggregated. Murray and coworkers also observed an increase in the size of the phosphine-stabilized AuNPs after ligand exchange with thiols.[21] Particle aggregation also was observed in all cases. This is attributed to the different solvation behaviors of the ionized head groups in water.[3] Ligand exchange performed with 11-bromo-1-undecanethiol (BUT) produced nanoparticles of different sizes and shapes (Figure 3.2C). We speculate that this is due to the bromine atoms which cause reorganization of the NP surface leading to the structures observed.[8] UV-vis absorption spectra of the DDT-, MUA-, MUOH- and BUT-AuNPs are shown in Figure 3.3. While plasmon resonance position does not change for DDT-AuNPs, MUA- and MUOH-AuNPs exhibit a red shift to about 530 nm. The shifts in the position of the absorption maxima (nm) indicate an increase in the size of the NPs as confirmed by TEM.

3.3.2 FTIR spectroscopy of MUA-AuNPs

The solubility of MUA-AuNPs has been established to be dependent on pH.[44] In this study, MUA-AuNPs adjusted to a basic pH were soluble in polar solvents while those at low pH were soluble in less polar solvents. At acidic pH, we observed that MUA-AuNPs were aggregated while at basic pH, the NPs did not aggregate. This is attributed to the protonation or deprotonation of the COOH group at low or high pH.[45, 46]

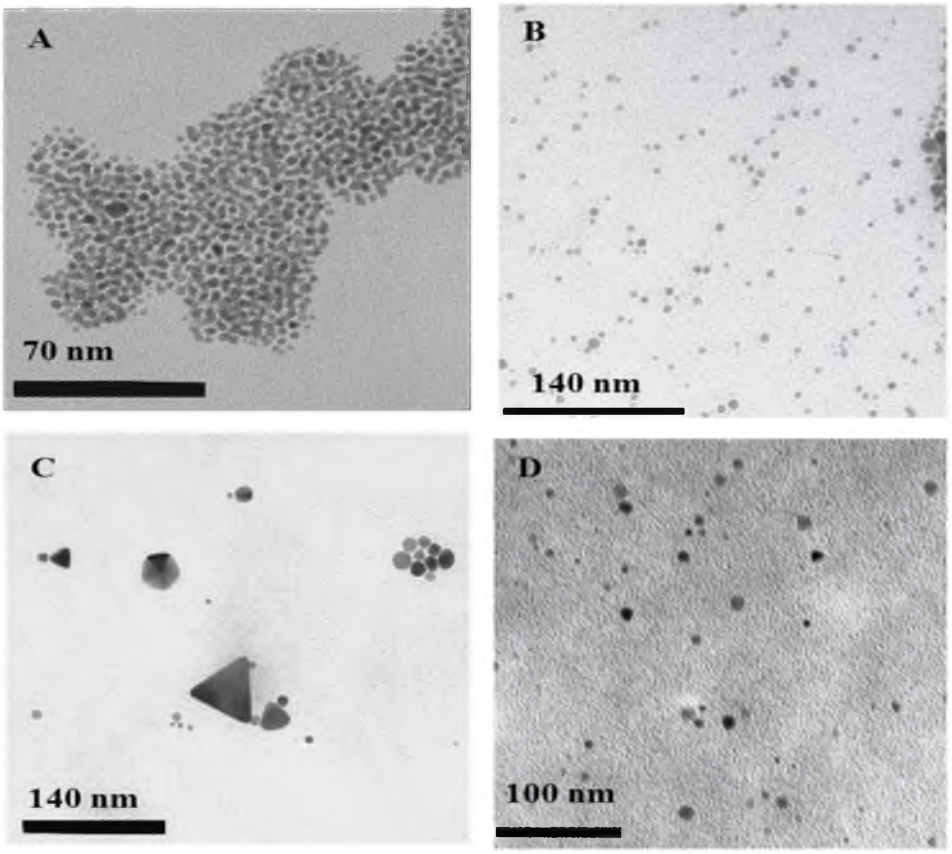

Figure 3.2. TEM image of (A) MUA-AuNPs, (B) MUOH-AuNPs, (C) BUT-AuNPs and (D) MUA-AuNPs after pH treatment.

At low pH, hydrogen bonding occurs leading to the observed aggregation and precipitation of the MUA-AuNPs. When the pH was adjusted to basic conditions (pH=9), no aggregation or precipitation was observed. However the size of the MUA-AuNPs after adjusting the pH increased from 2.3 ± 0.5 nm to 3.4 ± 0.7 nm. At pH=9, the carboxylic acid (–COOH) groups are converted to carboxylate ($–COO^-$) groups. Electrostatic repulsion between the carboxylate groups serves to keep the MUA-AuNPs from aggregating.[47]

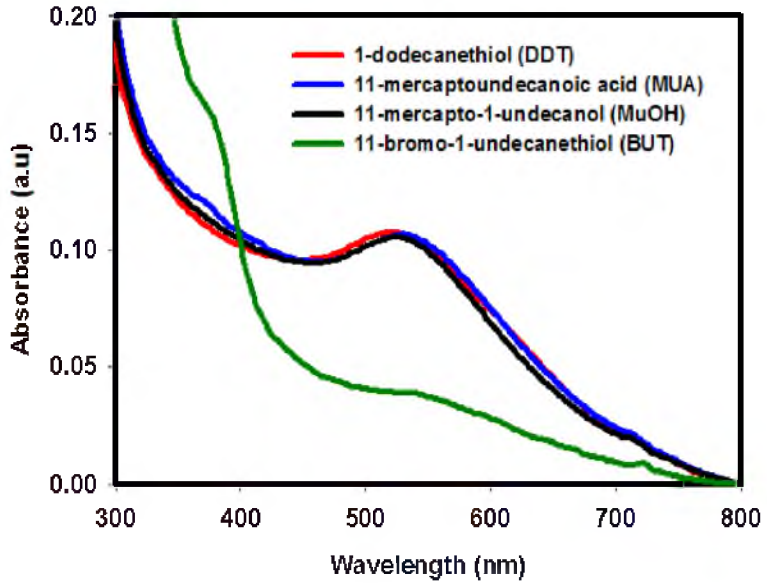

Figure 3.3. UV-vis absorption spectra of DDT-, MUA-, MUOH- and DDT-AuNPs.

This is confirmed by the TEM analysis of the NPs from the original solution and after pH adjustment as shown in Figure 3.2D. FTIR spectroscopy also was used to study the MUA-AuNPs. The FTIR spectra of pure MUA and MUA-AuNPs are shown in Figure 3.4. The asymmetric CH_2-stretching mode for MUA was observed at 2917 cm^{-1} while the mode observed at 2849 cm^{-1} was assigned to symmetric CH_2- stretching mode.[48] The band at 1693 cm^{-1} was assigned to the characteristic C=O stretch. After the ligand exchange, the stretching modes were observed at 2954, 2855 and 1722 cm^{-1} which were assigned to asymmetric CH_2- stretching, symmetric CH_2- and C=O stretching modes respectively. All of these modes shifted to higher energy indicating that the MUA is attached to the Au surface. Kim et al. observed the CH_2- asymmetric and symmetric stretching modes at 2922 and 2852 cm^{-1} respectively and 1700 cm^{-1} for the carbonyl stretching mode for MUA-AuNPs.[44] These values are comparable to what we observed in this study.

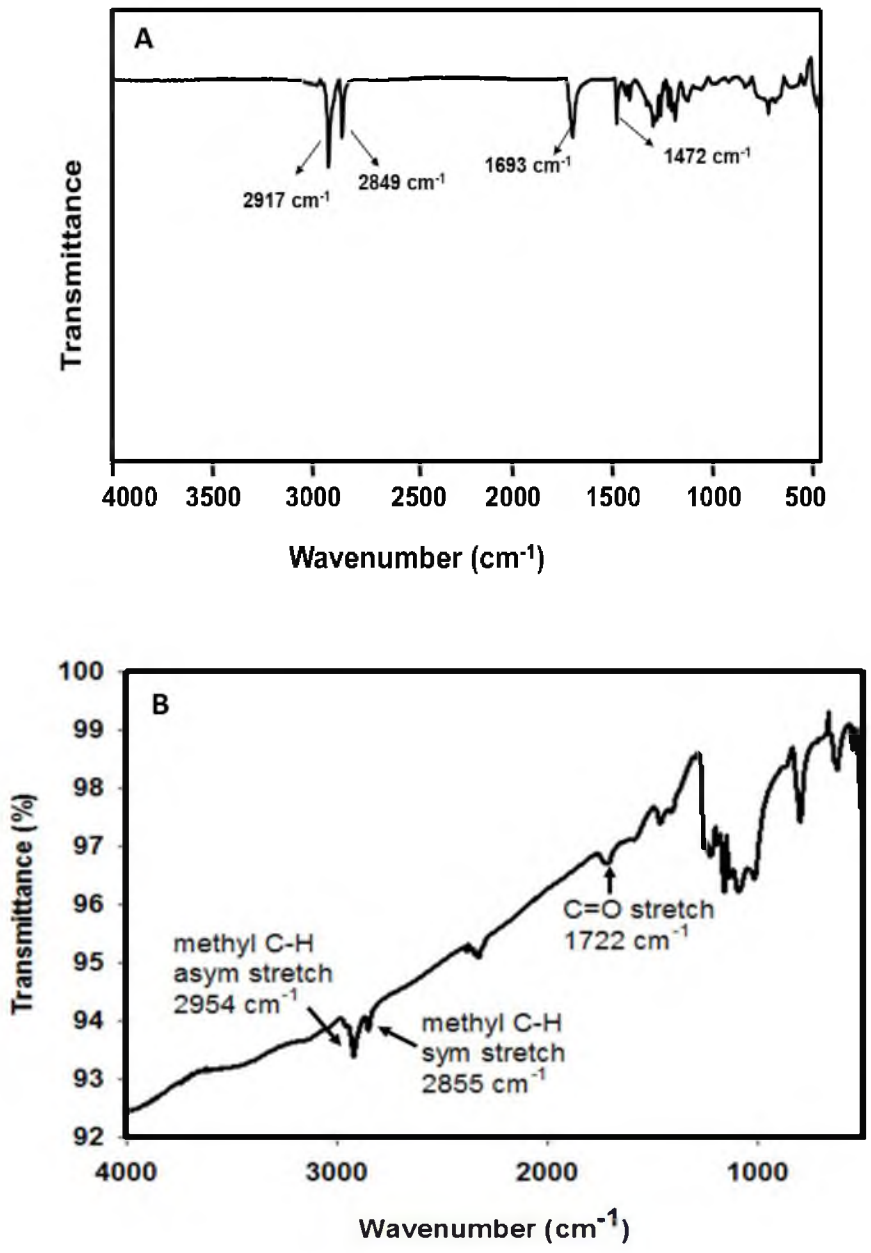

Figure 3.4. FTIR spectra of (A) pure MUA and (B) MUA-AuNPs before adjustment of pH.

Figure 3.4B presents the FTIR spectrum for MUA-AuNPs at low pH. The appearance of the C=O peak at 1722 cm^{-1} confirms that hydrogen bonding occurs between –COOH groups leading to the observed aggregation for this sample.

3.3.3 Ligand exchange reactions involving 2,2'- and 4,4'-bipyridines

We investigated the ligand exchange reactions involving TPP-AuNPs using 2,2'- and 4,4'-bipyridines (bipy). The bipyridines are expected to displace the TPP molecules which are attached to the AuNPs through coordination of P with Au. The bipyridines also are expected to attach to the AuNPs through coordination to nitrogen with Au. After ligand exchange, the 2,2'- and 4,4'-bipy AuNPs were dissolved in either ethanol or water for UV-vis analysis. The UV-vis absorption maxima shifted from 508 nm for TPP-AuNPs to 585 and 582 nm for 2,2'- and 4,4'-bipy AuNPs, respectively (Figure 3.5A). Aggregation was observed for 2,2'- and 4,4'-bipy AuNPs dissolved in both ethanol and water (Figure 3.5B-E). Attachment of the bipyridyl ligands to the AuNPs was confirmed by Raman spectroscopy using a Kr ion laser at 785 nm. Due to the aggregation of the bipy-AuNPs prepared using ligand exchange, a new method for synthesizing bipy-AuNPs *in-situ* using a modified 9-BBN reduction method will be discussed in Chapter 4.

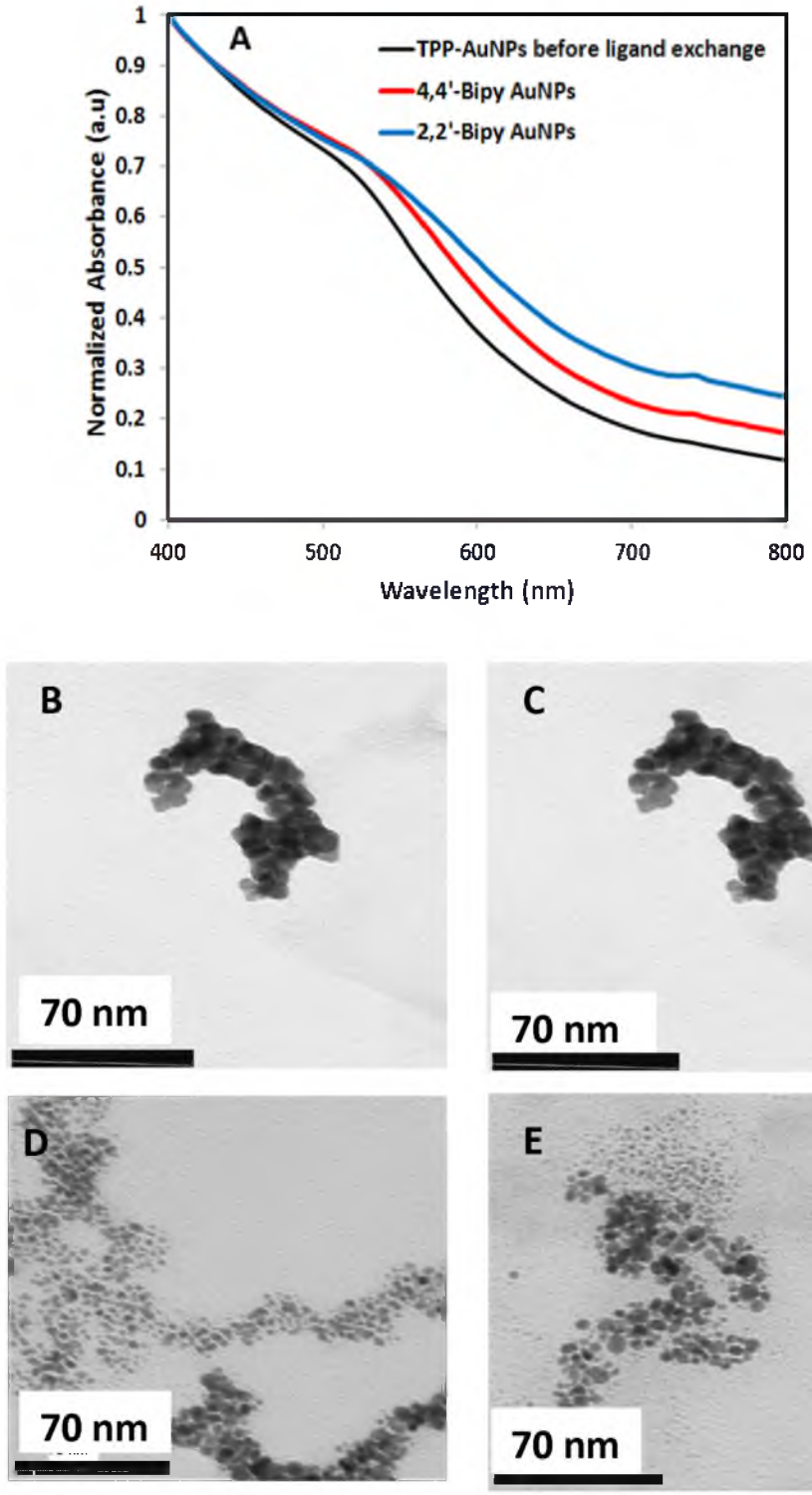

Figure 3.5. Bipyridyl AuNPs prepared by ligand exchange. (A) UV-vis absorption spectra of TPP-AuNPs and 2, 2'- and 4, 4'-bipy AuNPs. (B) 4,4'-bipy AuNPs in ethanol. (C) 2,2'-bipy AuNPs in ethanol. (D) 4,4'-bipyAuNPs in water. (E) 2,2'-bipy AuNPs in water.

3.3.4 Ligand exchange mechanism for phosphine stabilized AuNPs

We note that the ligand exchange mechanism for TPP-AuNPs depends on complex factors and as such, the mechanism is not clear. For example, it has been reported that the charge on the metal NPs affects the ligand exchange mechanism.[49] Obviously, the loss of Au atoms in the form of $Au(PPh_3)Cl$ must lead to a change in the oxidation state of the AuNPs cluster. This could affect how the exchange mechanism proceeds. During ligand exchange, PPh_3 does not desorb alone, rather $Au(PPh_3)Cl$ desorbs leading to loss of Au atoms.[5]

This loss of atoms may not be detected by analysis of TEM images of the AuNPs. Kuo *et al* confirmed the desorption of $Au(PPh_3)Cl$ from the TPP-AuNPs by ^{31}P NMR.[5] Yarger et al. have corroborated the observation that the desorption of $Au(PPh_3)Cl$ occurs during ligand exchange rather than the loss of PPh_3 alone using ^{1}H, ^{2}H and both solution and solid state ^{31}P NMR.[50] We also note that the experimentally proven loss of $Au(PPh_3)Cl$ rather than free PPh_3 is an indication that the core of the TPP-AuNPs clusters are surrounded by gold-phosphine complexes. The solubility of the displaced ligands (PPh_3 in our case) has been shown to affect the ligand exchange process.[51] The ligand exchange process has been reported to be diffusion limited.[52] Specifically for TPP-AuNPs, the exchange is a three stage event. [27] For TPP-AuNPs comparable in size to the ones used in the current study (1.5 nm – 1.7 nm in diameter), Hutchison and co-workers report that the initial stage of ligand exchange involves the loss of $Au(PPh_3)Cl$ as opposed to free PPh_3. This step leads to removal of the chlorine in the form of the complex $Au(PPh_3)Cl$. This step continues until all chlorides are removed. The remaining PPh_3 is then removed by dissociating from the NP surface as free PPh_3 to form a

phosphine-gold complex. Alternatively, PPh_3 may be transferred to $Au(PPh_3)Cl$. Trapping experiments for free PPh_3 indicate the later route is more plausible. [29] The final step involves the coordination of the incoming ligand with the Au.

3.4 Conclusion

We have shown that TPP-stabilized nanoparticles can be used as precursors for preparation of AuNPs functionalized with different types of ligands through ligand exchange reactions. The DDT-AuNPs produced by the ligand exchange process retained the size of the starting TPP-AuNPs. The particle size of the exchange product was found to be larger than the starting TPP-stabilized AuNPs for MUA and MUOH stabilized AuNPs. Exchanging triphenylphosphine ligands for 11-bromo-1-undecanethiol (BUT) lead to formation of NPs of different sizes and shapes. The solubility of NPs functionalized by different ligands was also shown to vary in different solvents depending on the functional group borne by the ligand. This was demonstrated to be the case for MUA whose solubility was established to be dependent on pH. This ligand exchange protocol could be useful in preparation of optically active phosphinate stabilized gold or other noble metal nanoparticles. These ligand exchange results demonstrate the potential for using the phosphine-stabilized AuNPs as precursors for functionalization with bipyridyl and thiol-based ligands.

3.5 References

(1) Kiely, C. J.; Fink, J.; Brust, M.; Bethell, D.; Schiffrin, D. J. *Nature* **1998**, *396*, 444-446.

(2) Schmid, G.; Simon, U. *Chem. Commun.* **2005**, 697-710.

(3) Woehrle, G. H.; Warner, M. G.; Hutchison, J. E. *J. Phys. Chem. B* **2002**, *106*, 9979-9981.

(4) Ackerson, C. J.; Jadzinsky, P. D.; Kornberg, R. D. *J. Am. Chem. Soc.* **2005**, *127*, 6550-6551.

(5) Kuo, C.-T.; Yu, J.-Y.; Huang, M.-J.; Chen, C.-h. *Langmuir* **2010**, *26*, 6149-6153.

(6) Brown, L. O.; Hutchison, J. E. *J. Am. Chem. Soc.* **1999**, *121*, 882-883.

(7) Guo, R.; Song, Y.; Wang, G.; Murray, R. W. *J. Am. Chem. Soc.* **2005**, *127*, 2752-2757.

(8) Caragheorgheopol, A.; Chechik, V. *Phys. Chem. Chem. Phys.* **2008**, *10*, 5029-5041.

(9) Häkkinen, H.; Barnett, R. N.; Landman, U. *Phys. Rev. Lett.* **1999**, *82*, 3264-3267.

(10) Montalti, M.; Prodi, L.; Zaccheroni, N.; Baxter, R.; Teobaldi, G.; Zerbetto, F. *Langmuir* **2003**, *19*, 5172-5174.

(11) Baralia, G. G.; Duwez, A.-S.; Nysten, B.; Jonas, A. M. *Langmuir* **2005**, *21*, 6825-6829.

(12) Ivanisevic, A.; McCumber, K. V.; Mirkin, C. A. *J. Am. Chem. Soc.* **2002**, *124*, 11997-12001.

(13) Dahl, J. A.; Maddux, B. L. S.; Hutchison, J. E. *Chem. Rev.* **2007**, *107*, 2228-2269.

(14) Nichols, R. J.; Burgess, I.; Young, K. L.; Zamlynny, V.; Lipkowski, J. *J. Electroanal. Chem.* **2004**, *563*, 33-39.

(15) Feng, Y.; Xing, S.; Xu, J.; Wang, H.; Lim, J. W.; Chen, H. *Dalton Trans.* **2010**, *39*, 349-351.

(16) Brown, L. O.; Hutchison, J. E. *J. Am. Chem. Soc.* **1997**, *119*, 12384-12385.

(17) Weare, W. W.; Reed, S. M.; Warner, M. G.; Hutchison, J. E. *J. Am. Chem. Soc.* **2000**, *122*, 12890-12891.

(18) Wang, W.; Murray, R. W. *Langmuir* **2005**, *21*, 7015-7022.

(19) Donkers, R. L.; Song, Y.; Murray, R. W. *Langmuir* **2004**, *20*, 4703-4707.

(20) Wolfe, R. L.; Balasubramanian, R.; Tracy, J. B.; Murray, R. W. *Langmuir* **2006**, *23*, 2247-2254.

(21) Balasubramanian, R.; Guo, R.; Mills, A. J.; Murray, R. W. *J. Am. Chem. Soc.* **2005**, *127*, 8126-8132.

(22) Schmid, G.; Klein, N.; Korste, L.; Kreibig, U.; Schonauer, D. *Polyhedron* **1988**, *7*, 605-608.

(23) Bartlett, P. A.; Bauer, B.; Singer, S. J. *J. Am. Chem. Soc.* **1978**, *100*, 5085.

(24) Jahn, W. *J. Struct. Biol.* **1999**, *127*, 106-112.

(25) Petroski, J.; Chou, M. H.; Creutz, C. *Inorg. Chem.* **2004**, *43*, 1597-1599.

(26) Brown, L. O.; Hutchison, J. E. *J. Phys. Chem. B* **2001**, *105*, 8911-8916.

(27) Woehrle, G. H.; Brown, L. O.; Hutchison, J. E. *J. Am. Chem. Soc.* **2005**, *127*, 2172-2183.

(28) Warner, M. G.; Reed, S. M.; Hutchison, J. E. *Chem. Mater.* **2000**, *12*, 3316-3320.

(29) Woehrle, G. H.; Hutchison, J. E. *Inorg. Chem.* **2005**, *44*, 6149-6158.

(30) Daniel, M. C.; Astruc, D. *Chem. Rev.* **2004**, *104*, 293-346.

(31) Phillips, R. L.; Miranda, O. R.; You, C.-C.; Rotello, V. M.; Bunz, U. H. F. *Angew. Chem. Int. Ed.* **2008**, *47*, 2590-2594.

(32) Zhu, M.; Aikens, C. M.; Hollander, F. J.; Schatz, G. C.; Jin, R. *J. Am. Chem. Soc.* **2008**, *130*, 5883-5885.

(33) Jadzinsky, P. D.; Calero, G.; Ackerson, C. J.; Bushnell, D. A.; Kornberg, R. D. *Science* **2007**, *318*, 430-433.

(34) Gruene, P.; Rayner, D. M.; Redlich, B.; van der Meer, A. F. G.; Lyon, J. T.; Meijer, G.; Fielicke, A. *Science* **2008**, *321*, 674-676.

(35) Heaven, M. W.; Dass, A.; White, P. S.; Holt, K. M.; Murray, R. W. *J. Am. Chem. Soc.* **2008**, *130*, 3754-3755.

(36) Shem, P. M.; Sardar, R.; Shumaker-Parry, J. S. *Langmuir* **2009**, *25*, 13279-13283.

(37) Wandlowski, T.; Ataka, K.; Mayer, D. *Langmuir* **2002**, *18*, 4331-4341.

(38) Armstrong, F. A.; Hill, H. A. O.; Walton, N. J. *Acc. Chem. Res.* **1988**, *21*, 407-413.

(39) Gittins, D. I.; Bethell, D.; Schiffrin, D. J.; Nichols, R. J. *Nature* **2000**, *408*, 67-69.

(40) Schnadt, J.; Bruhwiler, P. A.; Patthey, L.; O'Shea, J. N.; Sodergren, S.; Odelius, M.; Ahuja, R.; Karis, O.; Bassler, M.; Persson, P.; Siegbahn, H.; Lunell, S.; Martensson, N. *Nature* **2002**, *418*, 620-623.

(41) Joo, S. W. *Spectrosc. Lett.* **2006**, *39*, 85-96.

(42) Kimling, J.; Maier, M.; Okenve, B.; Kotaidis, V.; Ballot, H.; Plech, A. *J. Phys. Chem. B* **2006**, *110*, 15700-15707.

(43) Uibel, R. H.; Harris, J. M. *Appl. Spectrosc.* **2000**, *54*, 1868-1875.

(44) Kim, K.-H.; Yamada, M.; Park, D.-W.; Miyake, M. *Chem. Lett.* **2004**, *33*, 344-345.

(45) Sardar, R.; Bjorge, N. S.; Shumaker-Parry, J. S. *Macromolecules* **2008**, *41*, 4347-4352.

(46) Basu, S.; Ghosh, S. K.; Kundu, S.; Panigrahi, S.; Praharaj, S.; Pande, S.; Jana, S.; Pal, T. *J. Colloid Interface Sci.* **2007**, *313*, 724-734.

(47) Simard, J.; Briggs, C.; Boal, A. K.; Rotello, V. M. *Chem. Commun.* **2000**.

(48) Anderson, M. R.; Baltzersen, R. *J. Colloid Interface Sci.* **2003**, *263*, 516-521.

(49) Song, Y.; Murray, R. W. *J. Am. Chem. Soc.* **2002**, *124*, 7096-7102.

(50) Sharma, R.; Holland, G. P.; Solomon, V. C.; Zimmermann, H.; Schiffenhaus, S.; Amin, S. A.; Buttry, D. A.; Yarger, J. L. *J. Phys. Chem. C* **2009**, *113*, 16387-16393.

(51) Toikkanen, O.; Carlsson, S.; Dass, A.; Roì^nnholm, G.; Kalkkinen, N.; Quinn, B. M. *J. Phys. Chem. Lett.* **2009**, *1*, 32-37.

(52) Kassam, A.; Bremner, G.; Clark, B.; Ulibarri, G.; Lennox, R. B. *J. Am. Chem. Soc.* **2006**, *128*, 3476-3477.

CHAPTER 4

SYNTHESIS OF SOFT LIGAND STABILIZED GOLD NANOPARTICLES AND APPLICATION IN THE *IN-SITU* FORMATION OF BIPYRIDYL STABILIZED GOLD NANOPARTICLES

4.1 Introduction

Synthesis of nanomaterials with unique properties for diverse applications has been a focus area of nanomaterial research in the past few years. Their unique characteristics emanate from their different sizes,[1-3] shapes[4-6] and surface chemistry.[7-9] As a result, these materials can be utilized for biological, chemical, optical and electronic applications.[10-14] Metal nanoparticles form an important class of the nanomaterials studied. It is therefore necessary to understand the factors affecting the growth kinetics of the NPs in order to achieve control of their organization.[15-17] One of the most critical considerations when synthesizing NPs is the surface chemistry. The surface chemistry of the NPs is dictated to a great extent by the ligands present at the nanoparticle surface.[18, 19] As a result, the surface ligands play a vital role in determining the characteristics of the NPs produced. For example, introduction of capping agents such as citrates and thiols during nanoparticle synthesis has the effect of stopping the growth whereas weakly associated ligands allow for continued growth.[20-22]

Thus the type of ligands, whether strongly or weakly binding to nanoparticles determines the size and shape of the resulting nanoparticles.[7, 23]

A number of solution-based synthetic approaches have been used to generate spherical AuNPs either in aqueous or organic solvents.[24-31] Most of the methods involve the reduction of Au(III) in the presence of a ligand. The Brust method and its various modifications have been routinely used to synthesize smaller size AuNPs (1-5 nm size range).[32, 33] In the Brust approach, phase transfer of Au (III) from aqueous phase to organic phase is required and the strong reducing agent $NaBH_4$ generates AuNPs very rapidly. As a result, during the nanoparticle synthesis, the presence of capping agent, e.g. alkylthiols, is essential in order to control the nanoparticle size and prevent aggregation. Even though the borohydride-based method provides good control over particle size, the AuNPs are coated with a monolayer of thiols *in-situ* making further surface modification with alternative ligands more challenging.[34] This is because of the strong gold- sulphur interaction.[7] The use of strong reducing agents, $NaBH_4$ for example, also limits the types of ω-functionalized alkylthiols and amines that can be used as capping ligands for AuNP stabilization and functionalization. This limitation is due to the reduction of the functional groups of the capping ligands by the strong reducing agents.[35] In addition, the sizes of the nanoparticles produced using the Brust method vary from batch to batch.[35, 36]

In the recent past, other synthetic methods for preparation of small AuNPs have been developed; however, in each approach, inclusion of a capping ligand is essential to inhibit nanoparticle aggregation and enable controlled assembly and tuning of the optical properties of the AuNPs.[1] In order to overcome the limitations of the original Brust method or its various modifications where use of a phase transfer agent and strong

capping ligands are required, single step "surfactant-free" synthesis of AuNPs also has been reported.[37-39] In these approaches, the stability of nanoparticles is a major concern and particle precipitation is observed within one day after synthesis. In general, synthesis of stable AuNPs without any surfactant present in the reaction mixture is a challenge.

In order to synthesize AuNPs without the use of surfactants, the synthetic method requires a mild reducing agent which could generate nanoparticles at a slow rate with the resulting particles stabilized by coordinating ions or ligands which are already present in the reaction mixture from the gold salt precursor. The major advantage of this method would be obtaining nanoparticles capped by a weak stabilizer without need for strong capping ligand such as thiols. Depending on the intended application, the nanoparticles could be easily functionalized by replacing the weakly adsorbed molecules with ligands having a strong affinity for the AuNPs. The use of the mild reducing agent 9-BBN for *in-situ* synthesis of various ω-functionalized (acid, amide, or alcohol) alkylthiols or azide terminated disulfide-protected AuNPs has been reported by the Shumaker-Parry group.[31] AuNPs also can be directly functionalized with a variety of thiolated ligands during the synthetic process.[21] The protocol could be exploited to synthesize other noble metal nanoparticles, specifically, silver (Ag), palladium (Pd), and platinum (Pt) nanoparticles of narrow size dispersion.[31] We also have demonstrated that 9-BBN can be used to produce triphenylphosphine-stabilized AuNPs of about ~2.0 nm in a single step approach.[33]

Herein, we report the synthesis of ~4.0 nm AuNPs stabilized by soft ligands in organic solvents. The synthesis involves the reduction of a phosphine-based gold precursor by the mild reducing agent 9-Borabicyclo[3.3.1]nonane (9-BBN) without adding stabilizing agents. Soft ligands such as triethylphosphine (Et_3P) and chloride are

produced from the precursor materials. The novelty of this synthetic procedure is that stabilizing agents are not added during nanoparticle synthesis as the nanoparticles are produced at a slow rate and stabilized by soft ligands. The main advantage of the soft ligands is that they offer the potential for easy and complete displacement after synthesis by the desired strong binding ligands. Due to the relatively weak affinity of the phosphine ligands, *in-situ* addition of stronger ligands prevents the growth of nanoparticles and produces AuNPs with much more narrow size dispersion. This leads to longer term stabilization of the AuNPs. The utility of this synthesis is demonstrated by simple *in-situ* surface modification of the synthesized AuNPs with 2,2'- and 4,4'-bipyridyl leading to 2,2'- and 4,4'-bipyridyl-functionalized AuNPs. We also use this synthetic procedure to gain an insight into the growth kinetics of the soft ligand stabilized NPs based on the chloro(triethylphosphine) Au salt precursor. Using this knowledge, we are able to determine the precise time for addition of the ligands to arrest the growth process and obtain NPs of uniform size.

4.2 Experimental section

4.2.1 Chemicals

(3-mercaptopropyl)triethoxy-silane (MPTES), chloro(triethylphosphine)gold(I) (Et_3PAuCl), 0.5 M THF (tetrahydrofuran) solution of 9-Borabicyclo[3.3.1]nonane (9-BBN) , 2,2'-bipyridine (2,2'-bipy), 4,4'-bipyridine (4,4'-bipy) and 11-mercapto-1-undecanol (MUOH) were purchased from Sigma Aldrich. HPLC grade THF and acetonitrile were obtained from Fisher Scientific. All of the chemicals and solvents were used as received without any purification. The glassware used in the synthesis were

cleaned with aqua-regia, rinsed with a copious amount of nanopure water and dried over night prior to use. All of the reactions were carried out in air.

4.2.2 Synthesis of soft ligand stabilized gold nanoparticles

Et_3PAuCl (0.004 gm) was dissolved in 50-mL 1:1 mixture of acetonitrile and THF in air at room temperature. The solution was stirred for 5 min and and 0.06 mL of 0.5 M 9-BBN in THF solution was added. The solution was left to react without stirring for 20 min. The color of the solution gradually changed from colorless to reddish pink. One drop of the solution was deposited on the formvar coated carbon grid and analyzed by TEM. The AuNPs solution was stored at –20 ^{0}C.

4.2.3 Kinetics of nanoparticle growth

The same procedure for synthesis of soft ligand stabilized gold nanoparticles described above was followed. However, for one batch of the NPs, stirring was performed using a magnetic stir bar. In both cases, samples were collected at 5 min intervals for 1 h for UV-vis and TEM analyses.

4.2.4 Synthesis of 2,2'- and 4,4'-bipyridyl AuNPs

Et_3PAuCl (0.004 gm)was dissolved in 50-mL 1:1 mixture of acetonitrile and THF in air at room temperature. The solution was stirred for 5 min and 0.06 mL of 0.5 M 9-BBN in THF solution was added. The solution was left to react without stirring for 20 min. The color of the solution gradually changed from colorless to reddish pink. At this point, 0.062 g of bipyridyl was added and the solution was stirred for a minute and left to

react for an additional 20 min without stirring. The color of the solution changed to deep red. The solution was centrifuged and the solid was cleaned with hexanes. The NPs obtained were dissolved in toluene. One drop of the solution was deposited on the formvar coated carbon grid and analyzed by TEM.

4.2.5 Preparation of glass coverslips

The coverslips were cleaned by placing them in an aqueous 20% RBS detergent solution heated to 90 ^{o}C and sonicating for 5 min. The coverslips were copiously rinsed with distilled water and then immersed in a 1:1(v/v) solution of methanol and concentrated HCl for 30 min. The coverslips were rinsed thoroughly with distilled water and left to dry overnight in an oven at 60 ^{o}C.

4.2.6 Functionalization of glass coverslip surfaces with MPTES

Glass coverslips were functionalized with MPTES using the published procedure.[40] One batch of the clean coverslips prepared above was then placed in a 10% (v/v) solution of MPTES in anhydrous ethanol for 30 min. The coverslips were sonicated and then rinsed with anhydrous ethanol and dried at 100^{o}C for 3h.

4.2.7 Preparation of samples for XPS analysis

Three different samples were prepared:

(a) The gold nanoparticle solution prepared above was drop cast on the unsilanized glass coverslips and left to dry at room temperature.

(b) Glass coverslips functionalized with MPTES were incubated in the soft ligand stabilized gold nanoparticle solution for 2-3 h. The glass slides were then rinsed thoroughly with a 1:1 acetonitrile/THF solvent and dried in a stream of nitrogen.

(c) A self-assembled monolayer of MUOH was formed on the surface of the gold nanoparticles by incubating the Au-nanoparticle coated glass coverslips prepared in step (b) in a 1 mM solution of MUOH in ethanol for 2 h at room temperature. After formation of the MUOH SAMs, the surface was thoroughly rinsed with ethanol to remove unreacted thiols, dried using nitrogen, and stored at 4 ^{0}C in a nitrogen atmosphere.

4.2.8 UV-visible Spectroscopy and Transmission Electron Microscopy (TEM)

UV-vis extinction spectra were collected using a Perkin-Elmer Lambda 750 UV/Vis/NIR spectrophotometer. TPP-AuNPs solutions were drop cast onto 200 mesh formvar-coated copper grids (Electron Microscopy Sciences, PA). The excess solution was wicked off and the grids were air dried. TEM images were obtained using a Tecnai-12 instrument operating at 100 KV accelerating voltage (Microscopy Core Facility, University of Utah). Particle size analysis was conducted by analyzing ~1000 particles in the TEM images (TIF format) using Scion Image Beta 4.02 Software. In Scion Image, the known distance and unit were set. The 'Analyze Particle' parameter was used to generate a table of particle diameters. This table was then exported into Microsoft Excel 2010 for statistical analysis.

4.2.9 X-ray Photoelectron Spectroscopy (XPS)

XPS data were obtained on a Kratos AxisUltraDLD using a monochromatic Al kα source (1486.6 eV) with a pass energy of 40 eV and a step size of 0.1 eV. The spectrometer was calibrated using Ag $3d_{5/2}$ peak. The binding energy (BE) scale was calibrated using the C1s peak with a BE set at 284.8 eV. The dwell time was 300 ms and the peaks were analyzed relative to the C1s. The data were fitted to an asymmetrical Gaussian-Lorentzian line shape using CasaXPS version 2.3.14.

4.2.10 HAADF-STEM, HRTEM and SAED imaging

TPP-AuNPs samples were prepared following the same procedure used for TEM samples as described above. Micrographs were obtained using a FEI Titan 80-300 TEM operated at 300 kV at the CAMCOR High Resolution and Analytical Facility (University of Oregon, Eugene, OR). The instrument is equipped for bright field, dark field, and high angle annular dark field STEM imaging. The detector was a high-angle annular dark-field detector for HAADF-STEM. The collection angle of HAADF-STEM images was 10 mrad. The images were acquired at different magnifications and captured using a Gatan CCD. The camera length was 160 mm. The size of the images obtained was 1k x 1k for the original images. The pixel size was 478 pm x 478 pm. Selected-area electron diffraction (SAED) patterns also were obtained.

4.3 Results and discussion

4.3.1 Synthesis of soft ligand stabilized NPs

The synthetic procedure for the generation of soft ligand stabilized NPs follows Scheme 4.1. No additional ligands were introduced in the reaction mixture besides Et_3PAuCl as a gold salt precursor and 9-BBN as the reducing agent. The NPs are stabilized by the soft ligands, Et_3P and Cl^- ions which come from these components. Previously, it was observed that chloride ions could electrostatically adsorb on metal nanoparticles and provide stability of the colloids.[41] Chloride ions are essential stabilizers in gold-phosphine NPs and in other clusters where gold-halide compounds are used as precursors.[42] In addition, phosphine ligands are known to act as stabilizers in the production of stable metal nanoparticles in organic solvents.[32, 33]

The precursor salt, chloro(triethylphosphine) gold(I) has an absorbance at 300 nm (Figure 4.1).[43] The peaks at 267 and 276 nm in the absorption spectra of the Au precursor salt in Figure 4.1 are due to Au^+. The broad featureless absorbance in the UV-vis spectrum that is observed after addition of the reducing agent is an indication that the NPs are being formed.

Scheme 4.1. Synthetic procedure for the soft ligand stabilized NPs

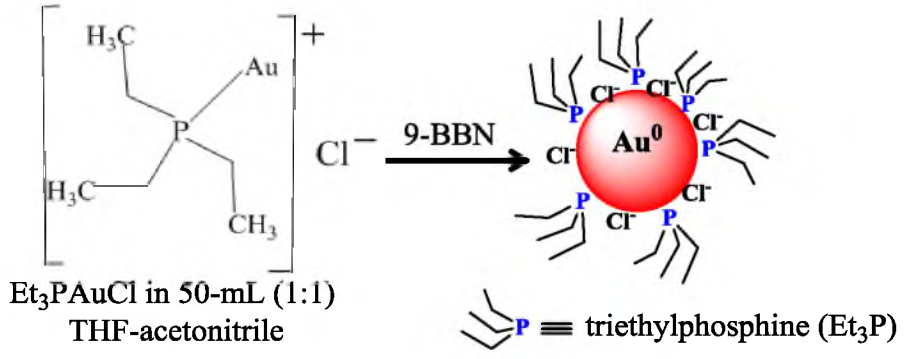

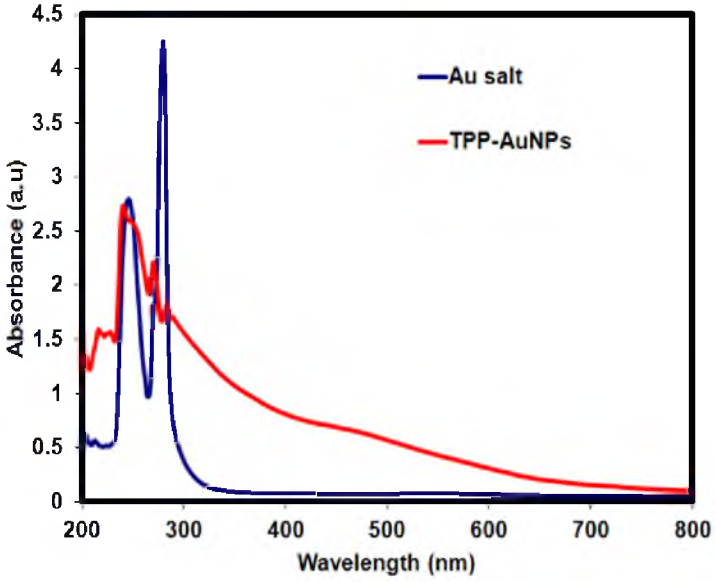

Figure 4.1. UV-vis absorption spectra of the chloro(triethylphsophine) gold(I) precursor salt and the TPP-AuNPs formed on addition of 9-BBN.

The color of the solution changes from colorless to light brown on addition of 9-BBN. As more NPs are formed, the absorbance of the solution increases in the 400-500 nm range. The color of the solution also changes to reddish-brown. No particle precipitation was observed. Differences were observed depending on if the reaction mixture was stirred or not stirred. Mechanical agitation disrupts the nucleation process and alters the aggregation growth process of the NPs.[44] Stirring introduces shear forces to the solution and while shear-induced enhancement of nucleation has been reported,[45, 46] mechanical shear has also been found to suppress growth by breaking up aggregated nanoparticles.[47] This is illustrated in Figure 4.2. When the reaction solution was stirred mechanically using a magnetic stir bar, the UV-vis spectra absorbance as well as the color of the solution did not change from the light brown color first observed on addition of 9-BBN. This was an indication that growth was not taking place.

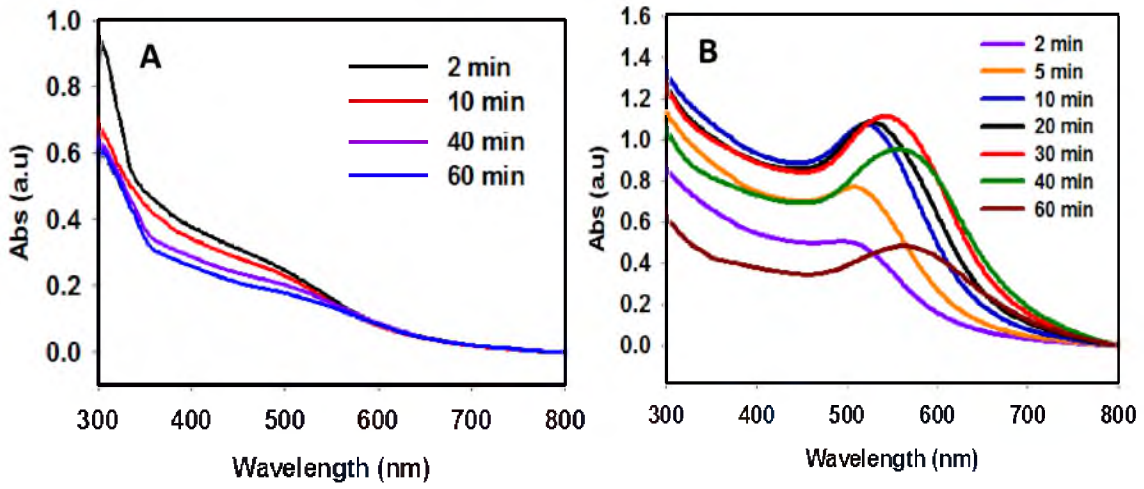

Figure 4.2. UV-vis absorption spectra of the (A) stirred and (B) unstirred TPP-AuNPs solutions indicating differences in the size evolution of the resulting NPs.

However, when stirring was stopped, the absorbance of the solution increased indicating growth of the NPs. For the solution that was not stirred, the absorbance of the solution increased gradually with time. The color of the solution changed from colorless, to reddish-brown, purple and finally bluish purple, indicating that the growth of the NPs continued. Aggregates were formed unless the process was stopped, for example by addition of strongly stabilizing ligands as we shall demonstrate later in this chapter. Stirring the mixture changes the nuclei concentration leading to different sizes of the NPs obtained between the stirred and unstirred mixtures.[36] The solution that was not stirred produced consistent NP sizes and therefore was the synthetic procedure adopted for subsequent synthesis of the soft ligand stabilized nanoparticles in this study. We investigated the size evolution of the NPs using this synthetic procedure. Samples were taken from this solution every 5 min for UV-vis (Figure 4.2B) and TEM analysis. The UV-vis data in Figure 4.2B suggest that the NPs continue to grow in size with time. A close examination of the spectra reveals that between 15 and 25 min after addition of 9-

BBN, there is no change in the peak absorbance amplitude and the spectra do not shift. Afterwards, there is a marked red shift and broadening of the absorbance band accompanied by a reduction in the absorbance amplitude indicating formation of large aggregates. When the reaction was allowed to proceed for 60 min, precipitation was observed. TEM analysis of the solution corroborates this analysis (Figure 4.3). The images confirm that the during the NP growth process, the NPs are polydisperse. However, at the point where the absorbance peak position and amplitude do not change, the NPs exhibit narrow size dispersion. The size of the NPs at this point was determined to be 3.6 ± 0.94 nm. The monodisperse NPs aggregated when the solution was allowed to stand for longer forming large aggregates (Figure 4.3D). HRTEM, HAADF-STEM and SAED were used to further characterize the morphology and structure of the NPs formed at 25 min (Figure 4.4). HRTEM showed NPs with well-defined lattice fringes. The NPs were indexed to Au fcc using SAED.

The shape and faceting of the NPs as obtained by HRTEM indicates that the NPs are likely formed by the coalescence of individual smaller NPs. The NPs likely coalesce along common facets to form twinned particles. Contrast differences in HRTEM images, where some regions are darker than others is an indication of twins.[48] A close observation of Figures 4.4B and C confirms the contrast differences in the NPs. The SAED pattern of the NPs was indexed to the (111), (200), (220) and (311) of a face-centered cubic (fcc) Au lattice. The spotty nature of the SAED pattern also supports the presence of twins. This result provides information related to the NP formation mechanism which will be discussed in detail in the section below.

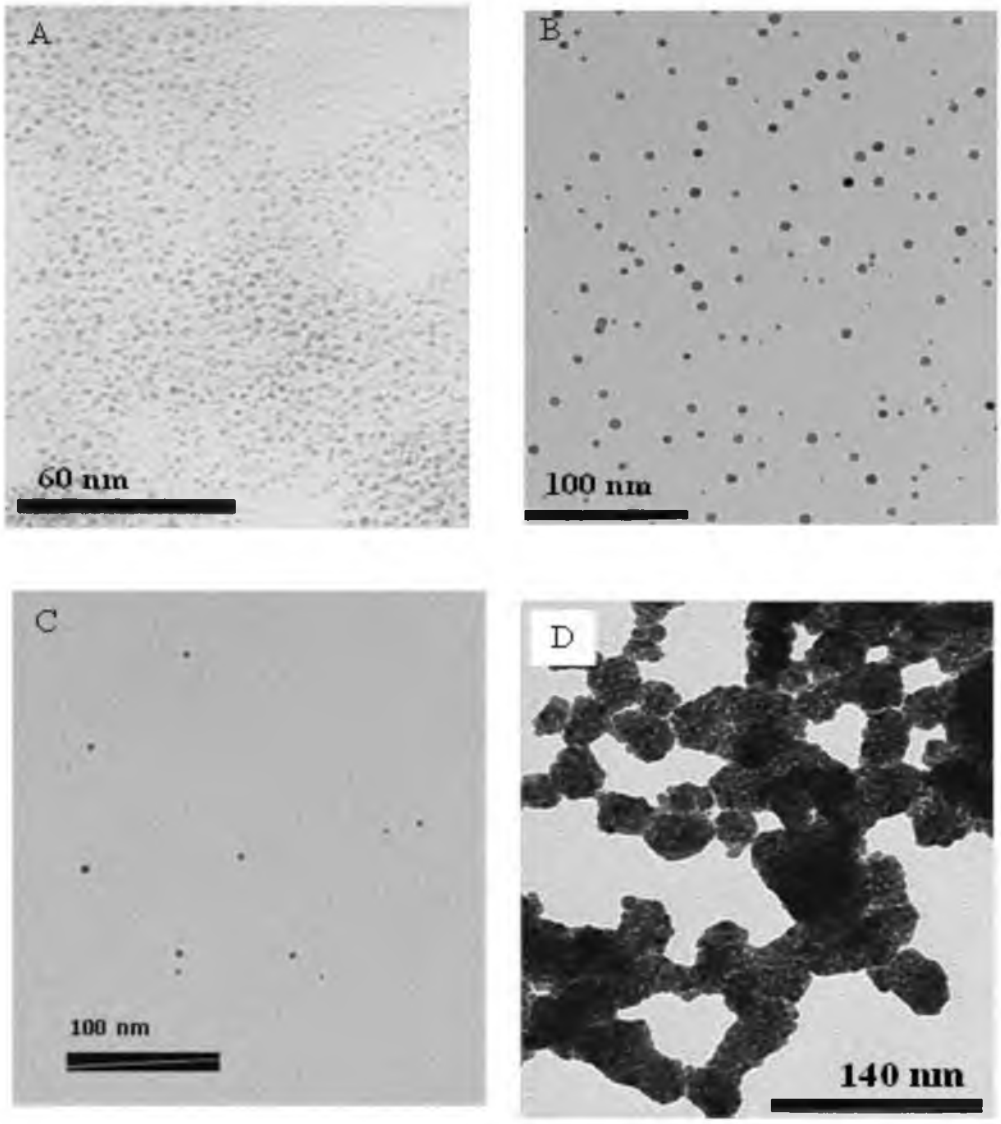

Figure 4.3. TEM images of the NPs at different time points during the synthesis: (A) 5 min, (B) 15 min, (C) 25 min and (D) 60 min after addition of 9-BBN.

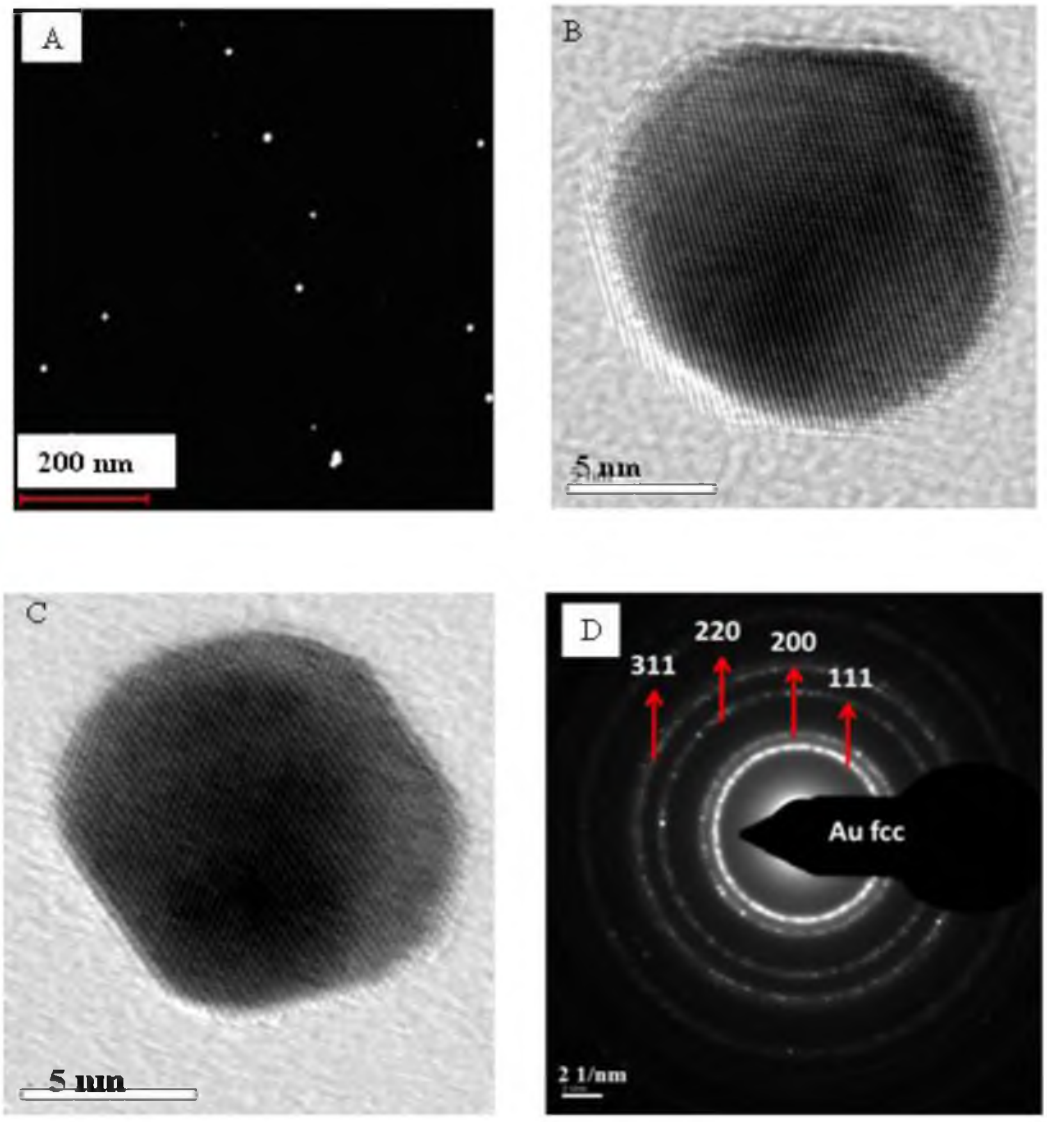

Figure 4.4. (A) HAADF-STEM image of the NPs at 25 min in Figure 3C above. (B) and (C) Representative HRTEM images of the NPs at 25 min. (D) SAED diffraction pattern of the NPs which was indexed to Au fcc.

4.3.2 Growth kinetics of the soft ligand stabilized NPs

Extensive work has been done to determine the growth kinetics and mechanism of NP growth.[36, 49-52] In order to describe growth kinetics and mechanisms for nanoparticles, it is important to establish the origin and identity of the species present in the reaction mixture. It is also important to determine whether the presence of the species is supported by the predicted mechanisms. However, a review of the literature confirms that the understanding of the mechanisms leading to the formation of NPs still has gaps owing to lack of time resolved *in-situ* information about precursor reduction and the NP growth process. Real time *in-situ* monitoring of precursor reduction, oxidation states of metal, size distribution and number of particles formed can provide crucial information on the nucleation and growth of the NPs.[53, 54] The NP formation reactions are usually rapid, occurring in the millisecond time scale and therefore cannot be monitored with commonly available instruments like UV-vis and TEM.[54] As a result, it is challenging to establish with certainty the identities of the species formed during the short time period of the reaction and nanoparticle formation.

The classical theory of the growth mechanism of monodisperse colloids was proposed by LaMer and Dinegar.[49] LaMer theory is based on a nucleation and diffusion model. Nucleation occurs in a short burst during which time gold atoms nucleate to form a primary particles. In the growth stage, nucleation does not occur, instead, particles grow by the deposition of atoms onto the primary particles through a diffusion driven process.[38] This model however ignores particle-particle interactions. [55] A close examination of the NPs produced in this study shows that the NPs are not single crystals but are made up of smaller NP units (Figure 4.4B and 4.4C). This has been observed for

other NP systems as well.[43, 51] Recent studies have shown that the formation of NPs by most solution phase syntheses cannot be explained by the LaMer model. [56-60]

A model of growth based on an aggregation mechanism supported by both experiment and theoretical calculations has been proposed.[52, 61-65] These studies have established that this model accounts for most NP growth systems. Zheng et al.[62] confirmed this model by observing single particle growth trajectories for platinum nanoparticles. The study confirmed that particle interactions play an important role in the formation kinetics of the NPs. In the present study, we observed that the NPs had a broad size distribution, which narrowed with time. This is an indication of particle-particle interactions by coalescence or an aggregative growth mechanism. Bimodal distribution of NPs is evidence for aggregative growth.[55] Two populations of small and large NPs are observed before uniform size NPs were formed (Figure 4.3B) Coalescence or aggregation stops when all the particles have been consumed leading to the end of the growth process and the establishment of a narrow size distribution of the NPs.[66] Polte et al. observed that in the absence of a stabilizing agent, growth can continue for long periods of time (in their case, 24 h) driven entirely by coalescence and not monomer addition.[54] This model based on an aggregation mechanism accounts for the observations in this study and is summarized in Figure 4.5.

We can conclude that the NP growth process in this study proceeds by coalescence. After about 20-25 min, a uniform size distribution is established and the growth process can be arrested at this time point. This presents the opportunity to introduce desired ligands into the reaction mixture to stabilize the NPs. The NPs are not strongly stabilized by Et_3P and Cl^- ions.

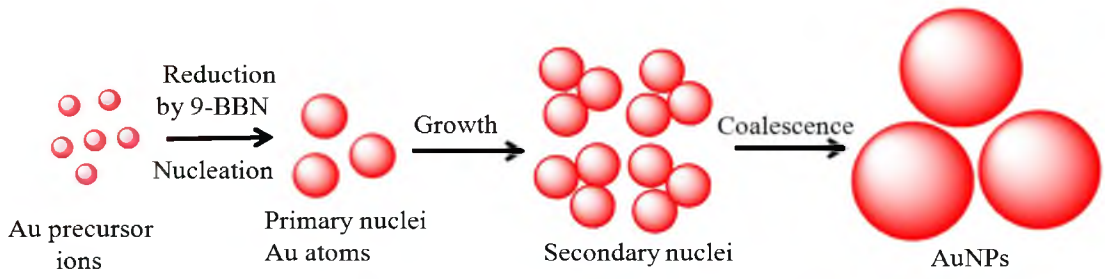

Figure 4.5. Growth stages of the soft ligand stabilized NPs following the aggregative growth model.

These weakly adsorbed ligands can be replaced by the incoming ligands. In this study, we employ this strategy to functionalize the NPs with 2, 2'-bipyridyl and 4, 4'-bipyridyl to make AuNPs stabilized by the respective bipyridyls.

4.3.3 Investigations to confirm the identity of the soft ligands

In order to investigate the identity of the stabilizing agents for the soft ligand stabilized AuNPs, two sets of experiments were performed. The aim of these experiments was to determine the ligands/ions present on the AuNPs surface by X-ray photoelectron spectroscopy (XPS). The AuNPs were immobilized on a 3-mercaptopropyltriethoxy silane (MPTES) modified glass surface. The thiol functional group on the MPTES was used to bind the AuNPs. The procedure for the silanization of the glass surface is described in detail in the experimental section. Immobilization of the AuNPs on a silanized glass surface presents a way to control the assembly of the AuNPs on the glass surface and to obtain uniform coverage of the AuNPs on the glass surface. The results obtained before and after replacement of the soft ligands can thus be easily compared. In the first experiment, the MPTES functionalized glass coverslips were incubated for 2 h in the freshly synthesized AuNPs solution.

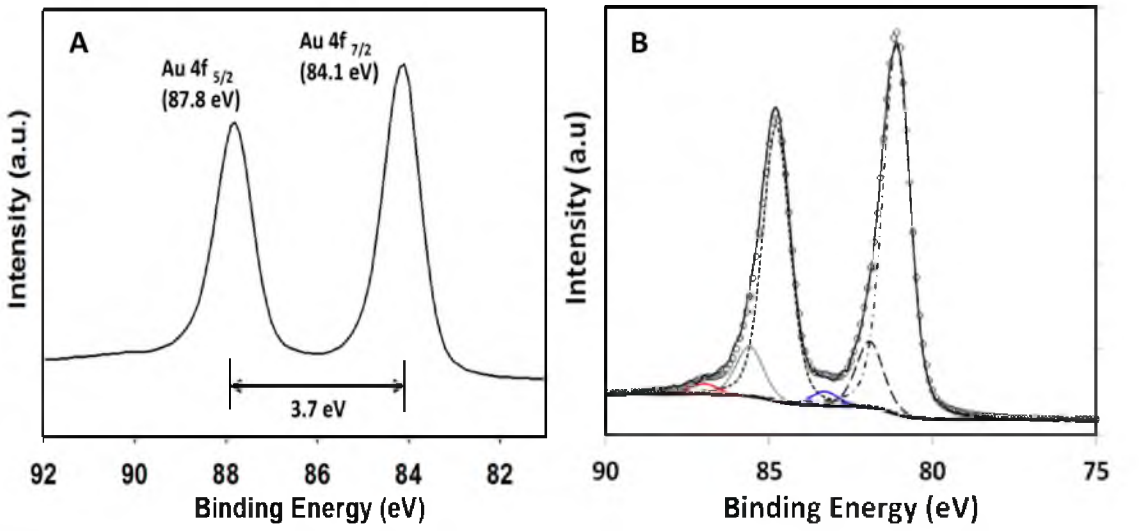

Figure 4.6. (A) XPS high resolution scan for the Au 4f photoelectron peak for the AuNPs on MPTES functionalized glass. The peak position and peak to peak distance of the doublet are consistent with Au^0. (B) XPS curve fitting of the Au 4f peak using a Gaussian-Lorentzian line shape.

The AuNPs functionalized glass substrate was then washed with copious amount of solvents in order to remove loosely adsorbed molecules or ions from nanoparticles surface. Figure 4.6A shows the XPS peak position of gold 4f doublet, $4f_{5/2}$ (87.8 eV), $4f_{7/2}$, (84.1 eV). The peak-to-peak distance (3.7 eV) clearly verifies that most of the gold was present in the Au^0 oxidation state.[9] This was confirmed by fitting the Au 4f peak using a Gaussian-Lorentzian line shape (Figure 4.6B). The results indicate that 89.8 % of the Au is present as Au (0) while Au (I) and Au (III) make up 1.8 % and 8.4 % , respectively. The peaks associated with P (2p) at 131.6 eV from Et_3P and Cl (2P) at 198 eV also were observed.[33, 67]

In the second set of experiments, the freshly prepared AuNPs were dropcast on an unsilanized glass coverslip. The aim of this step was to ascertain the presence of the ligands on the unfunctionalized glass surface for comparison with the functionalized surface in the first experiment. In this case, peaks associated with P (2p) at 131.6 eV from

Et_3P and Cl (2P) at 198 eV were again observed. The XPS results indicate that the AuNPs were stabilized by a mixture of Et_3P and chloride ions which were electrostatically adsorbed on the surface of the gold nanoparticles. These soft ligands provided the stability of the AuNPs in organic solvent and prevented agglomeration.

4.3.4 Removal of Et_3P and Cl^- ions

In order to investigate the ease of replacing the stabilizing agents with stronger ligands such thiols, ligand exchange reactions were performed on the NPs. *Ex-situ* modification of the surface bound NPs by the thiol, 11-mercaptoundecanol (MUOH) was done on a silanized glass surface. As described previously, the AuNPs stabilized by Et_3P and Cl^- ions were incubated on MPTES functionalized glass surface. The AuNPs containing glass surface was then rinsed with 1:1 acetonitrile/THF solvent and dried by flow of N_2. The nanoparticles were then incubated with a 1mM ethanolic solution of 11-mercaptoundecanol (MUOH) for 2 h at room temperature. The sample was washed using copious amount of ethanol in order to remove loosely bound thiols as well as other molecules or ions from the AuNPs surface. The sample was then analyzed by XPS. Interestingly peaks associated with P (2p) were not observed.

The data showed a peak for S (2p) at 162.4 eV (Figure 4.7) which points to a sulfur-Au interaction through a thiolate bond [68, 69] along with gold 4f doublets $4f_{5/2}$ (87.8 eV) and $4f_{7/2}$, (84.1 eV). XPS high resolution scans for the P (2p) region for the sample before and after ligand exchange shows that phosphorus is absent after ligand exchange (Figure 4.7). This result suggests that when the mixture of Et_3P and Cl^- ions stabilized AuNPs was incubated in the MUOH solution, the thiol ligands replaced the Et_3P

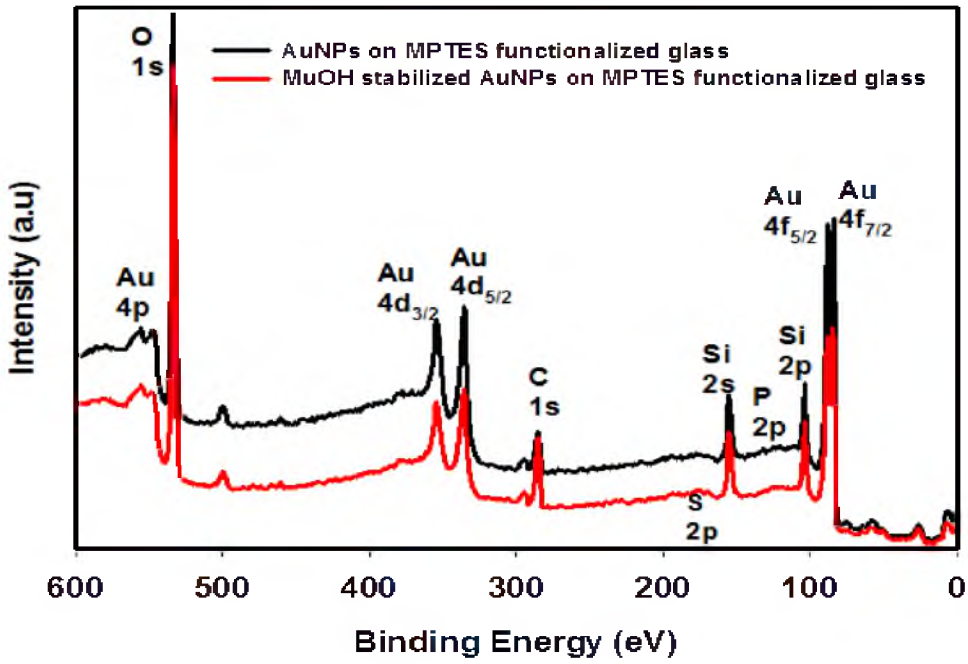

Figure 4.7. XPS survey scans for the AuNPs on MPTES functionalized glass and MUOH stabilized AuNPs on MPTES functionalized glass.

molecules from the NP surface and produced thiolated AuNPs. The reason for this is that Et_3P does not form strong Au-P bonds and can be displaced by the thiols to form the stronger Au-S bond.

4.3.5 *In-situ* synthesis of 2,2'- and 4,4'-bipyridyl AuNPs

The 9-BBN induced generation of soft ligand stabilized AuNPs was performed as described previously. TEM analysis was done during the NP formation at different time periods to determine the particles size and dispersion. Results show that after 25 min, the AuNPs are of narrow size distribution. Due to the slow reduction of the reaction induced by 9-BBN, introduction of the ligands at the 25 min time point enables the growth process to be terminated, which would not be possible if a stronger reducing agent like $NaBH_4$ was used . The result is that AuNPs of narrow size dispersion functionalized with

the desired ligand are obtained. However, if the ligands were not introduced at that time point, TEM analysis indicates that the particles would undergo further growth which eventually produces polydisperse particles. We therefore added 2, 2'- and 4, 4'-bipyridyls to the reaction mixture at the 25 min time point in order to terminate the growth process of the nanoparticles and generate AuNPs stabilized with the respective bipyridyl ligands according to Scheme 4.2.

On addition of 2,2'-bipyridyl and 4,4'-bipyridyl dissolved in THF to the AuNP solution, the color of the solution changed from reddish pink to deep red. The mixture was allowed to react for 20 min and the color of the solution changed to purple with time. This was an indication that the bipyridyls had attached to the AuNP surface.[70] Precipitation was not observed but solids were obtained after centrifugation of the AuNP solution. After cleaning, the solid was dissolved in ethanol. We observed that the bipyridyl stabilized AuNPs could only dissolve in polar solvents.

Scheme 4.2. Synthesis of 2, 2'- and 4, 4'-bipyridyl stabilized AuNPs.

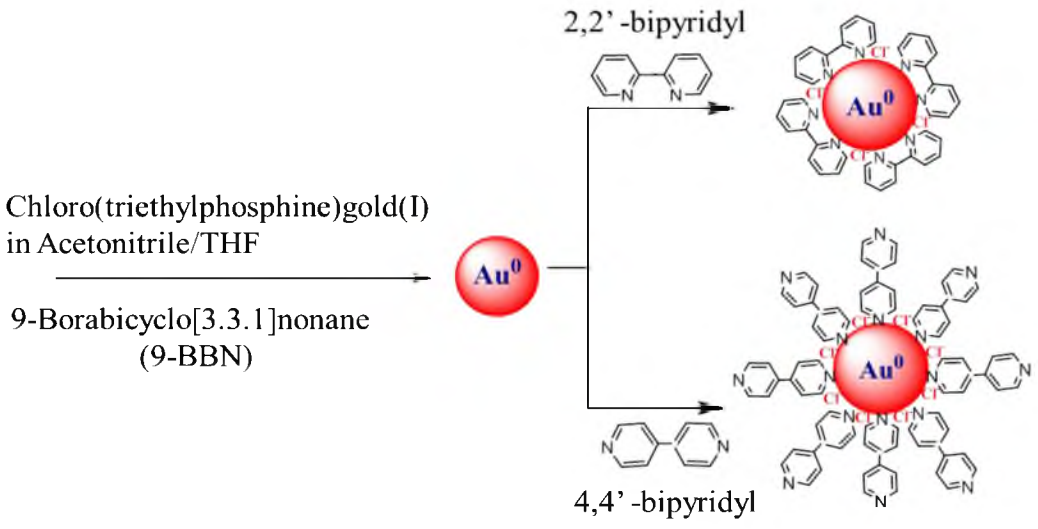

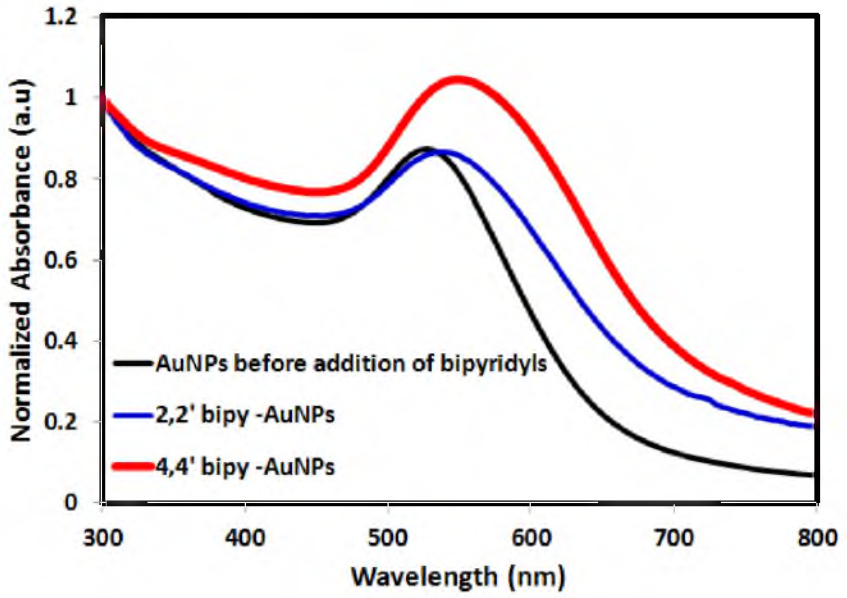

Figure 4.8. UV-vis absorption spectra of the 2,2'-bipyridyl and 4,4'-bipyridyl AuNPs.

The two bipyridyls attach to the gold via the nitrogen atom. The UV-vis spectra of the bipyridyl AuNPs was slightly different owing to the different orientations of the 2,2'-bipy and 4.4'-bipy on the surface of the gold.[71, 72] This difference is due to the different position of the nitrogen atoms in the respective molecules. The UV-vis spectra of the soft ligand NP solution had maximum absorbance (λ_{max}) at ~ 530 nm, while the 2,2'-bipyridyl and 4,4'-bipyridyl AuNPs exhibited maximum absorbance at 535 nm and 545 nm respectively (Figure 4.8).

Samples of the 2,2'-bipyridyl and 4,4'-bipyridyl AuNPs were deposited on copper grids for TEM analysis. The size of the NPs before functionalization with the bipyridyl ligands was 3.6 ± 0.94 nm. The size of the 4,4'-bipy and 2,2'-bipyridyl AuNPs was determined to be 3.5 ± 0.55 nm and 3.1 ± 0.95 nm respectively. TEM images of the NPs are presentedin Figure 4.9. We note that there was no significant change in the sizes of the NPs after functionalization with the bipyridyl ligands.

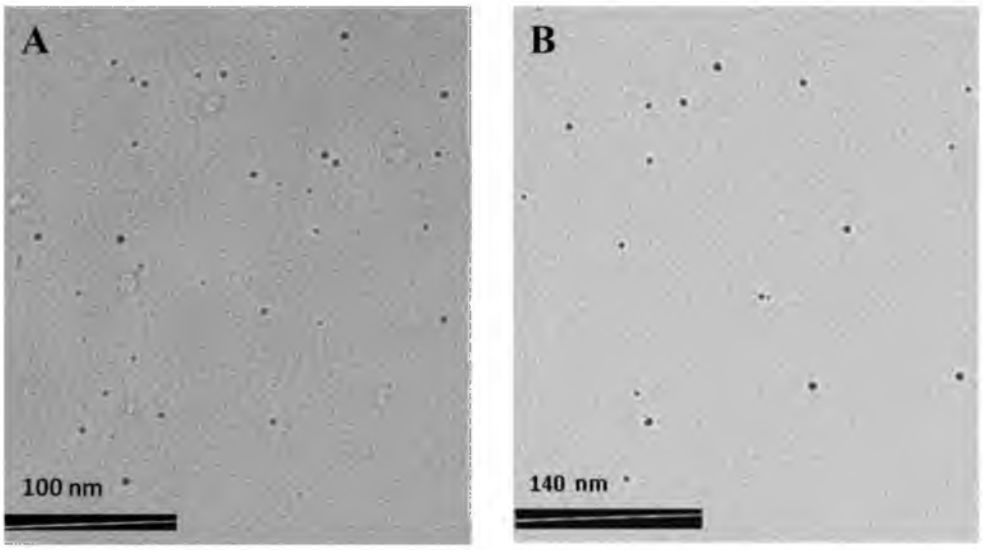

Figure 4.9. TEM images of (A) 4,4'-bipy AuNPs and (B) 2,2'-bipy AuNPs.

In order to investigate the nature of interaction between the bipyridyl ligands and the AuNPs, XPS measurements were performed on the 2,2'- and 4,4'-bipyridyl AuNPs deposited on silicon wafers. The N 1s spectra were resolved by fitting into three components at 399.5, 401.4 and 403.4 eV for 2,2'-bipyridyl AuNPs and 399.6, 400.3 and 402.8 eV for 4,4'-bipyridyl AuNPs (Figure 4.10 A and B). The peaks at 399 eV indicate that the bipyridyls are coordinated to the AuNPs compared to 398 eV for free ligands.[73-75] The shift to higher binding energy occurs because the bipyridyls donate electrons to the Au atoms via the nitrogen atom.[76] respectively (Figure 4.10C and D). The peaks at 401-403 eV are due to the protonation of the of the bipyridyl nitrogen.[74, 75] Therefore, the high binding energy peaks indicate the presence of a N^+ species. The C 1s spectra for both 2,2'- and 4,4'-bipyridyl AuNPs show peaks at 285.9 and 285.2 eV.

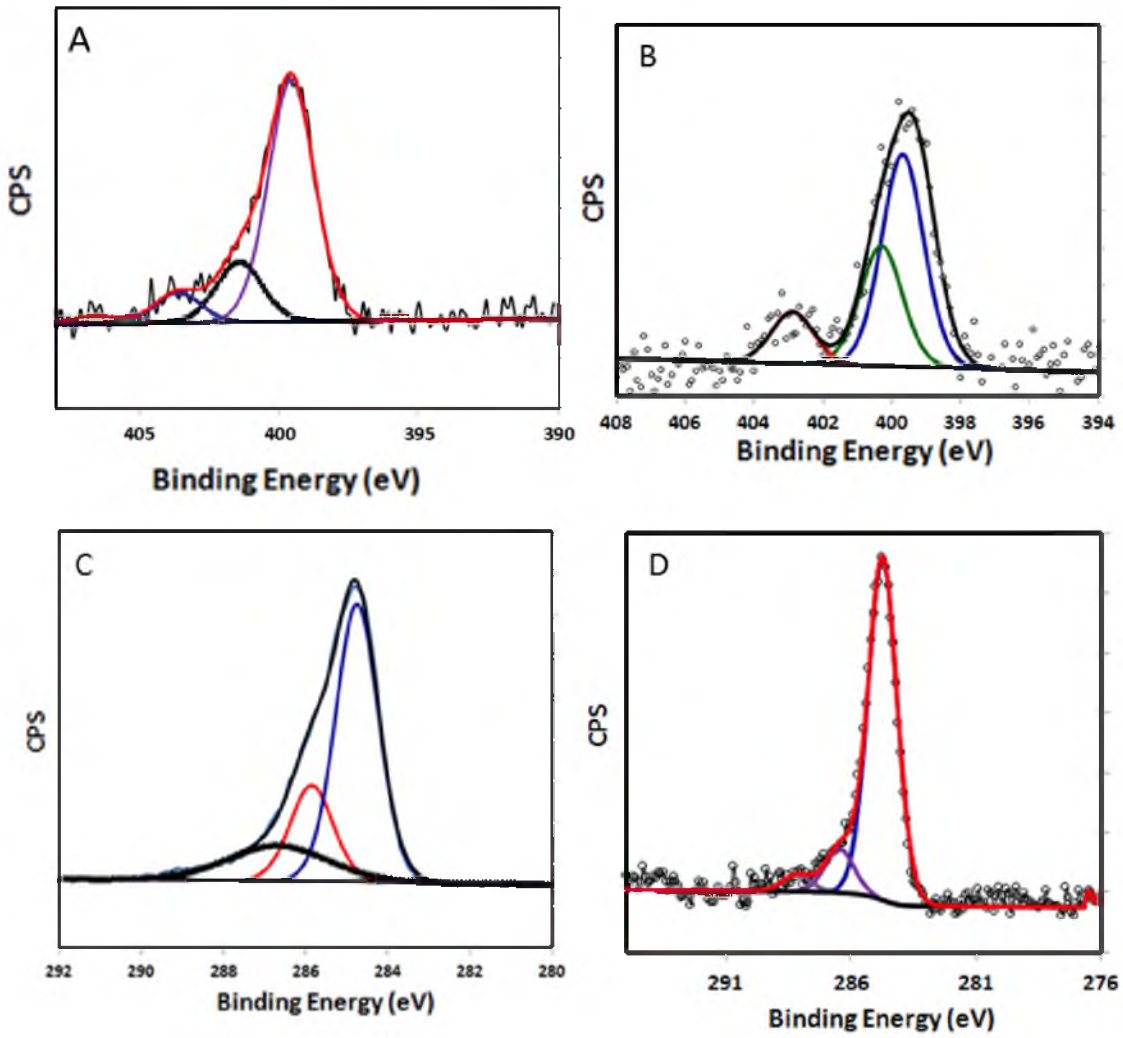

Figure 4.10. N 1s spectra of (A) 2,2'-bipyridyl AuNPs and (B) 4,4'-bipyridyl AuNPs. C 1s spectra of (C) 2,2'-bipyridyl AuNPs and (D) 4,4'-bipyridyl AuNPs.

These peaks are attributed to the aromatic carbons of the bipyridyl ligands.[73] The peaks at 284.8 eV are assigned to adventitious carbon. The peaks at a higher binding energy of 287.8 and 288.3 eV for 2,2'- and 4,4'-bipyridyl AuNPs, respectively, are due to hydrogen bonding of the bipyridyl nitrogen.[75] The Au 4f spectra indicate that Au exists primarily as Au atoms.

These XPS results confirm that the bipyridyl ligands are attached to the AuNPs. Bipyridyl molecules and especially 4,4'-bipyridyl have been known to enhance redox reactions and as a result, they have generated great interest in electron transfer reactions.[77] Bipyridyls attached to metal surfaces have also been used as nanoscale electronic switches and could be useful in the fabrication of molecular electronic devices.[78]

4.4 Conclusion

A single-step synthesis using the mild reducing agent 9-BBN and the gold salt, Et_3PAuCl to produce gold nanoparticles (AuNPs) without incorporating additional stabilizing agents in the reaction mixture has been presented. 9-BBN has been shown to be a mild reducing agent that enables the slow generation of AuNPs which allows greater control over the synthetic process. XPS analysis indicates that chloride ions and Et_3P from the precursor co-adsorb on the surface of the nanoparticles and act as capping ligands to stabilize the particles. The average size of the NPs was determined by TEM to be 4 nm. This synthetic procedure exhibited great sensitivity to changes in reaction conditions. For example, changes in nuclei concentration caused by mechanical agitation led to arrest of the growth of the NPs. We also observed that during the growth process

of the NPs, polydisperse NPs are initially formed. The size distribution of the NPs narrowed about 25 min into the growth process, producing NPs with uniform size. HRTEM and SAED analysis of the NPs indicated that the NPs are formed by coalescence of individual smaller NPs. We demonstrated that *in-situ* addition of capping ligands such as bipyridyls to replace the soft ligand Et_3P restricted nanoparticle growth and significantly narrowed the size dispersion of the NPs. Incorporation of the ligand also provided long term stabilization of the resulting NPs. 2,2'- and 4,4'-bipyridyl-functionalized AuNPs were prepared using strategy. These results show that the formation of the soft ligand stabilized NPs is best described by an aggregative growth model.

4.5 References

(1) Song, J.; Kim, D.; Lee, D. *Langmuir* **2011**, *27*, 13854-13860.

(2) Brown, L. O.; Hutchison, J. E. *J. Am. Chem. Soc.* **1999**, *121*, 882-883.

(3) Varnavski, O.; Ramakrishna, G.; Kim, J.; Lee, D.; Goodson, T. *J. Am. Chem. Soc.* **2009**, *132*, 16-17.

(4) Kim, F.; Song, J. H.; Yang, P. *J. Am. Chem. Soc.* **2002**, *124*, 14316-14317.

(5) Mahmoud, M. A.; Saira, F.; El-Sayed, M. A. *Nano Lett.* **2010**, *10*, 3764-3769.

(6) Mahmoud; Tabor, C. E.; El-Sayed, M. A.; Ding, Y.; Wang, Z. L. *J. Am. Chem. Soc.* **2008**, *130*, 4590-4591.

(7) Dahl, J. A.; Maddux, B. L. S.; Hutchison, J. E. *Chem. Rev.* **2007**, *107*, 2228-2269.

(8) Jahn, W. *J. Struct. Biol.* **1999**, *127*, 106-112.

(9) Leff, D. V.; Brandt, L.; Heath, J. R. *Langmuir* **1996**, *12*, 4723-4730.

(10) Lopez, N.; Janssens, T. V. W.; Clausen, B. S.; Xu, Y.; Mavrikakis, M.; Bligaard, T.; Nørskov, J. K. *J. Catal.* **2004**, *223*, 232-235.

(11) Daniel, M.-C.; Astruc, D. *Chem. Rev.* **2004**, *104*, 293-346.

(12) Han, J.; Liu, Y.; Guo, R. *J. Am. Chem. Soc.* **2009**, *131*, 2060-2061.

(13) Debouttière, P. J.; Roux, S.; Vocanson, F.; Billotey, C.; Beuf, O.; Favre-Réguillon, A.; Lin, Y.; Pellet-Rostaing, S.; Lamartine, R.; Perriat, P.; Tillement, O. *Adv. Funct. Mater.* **2006**, *16*, 2330-2339.

(14) Liu, Y.; Tsunoyama, H.; Akita, T.; Xie, S.; Tsukuda, T. *ACS Catalysis* **2011**, *1*, 2-6.

(15) Wang, S.; Yao, H.; Sato, S.; Kimura, K. *J. Am. Chem. Soc.* **2004**, *126*, 7438-7439.

(16) Park, J.; Joo, J.; Kwon, S. G.; Jang, Y.; Hyeon, T. *Angew. Chem. Int. Ed.* **2007**, *46*, 4630-4660.

(17) Peng, Z. A.; Peng, X. *J. Am. Chem. Soc.* **2002**, *124*, 3343-3353.

(18) Montalti, M.; Prodi, L.; Zaccheroni, N.; Baxter, R.; Teobaldi, G.; Zerbetto, F. *Langmuir* **2003**, *19*, 5172-5174.

(19) Kuo, C.-T.; Yu, J.-Y.; Huang, M.-J.; Chen, C.-H. *Langmuir* **2010**, *26*, 6149-6153.

(20) Mpourmpakis, G.; Vlachos, D. G. *Phys. Rev. Lett.* **2009**, *102*, 155505.

(21) Sardar, R.; Shumaker-Parry, J. S. *J. Am. Chem. Soc.* **2011**, *133*, 8179-8190.

(22) Mpourmpakis, G.; Caratzoulas, S.; Vlachos, D. G. *Nano Lett.* **2010**, *10*, 3408-3413.

(23) Balasubramanian, R.; Guo, R.; Mills, A. J.; Murray, R. W. *J. Am. Chem. Soc.* **2005**, *127*, 8126-8132.

(24) Turkevich, J.; Stevenson, P. C.; Hillier, J. *Discuss. Faraday Soc.* **1951**, *11*, 55.

(25) Schmid, G.; Pfeil, R.; Boese, R.; Bandermann, F.; Meyer, S.; Calis, G. H. M.; van der Velden, J. W. A. *Chem. Ber.* **1981**, *114*, 3634-3642.

(26) Kim, S.-W.; Kim, S.; Tracy, J. B.; Jasanoff, A.; Bawendi, M. G. *J. Am. Chem. Soc.* **2005**, *127*, 4556-4557.

(27) Schmid, G. *Inorg. Synth.* **1990**, *27*, 214-218.

(28) Brust, M.; Walker, M.; Bethell, D.; Schiffrin, D. J.; Whyman, R. *Chem. Commun.* **1994**, *7*, 801-802.

(29) Warner, M. G.; Reed, S. M.; Hutchison, J. E. *Chem. Mater.* **2000**, *12*, 3316-3320.

(30) Jana, N. R.; Peng, X. *J. Am. Chem. Soc.* **2003**, *125*, 14280-14281.

(31) Sardar, R.; Shumaker-Parry, J. S. *Chem. Mater.* **2009**, *21*, 1167-1169.

(32) Weare, W. W.; Reed, S. M.; Warner, M. G.; Hutchison, J. E. *J. Am. Chem. Soc.* **2000**, *122*, 12890-12891.

(33) Shem, P. M.; Sardar, R.; Shumaker-Parry, J. S. *Langmuir* **2009**, *25*, 13279-13283.

(34) Fink, J.; Kiely, C. J.; Bethell, D.; Schiffrin, D. J. *Chem. Mater.* **1998**, *10*, 922-926.

(35) Roth, P. J.; Theato, P. *Chem. Mater.* **2008**, *20*, 1614-1621.

(36) Liu, X.; Worden, J. G.; Huo, Q.; Brennan, J. P. *J. Nanosci. Nanotechnol.* **2006**, *6*, 1054-1059.

(37) Schulz-Dobrick, M.; Sarathy, K. V.; Jansen, M. *J. Am. Chem. Soc.* **2005**, *127*, 12816-12817.

(38) Hiramatsu, H.; Osterloh, F. E. *Chem. Mater.* **2004**, *16*, 2509-2511.

(39) Reilly, S. M.; Krick, T.; Dass, A. *J. Phys. Chem. C* **2010**, *114*, 741-745.

(40) Sardar, R.; Shumaker-Parry, J. S. *Nano Lett.* **2008**, *8*, 731-736.

(41) Ott, L. S.; Finke, R. G. *Inorg. Chem.* **2006**, *45*, 8382-8393.

(42) Bardaji, M.; Uznanski, P.; Amiens, C.; Chaudret, B.; Laguna, A. *Chem. Commun.* **2002**, 598-599.

(43) Liu, X.; Atwater, M.; Wang, J.; Dai, Q.; Zou, J.; Brennan, J. P.; Huo, Q. *J. Nanosci. Nanotechnol.* **2007**, *7*, 3126-3133.

(44) Li, D.; Kaner, R. B. *J. Am. Chem. Soc.* **2005**, *128*, 968-975.

(45) Ackerson, B. J.; Pusey, P. N. *Phys. Rev. Lett.* **1988**, *61*, 1033-1036.

(46) Amos, R. M.; Rarity, J. G.; Tapster, P. R.; Shepherd, T. J.; Kitson, S. C. *Physical Review E* **2000**, *61*, 2929-2935.

(47) Blaak, R.; Auer, S.; Frenkel, D.; Löwen, H. *Phys. Rev. Lett.* **2004**, *93*, 068303.

(48) Wang, Z. L. *J. Phys. Chem. B* **2000**, *104*, 1153-1175.

(49) LaMer, V. K.; Dinegar, R. H. *J. Am. Chem. Soc.* **1950**, *72*, 4847-4854.

(50) Brennan, J. P.; Liu, X.; Huo, Q. *J. Comput. Theor. Nanosci.* **2007**, *4*, 127-132.

(51) Privman, V.; Goia, D. V.; Park, J.; Matijevic, E. *J. Colloid Interface Sci.* **1999**, *213*, 36-45.

(52) Compton, O. C.; Osterloh, F. E. *J. Am. Chem. Soc.* **2007**, *129*, 7793-7798.

(53) Abecassis, B.; Testard, F.; Spalla, O.; Barboux, P. *Nano Lett.* **2007**, *7*, 1723-1727.

(54) Polte, J.; Erler, R.; Thünemann, A. F.; Sokolov, S.; Ahner, T. T.; Rademann, K.; Emmerling, F.; Kraehnert, R. *ACS Nano* **2010**, *4*, 1076-1082.

(55) Shields, S. P.; Richards, V. N.; Buhro, W. E. *Chem. Mater.* **2010**, *22*, 3212-3225.

(56) Besson, C.; Finney, E. E.; Finke, R. G. *J. Am. Chem. Soc.* **2005**, *127*, 8179-8184.

(57) Finney, E. E.; Finke, R. G. *Chem. Mater.* **2008**, *20*, 1956-1970.

(58) Matijevic, E. *Chem. Mater.* **1993**, *5*, 412-426.

(59) Privman, V. *Ann. N.Y. Acad. Sci.* **2009**, *1161*, 508-525.

(60) Kumar, S.; Davis, T. M.; Ramanan, H.; Penn, R. L.; Tsapatsis, M. *J. Phys. Chem. B* **2007**, *111*, 3398-3403.

(61) Suber, L.; Sondi, I.; Matijevic, E.; Goia, D. V. *J. Colloid Interface Sci.* **2005**, *288*, 489-495.

(62) Zheng, H.; Smith, R. K.; Jun, Y.-w.; Kisielowski, C.; Dahmen, U.; Alivisatos, A. P. *Science* **2009**, *324*, 1309-1312.

(63) Park, J.; Privman, V.; Matijevic, E. *J. Phys. Chem. B* **2001**, *105*, 11630-11635.

(64) van Embden, J.; Sader, J. E.; Davidson, M.; Mulvaney, P. *J. Phys. Chem. C* **2009**, *113*, 16342-16355.

(65) Njoki, P. N.; Luo, J.; Kamundi, M. M.; Lim, S.; Zhong, C.-J. *Langmuir* **2010**, *26*, 13622-13629.

(66) Sugimoto, T. *Fine particles : Synthesis, Characterization, and Mechanisms of Growth* Marcel Dekker New York 2000.

(67) Uvdal, K.; Persson, I.; Liedberg, B. *Langmuir* **1995**, *11*, 1252-1256.

(68) Vericat, C.; Benitez, G. A.; Grumelli, D. E.; Vela, M. E.; Salvarezza, R. C. *J. Phys.: Condens. Matter* **2008**, *20*, 184004.

(69) Bourg, M.-C.; Badia, A.; Lennox, R. B. *J. Phys. Chem. B* **2000**, *104*, 6562-6567.

(70) Joo, S. W. *Spectrosc. Lett.* **2006**, *39*, 85-96.

(71) Wandlowski, T.; Ataka, K.; Mayer, D. *Langmuir* **2002**, *18*, 4331-4341.

(72) Noda, H.; Minoha, T.; Wan, L.-J.; Osawa, M. *J. Electroanal. Chem.* **2000**, *481*, 62-68.

(73) Chong, S. V.; Tallon, J. L. *J. Phys. Chem. Solids* **2010**, *71*, 303-308.

(74) Hamoudi, H.; Döring, K.; Chesneau, F.; Lang, H.; Zharnikov, M. *J. Phys. Chem. C* **2012**, *116*, 861-870.

(75) Zubavichus, Y.; Zharnikov, M.; Yang, Y.; Fuchs, O.; Umbach, E.; Heske, C.; Ulman, A.; Grunze, M. *Langmuir* **2004**, *20*, 11022-11029.

(76) Liu, W.; Yang, X.; Xie, L. *J. Colloid Interface Sci.* **2007**, *313*, 494-502.

(77) Monk, P. M. S. *The Viologens: Physicochemical Properties, Synthesis and Applications of the Salts of 4,4'-Bipyridine*; Wiley: Chichester, New York 1998.

(78) Gittins, D. I.; Bethell, D.; Schiffrin, D. J.; Nichols, R. J. *Nature* **2000**, *408*, 67-69.

CHAPTER 5

INVESTIGATION OF THE FACTORS AFFECTING THE STABILITY AND STRUCTURE OF TPP-AuNPs IN AQUEOUS MEDIUM

5.1 Introduction

Metallic nanoparticles have been the focus of research in recent times because of their unique properties emanating from their size and shape.[1, 2] Of these NPs, gold NPs (AuNPs) have elicited interest due to applications in catalysis,[3, 4] biotagging,[5, 6] biological assays,[7] sensors,[8, 9] electronics,[10, 11] imaging contrast agents[12] and drug delivery.[13] An understanding of controlling stability in colloidal systems is important so as to know how to prevent aggregation which can render the NPs unusable for most of these applications. Interparticle interactions are determined by a host of forces, including van der Waals attractive and Coloumbic repulsive forces. The nature of the solvent and the ligands or charges on the surface of the NPs plays an important role. [14] In addition, the electronic character of the AuNPs is affected to a great extent by the solvent environment of the particles.[15, 16] A wide variety of stabilizers have been reported in literature, including organic ligands such as phosphines, amines and thiols, polymers, dendrimers, solvents, microgels and ionic liquids.[17-23] Generally, stabilization of NPs and colloids can be explained by two phenomena: electrostatic and steric stabilization. Electrostatic

stabilization is due to adsorption of ions on the NPs leading to the generation of an electrical double layer as explained by the Derjaugin-Landau-Verwey-Overbeek (DLVO) theory.[24, 25] A balance between Coloumbic repulsive and van der Waals attractive forces of the charged NPs is maintained. Steric stabilization occurs due to adsorption of bulky molecules on the surface of the NPs. These molecules minimize the van der Waals attractions of the NPs.[23]

For biomedical and bioanalytical applications, it is important that the nanoparticles be soluble and stable in water. This has led to development of synthetic methods which involve post synthetic modification of hydrophobic ligand-stabilized NPs to make them water soluble and stable. Of the noble metal NPs used in biological applications, AuNPs are easy to synthesize and as a result have been preferred because of their resistance to oxidation in water and electrolytic solutions compared to other metal NPs, for example silver.[26] Several strategies for making water soluble NPs have been reported. For example, water soluble AuNPs stabilized by derivatized hydrophilic phosphines for protein labeling[27] and peptide stabilized NPs[26] have been reported. PEGylation of AuNPs[28] and the use of dual-interaction ligands[29] are other strategies that have been used to prepare water-soluble NPs. One of the challenges is balancing the need for stability of the NPs and the ability to use the NPs for biological applications. For example, functionalizing the NPs with silica shells imparts them with stability but hinders their application for biological studies.[30] PEGylated AuNPs have also been reported to be long circulating in the body, thus impacting timely clearance from the body.[28] An increase in the hydrodynamic radius of PEGylated NPs is also undesirable because it makes uptake into cells challenging.[31] While post synthetic functionalization

with the appropriate ligands imparts water solubility to the NPs, modified NPs can exhibit low stability as well as nonspecific binding with biomolecules.[32] In some cases, it is important to preserve the ligands for applications such as imaging.[6, 33] Preserving the ligands ensures better visibility of the NPs especially when the NPs are localized at specific positions or are used to mark specific sites.[34] The water soluble Au_{55} cluster also needs to keep the triphenylphosphine-monosulfonic acid ligand to maintain its stability.[6] The hydrophobic ligand stabilized cluster is unstable in organic solvents. The water soluble Au_{55} cluster is prepared by using the substituted ligand, triphenylphosphine-monosulfonic acid.[35] The charged ligand increases the stability of the cluster in water.

The driving forces involved with NP aggregation are complex. Solvent effects,[23] intermolecular hydrogen bonding,[36] electrostatic or van der Waals forces[37] and chemical binding[38] can individually or cooperatively cause aggregation. These forces can be manipulated to induce and selectively control aggregation of NPs to achieve a variety of Au architectures, such as 1D, 2D or 3D assemblies with tunable optoelectronic properties.[39] For instance, using a solvent with a specific dielectric constant can cause changes in the electrostatic and dipolar interaction potentials and lead to aggregation.[25] Addition of salt to AuNP solution leads to shielding of charge repulsion culminating in the collapse of the Debye layer and subsequent aggregation.[24] A major challenge is to understand and ultimately control NP stability.

Investigation of the stability of NPs requires the use of multiple methods in order to corroborate data obtained by the different methods. *In-situ* methods are preferred to *ex-situ* ones because of problems associated with sample aggregation during sample preparation for analysis. For example, transmission electron microscopy (TEM) is used

routinely to assess aggregation but it is difficult to rule out aggregation artifacts due to reorganization induced by drying on the TEM grid.[40] *In-situ* monitoring of the shape and position of the surface plasmon bands of the NPs can provide information about aggregation, especially when monitoring this process over time. Changes in the hydrodynamic radius of the NPs as measured by dynamic light scattering (DLS) as well as variation in the zeta potential also can indicate whether the NPs are aggregated. *In-situ* small-angle X-ray scattering (SAXS) provides information about the size and shape of the NPs whereas wide-angle X-ray scattering (WAXS) gives information about crystal dimensions.[40] X-ray absorption fine structure (XAFS) can be used to obtain information about aggregation dynamics.[41] However, these techniques can only be performed at a synchrotron radiation facility thereby limiting their availability.

Herein, we report the results of the investigation of the stability of triphenylphosphine stabilized AuNPs.[19] This is the first reported case of TPP-AuNPs being soluble in water without derivatizing the phosphine ligand. We investigated the influence of ionic strength and the concentration of $NaBH_4$ on the stability of the TPP-AuNPs. We also investigated the effect of temperature, dilution effects and solvation in different solvents on the thermodynamic and kinetic stability of the NPs.

5.2 Experimental section

5.2.1. Chemicals

All chemicals and solvents were used as received. Sodium borohydride ($NaBH_4$) powder (98%) was obtained from Alfa Aesar. Sodium chloride (NaCl), magnesium chloride ($MgCl_2$) and potassium chloride (KCl) were obtained from Mallinckrodt Baker.

Sodium nitrate ($NaNO_3$) was obtained from J.T. Baker. Sodium sulfate (Na_2SO_4) was obtained from Macron Chemicals. Sodium perchlorate ($NaClO_4$), (3-Aminopropyl)triethoxysilane (APTES) and dimethylformamide (DMF) were obtained from Sigma-Aldrich. Ethanol was obtained from Decon Labs while acetonitrile (HPLC grade) was obtained from Fisher Scientific. MilliQ water, (>18 MΩ) was also used.

5.2.2. Preparation of TPP-AuNPs

TPP-AuNPs were prepared according to a procedure developed our lab.[19] The black solid obtained was dissolved in MilliQ water, (>18 MΩ) to obtain TPP-AuNP solution which was brown in color. The TPP-AuNP solution was sonicated in a Branson ultrasonic cleaner. The solution was centrifuged for 30 min at 4000 r.p.m and the small aggregates at the bottom of the tube were discarded. The supernatant was centrifuged two more times and the final solution was used in this study.

5.2.3. Determination of the effect of $NaBH_4$ on PPh_3 on TPP-AuNPs

APTES functionalized glass slides were immersed in a solution of TPP-AuNPs for 12 h. The glass slides were rinsed with milliQ water to remove unbound TPP-AuNPs. One batch of the glass slides was immersed in a solution of 0.1M $NaBH_4$ for 30 min, rinsed with water and dried in a stream of nitrogen gas. The batch that was immersed in $NaBH_4$ was used to quantify how much phosphorus remained on the TPP-AuNPs by X-ray Photoelectron Spectroscopy (XPS) while the batch that was not immersed was used as the reference for phosphorus.

5.3 Instrumentation

5.3.1 UV-visible Spectroscopy

UV-vis extinction spectra at room temperature were collected using a Perkin-Elmer Lambda 750 UV/Vis/NIR spectrophotometer over the 300-600 nm range. All data were corrected for background absorption using water.

5.3.2 X-ray Photoelectron Spectroscopy (XPS)

XPS data were obtained on a Kratos AxisUltraDLD using monochromatic Al kα source (1486.6 eV) with a pass energy of 40 eV and a step size of 0.1 eV. The spectrometer was calibrated using Ag 3d5/2 peak. The binding energy (BE) scale was calibrated using the C1s peak with a BE set at 285.0 eV. The dwell time was 300 ms and the peaks were analyzed relative to the C1s. The samples were prepared by drop casting the AuNP solution on a silicon wafer which had been thoroughly cleaned using piranha solution, rinsed copiously with nanopure water and ethanol. The sample was then dried under a stream of nitrogen gas.

5.3.3 Transmission Electron Microscopy (TEM)

TPP-AuNPs solutions were drop cast onto 200 mesh formvar-coated copper grids (Electron Microscopy Sciences, PA). The excess solution was wicked off and the grids air dried. TEM images were obtained using a Tecnai-12 instrument operating at 100 KV accelerating voltage (Microscopy Core Facility, University of Utah). Particle size analysis was conducted by analyzing ~1000 particles in the TEM images (TIF format) using Scion Image Beta 4.02 Software. In Scion Image, the known distance and unit were

set. The 'Analyze Particle' parameter was used to generate a table of particle diameters. This table was then exported into Microsoft Excel 2010 for statistical analysis.

5.3.4 HAADF-STEM, HRTEM and SAED imaging

TPP-AuNPs samples were prepared following the same procedure used for TEM samples as described above. Micrographs were obtained using a FEI Titan 80-300 TEM operated at 300 kV at the CAMCOR High Resolution and Analytical Facility (University of Oregon, Eugene, OR). The instrument is equipped for bright field, dark field, and high angle annular dark field STEM imaging. A high-angle annular dark-field detector was used for HAADF-STEM. The collection angle of HAADF-STEM images was 10 mrad. The images were captured at different magnifications using a Gatan CCD. The dimension of the images obtained was 1k x 1k pixels. Selected-area electron diffraction (SAED) patterns also were obtained.

5.3.5 Attenuated Total Reflectance Infrared Spectroscopy (ATR-IR)

A Perkin-Elmer Spectrum 100 Fourier transform infrared (FTIR) spectrometer equipped with a Pike MIRacle™ ZnSe ATR crystal was used for ATR-IR analysis. TPP-AuNPs samples were prepared by depositing 20 µl of the solution containing the TPP-AuNPs on the ZnSe crystal. The sample was then dried under nitrogen before ATR-IR analysis. Each spectrum was obtained by averaging 4 four scans at 4 cm^{-1} resolution.

5.3.6 Zeta potential

The effective charge on the NP surfaces was determined by measuring the zeta potential using a NICOMP™ 380 ZLS (Particle Sizing Systems, CA). The numbers used for analysis were the average of three measurements. Data were fit using the Smoluchowski equation.

5.3.7. ^{31}P NMR

^{31}P NMR spectra were obtained using a Varian Inova 500 MHz NMR working at a ^{31}P frequency of 202.2 MHz. A direct broadband ^{1}H decoupled probe was used. The ^{31}P chemical shifts were referenced to the signal of 85% H_3PO_4 at 0.00 ppm. ^{31}P spectra were obtained for TPP, TPPO and TPP-AuNPs at 8°C with a sweep width of 40,000 Hz and a relaxation delay of 40.4 sec. The acquisition time was 1 second with a 90^0 pulse width of 44 μs and four transients (TPP) and 1024 transients for TPP-AuNPs. Samples were dissolved in D_2O, filtered and placed in a 7 mm NMR tube for analysis.

5.4 Results and discussion

5.4.1 Structure and stability of TPP-AuNPs in water

UV-vis spectroscopy was used to monitor changes in the extinction and wavelength of the localized surface plasmon resonance (LSPR) of NPs. Broadening and shifting of the resonance peak toward longer wavelengths indicated aggregation of the NPs. Transmission electron microscopy (TEM) was used to confirm whether the NPs were aggregated or not.

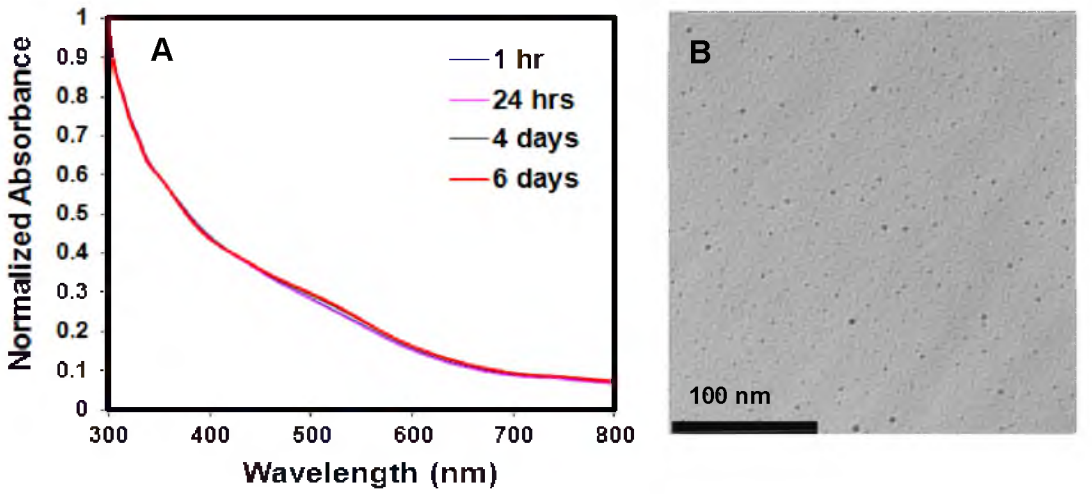

Figure 5.1. (A) UV-visible absorption spectra of the TPP-AuNPs showing the stability of the colloid solution over 6 days. (B) TEM image of the TPP-AuNPs on day 1.

In this study, the UV-vis absorption spectra of the TPP-AuNPs in water were recorded during the course of a week in order to monitor changes in shape and position of the spectra which would indicate aggregation of the TPP-AuNPs. The TPP-AuNPs displayed nearly featureless UV-vis spectra which did not red shift or broaden over 6 days (Figure 5.1A), which was an indication of the stability of the NPs.

The NP stability also was confirmed by TEM of the particles over the time course of the monitoring period. A close examination of the TEM images indicated that spherical NPs were dominant with an average NP diameter of 4.3 ± 1.4 nm (Figure 5.1B).There were no discernible changes in the size and shape of the NPs after 6 days. The effective charge on the surface of the TPP-AuNPs also was monitored by measuring the zeta potential over the same time period, and the values remained constant. The average zeta potential for the aqueous samples at pH 7.55 was 34.9 ± 4.6 mV, indicating the NPs were positively charged.

We used a combination of approaches to characterize the morphology and structure of the TPP-AuNPs including TEM, high resolution TEM (HRTEM), high angle annular dark field scanning transmission electron microscopy (HAADF-STEM) and selected-area electron diffraction (SAED). HRTEM and HAADF-STEM analysis provided high resolution analysis of the TPP-AuNPs. Figure 5.2A is a representative dark field HAADF-STEM image of the TPP-AuNPs. Compared to the bright field TEM image in Figure 5.1B, the HAADF-STEM image shows remarkable contrast between the high-Z TPP-AuNPs and the low-Z carbon support of the TEM grid. Information about how the NPs are faceted was derived from HRTEM. Close inspection of the HRTEM images indicated that approximately half of the NPs were single phase crystals, while the rest exhibited multiple twinning. The HRTEM and SAED pattern showed that a majority of the NPs were highly crystalline. Figure 5.2B is a representative image of the NPs and it shows a NP with distinct lattice fringes, with a lattice spacing for the (111) planes of 0.24 nm. Figure 5.2C shows a SAED pattern of the NPs which was indexed to the (111), (200), (220) and (311) of a face-centered cubic (fcc) Au lattice. The predominantly single crystalline NPs were found to exhibit fcc packing. This is in agreement with previous reports where NPs with (111) planes with lattice spacing of 2.36 Å were determined to be face centered cubic AuNPs.[42] The pristine (un-twinned) NP as shown in the representative image in Figure 5.2B had a truncated octahedral shape which has been reported to be the shape which affords the lowest energy to fcc AuNPs within the 4 nm size range.[43] Twinning defects which are a characteristic feature of fcc structures[44, 45] also were observed in the HRTEM images.

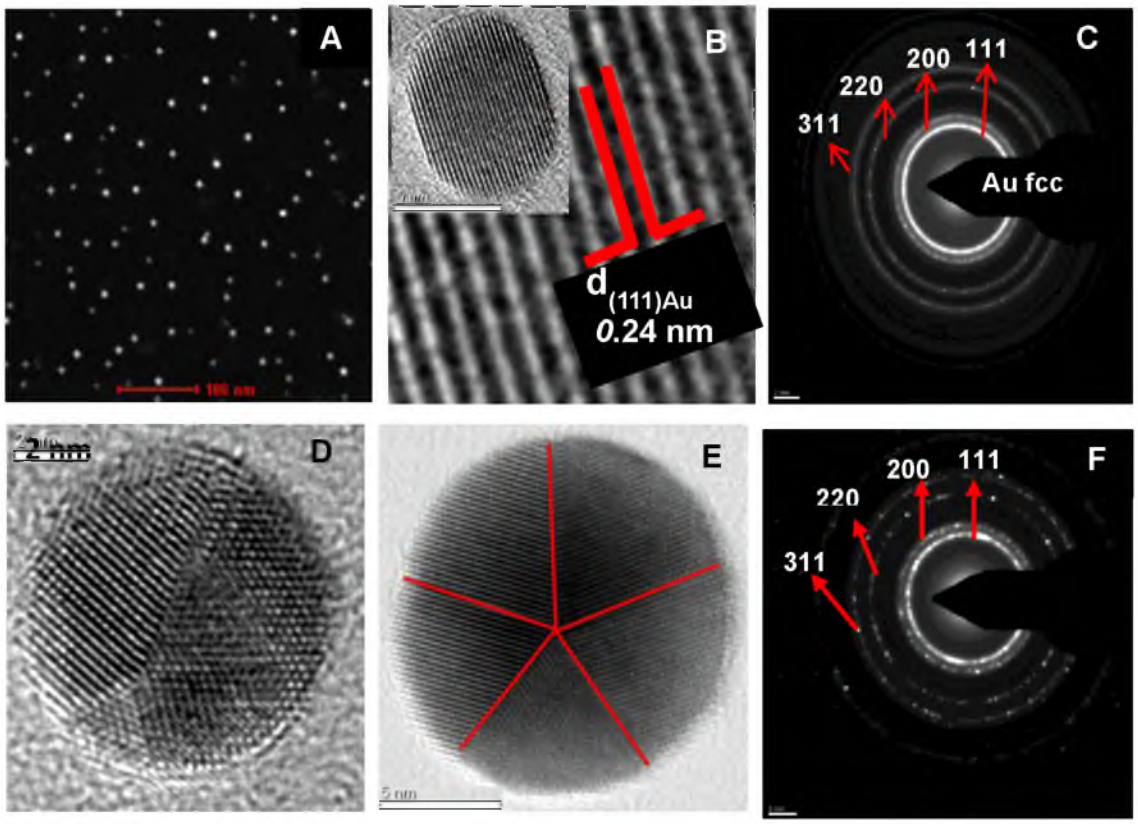

Figure 5.2. (A) HAADF-STEM image of the TPP-AuNPs. (B) Representative HRTEM image showing (111) lattice fringes of a single crystalline NP. (C) SAED pattern depicting the crystalline nature of the NPs. (D) HRTEM image showing a multiply twinned (decahedral) NP. (E) HRTEM image showing a multi-phase and twinned NP and (F) SAED diffraction pattern of the twinned NPs which was indexed to Au fcc.

Twinning occurs during the crystal formation and growth process and is thus one of the crystallographic imperfections observed in many nanomaterials.[44, 46, 47] These twinning defects which lead to a variety of morphologies have been known to occur frequently in noble metal NPs including Au where the bulk arrangement is fcc.[48, 49] While un-twinned NPs, such as the particle shown in Figure 5.2B, were observed in this study, singly twinned and decahedral NPs with multiple twinning also were present (Figures 5.2D).

For NPs in the size range of ~5 nm, decahedra with five-fold twinning have been reported to be more stable than other particles, for example octahedral NPs which are stable for larger size NPs.[50] The corresponding SAED diffraction pattern of the multiply twinned NPs is shown in Figure 5.2F and was indexed to Au fcc structure. Some of the structures observed show a six sided NP (Figure 5.3). Close observation of the magnified image clearly indicates this is not hcp AuNP but fcc AuNP which is composed of two twins as shown by the lines in the image.

This could have resulted from two small NPs that coalesced through twinning to form a larger NP, a phenomenon which has been reported in the literature. [51] Structural transformations and distortions induced by the electron beam during imaging due to local heating, atom displacement, bond breakage and atom ionization also have been known to result.[47, 50, 52] The extent to which samples in this study were affected by the electron beam during TEM, HRTEM, HAADF-STEM and SAED imaging is not apparent.

In summary, we observed that the TPP-AuNPs were soluble and stable in water. The NPs also were positively charged. In order to understand the driving forces behind the two observations and to obtain evidence for the behavior of the NPs in water, we investigated the surface chemistry of the TPP-AuNPs. The aim of study was to address two questions: Why are the NPs soluble in water while the ligand capping them is hydrophobic? What is the origin of the overall positive charge on the NPs? We used a combination of XPS, ATR-IR and ^{31}P NMR to obtain information on the structure and coordination of the TPP ligand on the AuNPs.

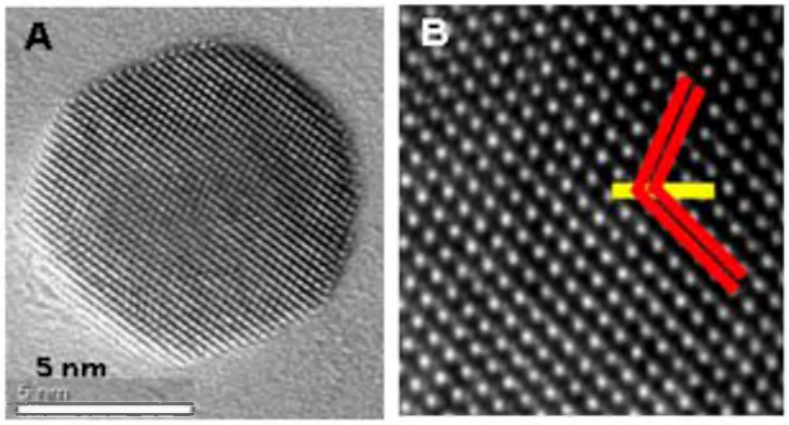

Figure 5.3. (A) HRTEM image of a decahedral AuNP showing (111) twinning. (B) Magnified image of the surface of the NP in A showing the arrangement of the NP grains.

We also induced aggregation of the TPP-AuNPs by addition of $NaBH_4$ and ions with different charges. The effect of temperature and dilution on the aggregation of the NPs as well as the behavior of the TPP-AuNPs in different solvents also was studied. The results of this investigation are presented in the following sections.

5.4.2 XPS investigation of triphenylphosphine adsorption on AuNPs

We used XPS analysis to study the adsorption of TPP to the AuNPs. TPP is expected to bind to Au through the lone pair orbital of phosphorus.[53, 54] To obtain XPS spectra of the TPP-AuNPs, a sample of the NPs was drop cast on a silicon wafer and dried. Figure 5.4 shows high resolution scans of the P(2p), C(1s) and O(1s) that have been deconvoluted. The phosphorus peak is a spin-orbit split doublet with the $P(2p_{3/2})$ peak at 131.6 eV. This can be attributed to the coordination of the TPP molecules attached to Au. After deconvolution, a small additional peak at 133 eV is observed. This is an indication that some of the TPP is oxidized to TPPO.[55] The $P(2p_{3/2})$ binding energy position for free TPP is 130.2 eV while that for TPPO is 132.8 eV.[56, 57]

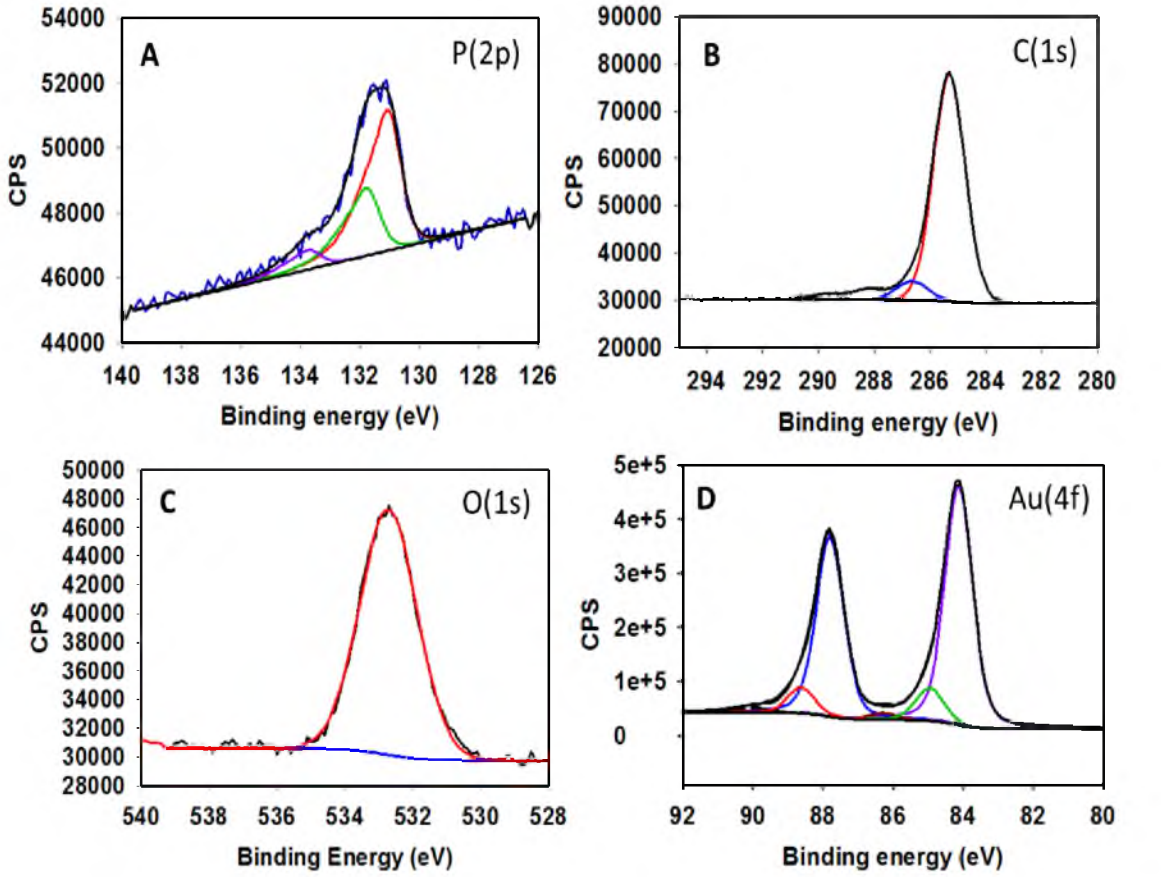

Figure 5.4. High resolution scans of TPP-AuNPs (A) P(2p), (B) C(1s), (C) O(1s) and (D) Au(4f). All spectra were fit using a Gaussian-Lorentzian line shape.

When TPP is oxidized to TPPO, a shift to higher binding energy is expected since P is in a more electronegative environment due to the presence of oxygen.[53] Even though the data shows P binds to Au, it has been reported that P-Au bonding causes molecular orientation changes which induce cross sectional changes of the P(2p) peak. This reduces the intensity of the P(2p) peak.[56] The low intensity of the P(2p) could also be due to few TPP molecules adsorbed on Au due to the molecular structure of TPP. The ratio of Au:P for samples in this study was 8:1.

The carbon C(1s) XPS spectrum shows a sharp symmetric peak at 285.3 eV (Figure 5.4B). The C(1s) spectrum also exhibited shake-up satellite peaks at higher binding energies compared to the main C(1s) peak. Shake- up satellites are known to occur in aromatic systems.[55] Deconvolution of the C(1s) spectrum showed peaks at 286.6 eV, 288.2 eV and 289.7 eV which could indicate the presence of C-O-P linkage, carboxyl groups and shake-up satellites due to π-π^* transitions of the aromatic carbon atoms of the phosphine phenyl rings.[58, 59]

A narrow oxygen peak O(1s) peak was observed at 532.7 eV (Figure 5.4C). Fitting of the O(1s) high resolution spectra did not point to different chemical environments for oxygen. The O(1s) peak at 532.7 eV signaled the presence of C-OH or C-O-P linkage.[59] This could be due to the contribution of oxygen from TPPO.[55] The intensity ratio of C(1s) and O(1s) is 1.6 while that of P($2p_{3/2}$) and O(1s) is 1.02. This indicates a significant contribution from oxygen from the air or from tightly bound water that was not removed during the drying step of sample preparation or in the vacuum conditions in the XPS system.[56]

The results indicated that the phosphorus bonded to Au is not oxidized. However, since deconvolution of the P($2p_{3/2}$) indicated the presence of TPPO, it is likely that some of the oxygen is bonded to P to form a P-O-H layer. This layer was investigated by ATR-IR and the results are discussed below.

5.4.3 ATR-IR investigation of triphenylphosphine adsorption on AuNPs

ATR-IR spectroscopy can provide information about the structure and identity of the molecules adsorbed on Au surface. Compared to other triphenyl compounds, TPP is less sterically hindered and thus binds strongly to metals including Au, Pt, Pd and Rh.[56, 60] TPP, TPPO and TPP-AuNPs were analyzed by ATR-IR. The ATR-IR spectra of pure TPP and pure TPPO showed C-H stretching vibrations at 2973 and 288cm^{-1} (Figure 5.5). The signals at 1438 cm^{-1} were attributed to CH_2 scissoring. The bands around 1000 cm^{-1} likely emanate from P-O-C units that are partly oxidized.[60] The spectrum for TPPO showed a bands at 541 cm^{-1} and 1120 cm^{-1} which were not observed for TPP and TPP-AuNPs. These peaks were attributed to a P=O stretching vibration from the TPPO.[55, 61] Absence of P=O vibration in the TPP-AuNPs spectrum indicated the adsorption of oxygen-free TPP on Au.

The adsorption of TPP or TPPO on Au will be in favor of the ligand (in this case, TPP) that can donate an electron pair to Au.[62] P=O also tends to align itself parallel to the Au surface, leading to the non-observance of its signal in ATR-based IR analysis.[63] We also noticed that the intensity of the TPP-AuNPs was weak. This could be due to the structure of TPP which causes the molecules to pack less densely on the Au surface leading to a weak signal.[64] We observed evidence of P-O-H vibrations in the ATR-IR spectra. The boxed region in Figure 5.5A is where P-O-H vibrations are expected. It has been reported that P-O-H vibrations occur in the 2700-2300 cm^{-1} region and are attributed to intermolecular hydrogen bonds.[65] The peak at 2360 cm^{-1} was assigned to P-O-H. The broad band at 3306 cm^{-1} was attributed to O-H stretching of water due to

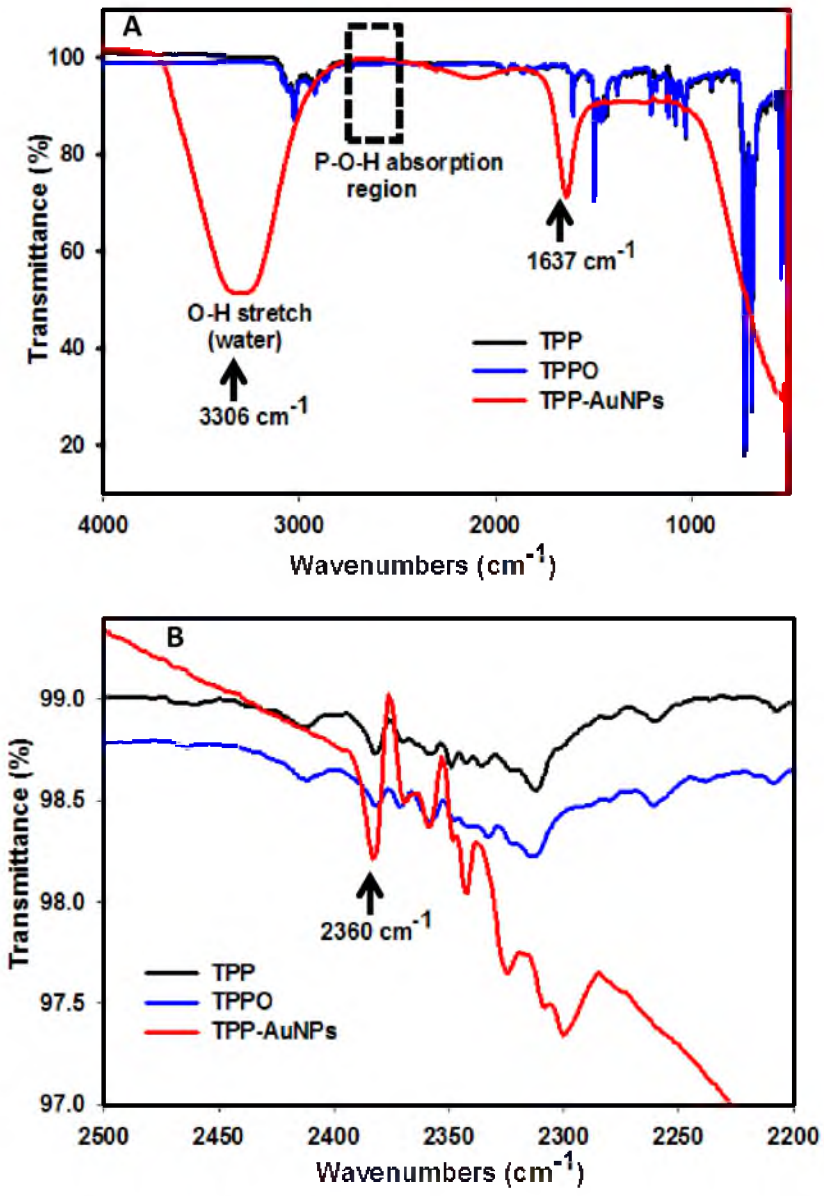

Figure 5.5. (A) ATR-IR spectrum of TPP, TPPO and TPP-AuNPs. (B) The 2500-2200 cm^{-1} region has been enlarged to show the area where the P-O-H signal was observed.

hydrogen bonding while the band at 1637 cm^{-1} was due to O-H bending.[66] These data point to the presence of TPP that has been transformed to TPPO and we speculate that a hydrogen bonded TPPO layer is present.

5.4.4. ^{31}P NMR investigation of TPP adsorption on AuNPs

To further investigate the coordination of TPP and TPPO to the AuNPs, ^{31}P NMR spectroscopy was performed. The ^{31}P NMR shifts of TPP, TPPO and TPP-AuNPs were obtained using solution state NMR. The samples were dissolved in deuterium oxide (D_2O) and filtered. TPP and TPPO are sparingly soluble in D_2O. Coordination of either TPP or TPPO to AuNPs is expected to result in a downward shift of the ^{31}P NMR chemical shifts.[67] At 8 ^{0}C, the NMR data exhibited a peak at 37 ppm for TPPO, and two peaks for TPP-AuNPs at 37 and 46 ppm (Figure 5.6). The TPP did not show any signal. We attribute this to the insolubility of TPP in D_2O. Gonella et al. previously observed peaks for TPPO in solution state ^{31}P NMR at 38.87–40.81 ppm.[68] A close inspection of the TPP-AuNPs spectrum showed that the ^{31}P chemical shift at 37 ppm was identical to that for TPPO. This chemical shift was assigned to TPPO monohydrate. The second peak at 46 ppm is narrow and down shifted. This could be due to the formation of a weak Au-TPPO complex in water.[69]

Phosphines are easily oxidized in air forming phosphine oxides.[53, 56] Phosphine oxides tend to form hydrogen bonds thereby increasing solubility of the molecules in water. Combined, the XPS, ATR-IR and ^{31}P NMR analyses provided strong evidence for the presence of TPPO and hydrogen bonded TPPO. Adsorption of TPP on the Au surface

likely leads to the removal of Au atoms from the NP surface.[70] These atoms can become trapped and stabilized by the TPP ligands and are not easily removed.[70]

Thermogravimmetric analysis of a sample of TPP-AuNPs indicated that after evaporation of the solvent, there was a second labile layer of TPP that was removed upon further heating of the sample. Interestingly, XPS analysis showed that TPP rather than TPPO was bonded to the AuNPs. The phenyl rings of the TPP molecules previously were observed to adsorb on the ring edge of the NPs in a vertical (standing up) position and oriented away from the Au surface.[71-73] A combination of π-π stacking interactions and hydrogen bonding in compounds containing TPP ligands has been reported.[74, 75]

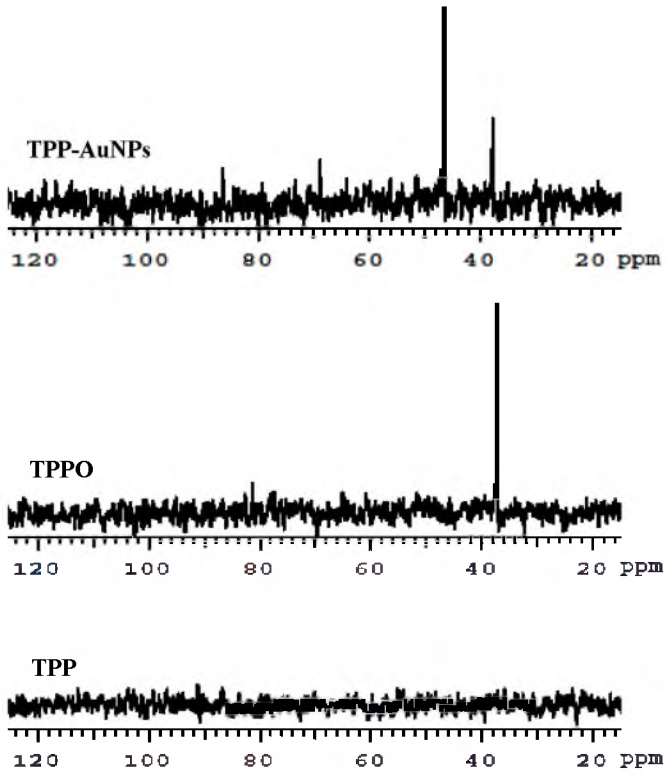

Figure 5.6. ^{31}P NMR spectrum of TPP, TPPO and TPP-AuNPs in D_2O.

Rearrangement of the phenyl rings could occur to maximize the π-π overlap of the phenyl rings.[74] These interactions lead to increased stability of the structures. It is possible that π-π stacking of the phenyl rings of the TPP occurs for the TPP-AuNPs, resulting in two layers of TPP: one attached to Au via the P atom and the other stacked on this Au-TPP layer. It is the outer layer that is responsible for H-bonding. This could explain why TPP-AuNPs in this study are soluble in water.

5.4.5 Effect of $NaBH_4$ on TPP-AuNPs aggregation

In order to gain further insights into how the NPs are stabilized, aggregation was induced by addition of $NaBH_4$ and the ionic strength of the solution varied by addition of different concentrations of salt. The pH of the TPP-AuNPs as a function of the $NaBH_4$ added showed that the pH remained constant over the period the solutions were monitored. Typically, $NaBH_4$ decomposes in non-basic aqueous solutions accompanied by the release of hydrogen gas. [76, 77] This decomposition was avoided by working at a basic pH. The original TPP-AuNPs solution had a pH of 7.15 and addition of $NaBH_4$ made the solution basic. We used UV-vis spectroscopy to monitor the effect of the addition of $NaBH_4$ on the TPP-AuNPs over the time course of one week. On addition of different concentrations of $NaBH_4$ to solutions of TPP-AuNPs, the LSPR of the TPP-AuNPs was observed to red shift. The red shift was more pronounced when higher concentrations of $NaBH_4$ were added. Addition of 40 mM $NaBH_4$ led to the biggest red shift for the LSPR peak in the shortest time, indicating the greatest rate of aggregation (Figure 5.7). The aggregated NPs were stable as evidenced by the UV-vis spectra in Figure 5.7 before they crashed out of solution.

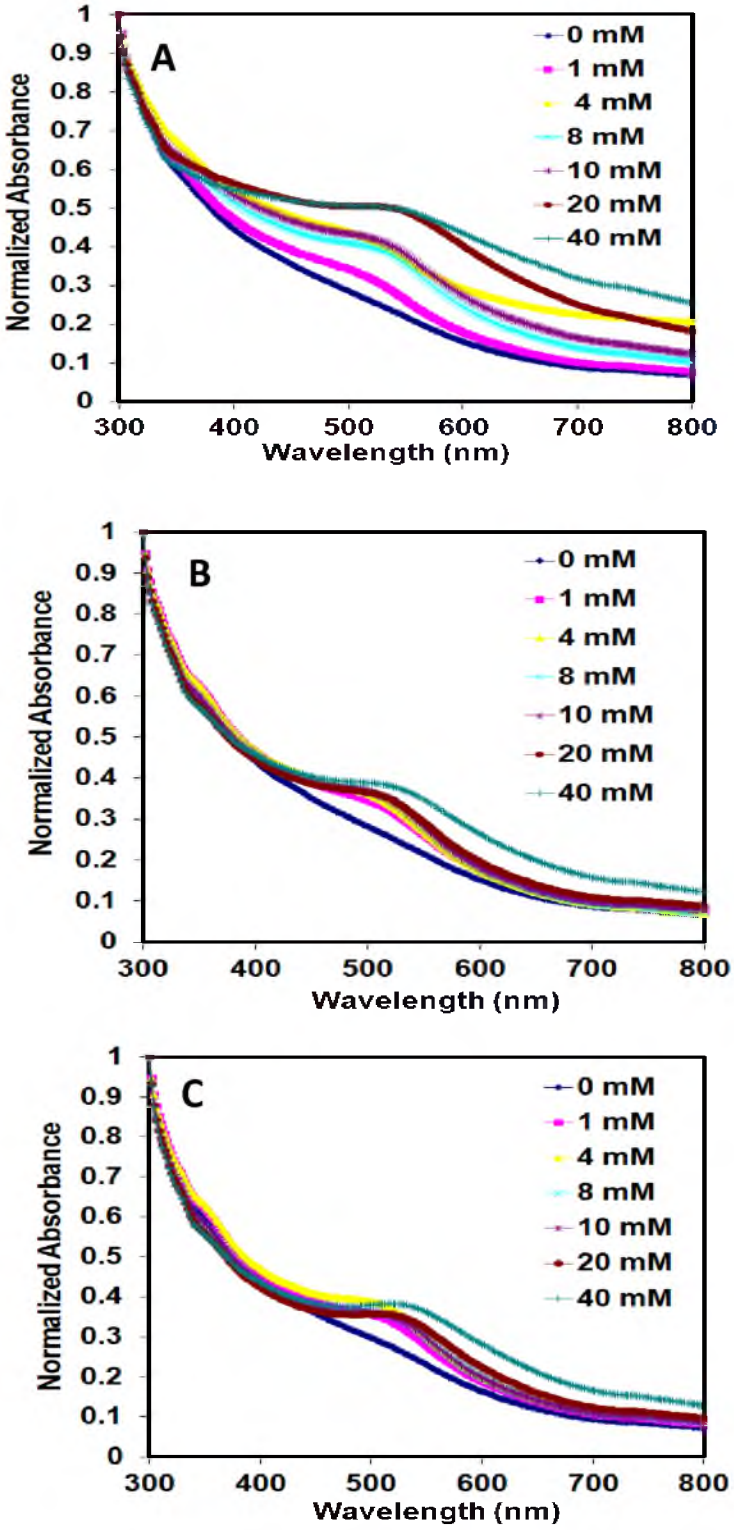

Figure 5.7. UV-vis absorption spectra showing the evolution of the LSPR bands of the TPP-AuNPs after addition of different concentrations of $NaBH_4$ as indicated in the legends after (A) 1 h (B) 24 h (C) 6 days.

For example, we noticed that the peak position of the sample to which 40 mM $NaBH_4$ was added did not change over six days. We also observed that the extent of aggregation and the rate of the LSPR red shift depended on the concentration of $NaBH_4$ added. The LSPR red shift reached a maximum after ~1 h, and then it blue shifted. (Figure 5.8A and 5.8B). There was no change in peak position after 24 h and the original spectrum was not recovered.

Mulvaney et al. reported that the electron density of metallic nanomaterials (NPs and nanorods) is increased on addition of $NaBH_4$ to a solution containing the nanomaterials.[78] The injection of electrons into the AuNPs causes changes in the optical properties of the NPs.[78, 79] The increase in the electron density on the surface of the NPs should induce a blue shift in the LSPR peak.[78] Contrary to this report, we observed a red shift in the LSPR of TPP-AuNPs accompanied by the generation of hydrogen gas in this study. The red shift stopped and the generation of hydrogen ceased coinciding with the discharging of the BH_4^- ions. A blue shift occurred after this discharge. TEM analysis of the TPP-AuNPs indicated that the NPs were aggregated (Figure 5.9). This aggregation was dominant such that the blue shift caused by the injection of electrons onto the NP surface was masked and therefore not observed. The aggregated polycrystalline NPs were indexed to face-centered cubic (fcc) Au lattice. We propose that the injection of electrons into the NP surface caused desorption of the stabilizing ligand (TPP) which led to the aggregation of the NPs. To investigate this assertion further, a monolayer of TPP-AuNPs was deposited on a glass slide functionalized with 3-aminopropyltriethoxysilane (APTES). One set of slides was treated with 0.1M $NaBH_4$ for 30 min while the other set was untreated and used as a reference to quantify the amount of phosphorus present.

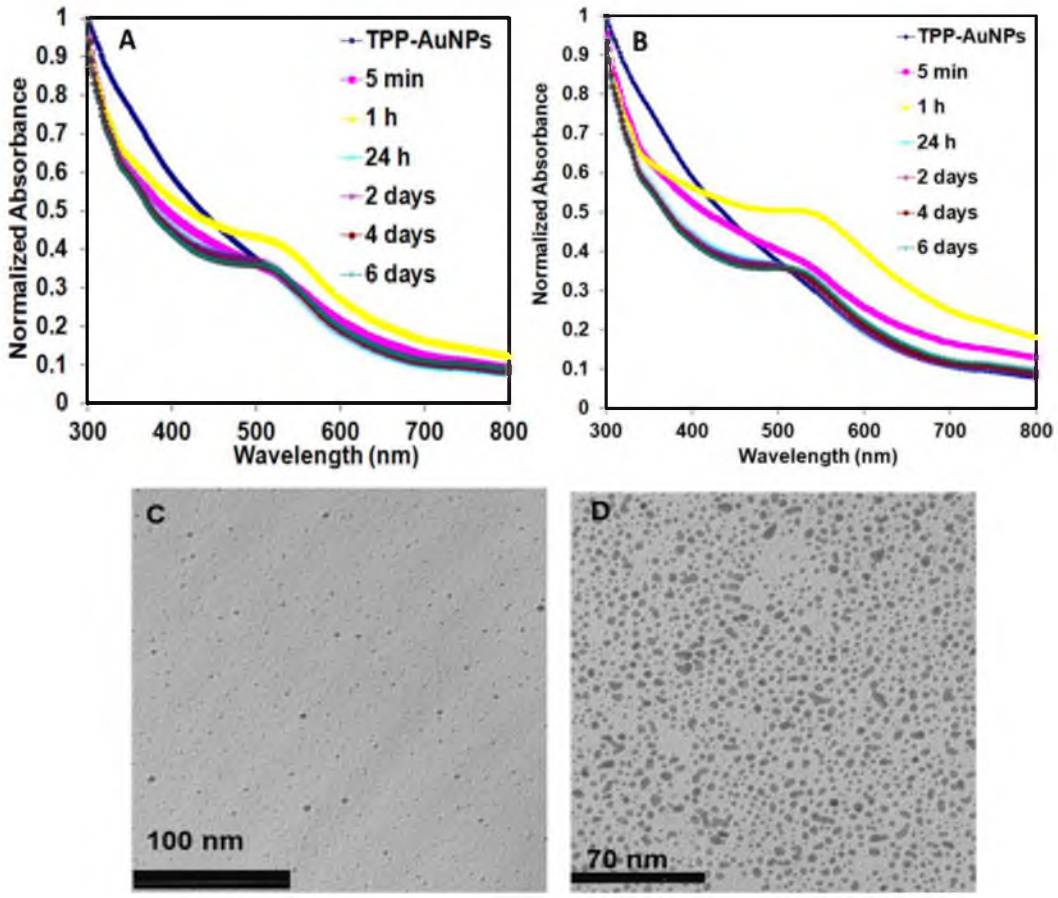

Figure 5.8. UV-vis absorption spectra showing the evolution of the LSPR bands of the TPP-AuNPs after addition of (A) 10 mM $NaBH_4$ and (B) 20 mM $NaBH_4$ over several days as indicated in the legends. (C) TEM image of the TPP-AuNPs before addition of $NaBH_4$ (D) TEM image of the TPP-AuNPs 24 h after addition of 10 mM $NaBH_4$.

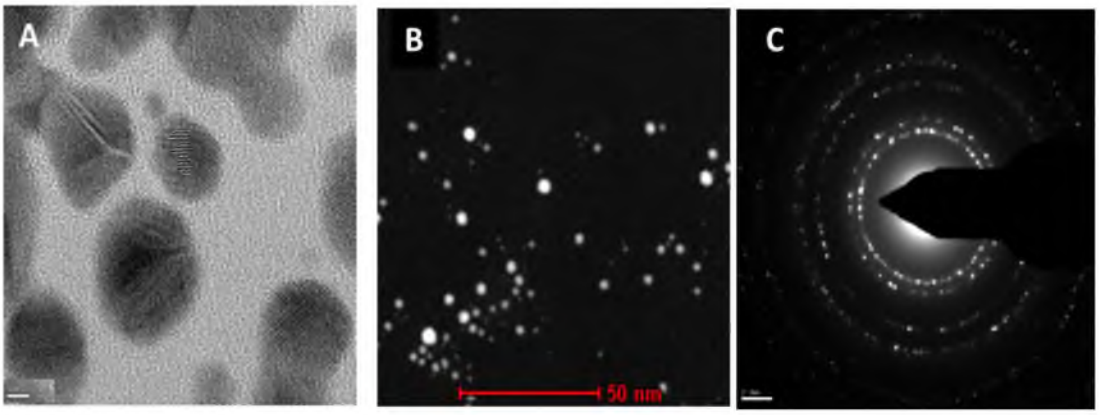

Figure 5.9. (A) Representative HRTEM image (scale bar = 2 nm) of the aggregated TPP-AuNPs after addition of 20 mM $NaBH_4$. (B) HAADF-STEM image of the TPP-AuNPs in A. (C) SAED diffraction pattern of the NPs.

The results indicated that ~53% of TPP on the surface of the TPP-AuNPs was displaced on addition of $NaBH_4$. This left the NPs without adequate stabilization and, as a result, the particles aggregated.

5.4.6. Effect of ionic strength of $NaBH_4$ on TPP-AuNPs

Metal colloids can be induced to aggregate by the addition of ions, changing the balance between electrostatic repulsion and van der Waals attraction which is needed to maintain colloid stability.[23] Addition of salt increases the ionic strength of the solution and disrupts this balance by weakening the electrostatic repulsion by causing the Debye layer around the NPs to become thinner.[25] This results in aggregation of the NPs in the solution. The effect of ionic strength on the stability of TPP-AuNPs was determined at a fixed $NaBH_4$ concentration while different concentrations of salt (NaCl) were added. The UV-vis extinction spectra of the solutions were monitored for a week and are presented in Figure 5.10A. On addition of salt, shifts in the LSPR of the NPs to longer wavelengths are clearly evident when compared to a solution of untreated TPP-AuNPs. A decrease in

the absorbance intensity also is evident in the presence of high concentrations of NaCl as the NPs aggregate and fall out of solution. For NPs pretreated with 20 mM $NaBH_4$ and to which NaCl was added, aggregation occurred and the particles formed 3D aggregates (Figure 5.10C). The extent of aggregation as determined by the broadening and shift of the LSPR peaks to longer wavelengths also was found to be dependent on the concentration of salt. Another experiment was performed where the NPs were not pretreated with $NaBH_4$ as in the previous experiment. To these solutions, NaCl was added. Aggregation was observed to occur and the NPs fell out of the solution. Aggregates of different shapes and sizes with no organizational structure were observed, as opposed to the 3D structure observed with $NaBH_4$ pretreated TPP-AuNPs (Figure 5.10D-F).

Since the salt we used to cause aggregation had Na^+ and Cl^- ions, we wanted to rule out the contribution of either the cation or anion to the aggregation observed. We investigated the aggregation induced in the presence of two different salts (NaCl and $NaNO_3$) of the same concentration (20 mM) of each salt. The LSPR spectra were monitored for 24 h. The concentration of the TPP-AuNPs was kept constant. In the presence of both the NaCl and the $NaNO_3$, the TPP-AuNPs exhibited LSPR spectra with broadened peaks and we observed aggregates that settled at the bottom of the reaction cuvette. The extent of aggregation in both salt solutions was similar as evidenced by the UV-vis spectra. Both Cl^- and NO_3^- ions should be able to attach to the TPP-AuNPs even though Cl^- will be the stronger ligand of the two. Since Cl^- ions caused the same aggregation as the NO_3^- ions, the presence of these ions was ruled out as an important factor in the aggregation observed.

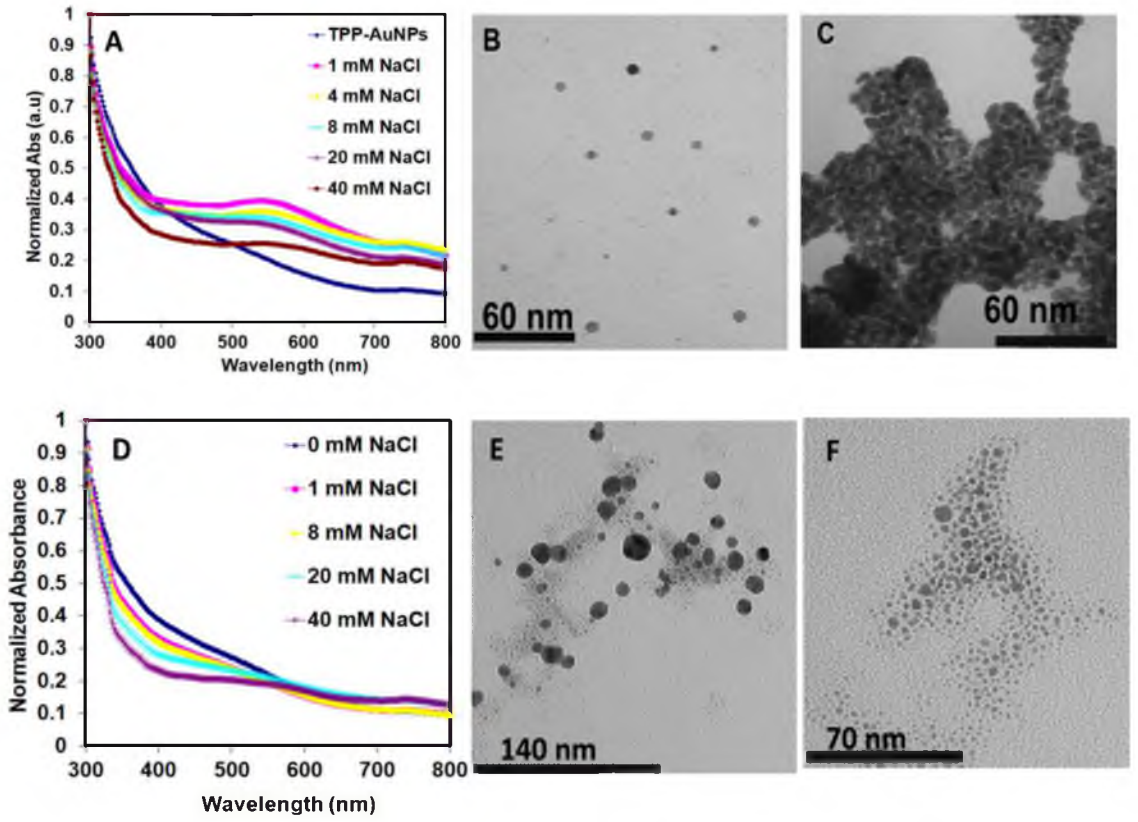

Figure 5.10. (A) UV-visible absorption spectra of the TPP-AuNPs on addition of different concentrations of NaCl to NP solutions pretreated with 20 mM $NaBH_4$ after 24 h. (B) TEM images of the TPP-AuNPs before and (C) after addition of NaCl. (D) UV-visible absorption spectra of the TPP-AuNPs on addition of different concentrations of NaCl to NP solutions (without $NaBH_4$ pretreatment) after 24 h. TEM images of the TPP-AuNPs 24 h after addition of (E) 1 mM NaCl and (F) 20 mM NaCl.

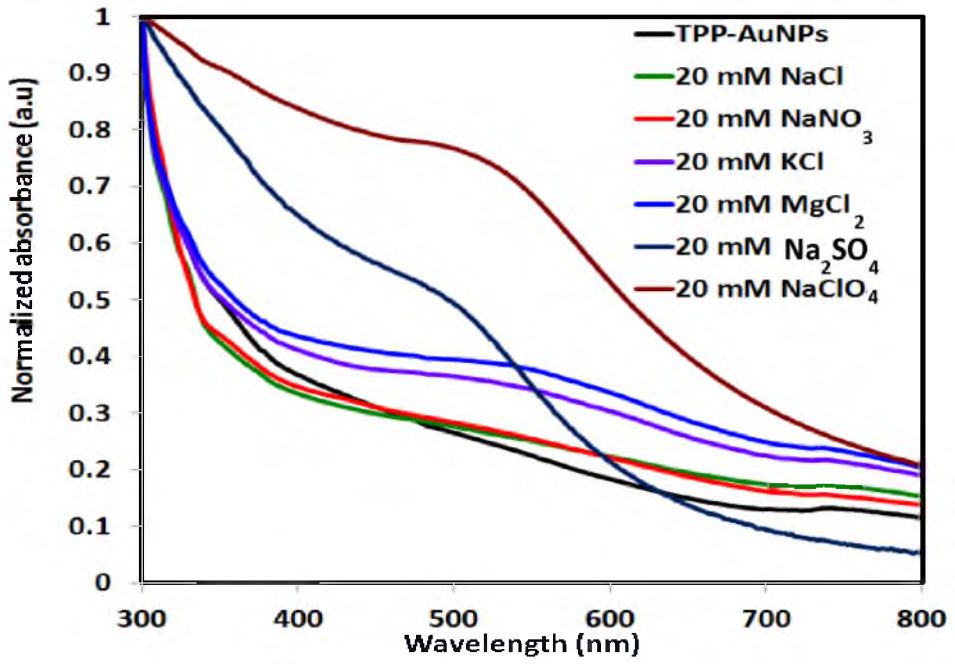

Figure 5.11. UV-visible absorption spectra of the aggregated TPP-AuNPs. Aggregation was monitored after being induced by addition of 20 mM NaCl, $NaNO_3$, KCl, $MgCl_2$, Na_2SO_4 and $NaClO_4$ after 24 h.

The same procedure was followed to investigate the contribution of cations to the observed aggregation. We checked for aggregation induced by adding KCl, $MgCl_2$ and NaCl of the same concentration to a TPP-AuNPs solution. $MgCl_2$ was observed to be more effective in causing aggregation than the other salts. Mg^{2+} is a divalent ion and as a result, it is more effective at causing aggregation than the monovalent salts because it can shield the NP surface charges more effectively.

Aggregation also was induced by using doubly charged anions: SO_4^{2-} and ClO_4^- ions. Both anions caused significant aggregation compared to the other salts (Figure 5.11). The doubly charged anions were able to shield the positive charge of the NPs effectively and cause significant aggregation and precipitation of the NPs. This

observation confirms that the NPs are positively charged as the zeta potential measurements indicated.

5.4.7. Temperature and dilution effects on the aggregation of TPP-AuNPs in water

NPs stabilized by strong ligands tend to resist permanent aggregation and can dissociate on dilution.[80] This is because dilution reduces the ionic strength of the solution. It also is expected that higher temperatures induce dissociation of aggregated NPs.[39] We expect that for weakly stabilized NPs, dissociation of the aggregates is not favored energetically. We investigated the effect of temperature and dilution on TPP-AuNPs treated with salt with a view to finding out whether the aggregation observed can be reversed. The approach, also used by Yang and co-workers, provides evidence of whether the aggregation is kinetically or thermodynamically controlled.[39] TPP-AuNPs were induced to aggregate by addition of NaCl in concentrations studied in the previous section. The aggregation was followed by UV-vis spectroscopy. The UV-vis spectra of the samples are shown in Figure 5.12 together with that of dispersed TPP-AuNPs for reference. To one of the samples (**S1**), 20 mM NaCl was added to the TPP-AuNPs solution and left to stand for 24 h at room temperature. The UV-vis spectrum shows a red-shift of the LSPR band of the sample which indicates aggregation. In order to test the effect of salt dilution, this sample was diluted twice to bring the final NaCl concentration to 10 mM. The sample was left to stand for 24 h (**S2**). The UV-vis absorption spectrum of this sample indicates that the aggregation was not reversible even on dilution of the

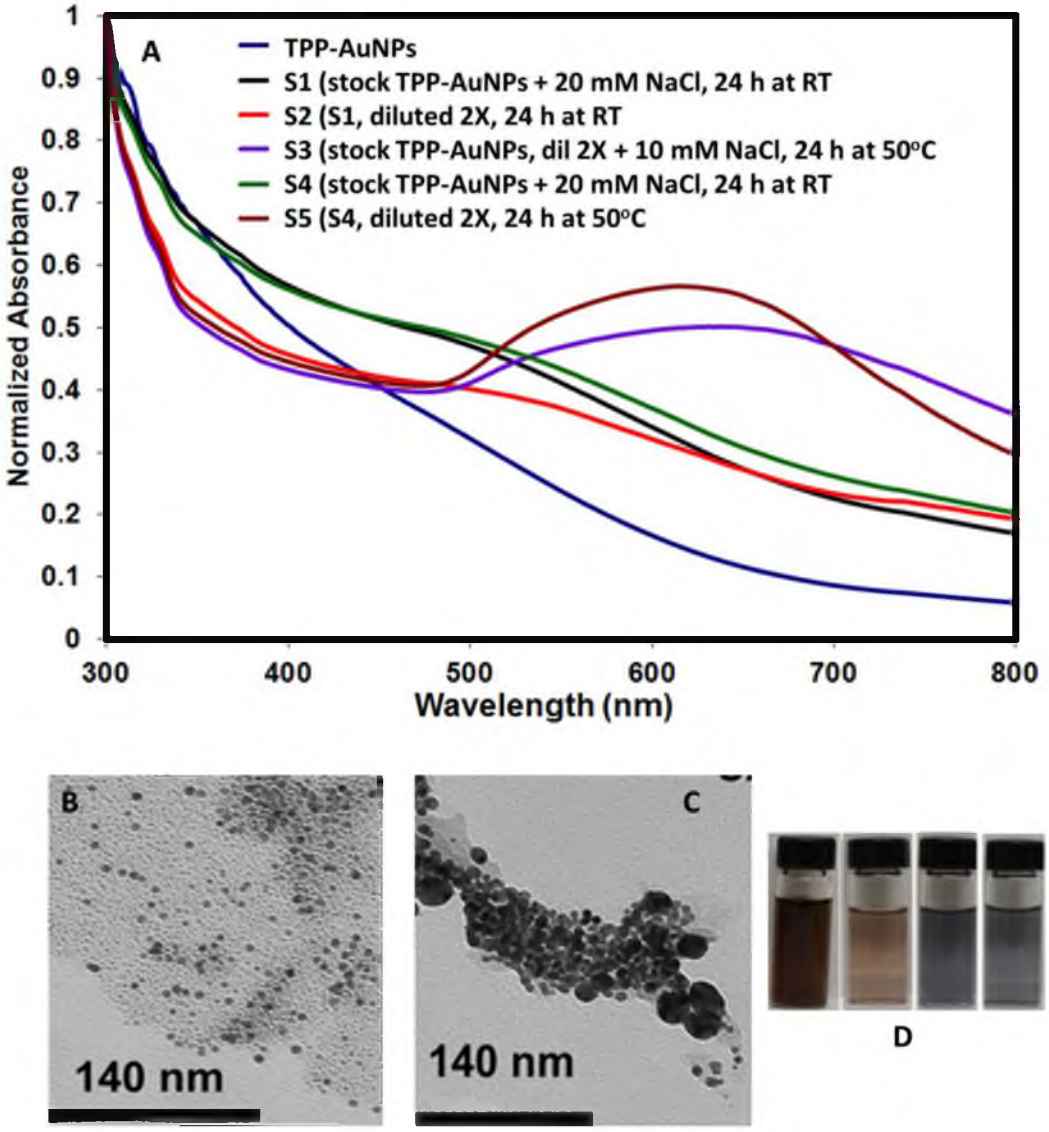

Figure 5.12. (A) UV-visible absorption spectra of the TPP-AuNPs aggregated by addition of NaCl. (B) TEM image of S. (C) Sample image of S. (D) Solution of the TPP-AuNPs, from left to right: stock TPP-AuNPs, S1, S3 and S5. The color change to purple clearly indicates aggregation.

sample. To another sample (**S3**), with half the concentration of TPP-AuNPs as **S1,** aggregation was induced by addition of 10 mM NaCl and incubation at 50°C for 24 h. The LSPR resulting peak measured for the TPP-AuNPs was significantly broadened and red-shifted indicating greater aggregation. It is evident therefore that the increased temperature did not trigger the dissociation of the aggregated TPP-AuNPs.

To test whether dilution of the sample would lead to dispersion of the aggregates, to a TPP-AuNPs solution with the same concentrations as S1, aggregation was induced by addition of 20 mM NaCl and left to stand for 24 h (**S4**). This sample was diluted twice and left to stand at 50°C for 24 h (**S5**). Both samples **S3** and **S5** have the same final concentrations of TPP-AuNPs and NaCl. The magnitude of aggregation for both samples was the same. We can therefore conclude that dilution and increased temperature did not reverse the aggregation observed. It is likely therefore, that the aggregation observed in this case is kinetically controlled. TEM analysis of the sample shows that the aggregates did not assemble in any organized manner.

5.4.8. Effect of solvents

According to the DLVO theory, the dielectric environment of the NPs affects their stability.[24] We therefore want to investigate whether the behavior of the TPP-AuNPs in water is different than that in other polar organic solvents. We notice that TPP-AuNPs in water have no noticeable LSPR band. When the NPs were dissolved in different polar solvents, the LSPR band was more distinguishable. Dissolving the particles in pure organic solvents reduced the stability of the NPs compared to the case where solvent is diluted with water or just pure water.

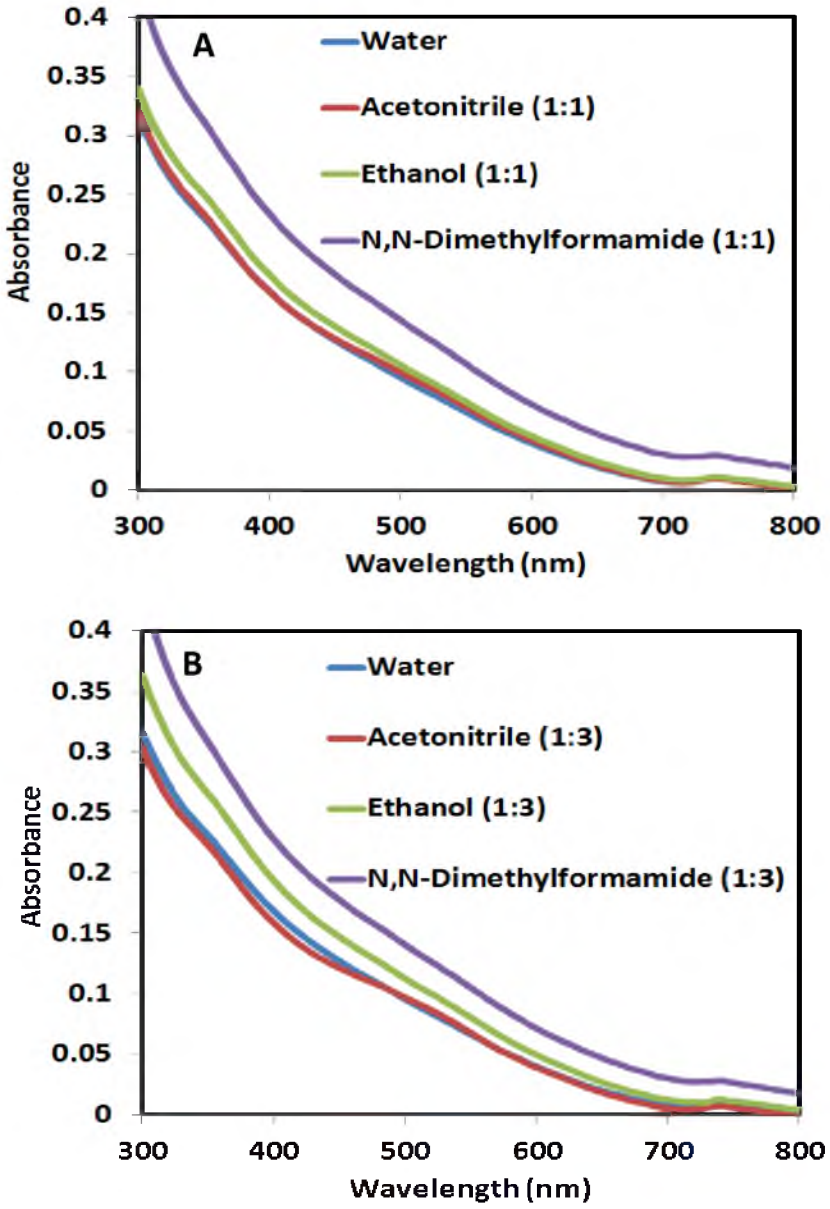

Figure 5.13. UV-visible absorption spectra of the TPP-AuNPs dissolved in solvents with different water: solvent ratios.

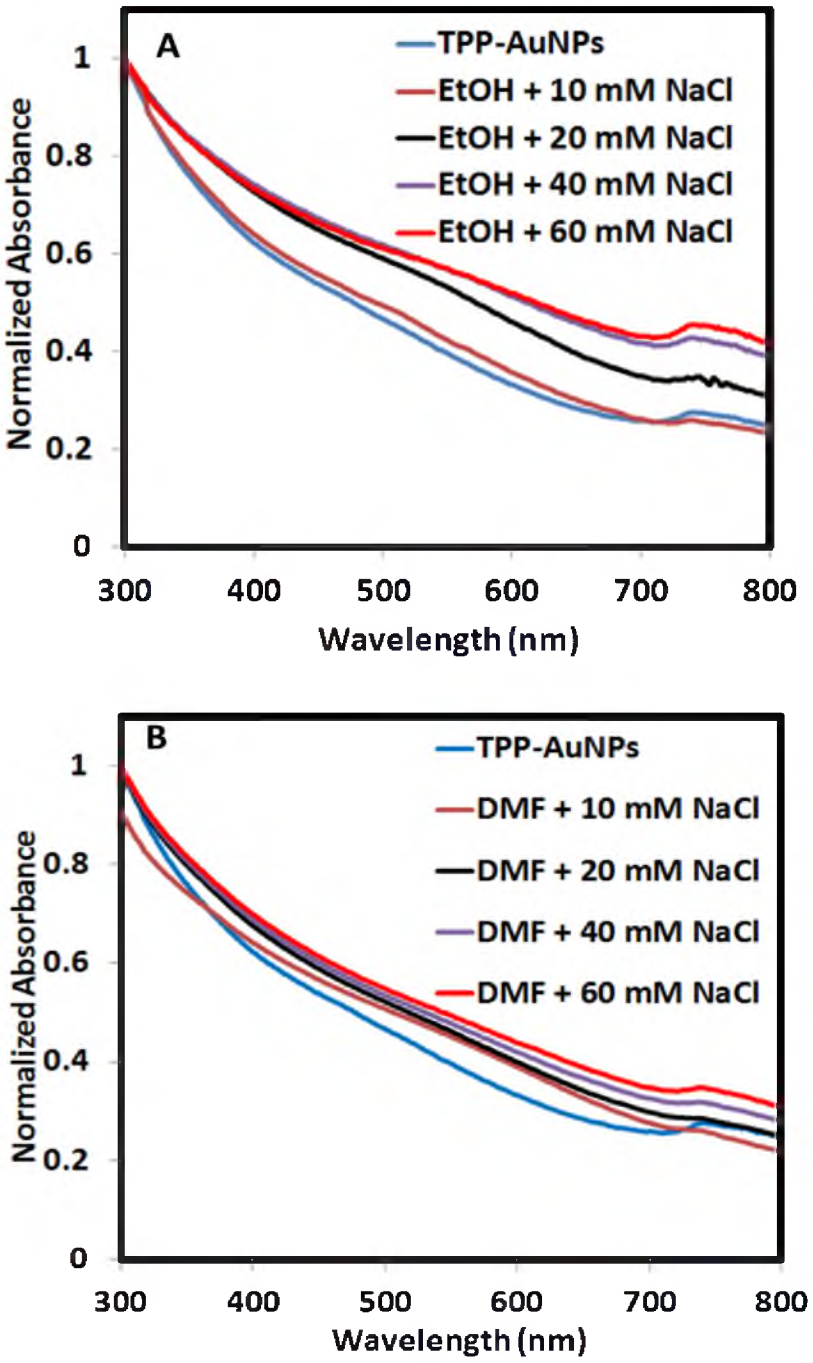

Figure 5.14. UV-visible extinction spectra of the TPP-AuNPs dissolved in (A) Ethanol and (B) DMF on addition of different concentrations of NaCl as indicated.

It has been reported that polar solvents with small dielectric constants can induce aggregation.[25] Stability of the NPs increased as determined by UV-vis spectroscopy and TEM imaging when the ratio of water to the solvents was changed to 1:1 and 1:3 (Figure 5.13). Acetonitrile and water did not show significant changes owing to their close refractive indices. Acetonitrile and water have nearly identical refractive index (RI).

No change in the shapes of the UV-vis spectra was observed. As more polar solvents were added to the aqueous solution of TPP-AuNPs, the absorption band shifted to longer wavelengths due to the decrease in dielectric constant. DMF which had the highest RI showed the most pronounced shift. One effect of using solvents of lower dielectric constants is that a decrease in the dielectric constant of the solvent of the NPs causes the dipolar interactions to increase as the electrostatic repulsion decreases.[25] As a result, the stability of the NPs decreases.

The presence of salt from the starting materials together with the organic solvents has been reported to induce assembly or aggregation of NPs.[80] In our case, only Cl^- ions are present and no cation is present to form a salt and initiate aggregation in a NP solution that has been purified. This is in comparison to citrate stabilized systems where both Na^+ and Cl^- are present from the starting salts. We chose to add salt to NP solutions in ethanol and DMF and observe how the electrical double layer is affected. The solvation power of water is greater than that of ethanol. Therefore, in ethanol the NPs have a thinner electrical double layer which is more susceptible to screening by addition of salt. The NPs are thus less stable against an increase in the ionic strength of the solution on addition of NaCl. Aggregation was observed for NPs dissolved in ethanol and DMF with the NPs in ethanol showing greater degree of aggregation (Figure 5.14).

5.4.9. Stabilization of TPP-AuNPs in water: Steric or electrostatic?

Nanoparticles can be stabilized by either of two modes: electrostatic and steric.[81] A third mode of stabilization which is a combination of the first two modes has been reported.[82] However this mode of stabilization has not been well defined.[23] For steric stabilization to be operative, the TPP ligands need to be coordinated to the AuNP, thereby limiting contact between the NPs and contributing to stability. The XPS results described earlier in this report indicate that the NPs contain about ~2% chlorine. The source of these Cl^- ions is the metal precursor salt, chloro(triethylphosphine)gold(I) which was used in the synthesis of TPP-AuNPs in this study. Chloride ions are well known nanoparticle stabilizers.[83, 84] Trace Cl^- ions could play an important part in the stabilization of the NPs. The adsorption of Cl^- ions on the surface NPs introduces the possibility of a DLVO-type electrostatic stabilization.[24] However, in our case, the TPP ligand also coordinates to the Au surface through the phosphorus as ATR-IR and ^{31}P NMR results earlier indicated. It is therefore possible that along with the Cl^- ions, the oxidized TPP ligands stabilize the NPs. The added stability of the NPs derives from an expanded Debye layer when the NPs are dissolved in a polar solvent. The overall zeta potential of the NPs was positive. Anions in solvents that have a high dielectric constant have been shown to contribute significantly to the stability of the NPs.[85] Therefore, the contribution of water to the stability of the TPP-AuNPs cannot be ignored.

The structure of the TPP-AuNPs could be represented as shown in Figure 5.15. The question remains as to whether this stabilization is truly a DLVO-type electrostatic stabilization or whether it is steric due to the bulky TPP ligands. When salt was added to the NPs in this study, aggregation was observed (refer to Figure 5.10), indicating a

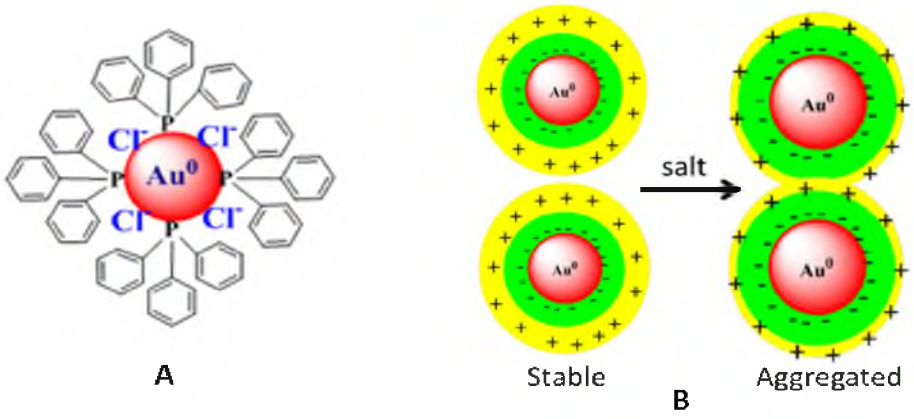

Figure 5.15. (A) A representation of the proposed structure of TPP-AuNPs showing how Cl^- ions and the TPP ligands are coordinated to Au. (B) Depiction of the collapse of the Debye layer on addition of salt.

collapse of the Debye layer. This pointed to a DLVO-type electrostatic stabilization that left the role of the TPP ligands in question. Addition of salt to sterically stabilized systems should not lead to aggregation of the NPs since no screening of charges is expected. Phosphines have been known to provide ligand stabilization to the NPs, which is basically steric stabilization.

Ott and Finke[23] argue that the presence of bigger clusters on TEM images which are clearly formed from coalescence of smaller clusters is an indication of ineffective stabilization by phosphines and amines. We have performed catalytic studies on these NPs in water on two model reactions (Chapter 6 and 7). The NPs were found to be catalytically active, with the experimentally determined kinetic parameters for the catalysis being comparable to those for supported systems.

Strongly stabilized NPs, especially those stabilized by thiols are usually catalytically inactive because the strong Au-S bonding reduces the number of atoms available for catalysis.[23, 86, 87] This supports the idea that the TPP ligands do not offer very strong stabilization to the NPs, leading to the catalytic activity observed for these

NPs. We therefore conclude that the mode of stabilization for TPP-AuNPs in water is electrosteric, in which both electrostatic and steric stabilization modes contribute to the overall stability of the NPs.

It has been reported that coordination of anions to the surfaces of neutral electrophilic metal nanoclusters can induce a positive electrostatic charge mirror.[84, 88] This positive charge is partial and it emanates from the attraction of the anions to the nanoparticle surface which is electrophilic.[23] The Au core also can be positively charged because the more electronegative Cl^- ions (compared to TPP molecules) pull electrons from the Au core.[15] The source of the overall positive charge on the NPs still remains unknown.

5.5 Conclusions

In summary, we have presented TPP-AuNPs that are soluble and stable in water. The increased stability was attributed to hydrogen binding as a result of π-π stacking of the phenyl rings of the TPP ligands. The absorption spectra of the NPs showed a featureless plasmon band. Zeta potential measurements also indicate that the NPs have an effective positive charge. A combination of methods used to study the structure and morphology of the NPs show that the NPs are face centered cubic. The NPs aggregate in the presence of $NaBH_4$ and different salts. Dilution and heating of the aggregates designed to cause a reversal of the aggregation were not successful. We therefore conclude that the aggregation is irreversible and kinetically controlled. The TPP-AuNPs in water can be used for several applications including catalysis.

5.6 References

(1) Sanchez, A.; Abbet, S.; Heiz, U.; Schneider, W. D.; Häkkinen, H.; Barnett, R. N.; Landman, U. *J. Phys. Chem. A* **1999**, *103*, 9573-9578.

(2) Schmid, G. *Chem. Rev.* **1992**, *92*, 1709-1727.

(3) Haruta, M. *Catal. Today* **1997**, *36*, 153-166.

(4) Tsunoyama, H.; Sakurai, H.; Ichikuni, N.; Negishi, Y.; Tsukuda, T. *Langmuir* **2004**, *20*, 11293-11296.

(5) Hainfeld, J. F. *Science* **1987**, *236*, 450-453.

(6) Jahn, W. *J. Struct. Biol* **1999**, *127*, 106-112.

(7) Han, M.; Gao, X.; Su, J. Z.; Nie, S. *Nat Biotech* **2001**, *19*, 631-635.

(8) Goettmann, F.; Moores, A.; Boissière, C.; Le Floch, P.; Sanchez, C. *Small* **2005**, *1*, 636-639.

(9) Raguse, B.; Chow, E.; Barton, C. S.; Wieczorek, L. *Anal. Chem.* **2007**, *79*, 7333-7339.

(10) Dorogi, M.; Gomez, J.; Osifchin, R.; Andres, R. P.; Reifenberger, R. *Phys. Rev. B* **1995**, *52*, 9071-9077.

(11) Berven, C. A.; Clarke, L.; Mooster, J. L.; Wybourne, M. N.; Hutchison, J. E. *Adv. Mater.* **2001**, *13*, 109-113.

(12) Debouttière, P. J.; Roux, S.; Vocanson, F.; Billotey, C.; Beuf, O.; Favre-Réguillon, A.; Lin, Y.; Pellet-Rostaing, S.; Lamartine, R.; Perriat, P.; Tillement, O. *Adv. Funct. Mater.* **2006**, *16*, 2330-2339.

(13) Gibson, J. D.; Khanal, B. P.; Zubarev, E. R. *J. Am. Chem. Soc.* **2007**, *129*, 11653-11661.

(14) Yoonessi, M.; Seikel, E.; Pender, M. J. *Langmuir* **2009**, *25*, 3369-3373.

(15) Periyasamy, G.; Remacle, F. *Nano Lett.* **2009**, *9*, 3007-3011.

(16) Petkov, V.; Peng, Y.; Williams, G.; Huang, B.; Tomalia, D.; Ren, Y. *Phys. Rev. B* **2005**, *72*, 195402.

(17) Vidoni, O.; Philippot, K.; Amiens, C.; Chaudret, B.; Balmes, O.; Malm, J.-O.; Bovin, J.-O.; Senocq, F.; Casanove, M.-J. *Angew. Chem. Int. Ed.* **1999**, *38*, 3736-3738.

(18) Özkar, S.; Finke, R. G. *Langmuir* **2002**, *18*, 7653-7662.

(19) Shem, P. M.; Sardar, R.; Shumaker-Parry, J. S. *Langmuir* **2009**, *25*, 13279-13283.

(20) Sardar, R.; Shumaker-Parry, J. S. *Chem. Mater.* **2009**, *21*, 1167-1169.

(21) Sardar, R.; Park, J.-W.; Shumaker-Parry, J. S. *Langmuir* **2007**, *23*, 11883-11889.

(22) Crooks, R. M.; Zhao, M.; Sun, L.; Chechik, V.; Yeung, L. K. *Acc. Chem. Res.* **2000**, *34*, 181-190.

(23) Ott, L. S.; Finke, R. G. *Coord. Chem. Rev.* **2007**, *251*, 1075-1100.

(24) Verwey, E. J. W.; Overbeek, E. T. J. *Theory of the Stability of Lyophobic Colloids*, 2 ed.; Dover Publications: Mineola, New York, 1999.

(25) Zhang, H.; Wang, D. *Angew. Chem. Int. Ed.* **2008**, *47*, 3984-3987.

(26) Doty, R. C.; Tshikhudo, T. R.; Brust, M.; Fernig, D. G. *Chem. Mater.* **2005**, *17*, 4630-4635.

(27) Jahn, W. *Z. Naturforsch. B* **1989**, *44*, 1313-1322.

(28) Eck, W.; Craig, G.; Sigdel, A.; Ritter, G.; Old, L. J.; Tang, L.; Brennan, M. F.; Allen, P. J.; Mason, M. D. *ACS Nano* **2008**, *2*, 2263-2272.

(29) Wu, H.; Zhu, H.; Zhuang, J.; Yang, S.; Liu, C.; Cao, Y. C. *Angew. Chem. Int. Ed.* **2008**, *47*, 3730-3734.

(30) Liz-Marzán, L. M.; Giersig, M.; Mulvaney, P. *Langmuir* **1996**, *12*, 4329-4335.

(31) Agasti, S. S.; You, C.-C.; Arumugam, P.; Rotello, V. M. *J. Mater. Chem.* **2008**, *18*, 70-73.

(32) Liu, W.; Howarth, M.; Greytak, A. B.; Zheng, Y.; Nocera, D. G.; Ting, A. Y.; Bawendi, M. G. *J. Am. Chem. Soc.* **2008**, *130*, 1274-1284.

(33) Hainfeld, J. F.; Slatkin, D. N.; Focella, T. M.; Smilowitz, H. M. *Br J Radiol* **2006**, *79*, 248-253.

(34) Hu, M.; Qian, L.; Brinas, R. P.; Lymar, E. S.; Kuznetsova, L.; Hainfeld, J. F. *J. Struct. Biol* **2008**, *161*, 83-91.

(35) Schmid, G.; Klein, N.; Korste, L.; Kreibig, U.; Schönauer, D. *Polyhedron* **1988**, *7*, 605-608.

(36) Thomas, K. G.; Barazzouk, S.; Ipe, B. I.; Joseph, S. T. S.; Kamat, P. V. *J. Phys. Chem. B* **2004**, *108*, 13066-13068.

(37) Park, H.-S.; Agarwal, A.; Kotov, N. A.; Lavrentovich, O. D. *Langmuir* **2008**, *24*, 13833-13837.

(38) Caswell, K. K.; Wilson, J. N.; Bunz, U. H. F.; Murphy, C. J. *J. Am. Chem. Soc.* **2003**, *125*, 13914-13915.

(39) Yang, M.; Chen, G.; Zhao, Y.; Silber, G.; Wang, Y.; Xing, S.; Han, Y.; Chen, H. *Phys. Chem. Chem. Phys.* **2010**, *12*, 11850-11860.

(40) Abécassis, B.; Testard, F.; Spalla, O.; Barboux, P. *Nano Lett.* **2007**, *7*, 1723-1727.

(41) Nishimura, S.; Takagaki, A.; Maenosono, S.; Ebitani, K. *Langmuir* **2009**, *26*, 4473-4479.

(42) Kuo, C.-H.; Chiang, T.-F.; Chen, L.-J.; Huang, M. H. *Langmuir* **2004**, *20*, 7820-7824.

(43) Barnard, A. S.; Lin, X. M.; Curtiss, L. A. *J. Phys. Chem. B* **2005**, *109*, 24465-24472.

(44) Barnard, A. S. *J. Phys. Chem. B* **2006**, *110*, 24498-24504.

(45) Oh, E.; Susumu, K.; Goswami, R.; Mattoussi, H. *Langmuir* **2010**, *26*, 7604-7613.

(46) Barnard, A. S.; Young, N. P.; Kirkland, A. I.; van Huis, M. A.; Xu, H. *ACS Nano* **2009**, *3*, 1431-1436.

(47) Elechiguerra, J. L.; Reyes-Gasga, J.; Yacaman, M. J. *J. Mater. Chem.* **2006**, *16*, 3906-3919.

(48) Marks, L. D. *Rep. Prog. Phys.* **1994**, *57*, 603.

(49) Zanchet, D.; Hall, B. D.; Ugarte, D. *J. Phys. Chem. B* **2000**, *104*, 11013-11018.

(50) Yacaman, M. J.; Ascencio, J. A.; Liu, H. B.; Gardea-Torresdey, J. *J. Vac. Sci. Technol. B* **2001**, *19*, 1091-1103.

(51) Wang, Y. Q.; Liang, W. S.; Geng, C. Y. *Nanoscale Res Lett* **2009**, *4*, 684 - 688.

(52) Wang, Z. L. *J. Phys. Chem. B* **2000**, *104*, 1153-1175.

(53) Uvdal, K.; Kariis, H.; Westermark, G.; Wirde, M.; Gelius, U.; Persson, I.; Liedberg, B. *Langmuir* **1998**, *14*, 7189-7196.

(54) Spessard, G. O.; Miessler, G. L. *Organometallic Chemistry*; Prentice-Hall,Inc: Upper Saddle River, NJ, 1997.

(55) Russo, M. V.; Furlani, A.; Altamura, P.; Fratoddi, I.; Polzonetti, G. *Polymer* **1997**, *38*, 3677-3690.

(56) Uvdal, K.; Persson, I.; Liedberg, B. *Langmuir* **1995**, *11*, 1252-1256.

(57) Zorn, G.; Gotman, I.; Gutmanas, E. Y.; Adadi, R.; Salitra, G.; Sukenik, C. N. *Chem. Mater.* **2005**, *17*, 4218-4226.

(58) Iucci, G.; Infante, G.; Polzonetti, G. *Polymer* **2002**, *43*, 655-663.

(59) Puziy, A. M.; Poddubnaya, O. I.; Ziatdinov, A. M. *Appl. Surf. Sci.* **2006**, *252*, 8036-8038.

(60) Kariis, H.; Westermark, G.; Persson, I.; Liedberg, B. *Langmuir* **1998**, *14*, 2736-2743.

(61) John, G. H.; May, I.; Sarsfield, M. J.; Steele, H. M.; Collison, D.; Helliwell, M.; McKinney, J. D. *Dalton Trans.*, **2004**, 734-740.

(62) Sandström, M.; Persson, I.; Persson, P. *Acta Chem. Scand.* **1990**, *44*, 653-675.

(63) Steiner, U. B.; Neuenschwander, P.; Caseri, W. R.; Suter, U. W.; Stucki, F. *Langmuir* **1992**, *8*, 90-94.

(64) Zeldin, M.; Mehta, P.; Vernon, W. D. *Inorg. Chem.* **1979**, *18*, 463-466.

(65) Thomas, L. C.; Chittenden, R. A. *J. Opt. Soc. Am.* **1962**, *52*, 829-829.

(66) Al-Abadleh, H. A.; Grassian, V. H. *Langmuir* **2002**, *19*, 341-347.

(67) Son, S. U.; Jang, Y.; Yoon, K. Y.; Kang, E.; Hyeon, T. *Nano Lett.* **2004**, *4*, 1147-1151.

(68) Gonnella, N. C.; Busacca, C.; Campbell, S.; Eriksson, M.; Grinberg, N.; Bartholomeyzik, T.; Ma, S.; Norwood, D. L. *Magn. Reson. Chem.* **2009**, *47*, 461-464.

(69) Kim, S.-W.; Kim, S.; Tracy, J. B.; Jasanoff, A.; Bawendi, M. G. *J. Am. Chem. Soc.* **2005**, *127*, 4556-4557.

(70) Jewell, A. D.; Sykes, E. C. H.; Kyriakou, G. *ACS Nano* **2012**, *6*, 3545-3552.

(71) Müllegger, S.; Hänel, K.; Strunskus, T.; Wöll, C.; Winkler, A. *ChemPhysChem* **2006**, *7*, 2552-2558.

(72) Muñoz-Márquez, M.; Guerrero, E.; Fernández, A.; Crespo, P.; Hernando, A.; Lucena, R.; Conesa, J. *J. Nanopart. Res.* **2010**, *12*, 1307-1318.

(73) Westermark, G.; Kariis, H.; Persson, I.; Liedberg, B. *Colloids Surf., A* **1999**, *150*, 31-43.

(74) Dayan, O.; Özdemir, N.; Dinçer, M.; Çetinkaya, B. *Acta Cryst.* **2007**, *C63*, m264-m266.

(75) Małecki, J. G.; Serda, M.; Musiol, R.; Polanski, J. *Polyhedron* 2012, *31*, 451-456.

(76) Schlesinger, H. I.; Brown, H. C.; Finholt, A. E.; Gilbreath, J. R.; Hoekstra, H. R.; Hyde, E. K. *J. Am. Chem. Soc.* 1953, *75*, 215-219.

(77) Chatenet, M.; Micoud, F.; Roche, I.; Chainet, E. *Electrochim. Acta* 2006, *51*, 5459-5467.

(78) Mulvaney, P.; Pérez-Juste, J.; Giersig, M.; Liz-Marzán, L.; Pecharromán, C. *Plasmonics* 2006, *1*, 61-66.

(79) Mulvaney, P. *Langmuir* 1996, *12*, 788-800.

(80) Han, X.; Goebl, J.; Lu, Z.; Yin, Y. *Langmuir* 2011, *27*, 5282-5289.

(81) Hunter, R. J. *Foundations of Colloid Science*, 2nd ed.; Oxford University Press Inc.: New York, 2001.

(82) Napper, D. H. *Polymeric stabilization of colloidal dispersions* Academic Press: London, 1984.

(83) Köhler, J. U.; Bradley, J. S. *Catal. Lett.* 1997, *45*, 203-208.

(84) Ott, L. S.; Finke, R. G. *Inorg. Chem.* 2006, *45*, 8382-8393.

(85) Ott, L. S.; Hornstein, B. J.; Finke, R. G. *Langmuir* 2006, *22*, 9357-9367.

(86) Templeton, A. C.; Wuelfing, W. P.; Murray, R. W. *Acc. Chem. Res.* 1999, *33*, 27-36.

(87) Long, C. G.; Gilbertson, J. D.; Vijayaraghavan, G.; Stevenson, K. J.; Pursell, C. J.; Chandler, B. D. *J. Am. Chem. Soc.* 2008, *130*, 10103-10115.

(88) Labib, M. E. *Colloids Surf.* 1988, *29*, 293-304.

CHAPTER 6

REDUCTION OF 4-NITROPHENOL BY SODIUM BOROHYDRIDE CATALYZED BY WATER SOLUBLE TRIPHENYLPHOSPHINE STABILIZED GOLD NANOPARTICLES

6.1 Introduction

Noble metal nanoparticles exhibit unique properties different from those of the bulk metals.[1-3] For example, gold in bulk is catalytically inactive due to its filled d-band.[4] However in the nanoscale form, gold exhibits significant catalytic activity.[3, 5] Gold nanoparticles (AuNPs) have been found to have unique catalytic properties which depend on their size and shape.[2, 5-7] This is a result of an increase in the Fermi potential and a subsequent reduction of the redox potential as the NPs become smaller.[8] Due to these properties, AuNPs have attracted great interest for potential industrial applications[9, 10] and use as model catalysts.[11] Since Haruta et al.[12-14] observed that small AuNPs showed high catalytic activity for CO oxidation at low temperatures, investigations of catalysis involving AuNPs in the literature have increased.[15-17] One of the goals of catalysis is to perform reactions under conditions that are mild and environmentally friendly, for example in water rather than in organic solvents. Such reactions catalyzed by colloidal

AuNPs are very useful in environmental remediation and other chemical industry applications. [18, 19] As an example, industrial plants (pharmaceutical, petrochemical and chemical) produce nitrophenols and their intermediates and derivatives as wastes enter into the environment from the production of synthetic dyes, insecticides, analgesic and antipyretic drugs, photographic developers and corrosion inhibitors among many other products.[20-23] While the quantities released may not allow adequate recovery of the waste, the amounts are enough to cause pollution concerns.

The U.S. Environmental Protection Agency has listed 4-nitrophenol along with several other phenols as priority pollutants with regards to water quality.[24] Methods for removal of these pollutants, for example catalytic liquid-phase oxidation which is done at high temperature,[25] increase the costs of dealing with these chemicals. Using metal NPs as catalysts, the reduction of 4-nitrophenol can be performed at room temperature. For cost considerations, low temperature catalytic reduction of phenols using NPs derived from noble metals could be an alternative approach of removing phenols from industrial waste water for example. Several different types of metal NPs have been used to catalyze the reduction of nitrophenols by $NaBH_4$ including Pt, Pd, Ni, Ag, Au as well as alloy NPs.[8, 26-28]

One of the main considerations for using NPs in catalysis is the stability of the particles under the reaction conditions. Nanoparticles that are not adequately stabilized aggregate which reduces the catalytic activity of the NPs. In order to minimize NP aggregation, several strategies have been used. The first strategy relies on incorporation of ligands to protect the NPs[29] and the second strategy involves the use of a high surface area solid to support the NPs.[17] Each strategy has advantages and disadvantages. For

example, supported AuNPs have been shown to exhibit enhanced catalytic activity due to interaction between the AuNPs and the support.[30] This can be an advantage; however this interaction also makes it challenging to gain an understanding of the catalysis because of the complexity introduced. Another challenge with supported materials can be low levels of NP incorporation into the support material. In order to obtain a high density of catalytically active NPs, high surface area support materials have been developed.[31] For these materials, leaching of supported AuNPs can be an issue.[15, 16] While ligand protected AuNPs provide a way to synthesize well controlled and stable structures for various applications, [32] AuNPs stabilized by organic ligands are generally considered to have diminished catalytic activity because the ligands shield the gold cores.[11, 32-34] However, recent research has shown that these stabilized AuNPs can have significant catalytic activity. [11, 30, 35] One reason for this observation is that the organic layers allow the passage of reactants and products through them.[36] The use of unsupported catalysts presents a unique opportunity to apply the NPs for various useful reactions in liquid-phase without the presence of the support which may hinder access to the active surface of the catalysts.[22] While the use of unsupported AuNP catalysts has inherent setbacks like aggregation of the catalysts, this approach provides a way to observe the kinetic behavior of the AuNPs during catalysis. Using dispersed particles also helps to analyze and correlate parameters such as the number of active sites for the AuNPs used. This information can be directly related to the activity of the AuNPs themselves without having to make considerations for the contribution of the solid support. In addition, the kinetic data obtained can be easily compared with that for supported systems.

The use of model reactions to evaluate the catalytic performance of the AuNPs is necessary because the kinetic parameters required for such an evaluation need to be collected quantitatively and precisely. Model reactions allow for the correlation of factors like size and shape of the NPs with the observed kinetic parameters. In addition, model reactions also provide easier comparison with other systems. Ideally, the model reactions chosen should proceed in a verifiable manner and produce only one product, with no by-products.[37] The reduction of 4-nitrophenol (4-NP) is one such model reaction used to demonstrate the catalytic activity of metal NPs.[7, 8, 37-39] In this study, we use the reduction of 4-NP to 4-aminophenol (4-AP) to quantitatively demonstrate the catalytic activity of triphenylphosphine AuNPs (TPP-AuNPs). Previous studies have shown that the reduction of 4-NP by $NaBH_4$ does not take place in the absence of NPs,[8] but upon addition of the NPs, the reaction proceeds. Electrons are transferred between 4-NP and $NaBH_4$ via the TPP-AuNPs. [8, 21, 40] We selected this reaction because it is rapid and can be easily characterized when AuNPs are added to the reaction mixture. We followed the reaction by monitoring the decrease in absorption peak amplitude of 4-NP at 400 nm over time by UV-vis spectroscopy. By using $NaBH_4$ whose concentration was much greater than that of 4-NP, the kinetics of the reaction could be described using pseudo-first- order kinetics[8] and we could assume that the reduction rate was independent of $NaBH_4$ concentration.

The objective of this study was to characterize the catalytic activity of the water soluble TPP-AuNPs using a simple model reaction; the reduction of 4-NP to 4-AP. The TPP-AuNPs were synthesized using a procedure developed in our laboratory.[41] The effect of the concentration of 4-NP and the TPP-AuNPs on the observed rate constants was investigated. We also determined the turn-over rate for this reaction. We report on the

percentage conversion of 4-NP to 4-AP as well as the observed induction times and recyclability of the TPP-AuNPs catalysts.

6.2 Experimental procedures

6.2.1 Materials

Sodium borohydride ($NaBH_4$)powder (98%) was obtained from Alfa Aesar. 4-nitrophenol (4-NP), chloro (triethylphosphine) gold (I) (97%), triphenylphosphine (TPP), trioctylphosphine (99.8%), 0.5 M THF solution of 9-Borabicyclo[3.3.1]nonane (9-BBN) and toluene (HPLC grade) were purchased from Sigma Aldrich. Acetonitrile (HPLC grade) and hexane were obtained from Fisher Scientific and EMD Chemicals respectively. All chemicals and solvents were used as received. Copper formvar/carbon grids (200 mesh) were acquired from Electron Microscopy Sciences.

6.2.2 Synthesis of TPP-AuNPs

In a mixture of acetonitrile and toluene (10:40 ml), 0.017 gm (0.05 mmol) of chloro(triethylphosphine)gold(I) (Et_3PAuCl) was dissolved. TPP (0.0786 gms, 0.3 mmol) was added to the mixture at room temperature. The contents were stirred for 30 min after which 0.4 ml of 9-BBN (0.2 mmol) was injected into the mixture. After an additional 30 min of stirring, a solid appeared. The reaction mixture was centrifuged and the solid was collected. The solid then was washed twice with hexane to remove any impurities. After drying by nitrogen flow, a black solid was obtained.

6.2.3 Preparation of catalyst

The black solid obtained above was dissolved in nanopure water, (>18 MΩ) and the mixture sonicated in a Branson ultrasonic cleaner. The solution was centrifuged for 30 min at 4000 r.p.m and the small aggregates at the bottom of the tube were discarded. The supernatant was centrifuged two more times and the final solution was used as the stock TPP-AuNP solution in the following catalysis investigations. For TEM analysis, a sample of the particles before the reaction was dropcast onto 200 mesh formvar-coated copper grid and excess solution removed using a filter paper to prevent particle aggregation. The grid was imaged after it dried.

6.2.4 Reduction of 4-NP

The reduction of 4-NP was carried out in a 2.5 ml quartz cuvette. In the cuvette, 2.33 ml of nanopure water was mixed with 10 µl of 0.01M 4-NP and 120 µl of 0.1M $NaBH_4$. Both solutions were freshly prepared. The color of the solution changed from colorless to yellow indicating that 4-NP had been converted to 4-nitrophenolate ions. The stock TPP-AuNP catalyst solution was diluted five times by taking 1 ml of the stock solution and adding 5 ml of nanopure water to it. The concentration of the diluted solution was determined by UV-vis spectroscopy. To the 4-NP solution, a 40 µl aliquot of the diluted TPP-AuNPs solution was added to make the total volume in the cuvette 2.5 ml. The final concentration of 4-NP was 4.0×10^{-5} M while that of $NaBH_4$ and TPP-AuNPs was 4.8×10^{-3} M and 3.7×10^{-10} M, respectively. Hydrogen gas was generated from the borohydride during the reduction reaction which assisted in the mixing of the solution. The pH of the solution was determined to be 10. The reaction was monitored by

collecting UV-vis absorption spectrum every 10 min. The same procedure was followed for a 4-NP concentration of 1.2×10^{-4} M. For the recycling experiments, 2 µl each of 4-NP and $NaBH_4$ were added to the cuvette after the first reaction (when all 4-NP in the initial reaction had been converted to 4-aminophenol). The total volume (2.504 ml) and hence the concentration of the reactants and catalyst did not change significantly from the initial volume (2.5 ml). Therefore, pseudo-first order kinetics analysis could still be used to determine the kinetics of this reaction. After the reactions, samples of the solution were drop cast onto 200 mesh formvar-coated copper grid and excess solution was removed using a filter paper to prevent particle aggregation. After drying, the sample on the grid was imaged using TEM.

6.2.5 Instrumentation

6.2.5.1 UV-visible Spectroscopy

UV-vis absorption spectra at room temperature were collected using a Perkin-Elmer Lambda 750 UV/Vis/NIR spectrophotometer over the 250-700 nm range. All data were corrected for background absorption using water. UV-vis absorption spectra at different temperatures (25.00, 30.00, 35.00 and 40.00 ^{o}C) were obtained using a U-4100 Hitachi spectrophotometer with TLC 42™ dual temperature controlled cuvette holders equipped with a matched and calibrated TC 225 temperature controller (Quantum Northwest Inc. WA). The temperature was maintained to within ± 0.02 ^{o}C of the desired temperature. All solutions were equilibrated for 5 min before the reaction was started.

6.2.5.2 Transmission Electron Microscopy

TPP-AuNPs solutions were drop cast onto 200 mesh formvar-coated copper grids (Electron Microscopy Sciences, PA). The excess solution was wicked away and the grids were air dried. TEM images were obtained using a Tecnai-12 instrument operating at 100 KV accelerating voltage (Microscopy Core Facility, University of Utah). Particle size analysis was done by counting at least 1000 particles in the TEM images using Scion Image Beta 4.02 Software.

6.2.5.3 HAADF-STEM, HRTEM and SAED imaging

TPP-AuNPs samples were prepared following the same procedure used for TEM samples as described above. Micrographs were obtained using a FEI Titan 80-300 TEM operated at 300 kV at the CAMCOR High Resolution and Analytical Facility (University of Oregon, Eugene, OR). The instrument is equipped for bright field, dark field, and high angle annular dark field STEM (HAADF-STEM) imaging. The collection angle of HAADF-STEM images was 10 mrad. The images were captured at different magnifications using a Gatan CCD. The dimension of the images obtained was 1k × 1k pixels for the original images. Selected-area electron diffraction (SAED) patterns also were obtained.

6.2.5.4 Zeta potential

Zeta potential of the NPs was determined using a NICOMP^{TM} 380 ZLS (Particle Sizing Systems, CA).

6.3 Results and discussion

6.3.1 Preparation of TPP-AuNPs

In this study, TPP-AuNPs dissolved in water are investigated as catalyst particle for the reduction of 4-NP by $NaBH_4$. The TPP-AuNPs were synthesized following a published procedure based on using 9-BBN as the reducing agent.[41] Briefly, chloro(triethylphosphine)gold(I) was dissolved in a mixture of acetonitrile and toluene. Triphenylphosphine (TPP) was added to the mixture at room temperature. After the mixing, 9-BBN was injected. A black solid was obtained after stirring for 30 min, which was collected by centrifugation, cleaned by washing twice with hexanes and dried under nitrogen. The final black solid was dissolved in water and used as the stock solution of TPP-AuNPs.

The NPs were found to be stable in water with a zeta potential of 34.9 ± 4.6 mV at a pH of 7.2. This is the first report of the solubility of TPP-AuNPs in water without post synthetic modification. UV-vis absorption spectroscopy indicated that the NPs were indeed small with no discernible localized surface plasmon resonance peak (Figure 6.1A). The size of the NPs as determined using transmission electron microscopy (TEM) was 4.3 ± 1.4 nm (Figure 6.1B). The NPs also were found to be single crystalline with (111) lattice fringes by high-resolution transmission electron microscopy (HRTEM) (Figure 6.1C). Selected area electron diffraction (SAED) confirmed the crystalline nature of the NPs.

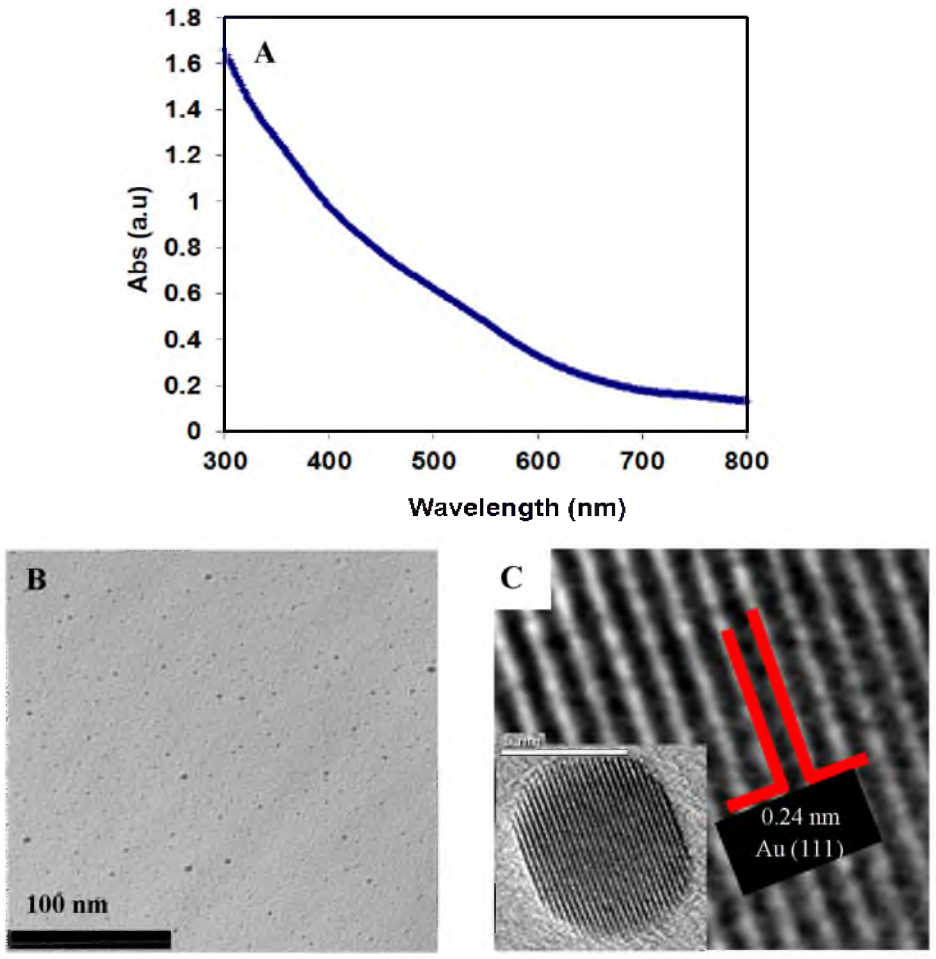

Figure 6.1. (A) UV-vis absorption spectrum of TPP-AuNPs in water. (B) TEM image of the TPP-AuNPs before being used as catalysts for the NP reduction reaction. (C) HRTEM image showing (111) lattice fringes of a single crystalline TPP-AuNP. Inset is a HRTEM image of a TPP-AuNP, scale bar = 5 nm.

6.3.2 Reduction of 4-nitrophenol catalyzed by TPP-AuNPs

Nitro compounds are known to be inert to reduction by $NaBH_4$ in the absence of a catalyst.[8] The catalytic activity of the prepared TPP-AuNPs was investigated using the reduction of 4-nitrophenol to 4-aminophenol by $NaBH_4$ as indicated in Scheme 6.1. This reaction is rapid and easily monitored by UV-vis spectroscopy. A detailed discussion of the mechanism of the reduction of 4-NP by $NaBH_4$ in the presence of TPP-AuNPs will follow later in this chapter. Briefly, TPP-AuNPs acted as an electron relay system to facilitate the transfer of electrons between 4-NP and the reducing agent, $NaBH_4$. The reaction conditions were set up such that $[BH_4^-] >> [4\text{-NP}]$ and [TPP-AuNPs]. As a result, the reaction followed pseudo first-order kinetics since at any one time, the concentration of BH_4^- was much greater than that of 4-NP and TPP-AuNPs. The reaction proceeded at a basic pH of 10. On addition of $NaBH_4$ to the reaction mixture, the color of the solution changed from colorless to yellow accompanied by evolution of hydrogen gas.

Scheme 6.1. The reduction of 4-NP to 4-AP by $NaBH_4$ catalyzed by TPP-AuNPs in water.

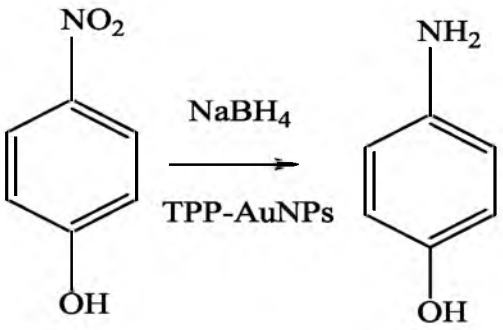

Reports suggest that the hydrogen gas liberated during the reaction purges oxygen as well as assists in the mixing of the reaction mixture.[23] The yellow color of the resulting solution indicated the conversion of 4-NP to 4-nitrophenolate ions under basic conditions. 4-NP and 4-nitrophenolate have absorption peaks at 317 and 400 nm, respectively, while 4-AP has a peak at 300 nm.

We followed the decrease in the amplitude of the 400 nm peak at different time points after adding the catalyst using UV-vis absorption measurements to determine the kinetics of the reaction. As mentioned previously, one of the most important considerations for choosing a model reaction is that only one product should be formed.[37] Isosbestic points indicated that 4-AP was the only product of the catalysis (Figure 6.2A). At room temperature and a catalyst concentration of 3.7×10^{-10} M, we observed that the reaction took about 120 min to complete for a 4-NP concentration of 4.0×10^{-5} M. The time for completion of the reduction decreased significantly when the concentration of the catalyst was increased, so the concentration was adjusted to allow for observation of changes in the peak amplitude using the simple UV-vis spectroscopy system. We used very dilute solutions of TPP-AuNPs as catalysts, and even addition of small amounts of catalyst to the reaction mixture caused a significant increase in the rate of reduction.

Our results also show that in the absence of catalyst the reduction reaction proceeds extremely slowly. In our control reaction, only about 2% of 4-NP had been converted to 4-AP over 6 days in the absence of catalyst (Figure 6.2B). Therefore, it is evident that the TPP-AuNPs serve as catalysts for this reduction reaction. A more detailed discussion of the effect of catalyst and 4-NP concentration on the rate of reduction of 4-NP will follow later in this chapter.

6.3.3 Determination of rate constants

As shown in Figure 6.2B, the reduction of 4-NP was negligible in the absence of TPP-AuNPs. The concentration of $NaBH_4$ was much greater than the concentration of 4-NP and TPP-AuNPs in all reaction mixtures. As a result, we used the approximation that the concentration of $NaBH_4$ was unchanged for the duration of the reaction. The observed rates of change of concentration of 4-NP with time (k_{obs}) were thus independent of the concentration of $NaBH_4$ and the reaction system was treated as pseudo first-order with respect to the concentration of 4-NP. We monitored the concentration of 4-NP as a function of time by monitoring the absorption peak at 400 nm which had an amplitude that was proportional to the concentration of 4-NP. Therefore, at time *t*, the ratio of the absorbance A_t to that at time *t=0,* (A_t/A_o) was equivalent to the ratio (C_t/C_o) of the concentration of 4-NP at time *t*, (C_t) and time t=0, (C_0). A linear correlation of ln A_t/A_o versus time verified the assumption that the reduction followed pseudo first-order kinetics (Figure 6.3).[7, 22, 26, 40]

The reaction progress was monitored until no 4-NP could be detected as evidenced by the absence of absorbance at 400 nm, indicating that all 4-NP had been converted to 4-AP or that the amount present was below the detection limit of the UV-vis spectrophotometer. Because induction times are a characteristic feature of the 4-NP reduction,[37] k_{obs} values were determined using the data from the linear part of the ln A_t/A_o versus time plot. The slope of this plot, -(d[4-NP]/[4-NP])/dt was used to obtain k_{obs}. The observed rate was found to be 0.0222 ± 0.0013 min^{-1} for concentrations of 4-NP = 4.0×10^{-5} M, $NaBH_4$ = 4.0×10^{-3} M and TPP-AuNPs = 3.7×10^{-10} M.

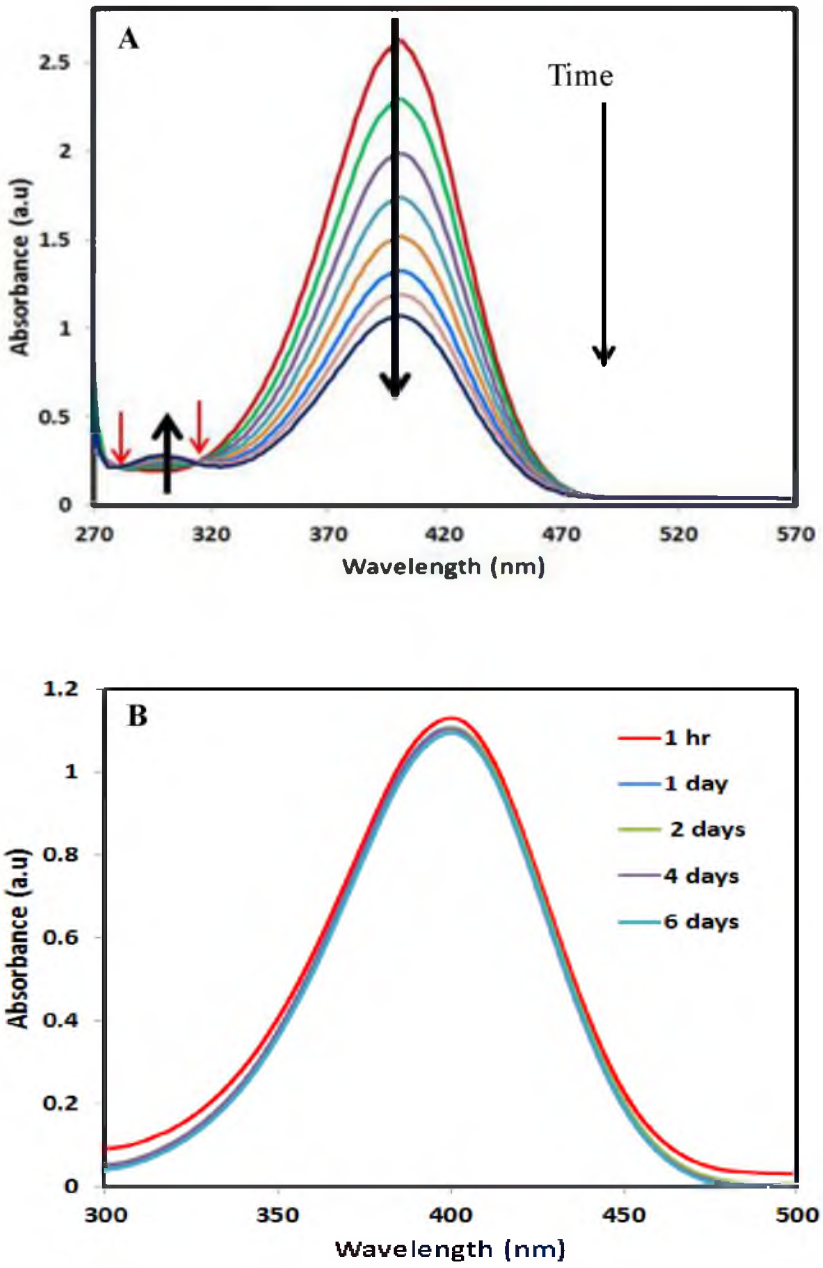

Figure 6.2. Time dependent UV-vis absorption spectra of the reduction of 4-NP by $NaBH_4$ at room temperature: (A) in the presence of TPP-AuNPs in water, (B) in the absence of TPP-AuNPs. The red arrows in A identify the isosbestic points indicating the complete conversion of 4-NP to 4-AP. Concentrations of 4-NP = 4.0×10^{-5} M, $NaBH_4$ = 4.0×10^{-3} M and TPP-AuNPs = 3.7×10^{-10} M were used.

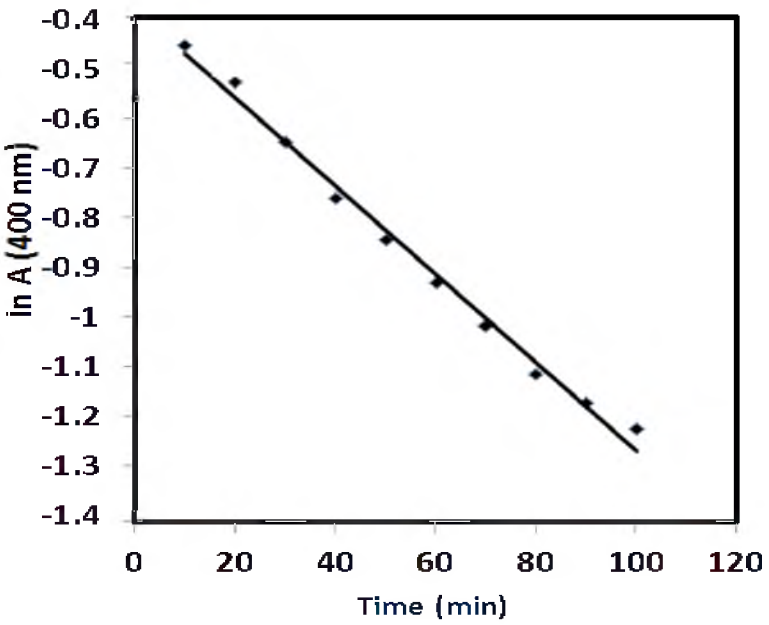

Figure 6.3. Plot of ln A vs time shows first-order kinetics for the reduction of 4-NP by $NaBH_4$.

The real rate of the reaction is thus (d[4-NP])/dt. This value is constant at all concentrations of the substrate and will be discussed in detail in sections 6.3.5 and 6.3.6.

6.3.4 Recyclability of the TPP-AuNPs catalysts

The recyclability of the TPP-AuNPs catalysts was investigated. Recycling of the AuNPs was studied by adding 2µl each of 4-NP and $NaBH_4$ to the 2.5 mL volume of reaction mixture in the reaction cuvette. The final concentration of 4-NP was 7.987×10^{-6} M. The total volume used for the recycling reaction study was 2.504 ml and hence the concentration of the reactants and catalyst did not change significantly from the initial volume (2.5 ml). Therefore, the kinetics could be treated as pseudo first-order. The percent conversion for the first cycle was ~98% as shown in Figure 6.4A.

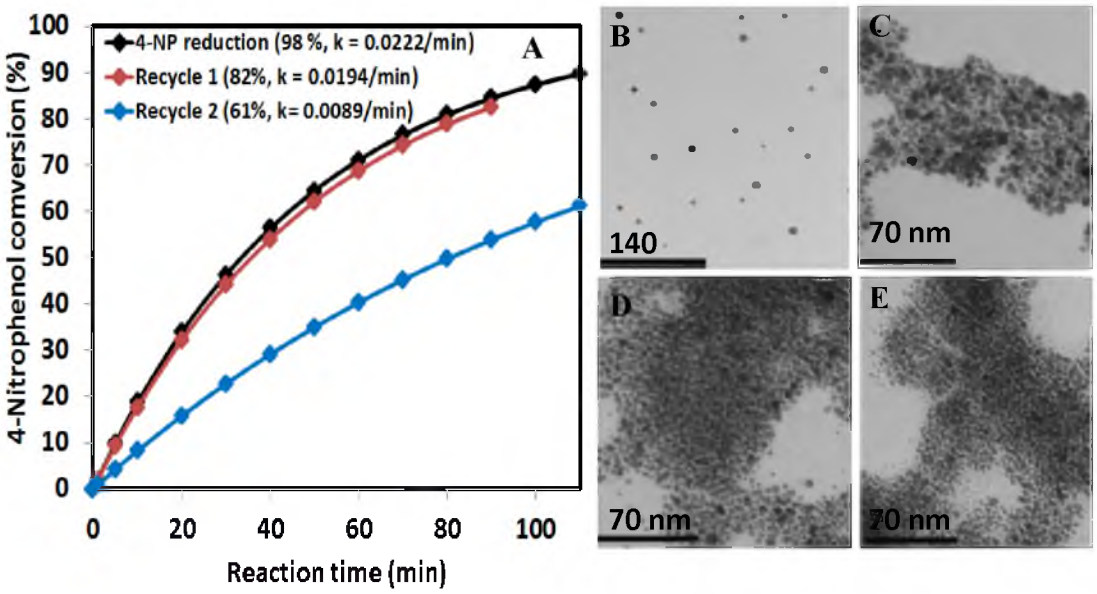

Figure 6.4. (A) Comparison of percent conversion of 4-NP to 4-AP between the first reaction cycle and the subsequent recycling runs. (B) TEM images of the TPP-AuNPs before reaction, (C) after the first reaction cycle, (D) after the first recycling reaction and (E) after the second recycling reaction.

This process was repeated again for a second recycling cycle after making sure that no 4-NP remained in the solution indicating the reduction had reached completion. The final total volume (2.508 ml) was not changed significantly from the initial volume (2.5 ml). The final concentration of 4-NP was 7.974×10^{-6} M. Therefore, pseudo first-order kinetics could still be used to determine the kinetics of this recycling reaction. There was a decrease in the k_{obs} of 4-NP between the two recycle runs from 0.0194 ± 0.0005 min^{-1} to 0.0089 ± 0.0003 min^{-1}. The percent conversion of 4-NP to 4-AP decreased significantly when the catalysts were recycled 96% to 61%. The reason for this is that the NPs aggregated (Figure 6.4B-E) thereby hindering access of 4-NP to the reactive sites on the surfaces of the NPs during subsequent reaction cycles. In addition, it has been reported that the amino group of 4-AP has strong affinity to Au surfaces, such

that when 4-AP adsorbs to the Au surfaces, it prevents 4-NP from accessing the Au surface.[42]

6.3.5 Dependence of 4-NP reduction on the concentration of 4-NP

We investigated the dependence of k_{obs} on the concentrations of 4-NP and the TPP-AuNPs (Figure 6.5). We fixed the concentrations of TPP-AuNPs and $NaBH_4$ at 3.712×10^{-10} M and 4.8×10^{-3} M, respectively, while varying the concentration of 4-NP. Based on the catalytic mechanism which is discussed in more detail later, the rate of electron transfer on the AuNPs surface affects the rate constant of the reaction. It has been reported that adsorption on and desorption from the surface of the TPP-AuNPs for 4-NP, BH_4^- and 4-AP is fast.[39] An inverse relationship between k_{obs} and the concentration of 4-NP was observed. As the concentration of 4-NP in the reaction mixture increased, k_{obs} decreased (Figure 6.5A). The rate of reduction of 4-NP i.e., -(d[4-NP])/dt is thus independent of the concentration of 4-NP in the reaction mixture. This indicated that at some point, the catalytic sites on the AuNPs became saturated as more 4-NP was added to the reaction mixture and adsorbed on the surface of the AuNPs. Therefore, the reaction rate at the NP surface was constant. A summary of the k_{obs} is given in Table 6.1. A plot of k_{obs} against 1/[4-NP] is linear, thus verifying that the rate of the reaction is indeed constant (Figure 6.5B) and independent of 4-NP concentration. Similar results were obtained by Wunder et al. [39] for Pt and Au NPs enclosed in spherical polyelectrolyte brushes. They observed a significant decrease in the k_{obs} as more 4-NP was added to the mixture for both PtNPs and AuNPs, providing more evidence for saturation of the NP surface with 4-NP.

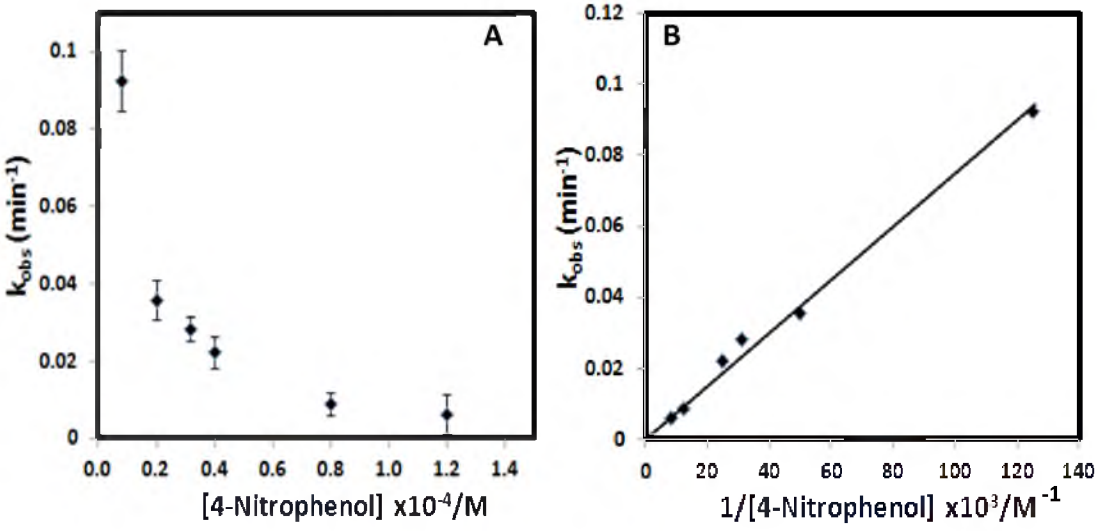

Figure 6.5. (A) Dependence of k_{obs} for the reduction of 4-NP by $NaBH_4$ on the concentration of 4-NP. (B) Dependence of the rate constant for the reduction of 4-NP by $NaBH_4$ on the concentration of 4-NP.

Table 6.1. Dependence of k_{obs} of 4-NP reduction on the concentration of 4-NP.

[4-NP]	k_{obs} (min^{-1})
8.0 x 10^{-6} M	0.0923 ± 0.0080
2.0 x 10^{-5} M	0.0357 ± 0.0050
3.2 x 10^{-5} M	0.0281 ± 0.0032
4.0 x 10^{-5} M	0.0222 ± 0.0041
8.0 x 10^{-5} M	0.0087 ± 0.0030
1.2 x 10^{-4} M	0.0061 ± 0.0050

6.3.6 Dependence of 4-NP reduction on the concentration of TPP-AuNPs

To investigate the dependence of k_{obs} on the concentration of TPP-AuNPs, we kept the concentrations of 4-NP and $NaBH_4$ constant at 4.0×10^{-5} M and 4.8×10^{-3} M, respectively, while varying the concentration of TPP-AuNPs. These concentrations were chosen to maintain a $NaBH_4$ concentration that was much greater than that of 4-NP in order to ensure that pseudo first-order kinetics still applied to this system. In addition, these concentrations had been optimized to ensure that the reaction proceeded neither too fast nor too slowly to be monitored by the UV-vis absorption spectroscopy. In order to make comparisons with other catalytic NP systems, we analyzed the activity of the NPs with respect to the number of surface atoms of the NPs. Surface atoms refer to the atoms at faces, corners, edges and defect sites. The fraction of surface atoms increases as the size of the NPs decreases.[43, 44] The atoms located on corners and edges have high surface energies and as a result, they are catalytically active.[45, 46] Since both the concentration and size of the TPP-AuNPs added to the reaction mixture were known, it was possible to calculate the number of surface atoms for that concentration of TPP-AuNPs. By calculation, a 4 nm particle has ~ 27% of atoms on the surface. As the number of surface atoms increased (corresponding to the concentration of TPP-AuNPs added), k_{obs} increased (Figure 6.6). The rate of reduction of 4-NP was proportional to the surface area of the TPP-AuNPs. The linear relationship between the number of surface atoms and the rate constant confirms that the rate of 4-NP reduction is constant and is limited by the concentration of the TPP-AuNPs. This result also implies that the surface atoms were responsible for the catalytic activity observed.

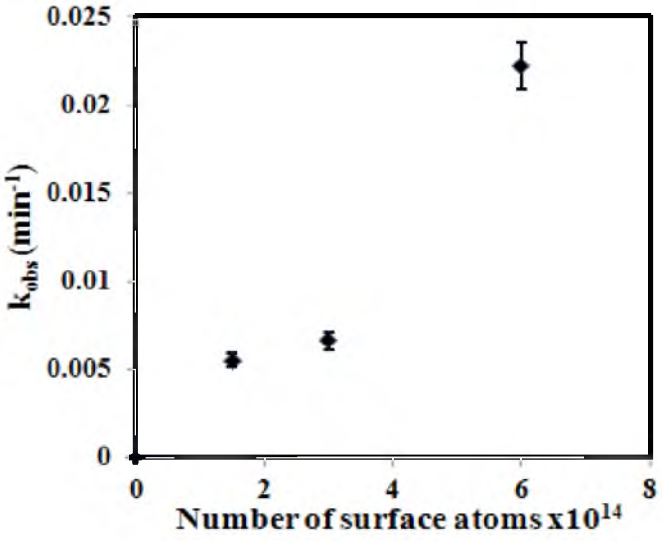

Figure 6.6. Dependence of k_{obs} of 4-NP reduction by $NaBH_4$ on the number of surface atoms with constant concentrations of 4-NP and $NaBH_4$.

6.3.7 Determination of the turn-over rate

The turn-over rate (TOR) for the reaction also was determined. The TOR represents the number of 4-NP molecules that are converted to 4-AP per catalytic site per unit time. However, it is difficult to measure the number of catalytically active sites for a given reaction.[47, 48] Therefore, in determining the TOR, the assumption was made that all surface sites were catalytically active.[49] The result obtained is thus a lower limit of the TOR.[48] In order to determine the TOR, the actual change in concentration of 4-NP that was turned over per unit time was determined and converted into molecules per unit time. This number was divided by the active surface area of the catalyst and then multiplied by the reactant molecule area to obtain TOR. The active surface area of the catalyst was the total surface area of the NPs added to the reaction mixture (4.49×10^3 cm^2). The reactant molecule area was 4.62×10^{-15} cm^2. For the reduction of 4-NP, a TOR of 876 min^{-1} was obtained. The TOR was found to be constant and independent of the catalyst

concentration. Liu et al. [50] reported TOR of 120 h^{-1} for the reduction of 4-NP catalyzed by polyethylenimine-isobutyramide capped AuNPs. Koga et al. also obtained TOR of 1400 h^{-1} for the reduction of 4-NP catalyzed by Au/Ag bimetallic NPs,[51] while TOR of 120 h^{-1} was determined for Au/AgNPs on ZnO. In another study, 0.1 mol % Au, Pd and Pt NPs were loaded onto TiO_2 resulting in TORs of 84, 97 and 7 min^{-1} respectively. [52] The TORs dramatically reduced when the NPs were loaded onto ZrO_2 and Al_2O_3. In summary, the TOR obtained with TPP-AuNPs is 36-400 times faster compared to literature reports. The implication is that water soluble TPP-AuNPs are better catalysts for the reduction of 4-NP.

6.3.8 Effect of temperature on the observed rate constants

To investigate the effect of temperature on the k_{obs}, reactions were performed at four different temperatures (298, 303, 308 and 313 K) for two concentrations of $NaBH_4$ (8.0×10^{-3} M and 1.2×10^{-2} M). The temperature for each sample was equilibrated for 5 min before the reactions were initiated. The concentration of 4-NP was kept constant at 4.0×10^{-5} M. Table 6.2 shows the dependence of k_{obs} on temperature for the two $NaBH_4$ concentrations.

Table 6.2. k_{obs} for the reduction of 4-NP at different temperatures.

Temperature (K)	k_{obs} (min^{-1}) with 8.0×10^{-3} M $NaBH_4$	k_{obs} (min^{-1}) with 1.2×10^{-2} M $NaBH_4$
298	0.0144 ± 0.0007	0.0447 ± 0.0026
303	0.0216 ± 0.0015	0.0560 ± 0.0028
308	0.0564 ± 0.0018	0.0764 ± 0.0040
313	0.1126 ± 0.0049	0.1195 ± 0.0070

It was evident that the rate of the reaction increased with an increase in temperature (Figure 6.7A). From this data, the activation energy (E_a) for the reaction was determined. The activation energy indicates how k_{obs} depend on the temperature. This relationship can be obtained from the Arrhenius equation (Equation 1):

$$\ln k_{obs} = -(E_a/RT) + \ln A \text{ .....(1)}$$

where k is the observed rate constant of the reaction, T is temperature in Kelvin, R is the universal gas constant and A is the Arrhenius factor. Figure 6.7B shows a plot of ln k_{obs} vs 1/T. This plot is linear for the reduction of 4-NP.

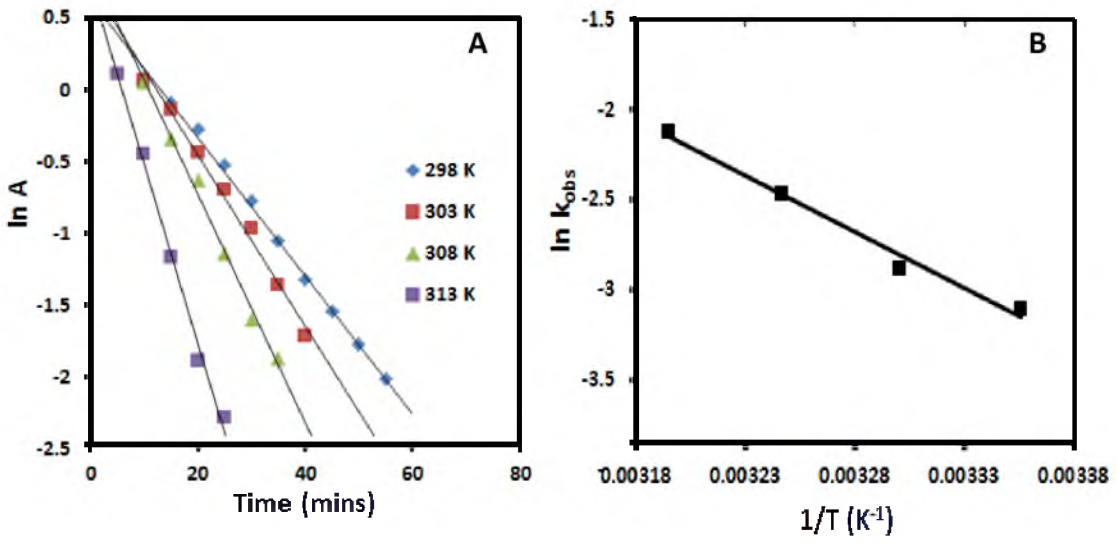

Figure 6.7. (A) Observed rate constants for the 4-NP reduction at different temperatures. (B) Arrhenius plot for the reduction of 4-NP by $NaBH_4$ catalyzed by TPP-AuNPs.

From the slope of the plot of ln k vs 1/T, the activation energy was determined to be 50.4 ± 2.1 kJ/mol. In addition, the pre-exponential factor was calculated from the intercept of the plot. The entropy of activation ($\Delta S^{\ddagger}$) also was determined using the equation $\ln A = \Delta S/R$.[46] The frequency factor was found to be 2.8×10^7 min^{-1} while $\Delta S^{\ddagger}$ was determined to be 145.5 ± 3.8 J/mol K. A review of literature for similar catalytic systems shows that these parameters are comparable to those obtained previously using NPs which have been immobilized or supported. We believe this is significant because our system is comprised of NPs that are not immobilized on a support. For unsupported systems, we expect the activation energy obtained to be much higher, which was not the case with the TPP-AuNPs. For example, using 2.2 nm AuNPs immobilized on spherical polyelectrolyte brushes, an activation energy of 49 kJ/mol was obtained.[37] For partially hollow Au nanoboxes and completely hollow Au nanoboxes, activation energies of 55 and 44 kJ/mol, respectively, were obtained.[7] Magnetically recoverable 3 nm AuNPs (chitosan-coated iron oxide magnetic nanocarrier) had an activation energy of 52 kJ/mol.[21] Comparing the surface area and the concentration of the TPP-AuNPs used in this study to those used by Kundu et al.,[53] the observed rate constants are comparable, 0.0222 min^{-1} vs 0.0276 min^{-1} even though we used much lower NP concentrations. A summary of the review of kinetic parameters for various catalytic systems is presented in Table 6.3.

Table 6.3. Kinetic parameters for different catalytic systems for the reduction of 4-nitrophenol.

Type of catalytic system	Kinetic parameters
2.2 nm AuNPs on spherical polyelectrolyte brushes[37]	E_a = 49 kJ/mol
Partially hollow Au nanoboxes[7]	E_a = 55 kJ/mol
Hollow Au nanoboxes[7]	E_a = 44 kJ/mol
Au nanocages[7]	E_a = 28 kJ/mol
CTAB-Au nanorods (nanorattles) 60 nm (L) X 30 nm (W)[54]	E_a = 38 kJ/mol
3 nm magnetically recoverable chitosan-coated iron oxide magnetic nanocarrier AuNPs[21]	E_a = 52 kJ/mol
Resin bead immobilized citrate stabilized AuNPs 20 nm[22]	E_a = 31 kJ/mol
Calcium alginate stabilized 5 nm AuNPs[23]	E_a = 21 kJ/mol
Cetyltrimethylammonium bromide (CTAB) stabilized 45 nm AuNPs[53] Number of particles per ml = 1.1×10^{20} Surface area = 6400 nm^2	k_{obs} = 0.0276 min^{-1}
Polyethylenimine-isobutyramide capped AuNPs[50]	TOR = 120 h^{-1}
Au, Pd and Pt NPs on TiO_2 [52]	TOR = 84, 97 and 7 min^{-1}
4 nm AuNPs (current study) Number of particles per ml = 1.396×10^{13} Surface area = 5.6×10^{14} nm^2	k_{obs}= 0.0222 min^{-1} TOR = 876 min^{-1}

6.3.9 Dependence of induction time on temperature and concentration of 4-NP

An induction period was observed for the reduction of 4-NP by borohydride in the presence of TPP-AuNPs. The induction time has been attributed to the restructuring of the AuNPs surface which involves the decomposition of the borohydride and the production of H-atoms[54] and the time needed for 4-NP to adsorb to the NP surface.[7, 37] Other researchers have attributed the induction to the time needed for oxygen in the system to be reduced.[23, 55] We conducted our experiments with water purged with nitrogen. The aim of purging the water with nitrogen was to remove dissolved oxygen. We compared the induction times for experiments in which the reagents were dissolved in water that was purged and water that was not purged. The induction times observed for the two sets of experiments were not significantly different. For example, for 8.0×10^{-6} M 4-NP, the observed induction times were 1.8 ± 0.7 min and 1.3 ± 0.7 min for the sample that was not purged and for the sample that was purged, respectively. The same trend was observed for the other concentrations of 4-NP used.

We also found that an increase in the concentration of $NaBH_4$ did not change the induction time, a finding that was also recently reported by Wunder et al.[37] We therefore set out to investigate the effect of other factors in this reduction on the induction times, namely, temperature and the concentration of 4-NP. To determine the effect of temperature on the induction time, the concentration of TPP-AuNPs, 4-NP and$NaBH_4$ were kept constant while the temperature was varied between 25, 30, 35 and 40 ^{o}C. There was a significant decrease in the induction times as the temperature was raised (Figure 6.8A). The induction time was found to increase as the concentration of 4-NP

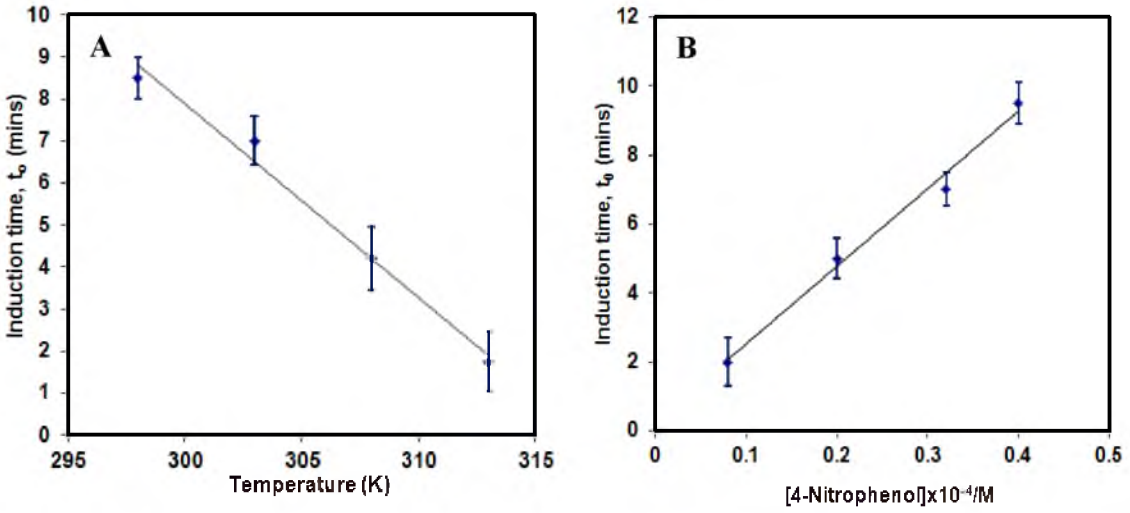

Figure 6.8. (A) Dependence of the induction time on temperature. [4-NP] = 4.0×10^{-5} M, [$NaBH_4$] = 8.0×10^{-3} M. (B) Dependence of the induction time on concentration of 4-NP. [$NaBH_4$]= 8.0×10^{-3} M, temperature = 25 °C.

increased (Figure 6.8B).

Due to the low NP concentrations used, the induction period lasted 8 min at 25 °C. When the temperature was raised to 40 °C, the induction period decreased to 1.8 min. To determine the effect of 4-NP concentration on the induction time, the concentration of TPP-AuNPs and $NaBH_4$ were kept constant. The temperature was also kept constant at 25 °C as the 4-NP concentration was varied. Adsorption of 4-NP on the surface of the TPP-AuNPs must occur for the reduction to take place.[39] This supports the hypothesis that, it is during this time that 4-NP rearranges the surface of the AuNPs to make the surface catalytically active. This point will become clearer in the following section where the mechanism of the reduction of 4-NP will be discussed.

In one study, analysis of the relationship between the induction time and the concentration of 4-NP revealed that the surface rearrangement process is induced by 4-NP.[37] This process is directly linked to the rate of the reduction reaction. This

rearrangement process is necessary for the catalysis to proceed. It is therefore safe to assume that the rate at which 4-NP adsorbs to the AuNP surface determines the length of the induction period.[7] As more 4-NP was added to the reaction mixture, most of the NP surface was covered by 4-NP to the disadvantage of BH_4^-, both of which must adsorb for the reduction to take place. An increase in temperature seemed to provide the energy needed for faster rearrangement of the NP surface. The reduction in induction times as a result of increase in the temperature under which the reaction is done has also been observed before.[7] Detailed induction times for both experiments are provided (Tables 6.4 and 6.5). A review of published results indicates that the surface chemistry of the NPs can play a role in determining the length of the induction period. In our case, we think that the TPP ligands may lengthen the induction period compared to citrate stabilized NPs due to the bulky nature of the TPP ligands. However, the catalytic activity as determined by the kinetic data indicates that there is still good accessibility to the surface of the NPs.

Table 6.4. Dependence of the induction time on temperature. [4-NP] = 4.0×10^{-5} M, [$NaBH_4$] = 8.0×10^{-3} M.

Temperature (K)	T_0 (min)
298	8.5 ± 0.5
303	7.0 ± 0.6
308	4.2 ± 0.8
313	1.8 ± 0.7

Table 6.5. Dependence of the induction time on concentration of 4-NP. [$NaBH_4$]= 8.0 × 10^{-3} M, temperature = 25 °C.

[4-NP] × 10^{-4} M	T_0 (min)
0.08	1.8 ± 0.7
0.2	4.7 ± 0.6
0.32	7.0 ± 0.5
0.4	9.5 ± 0.6

6.3.10 Mechanism of the reduction of 4-NP to 4-AP

The reduction of 4-NP to 4-AP is a 6 electron process.[23] The reaction starts with the conversion of 4-NP to 4-nitrophenolate ions on addition of $NaBH_4$. Since the concentration of $NaBH_4$ is much greater than the concentration of 4-NP, the pH of the solution is basic and this serves to slow down the degradation of the $NaBH_4$. The reduction of 4-NP to 4-AP takes place on the surface of the TPP-AuNPs. [39] This can be inferred from the relationship between the concentration of TPP-AuNPs and the rate constants of the reduction of 4-NP. The observed rate constants increased as the concentration of TPP-AuNPs increased. This increase was correlated to the number of surface atoms (Figure 6.6). The reaction proceeds with the transfer of electrons from the BH_4^- ions to the 4-NP with the TPP-AuNPs catalysts acting as the electron relay system to form the product, 4-AP which then desorbs from the surface of the NP. Several mechanisms for how the heterogeneous reduction of 4-NP proceeds have been proposed. Two models used to describe the reduction process are the Langmuir-Hinshelwood model[39] and the Eley-Rideal model.[54] The Eley-Rideal model assumes that only one reactant, in this case, hydrogen, is adsorbed on the surface of the catalyst. On the other

hand, the Langmuir-Hinshelwood model assumes both the reducing agent (BH_4^- ions) and the substrate (4-nitrophenolate ions) must be adsorbed onto the surface of the AuNPs for the reaction to proceed. According to the Langmuir-Hinshelwood model, a hydride is transferred from the BH_4^- ions to the metal NP surface. The nitrophenolate ions are then adsorbed on the NP surface. Hydride transfer to the adsorbed nitrophenolate ions occurs leading to the formation of the amino compound. Wunder et al. [39] have demonstrated that the reduction of 4-NP to 4-AP in the presence of metal NPs follows the Langmuir-Hinshelwood model. In our experiment, we had similar observation as in the experiments by Wunder et al. For example, we observed that the rate constant decreased when the concentration of 4-NP increased. We also observed that an increase in the concentration of $NaBH_4$ does not change the induction time. This leads us to propose that the reduction of 4-NP to 4-AP in the presence of TPP-AuNPs follows the Langmuir-Hinshelwood model.

Two routes for how the reduction takes place have been put forward. [56] The first route involves the conversion of the nitro compound to a hydroxylamine and then to an aniline (amino compound).[57] The second route involves the conversion of the nitro compound to a nitroso compound. Condensation of one nitroso compound molecule and one hydroxylamine molecule occurs to form an azo, hydrazo and aniline compound in that order. Corma et al.[56] used a combination of *in-situ* FTIR spectroscopy and kinetic experiments to study which of the two routes was followed for the reduction of nitro compounds. The intermediates species and reaction products in the reaction were identified. Using this information and the kinetic data generated, the first route was experimentally shown to be the preferred route for Au catalysts.

6.4 Conclusions

We have demonstrated that TPP-AuNPs soluble in water are catalytically active in the reduction of 4-NP by sodium borohydride to 4-AP. The reaction was determined to follow pseudo-first-order kinetics with respect to 4-NP. The rate constants were found to depend on several factors. The surface area of the catalyst was found to limit the rate constants at all concentrations of 4-NP. The surface of the catalyst was saturated at all concentrations and as a result, the rate of the reaction was proportional to the surface area of the catalyst. The turn-over rate also was found to be constant and independent of catalyst concentration. As the temperature and the amount of catalyst increased, the rate constants increased whereas they decreased as the amount of 4-NP increased. However, the rates were found to be independent of the concentration of 4-NP. An induction period was also observed which depended on the temperature and the concentration of 4-NP while remaining independent of the concentration of borohydride. The induction time was attributed to the time needed for the restructuring of the AuNP surface for catalysis. The activation energy for the reaction was 50 kJ/mol which was comparable to that for supported catalyst systems even though the catalytic system in this study did not have a catalyst support. Incorporating the TPP-AuNPs in a solid support could improve the percent conversion of 4-NP and catalyst recyclability and this aspect is under study.

6.5 References

(1) Schmid, G. *Chem. Rev.* **1992**, *92*, 1709-1727.

(2) Daniel, M.-C.; Astruc, D. *Chem. Rev.* **2004**, *104*, 293-346.

(3) Sanchez, A.; Abbet, S.; Heiz, U.; Schneider, W. D.; Häkkinen, H.; Barnett, R. N.; Landman, U. *J. Phys. Chem. A* **1999**, *103*, 9573-9578.

(4) Hammer, B.; Norskov, J. K. *Nature* **1995**, *376*, 238-240.

(5) Masatake, H. *Catal. Today* **1997**, *36*, 153-166.

(6) Min, B. K.; Friend, C. M. *Chem. Rev.* **2007**, *107*, 2709-2724.

(7) Zeng, J.; Zhang, Q.; Chen, J.; Xia, Y. *Nano Lett.* **2010**, *10*, 30-35.

(8) Pradhan, N.; Pal, A.; Pal, T. *Langmuir* **2001**, *17*, 1800-1802.

(9) Grunwaldt, J. D.; Molenbroek, A. M.; Topsøe, N. Y.; Topsøe, H.; Clausen, B. S. *J. Catal.* **2000**, *194*, 452-460.

(10) Hayashi, T.; Tanaka, K.; Haruta, M. *J. Catal.* **1998**, *178*, 566-575.

(11) Tsunoyama, H.; Ichikuni, N.; Sakurai, H.; Tsukuda, T. *J. Am. Chem. Soc.* **2009**, *131*, 7086-7093.

(12) Haruta, M.; Yamada, N.; Kobayashi, T.; Iijima, S. *J. Catal.* **1989**, *115*, 301-309.

(13) Haruta, M. *Catal. Surv. Jpn* **1997**, *1*, 61-73.

(14) Haruta, M.; Tsubota, S.; Kobayashi, T.; Kageyama, H.; Genet, M. J.; Delmon, B. *J. Catal.* **1993**, *144*, 175-192.

(15) Astruc, D. *Nanoparticles and catalysis*; Wiley-VCH: Weinheim, 2007.

(16) Corma, A.; Garcia, H. *Chem. Soc. Rev.* **2008**, *37*, 2096-2126.

(17) Haruta, M.; Date, M. *Appl. Catal., A* **2001**, *222*, 427-437.

(18) Alvarez-Puebla, R. A.; dos Santos, J. D. S.; Aroca, R. F. *Analyst* **2007**, *132*, 1210-1214.

(19) Filippini, D.; Weiß, T.; Aragón, R.; Weimar, U. *Sens. Actuators, B* **2001**, *78*, 195-201.

(20) Santos, A.; Yustos, P.; Quintanilla, A.; Garcia-Ochoa, F.; Casas, J. A.; Rodriguez, J. J. *Environ. Sci. Technol.* **2003**, *38*, 133-138.

(21) Chang, Y.-C.; Chen, D.-H. *J. Hazard. Mater.* **2009**, *165*, 664-669.

(22) Panigrahi, S.; Basu, S.; Praharaj, S.; Pande, S.; Jana, S.; Pal, A.; Ghosh, S. K.; Pal, T. *J. Phys. Chem. C* **2007**, *111*, 4596-4605.

(23) Saha, S.; Pal, A.; Kundu, S.; Basu, S.; Pal, T. *Langmuir* **2009**, *26*, 2885-2893.

(24) EPA, U. S. *Quality Criteria for Water*: Washington D.C, 1986.

(25) Levec, J.; Pintar, A. *Catal. Today* **1995**, *24*, 51-58.

(26) Mahmoud, M. A.; Saira, F.; El-Sayed, M. A. *Nano Lett.* **2010**, *10*, 3764-3769.

(27) Ghosh, S. K.; Mandal, M.; Kundu, S.; Nath, S.; Pal, T. *Appl. Catal., A* **2004**, *268*, 61-66.

(28) Lu, Y.; Mei, Y.; Drechsler, M.; Ballauff, M. *Angew Chem Int Ed.* **2006**, *45*, 813-816.

(29) Brust, M.; Kiely, C. J. *Colloids Surf, A* **2002**, *202*, 175-186.

(30) Turner, M.; Golovko, V. B.; Vaughan, O. P. H.; Abdulkin, P.; Berenguer-Murcia, A.; Tikhov, M. S.; Johnson, B. F. G.; Lambert, R. M. *Nature* **2008**, *454*, 981-983.

(31) Sau, T. K.; Pal, A.; Pal, T. *J. Phys. Chem. B* **2001**, *105*, 9266-9272.

(32) Gao, Y.; Shao, N.; Zeng, X. C. *ACS Nano* **2008**, *2*, 1497-1503.

(33) Zhu, M.; Aikens, C. M.; Hollander, F. J.; Schatz, G. C.; Jin, R. *J. Am. Chem. Soc.* **2008**, *130*, 5883-5885.

(34) Tsunoyama, H.; Nickut, P.; Negishi, Y.; Al-Shamery, K.; Matsumoto, Y.; Tsukuda, T. *J. Phys. Chem. C* **2007**, *111*, 4153-4158.

(35) Zhu, Y.; Qian, H.; Drake, B.; Jin, R. *Angew Chem Int Ed.* **2010**, *49*, 1295-1298.

(36) Somorjai, G. A.; Park, J. Y. *Angew Chem Int Ed.* **2008**, *47*, 9212-9228.

(37) Wunder, S.; Lu, Y.; Albrecht, M.; Ballauff, M. *ACS Catal.* **2011**, *1*, 908-916.

(38) Esumi, K.; Miyamoto, K.; Yoshimura, T. *J. Colloid Interface Sci.* **2002**, *254*, 402-405.

(39) Wunder, S.; Polzer, F.; Lu, Y.; Mei, Y.; Ballauff, M. *J. Phys. Chem. C* **2010**, *114*, 8814-8820.

(40) Lee, K. Y.; Hwang, J.; Lee, Y. W.; Kim, J.; Han, S. W. *J. Colloid Interface Sci.* **2007**, *316*, 476-481.

(41) Shem, P. M.; Sardar, R.; Shumaker-Parry, J. S. *Langmuir* **2009**, *25*, 13279-13283.

(42) Seh, Z. W.; Liu, S.; Zhang, S.-Y.; Shah, K. W.; Han, M.-Y. *Chem. Commun.* **2011**, *47*, 6689-6691.

(43) Chui, Y. H.; Chan, K. Y. *Phys. Chem. Chem. Phys.* **2003**, *5*, 2869-2874.

(44) Wen, C.; Liu, Y.; Tao, F. *Pure Appl. Chem* **2011**, *83*, 243–252.

(45) Narayanan, R.; Tabor, C.; El-Sayed, M. *Top Catal.* **2008**, *48*, 60-74.

(46) Narayanan, R.; El-Sayed, M. A. *Nano Lett.* **2004**, *4*, 1343-1348.

(47) Boudart, M. *Chem. Rev.* **1995**, *95*, 661-666.

(48) Somorjai, G. A.; Li, Y. *Introduction to Surface Chemistry and Catalysis*, 2nd ed.; John Wiley & Sons: Hoboken, New Jersey, 2010.

(49) Somorjai, G. A. *Chem. Rev.* **1996**, *96*, 1223-1236.

(50) Liu, X.-Y.; Cheng, F.; Liu, Y.; Liu, H.-J.; Chen, Y. *J. Mater. Chem.* **2010**, *20*, 360-368.

(51) Koga, H.; Umemura, Y.; Kitaoka, T. *Catalysts* **2011**, *1*, 69-82.

(52) Jin, Z.; Xiao, M.; Bao, Z.; Wang, P.; Wang, J. *Angew Chem Int Ed.* **2012**, *51*, 6406-6410.

(53) Kundu, S.; Lau, S.; Liang, H. *J. Phys. Chem. C* **2009**, *113*, 5150-5156.

(54) Khalavka, Y.; Becker, J.; Sonnichsen, C. *J. Am. Chem. Soc.* **2009**, *131*, 1871-1875.

(55) Lu, Y.; Mei, Y.; Walker, R.; Ballauff, M.; Drechsler, M. *Polymer* **2006**, *47*, 4985-4995.

(56) Corma, A.; Concepción, P.; Serna, P. *Angew Chem Int Ed.* **2007**, *46*, 7266-7269.

(57) Gelder, E. A.; Jackson, S. D.; Lok, C. M. *Chem. Commun.* **2005**, 522-524.

CHAPTER 7

REDUCTION OF HEXACYANOFERRATE (III) TO HEXACYANOFERRATE (II) BY SODIUM BOROHYDRIDE CATALYZED BY WATER SOLUBLE TRIPHENYLPHOSPHINE STABILIZED GOLD NANOPARTICLES

7.1 Introduction

Catalysis based on using transition metal nanoparticles (NPs) in the nanometer size range has experienced tremendous growth in recent years.[1, 2] Catalytic activity of NPs has been found to generally increase as the NP size decreases primarily because of the large increase in the surface area to volume ratio, especially compared to bulk metals.[1, 3-7] Bulk gold is known to be chemically inert to the extent that normally reactive molecules, including H_2 and CO, do not adsorb on the surface of gold.[8, 9] However, Haruta demonstrated that Au in the form of small AuNPs can have excellent catalytic activity.[3] For AuNPs, this catalytic activity derives from size effects as well as the stabilization of the $6s^2$ electron pair and the reactivity of the 5 d electrons due to relativistic effects.[8, 10] Many studies of AuNP catalysis have been based on dispersing the NPs on oxide supports. Some of the oxides used are ZrO_2, Fe_2O_3, Co_3O_4 , TiO_2 and Al_2O_3 among others.[11-13] For most metal NPs, the atoms at the surface, edges and corners

have a positive oxidation state compared to the inner atoms which have a zero oxidation state.[14] The metal oxide support provides the electronic density needed to stabilize these surface atoms. On deposition onto metal oxide supports, a greater fraction of surface atoms comes into contact with the support for small NPs.[8] Therefore, the most catalytically active atoms are the ones at the interface between the NP and the support.[14] Dispersing the catalysts on the metal oxide supports exposes a higher fraction of surface atoms for catalysis. For this reason, supported NPs have been shown to have high activities at low temperatures for CO oxidation and NO reduction. [3, 11] One setback of oxide surface supported AuNP catalysts is sintering as a result of the movement of the AuNPs on the oxide surface at high temperatures which leads to deactivation of the catalyst.[15] Development of oxide catalyst support systems that do not sinter is therefore an active field of research.[16-18] Other materials have been used as supports for Au based catalysts, such as carbon nanotube-inorganic oxide hybrid nanoparticles,[19] activated-carbon,[20] mesoporous silica core–shell nanocatalysts[21] and boron nitride.[22]

Use of AuNPs as catalysts in the solution phase is not unprecedented. Colloidal gold has been used for the reduction of aromatic nitro compounds [23] and eosin reduction.[24] Polymer-stabilized AuNPs have been used for the aerobic alcohol oxidation [25, 26] and aerobic homocoupling of arylboronic acid in water.[27] Using unsupported AuNPs can provide a platform with which the catalytic activity of different AuNP systems can be compared and contrasted directly without factoring in the contributions of the support materials. This comparison is further made easier by the use of well characterized model reactions.

Herein, we demonstrate the catalytic activity of water soluble triphenylphosphine stabilized gold nanoparticles (TPP-AuNPs) using a model reaction: the reduction of hexacyanoferrate (III) to hexacyanoferrate (II) by sodium borohydride. The objective of this study is to investigate the catalytic activity of TPP-AuNPs in electron transfer reactions. The TPP-AuNPs were synthesized using the reducing agent, 9-BBN based on a method developed in our lab.[28] We investigate various factors affecting the reduction including the concentrations of hexacyanoferrate (III), the catalyst (TPP-AuNPs) and borohydride. We also investigate how temperature affects the reaction rates and determine the activation energy and other kinetic parameters for this model reaction.

7.2 Experimental section

7.2.1 Materials

Potassium ferricyanide and sodium borohydride powder (98%) were obtained from Mallinckrodt Baker and Alfa Aesar respectively. Chloro(triethylphosphine)gold(I) (97%), triphenylphosphine (99%), trioctylphosphine (99.8%), 0.5 M 9-Borabicyclo[3.3.1]nonane (9-BBN) solution in THF and toluene (HPLC grade) were purchased from Sigma Aldrich. Acetonitrile (HPLC grade) and hexanes were obatined from Fisher Scientific and EMD Chemicals respectively. All chemicals and solvents were used as received. Copper formvar/carbon grids (200 mesh) were acquired from Electron Microscopy Sciences.

7.2.2 Synthesis of TPP-AuNPs

In a mixture of acetonitrile and toluene (10:40 ml), 0.017 gm (0.05 mmol) of chloro(triethylphosphine)gold(I) (Et_3PAuCl) was dissolved. TPP (0.0786 gms, 0.3 mmol) was added to the mixture at room temperature. The contents were stirred for 30 min after which 0.4 ml of 9-BBN (0.2 mmol) was injected into the mixture. After an additional 30 min of stirring, a solid appeared. The reaction mixture was centrifuged and the solid was collected. The solid was washed twice with hexane to remove any impurities. After drying by nitrogen flow, a black solid was obtained.

7.2.3 Preparation of catalyst

The black solid obtained above was dissolved in nanopure water, (>18 MΩ) and the mixture sonicated in a Branson ultrasonic cleaner. The solution was centrifuged for 30 min at 4000 r.p.m. and small aggregates at the bottom of the tube were discarded. The supernatant was centrifuged two more times and the final solution was used as the catalyst in the reactions described below. Samples of the catalyst particles were dropcast onto 200 mesh formvar-coated copper grid and imaged by transmission electron microscopy (TEM) after drying in air.

7.2.4 Reduction of hexacyanoferrate (III)

From potassium hexacyanoferrate (III) salt, 0.01 M stock solution of hexacyanoferrate (III) was prepared. A stock solution of 0.1M $NaBH_4$ also was prepared. Freshly prepared solutions of these reagents were used in all cases. The reduction of hexacyanoferrate (III) was carried out in a 2.5 ml quartz cuvette. To study the effect of

catalyst concentration on the rate constant, studies were performed at four different concentrations of $NaBH_4$ (4.0×10^{-3} M, 8.0×10^{-3} M, 1.6×10^{-2} M, 2.4×10^{-2} M). Three concentrations of the catalyst (1.72×10^{-10} M, 3.44×10^{-10} M and 6.88×10^{-10} M) were used. The concentration of hexacyanoferrate (III) was kept constant at 8.0×10^{-4} M. For example, 200 µl of 0.01 M hexacyanoferrate (III) solution was added to 200 µl of 0.1M $NaBH_4$ and 10 µl of TPP-AuNPs. The mixture was made up to 2.5 ml with nanopure water for the following final concenterations: Hexacyanoferrate, 8.0×10^{-4} M ; $NaBH_4$, 8.0×10^{-3} M and TPP-AuNPs, 1.72×10^{-10} M. The pH of the solution was determined to be 10. The reaction was monitored by following the decrease in intensity of the hexacyanoferrate (III) peak at 420 nm as a function of time using UV-vis absorption spectra collected across a spectral range of 300-600 nm. Similar procedures were followed to determine the effect of the concenteration of $NaBH_4$ and hexacyanoferrate (III) on the reaction rate. After the reactions, samples of the solutions were prepared for TEM analysis.

7.2.5 Determination of activation energy

In order to determine the activation energy, the rate constants for the reaction were determined following the procedure decribed in section 7.2.4 was followed. Briefly, the decrease in intensity of the hexacyanoferrate (III) peak at 420 nm as a function of time was monitored using UV-vis absorption spectroscopy. However, for these experiments, the conccentration of hexacyanoferrtae (III) and TPP-AuNPs was kept constant while the concentration of $NaBH_4$ was varied and the rate constants were

determined at 25, 30, 35 and 40 °C. All solutions were equilibrated for 5 min before starting the reaction.

7.2.6 Instrumentation

7.2.6.1 UV-visible Spectroscopy

UV-vis absorption spectra at room temperature were collected using a Perkin-Elmer Lambda 750 UV/Vis/NIR spectrophotometer over the 300-600 nm range. All data were corrected for background absorption using water. UV-vis absorption spectra at different temperatures (25, 30, 35 and 40 °C) were obtained using a U-4100 Hitachi spectrophotometer with TLC 42™ dual temperature controlled cuvette holders equipped with a matched and calibrated TC 225 temperature controller (Quantum Northwest Inc. WA). The temperature was maintained to within ± 0.02 °C of the desired temperature.

7.2.6.2 Transmission Electron Microscopy (TEM)

TPP-AuNPs solutions were drop cast onto 200 mesh formvar-coated copper grids. The excess solution was wicked off and the grids air dried. TEM images were obtained using a Tecnai-12 instrument operating at 100 KV accelerating voltage (Microscopy Core Facility, University of Utah). Particle size analysis was done by counting at least 1000 particles in the TEM images using Scion Image Beta 4.02 Software.

7.2.6.3 HAADF-STEM, HRTEM and SAED imaging

TPP-AuNPs samples were prepared following the same procedure used for preparation of TEM samples as described above. Micrographs were obtained using a FEI

Titan 80-300 TEM operated at 300 kV at the CAMCOR High Resolution and Analytical Facility (University of Oregon, Eugene, OR). The instrument is equipped for bright field, dark field, and high angle annular dark field STEM imaging. The collection angle of HAADF-STEM images was 10 mrad. The images were taken at different magnifications and captured using a Gatan CCD. The dimension of the images obtained was 1k × 1k pixels. Selected-area electron diffraction (SAED) patterns also were obtained.

7.2.6.4 Zeta potential

Zeta potential of the NPs was determined using a NICOMP^{TM} 380 ZLS (Particle Sizing Systems, CA).

7.3 Results and discussion

7.3.1 Structure of TPP-AuNPs

The TPP-AuNPs were synthesized using a one-step procedure which utilizes the mild reducing agent 9-BBN to produce nanoparticles with a narrow size dispersion.[28] For the catalysis study, the TPP-AuNPs were dispersed in water. Figure 7.1A shows a TEM image of the NPs. The size of the TPP-AuNPs was determined from the TEM images to be 4.3 ± 1.4 nm in diameter. HRTEM imaging of the NP samples indicates that they have clear lattice fringes where the lattice spacing of the (111) planes is 0.24 nm. Figure 7.1B presents a representative HRTEM showing an un-twinned, single NP which represents the majority of the NP population. The NPs exhibit fcc packing of the Au atoms. Figure 7.1C shows a representative high angle annular dark field (HAADF) image of the TPP-AuNPs.

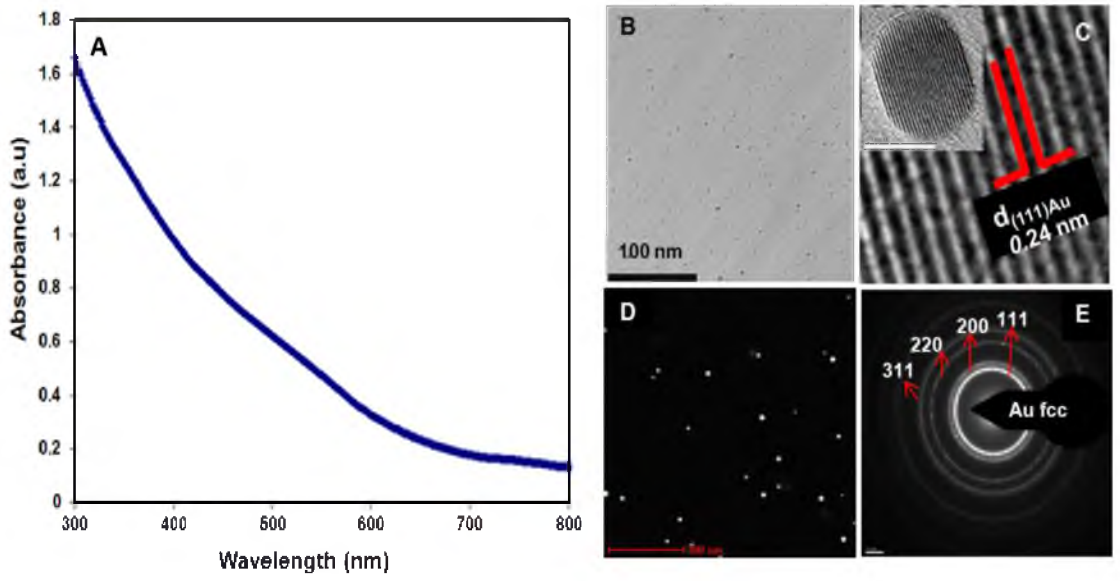

Figure 7.1. (A) UV-vis absorption spectrum of TPP-AuNPs in water. (B) TEM image of the TPP-AuNPs. (C) HRTEM image showing (111) lattice fringes of a single crystalline NP. Inset is a HRTEM image of a TPP-AuNP, scale bar = 5nm. (D) HAADF-STEM image of the TPP-AuNPs. (E) SAED diffraction pattern depicting the crystalline nature of the NPs.

The high contrast between the high-Z AuNPs and the low-Z carbon formvar support provided by HAADF-STEM allows for a more accurate determination of the size of the NPs compared to TEM. Selected area electron diffraction (SAED) pattern shows the crystalline structure of the NPs (Figure 7.1D). The electron diffraction rings have been indexed to the fcc lattice of Au. The TPP-AuNPs were found to be stable with a zeta potential of 34.9 ± 4.6 mV at a pH of 7.2. The UV-vis absorption spectrum of the NPs was monitored for a week and we observed no change in intensity, peak shape or position indicating that the NPs are stable and remain in solution.

7.3.2 Reduction of $Fe(CN)_6^{3-}$ to $Fe(CN)_6^{4-}$

We used the reduction of hexacyanoferrate (III) by sodium borohydride as a model electron transfer reaction to investigate the catalytic activity of AuNPs.[29] The reaction proceeds according to the redox reaction below.[30]

$$BH_4^- + 8Fe(CN)_6^{3-} + 3H_2O \longrightarrow H_2BO_3^- + 8Fe(CN)_6^{4-} + 8H^+$$

Motivations for choosing this reaction are that it is simple, proceeds at room temperature and can be monitored by UV-vis spectroscopy.[31] The reaction takes place in an alkaline environment which serves to slow down the decomposition of borohydride by hydrolysis.[32] We set up the reaction conditions such that the borohydride concentration is much greater than the concentration of hexacyanoferrate (IIII). The reaction therefore follows first-order kinetics. Borohydride injects electrons onto the surface of TPP-AuNPs thereby increasing their electron density and cathodically polarizing them.[33, 34] The reduction of hexacyanoferrate (III) ions occurs when they diffuse to the surface of the TPP-AuNPs and are reduced by the excess electrons. The hexacyanoferrate (III) ions have a characteristic peak centered at 420 nm.[35] As the reaction proceeds, the decrease in the amplitude of the peak at 420 nm is monitored as a function of time. In the absence of the AuNPs, the reaction takes a long time to reach completion. Addition of TPP-AuNPs to the reaction mixture speeds up the reaction significantly compared to the uncatalyzed reaction (Figure 7.2). The reactions were performed using nanopure water that had been purged with nitrogen to expel dissolved oxygen. Dissolved oxygen can slow down the reaction because it needs to be reduced first. In the process of oxygen reduction, some of

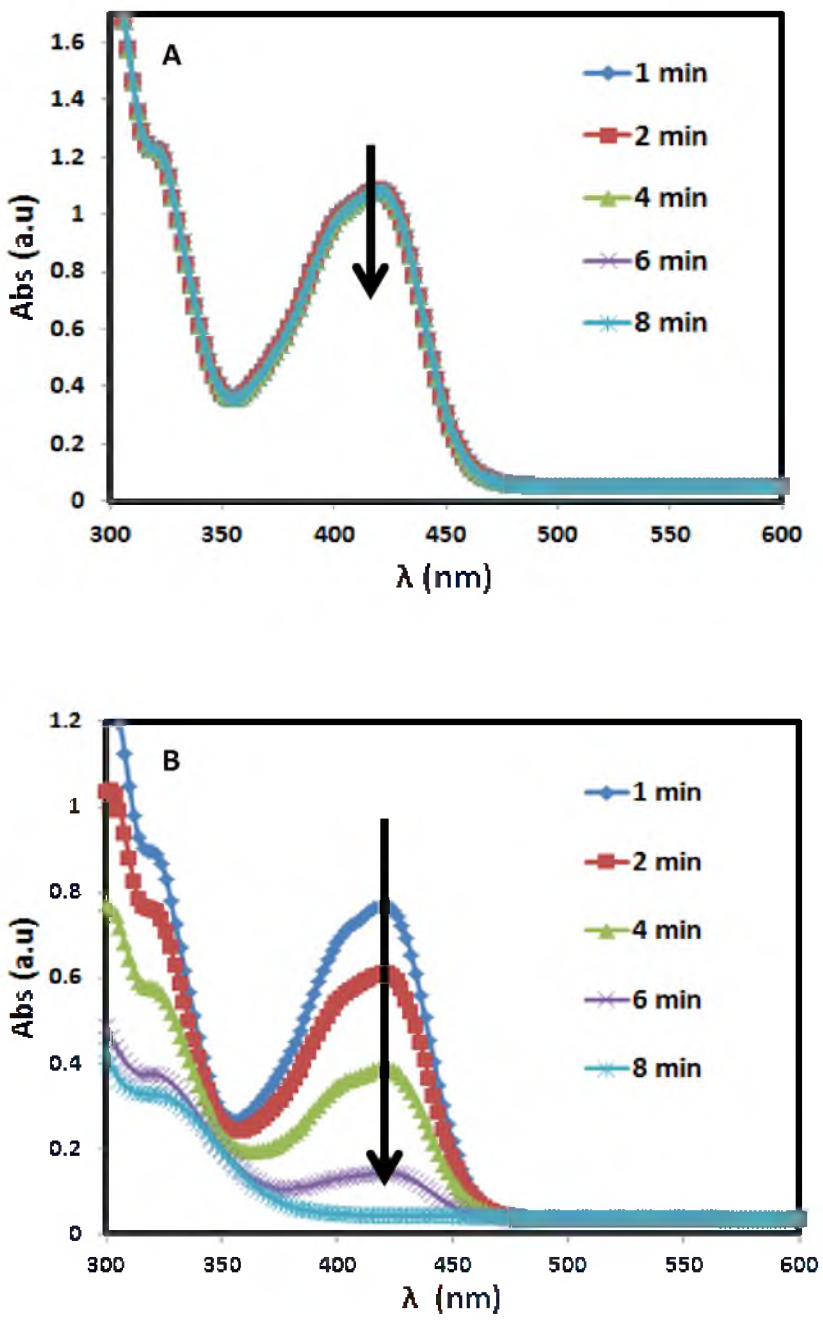

Figure 7.2. UV-visible absorption spectra of hexacyanoferrate (III) reduction by $NaBH_4$ in (A) the absence and (B) presence of TPP-AuNPs.

the $NaBH_4$ is consumed.[36] The rate of change of the concentration of hexacyanoferrate (III) with time (k_{obs}) for the reaction was obtained from the slope of ln A against time:

$$k_{obs} = -(d[Fe(CN)_6^{3-}] / [Fe(CN)_6^{3-}]) / dt$$

We note that k_{obs} is a composed of the real rate of reduction of $Fe(CN)_6^{3-}$ i.e., $d[Fe(CN)_6^{3-}] / dt$ and a factor $1/ [Fe(CN)_6^{3-}]$. Several factors were found to affect k_{obs} and will be discussed in the following sections.

7.3.3 Dependence of the rate of reduction of $Fe(CN)_6^{3-}$ on the $[Fe(CN)_6^{3-}]$

The effect of the concentration of hexacyanoferrate (III) ions on the k_{obs} was also investiagted. The concentration of $NaBH_4$ and TPP-AuNPs were kept constant at 8.0 $\times 10^{-3}$ M and 1.72 $\times 10^{-10}$ M respectively as the concentration of hexacyanoferrate (III) was varied. The data obtained indicates that the smaller the amount of hexacyanoferrate (III) added to the reaction mixture, the faster the reaction proceeded according to the observed rate constants, and vice versa (Figure 7.3A). This inverse relationship between the concentration of hexacyanoferrate (III) and the k_{obs} indicates that the real rate of reduction of $Fe(CN)_6^{3-}$ i.e., $d[Fe(CN)_6^{3-}] / dt$ is independent of the concentration of hexacyanoferrate (III). Figure 7.3B also shows that this rate is constant at all concentrations of hexacyanoferrate (III).

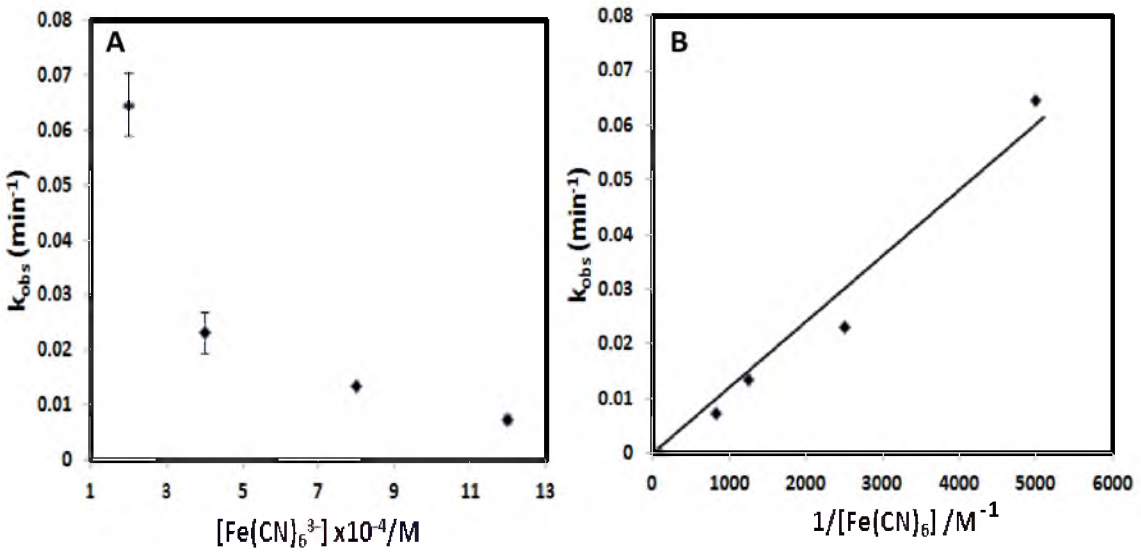

Figure 7.3. (A) Effect of hexacyanoferrate (III) concentration on the observed rate constants. (B) Dependence of the rate constant for the reduction of hexacyanoferrate (III) by $NaBH_4$ on the concentration of hexacyanoferrate (III). The concentration of $NaBH_4$ and TPP-AuNPs were kept constant.

7.3.4 Dependence of the rate of reduction of $Fe(CN)_6^{3-}$ on the $[NaBH_4]$

We investigated how the concentration of sodium borohydride affected k_{obs}. The electron-transfer reduction was performed at a constant concentration of hexcyanoferrate (III) ions (8.0×10^{-4} M) while the concentrations of $NaBH_4$ and TPP-AuNPs were varied. The pH of the reaction mixture remained alkaline during the reaction because of the excess $NaBH_4$ added. Figure 7.4 shows the dependence of k_{obs} on the concentration of $NaBH_4$ at different concentrations of TPP-AuNPs. As the concentration of $NaBH_4$ increased, k_{obs} values also were observed to increase. A summary of the k_{obs} showing the effect of $[NaBH_4]$ on the k_{obs} at different [TPP-AuNPs] is given in Table 7.1.

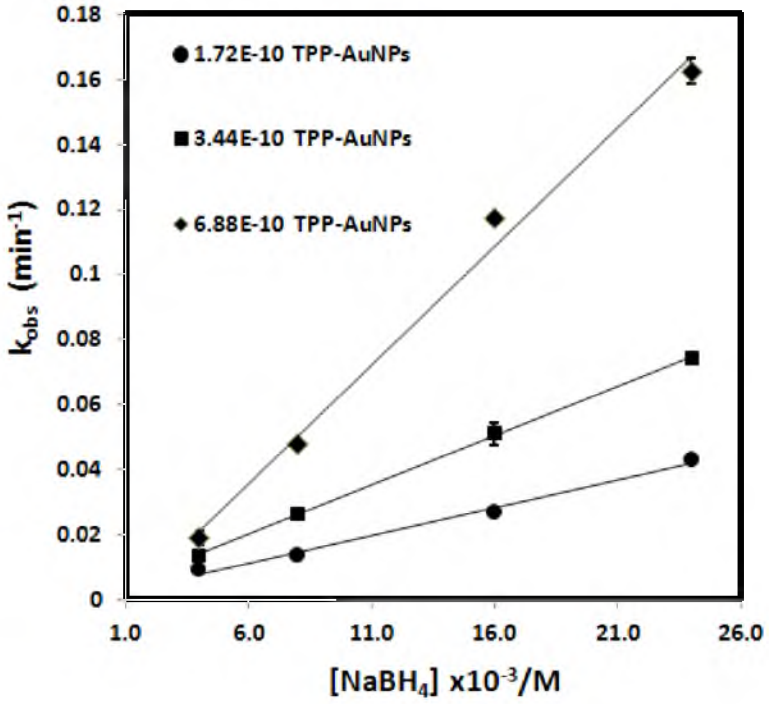

Figure 7.4. Effect of $NaBH_4$ concentration on the observed rate constants at different TPP-AuNPs concentrations. The solution pH=10 in both cases.

Table 7.1. Effect of TPP-AuNPs concentration on the observed rate constants (k_{obs}) at different $NaBH_4$ concentrations.

		[$NaBH_4$]			
[TPP-AuNPs]	[$Fe(CN)_6^{3-}$]	4.0×10^{-3} M	8.0×10^{-3} M	1.6×10^{-2} M	2.4×10^{-2} M
1.72×10^{-10} M	8.0×10^{-4} M	0.0091 ± 0.0002 min^{-1}	0.0134 ± 0.0002 min^{-1}	0.0269 ± 0.0004 min^{-1}	0.0432 ± 0.0013 min^{-1}
3.44×10^{-10} M	8.0×10^{-4} M	0.0135 ± 0.0004 min^{-1}	0.0263 ± 0.0007 min^{-1}	0.0511 ± 0.0033 min^{-1}	0.0743 ± 0.0005 min^{-1}
6.88×10^{-10} M	8.0×10^{-4} M	0.0190 ± 0.0020 min^{-1}	0.0481 ± 0.0002 min^{-1}	0.1172 ± 0.0012 min^{-1}	0.1625 ± 0.0038 min^{-1}

7.3.5 Dependence of the rate of reduction of $Fe(CN)_6^{3-}$ on the [TPP-AuNPs]

We also investigated how different concentrations of the catalyst affected k_{obs}. For this determination, the concentration of hexacyanoferrate (III) ions was kept constant at 8.0×10^{-4} M while the concentrations of $NaBH_4$ and TPP-AuNPs were varied. The observed rate constants were found to increase linearly with concentration of TPP-AuNPs as shown in Figure 7.5. A detailed summary of the k_{obs} showing the effect of TPP-AuNPs concentration on the observed rate constants at different $NaBH_4$ concentrations is given in Table 7.2. The rate of the reaction is proportional to the catalyst (TPP-AuNPs) surface area. The implication of this result is that the surface of the catalyst is saturated at all concentrations. It follows that the rate of reaction is thus limited by the catalyst surface area.

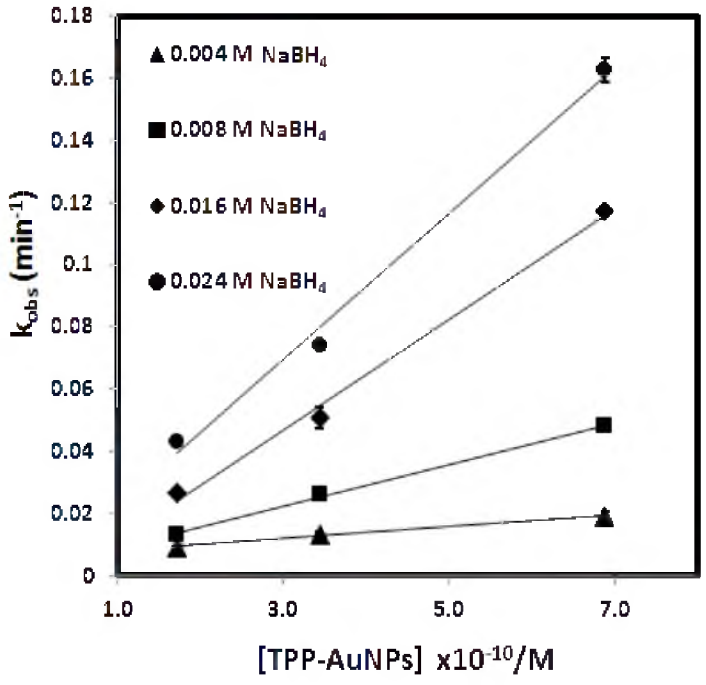

Figure 7.5. Effect of [TPP-AuNPs] on the observed rate constants at different $NaBH_4$ concentrations. The solution pH=10.

Table 7.2. Effect of $NaBH_4$ concentration on the observed rate constants (k_{obs}) at different concentrations of TPP-AuNPs.

		[TPP-AuNPs]		
$[NaBH_4]$	$[Fe(CN)_6^{3-}]$	1.72×10^{-10} M	3.44×10^{-10} M	6.88×10^{-10} M
4.0×10^{-3} M	8.0×10^{-4} M	0.0091 ± 0.0002 min^{-1}	0.0135 ± 0.0004 min^{-1}	0.019 ± 0.002 min^{-1}
8.0×10^{-3} M	8.0×10^{-4} M	0.0134 ± 0.0002 min^{-1}	0.0263 ± 0.0007 min^{-1}	0.0481 ± 0.0002 min^{-1}
1.6×10^{-2} M	8.0×10^{-4} M	0.0269 ± 0.0004 min^{-1}	0.0511 ± 0.0033 min^{-1}	0.1172 ± 0.0012 min^{-1}
2.4×10^{-2} M	8.0×10^{-4} M	0.0432 ± 0.0013 min^{-1}	0.0743 ± 0.0005 min^{-1}	0.1625 ± 0.0038 min^{-1}

The number of surface atoms of the TPP-AuNP catalyst was calculated by taking into account the volume of TPP-AuNPs of known concentration and size (diameter). A linear dependence of the rate constants on the surface area of the TPP-AuNPs also was observed. A dependence of the k_{obs} on the calculated number of surface atoms corroborates the assertion that the reaction takes place on the surface of the AuNPs (Figure 7.6).

The rate of hexacyanoferrate (III) ions converted to hexacyanoferrate (II) ions per unit time was determined to be 1.61×10^{16} ions per minute. The rate of hexacyanoferrate (III) ions converted to hexacyanoferrate (II) ions per unit area of the TPP-AuNPs catalyst per unit time also was determined. The assumption was made that all surface sites were catalytically active.[37] This assumption was necessitated by the difficulty in measuring the number of catalytically active sites for a given reaction.[38, 39] The rate was found to be 2.7×10^{16} ions cm^{-2} min^{-1}.

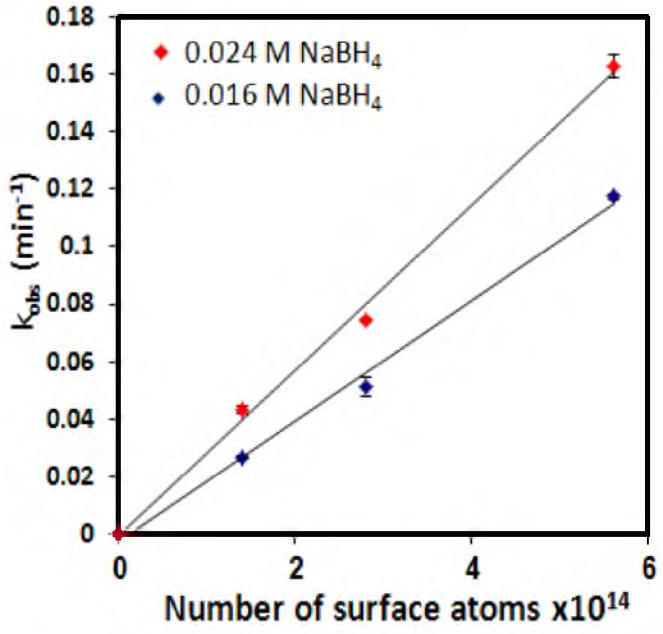

Figure 7.6. (A) The relationship between the number of surface atoms and the observed rate constants.

7.3.6 Effect of temperature

To investigate the effect of temperature on the reduction of hexacyanoferrate (III) by $NaBH_4$, the reaction was performed at 25, 30, 35 and 40 ^{o}C. The concentrations of hexacyanoferrate (III) and TPP-AuNPs were kept constant as the temperature was varied. The temperature of the solutions was equilibrated for 5 min prior to the reactions. The absorbance was monitored at 420 nm in each case and a first order plot of ln A vs time made to obtain the observed rate constant from the slope of the graph at each temperature (Figure 7.7A). There is a linear relationship between the average rate constant observed and the temperature (Figure 7.7B). This is expected from the Arrhenius equation. A summary of the k_{obs} at different temperatures is presented (Table 7.3).

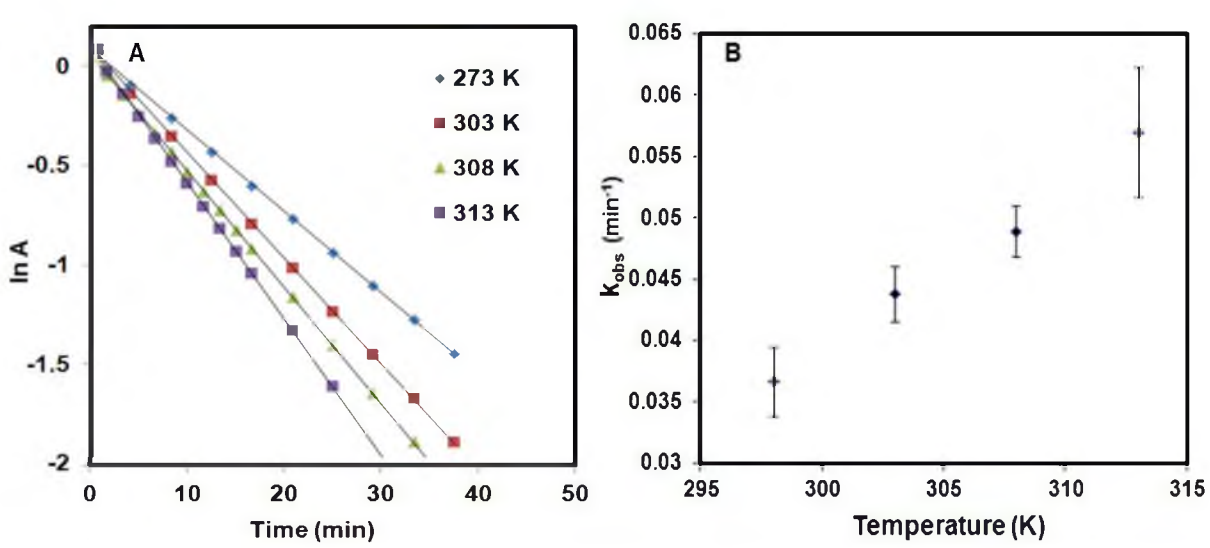

Figure 7.7. (A) First-order kinetic plot of the reduction of hexacyanoferrate (III) by $NaBH_4$ catalyzed by TPP-AuNPs and (B) Relationship between temperature and the observed rate constants.

Table 7.3. Summary of the observed rate constants (k_{obs}) obtained at different temperatures

Temperature	k_{obs} (min^{-1}) with 2.0×10^{-3} M $NaBH_4$	k_{obs} (min^{-1}) with 4.0×10^{-3} M $NaBH_4$
25^0C	0.0149 ± 0.0021	0.0356 ± 0.0028
30^0C	0.0222 ± 0.0016	0.0438 ± 0.0022
35^0C	0.0279 ± 0.0025	0.0489 ± 0.0040
40^0C	0.3425 ± 0.0038	0.0569 ± 0.0021

The activation energy (E_a) was determined from the Arrhenius equation (Equation 1):

$$\ln k_{obs} = -(E_a/RT) + \ln A \text{ .....(1)}$$

where k is the observed rate constant of the reaction, T is temperature in Kelvin, R is the universal gas constant and A is the Arrhenius factor. Using equation 1, a plot of ln *k* vs 1000/T was used to obtain the activation energy from the slope ($-E_a/R$) as shown in Figure 7.6.

The activation energy was determined to be 23.6 ± 2.8 kJ/mol. The pre-exponential factor was calculated from the intercept of the plot. The entropy of activation ($\Delta S^{\ddagger}$) also was determined using equation 2. The frequency factor was 977.8 ± 147.6 min^{-1} while the entropy of activation was 57.2 ± 1.3 J/mol K.

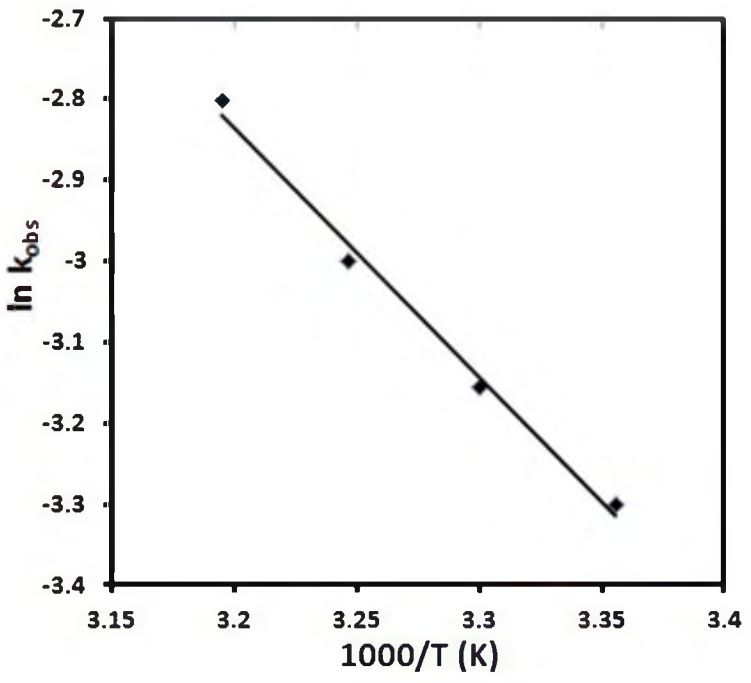

Figure 7.6. Arrhenius plot for the hexacyanoferrate(III) reduction by $NaBH_4$ catalyzed by TPP-AuNPs in water.

$$\ln A = \Delta S^{\ddagger} / R \quad \text{.....(2)}$$

Studies have shown that if the capping layers allow the movement of molecules to the reactive surfaces on the metal NPs, the catalytic reactions are not affected significantly.[2] For example, using PtNPs stabilized by different types of ligands, from polymers to thiols, the turnover rate for the oxidation of CO variation was 30%.[40] In this present study, 4 nm TPP-AuNPs were used. Small NPs in solution are susceptible to aggregation due to the high surface energy they possess.[29] To overcome this setback, a strong passivating agent is needed to stabilize the NPs. However, a strong stabilizer binds strongly to the NPs and reduces the number of active sites for catalysis. Weaker stabilizing agents do not provide adequate stabilization even though they leave more active sites accessible for catalysis. Aggregation of the AuNPs was observed in our study. This can be attributed to the fact that TPP does not provide strong stabilization for the AuNPs.

The activation energy of 23.6 ± 2.8 kJ/mol for this study is comparable to that obtained for electron transfer reaction between hexacyanoferrate (III) and $NaBH_4$ or thiosulfate ions in other reported studies. For example, the activation energy for the uncatalyzed hexacyanoferrate reduction was found to be 30 kJ/mol with a frequency factor of 5.9×10^{11} sec^{-1} as determined by Freund.[30] Carregal-Romero et al. used 15 nm citrate stabilized AuNPs to catalyze the reduction of hexacyanoferrate (III) by $NaBH_4$. An activation energy of 15.6 kJ/mol and an entropy of activation of -180 J/mol K were determined for this reaction.[29] In another report, thiosulfate was used as the reducing agent instead of $NaBH_4$ with 25 nm citrate stabilized AuNPs.[41] Activation energy of 29 kJ/mol was obtained. In comparison, when gold nanocages of about 80 nm in diameter stabilized by PVP were used to catalyze the same reaction, the experimentally determined activation energy was 24 kJ/mol.[41] The difference in the two results was attributed

mainly to the stabilization of the two catalysts. While both the nanocages and the citrate stabilized AuNPs increased in size in the presence of thiosulfate, the citrate stabilized AuNPs dissolved and aggregated more owing to the inferior protection by citrate ions. Their catalytic activity was also significantly diminished as a result. PVP- PtNPs 5 nm in diameter also have been used to catalyze the reduction of hexacyanoferrate (III) by thiosulfate ions.[35] In this case, activation energy of 23 kJ/mol was obtained. Direct comparison of the data from various studies is complicated by the different reducing agents used. For example, thiosulfate binds to the surface of the NPs and causes the collision frequency between the reagents to decrease.[42] Low rate constants are observed for such reactions. In a majority of the studies, concentrations of the catalysts used are not reported, making comparison of data even for NPs of similar size difficult.

7.4 Conclusion

We have demonstrated that TPP-AuNPs in aqueous solution can be used as effective catalysts for the electron-transfer reaction involving the reduction of hexacyanoferrate (III) by $NaBH_4$. We observed that in the absence of TPP-AuNPs, the reduction of hexacyanoferrate (III) by $NaBH_4$ to hexacyanoferrate (II) followed zero-order kinetics with respect to the concentration of hexacyanoferrate. However, on addition of TPP-AuNPs, the reaction followed first-order kinetics. The rate of reduction was found to depend linearly on the concentration of $NaBH_4$ at the concentrations of $NaBH_4$ studied. The rate of the reduction was found to be constant and to be limited by the catalyst surface. The relationship between the surface area, concentration of TPP-AuNPs and the rate constant was found to be linear. The observed rate constant was proportional to the number of surface atoms of the NPs. Increase in temperature also led to increase in the

observed rate constants. Removal of capping materials could increase the observed rates and decrease the apparent E_a thereby making these TPP-AuNPs effective redox catalysts.

7.5 References

(1) Aiken III, J. D.; Finke, R. G. *J. Mol. Catal. A: Chem.* **1999**, *145*, 1-44.

(2) Somorjai, G. A.; Park, J. Y. *Angew Chem Int Ed.* **2008**, *47*, 9212-9228.

(3) Haruta, M. *Catal. Today* **1997**, *36*, 153-166.

(4) Yuan, Y.; Asakura, K.; Wan, H.; Tsai, K.; Iwasawa, Y. *Catal. Lett.* **1996**, *42*, 15-20.

(5) Okumura, M.; Nakamura, S.; Tsubota, S.; Nakamura, T.; Azuma, M.; Haruta, M. *Catal. Lett.* **1998**, *51*, 53-58.

(6) Schwartz, V.; Mullins, D. R.; Yan, W.; Chen, B.; Dai, S.; Overbury, S. H. *J. Phys. Chem. B* **2004**, *108*, 15782-15790.

(7) El-Sayed, M. A. *Acc. Chem. Res.* **2001**, *34*, 257-264.

(8) Bond, G. C. *Catal. Today* **2002**, *72*, 5-9.

(9) Wang, J.; Koel, B. E. *J. Phys. Chem. A* **1998**, *102*, 8573-8579.

(10) Pyykko, P. *Chem. Rev.* **1988**, *88*, 563-594.

(11) Epling, W. S.; Hoflund, G. B.; Weaver, J. F.; Tsubota, S.; Haruta, M. *J. Phys. Chem* **1996**, *100*, 9929-9934.

(12) Knell, A.; Barnickel, P.; Baiker, A.; Wokaun, A. *J. Catal.* **1992**, *137*, 306-321.

(13) Haruta, M. *Catal. Surv. Jpn* **1997**, *1*, 61-73.

(14) Astruc, D. *Nanoparticles and catalysis*; Wiley-VCH: Weinheim, 2007.

(15) Yang, F.; Chen, M. S.; Goodman, D. W. *J. Phys. Chem. C* **2008**, *113*, 254-260.

(16) Arnal, P. M.; Comotti, M.; Schüth, F. *Angew Chem Int Ed.* **2006**, *45*, 8224-8227.

(17) Laurin, M.; Johanek, V.; Grant, A. W.; Kasemo, B.; Libuda, J.; Freund, H. J. *J. Chem. Phys.* **2005**, *123*, 054701-054712.

(18) Zhdanov, V. P.; Kasemo, B. *Surf. Sci. Rep.* **2000**, *39*, 25-104.

(19) Shen, M.; Resasco, D. E. *Langmuir* **2009**, *25*, 10843-10851.

(20) Zhu, J.; Figueiredo, J. L.; Faria, J. L. *Catal. Commun.* **2008**, *9*, 2395-2397.

(21) Joo, S. H.; Park, J. Y.; Tsung, C.-K.; Yamada, Y.; Yang, P.; Somorjai, G. A. *Nat Mater* **2009**, *8*, 126-131.

(22) Turner, M.; Golovko, V. B.; Vaughan, O. P. H.; Abdulkin, P.; Berenguer-Murcia, A.; Tikhov, M. S.; Johnson, B. F. G.; Lambert, R. M. *Nature* **2008**, *454*, 981-983.

(23) Panigrahi, S.; Basu, S.; Praharaj, S.; Pande, S.; Jana, S.; Pal, A.; Ghosh, S. K.; Pal, T. *J. Phys. Chem. C* **2007**, *111*, 4596-4605.

(24) Sau, T. K.; Pal, A.; Pal, T. *J. Phys. Chem. B* **2001**, *105*, 9266-9272.

(25) Tsunoyama, H.; Sakurai, H.; Negishi, Y.; Tsukuda, T. *J. Am. Chem. Soc.* **2005**, *127*, 9374-9375.

(26) Tsunoyama, H.; Ichikuni, N.; Tsukuda, T. *Langmuir* **2008**, *24*, 11327-11330.

(27) Tsunoyama, H.; Sakurai, H.; Ichikuni, N.; Negishi, Y.; Tsukuda, T. *Langmuir* **2004**, *20*, 11293-11296.

(28) Shem, P. M.; Sardar, R.; Shumaker-Parry, J. S. *Langmuir* **2009**, *25*, 13279-13283.

(29) Carregal-Romero, S.; Perez-Juste, J.; Herves, P.; Liz-Marzan, L. M.; Mulvaney, P. *Langmuir* **2010**, *26*, 1271-1277.

(30) Freund, T. *J. Inorg. Nucl. Chem.* **1959**, *9*, 246-251.

(31) Narayanan, R.; El-Sayed, M. A. *J. Am. Chem. Soc.* **2004**, *126*, 7194-7195.

(32) Chatenet, M.; Micoud, F.; Roche, I.; Chainet, E. *Electrochim. Acta* **2006**, *51*, 5459-5467.

(33) Henglein, A.; Meisel, D. *Langmuir* **1998**, *14*, 7392-7396.

(34) Mulvaney, P.; Pérez-Juste, J.; Giersig, M.; Liz-Marzán, L.; Pecharromán, C. *Plasmonics* **2006**, *1*, 61-66.

(35) Narayanan, R.; El-Sayed, M. A. *Nano Lett.* **2004**, *4*, 1343-1348.

(36) Lu, Y.; Mei, Y.; Walker, R.; Ballauff, M.; Drechsler, M. *Polymer* **2006**, *47*, 4985-4995.

(37) Somorjai, G. A. *Chem. Rev.* **1996**, *96*, 1223-1236.

(38) Boudart, M. *Chem. Rev.* **1995**, *95*, 661-666.

(39) Somorjai, G. A.; Li, Y. *Introduction to Surface Chemistry and Catalysis*, 2nd ed.; John Wiley & Sons: Hoboken, New Jersey, 2010.

(40) Park, J. Y.; Lee, H.; Renzas, J. R.; Zhang, Y.; Somorjai, G. A. *Nano Lett.* **2008**, *8*, 2388-2392.

(41) Yen, C.-W.; El-Sayed, M. A. *J. Phys. Chem. C* **2009**, *113*, 19585-19590.

(42) Narayanan, R.; El-Sayed, M. A. *J. Phys. Chem. B* **2005**, *109*, 18460-18464.

CHAPTER 8

CONCLUSION AND FUTURE WORK

8.1 Conclusion

A simple and versatile method for preparing monodisperse triphenylphosphine (TPP) stabilized AuNPs with diameters of less than 2 nm has been presented. This method is a single step procedure which uses a mild reducing agent 9-Borabicyclo[3.3.1]nonane (9-BBN). In addition, the approach is inexpensive and greener because the use of phase transfer reagents and the attendant rigorous purification steps are eliminated. We demonstrated that the particle size can be tuned by carefully controlling the conditions under which the reduction takes place. The phosphine-stabilized AuNPs exhibit size dependent localized surface plasmon resonance (LSPR) behavior as measured by UV-visible spectroscopy. We also have shown that the TPP-stabilized nanoparticles can be used as precursors for preparation of AuNPs functionalized with other ligands through ligand exchange reactions. The synthetic protocol could also be useful in the preparation of other noble metal nanoparticles stabilized with different ligands.

The ability to control the growth process is enhanced when 9-BBN is used as the reducing agent. Nanoparticles stabilized by soft ligands were prepared and then capped

in-situ with the desired ligands. The NP growth process was found to proceed by the aggregative growth model. By following the NP growth process, it was possible to arrest the growth process and avoid coalescence of the weakly stabilized NPs by introducing ligands into the NP solution. This is a useful way of introducing desired functionalities to NPs when the ligand exchange process is hampered by factors such as the pH dependent solubility of the ligands. We demonstrated that *in-situ* addition of capping ligands such as bipyridyls to replace the soft ligand Et_3P, restricted nanoparticle growth and significantly narrowed the size dispersion of the NPs. This also had the effect of providing long term stability to the bipyridyl NPs.

The TPP-AuNPs are soluble in water, thereby expanding their potential applications. The increased stability was attributed to hydrogen bonding as a result of π-π stacking of the phenyl rings of the triphenylphosphine ligands. The stability of the TPP-AuNPs in water was investigated as a function of salt and sodium borohydride concentration, solvents with different dielectric constants, pH and temperature. High resolution imaging and selected area electron diffraction indicated that the NPs were mostly spherical and crystalline with fcc packing. The NPs were found to be stable in water as evidenced by UV-vis spectra and zeta potential measurements over time. The addition of salt and $NaBH_4$ induced aggregation of the NPs. Addition of $NaBH_4$ caused the displacement of the TPP ligand as shown by XPS phosphorus measurements. Control experiments with different anions ruled out their role in inducing the aggregation. High valence salts were found to induce greater aggregation. The role of solvents on the stability of the NPs indicates that the NPs are more stable in water/solvent mixtures

where the solvents have a high dielectric constant. Dissolving the NPs in pure solvents (except water) alone caused aggregation.

The catalytic activity of the TPP-AuNPs in water was also investigated by using two model reactions which proceed by different pathways. The reduction of 4-nitrophenol (4-NP) by sodium borohydride catalyzed by the TPP-AuNPs served as one of the model reactions. The TPP-AuNPs were recycled, however aggregation of the NPs was observed at the end of the reduction. The turn-over rate for the unsupported TPP-AuNPs was 400 times faster than that for supported gold catalytic systems, indicating the good catalytic activity of TPP-AuNPs. The other model reaction used to test the catalytic efficiency of the TPP-AuNPs was the redox reduction of hexacyanoferrate (III) to hexacyanoferrate (II) by sodium borohydride. A linear relationship between the rate constant and the nanoparticle concentration as well as the surface area of the NPs was observed. This work demonstrated that TPP-AuNPs can act as efficient catalysts for electron transfer/redox reactions in an aqueous environment.

We have therefore presented a new method for making TPP-AuNPs and showed that the synthetic protocol is very versatile. It can be adapted to make NPs functionalized with different ligands by capping the NPs *in-situ* with the desired ligands. The TPP-AuNPs were also shown to be soluble in water and can serve as catalysts for a variety of applications.

8.2 Future work

Recent studies described in this dissertation have shown that the nucleation process occurs very fast and cannot be adequately monitored using *ex-situ* microscopy

and UV-vis spectroscopy. Most laboratory kinetics set ups have acquisition times in the range of minutes. Thus a fast method for monitoring the formation of the nanoparticles is needed. In addition, there are multiple thermodynamic and kinetic factors that determine the NP growth mechanism. For example the nucleation stage is very sensitive to factors such as reactant concentration, temperature, molar ratios of reactants, presence of surfactants and speed of stirring. Slight variations in these experimental conditions lead to changes in nuclei concentration and nanoparticles of various sizes. The growth kinetics and mechanisms of AuNPs formed using 9-BBN as a reducing agent need to be investigated using time resolved *in-situ* studies methods including XAFS, XANES, SAXS, and WAXS coupled with *in-situ* TEM and UV-vis spectroscopy. A synchrotron facility beamline that can provide time resolution of at least 200 ms is needed for this study.[1]

The stability of the NPs was studied using aggregation-based methods. The methods used for aggregation-based studies including TEM and UV-vis had problems related to sample preparation. XPS and ATR-IR also produced low signals due to the geometry of TPP and TPPO on the AuNP surface. A kinetic measurement based method for determining NP stability was recently reported.[2] This method uses kinetic probes for real time monitoring of aggregation kinetics. Using this approach, temperature induced NP aggregation rates can be obtained. These data allow the quantification of NP stability and stability ranking.[3]

A catalyst support system for the catalytically active TPP-AuNPs that achieves maximum loading of the NPs and homogenous dispersion of the NPs needs to be developed. This catalyst support system should also ensure recyclability of the NPs.

8.3 References

(1) Polte, J.; Erler, R.; Thünemann, A. F.; Sokolov, S.; Ahner, T. T.; Rademann, K.; Emmerling, F.; Kraehnert, R. *ACS Nano* **2010**, *4*, 1076-1082.

(2) Ott, L. S.; Finke, R. G. *Coord. Chem. Rev.* **2007**, *251*, 1075-1100.

(3) Ott, L. S.; Finke, R. G. *Chem. Mater.* **2008**, *20*, 2592-2601.